SNAP 11 Program
Final Summary Report

February 1962 through January 1967

Volume 2--Detailed Technical Discussion

MARTIN MARIETTA

DISCLAIMER

This report was prepared for the U. S. Atomic Energy Commission under Contract AT(30-1)-2952.

~~CONFIDENTIAL~~

MND-2952-70, 2 C-92a
M-3679, 49th Edition
AEC Research and Development Report.

UNCLASSIFIED

SNAP 11 Program
Final Summary Report

February 1962 through January 1967

Volume 2--Detailed Technical Discussion

MND-2952-70-2

Published: May 1967

Classification cancelled (or changed to)
by authority of DOC
by H. J. C. TIC, date SEP 4 - 1973

Approved by:

W. Brittain
W. Brittain
Project Engineer

W. P. Haass
W. P. Haass
Program Manager

~~DEFENSE~~
INFORMATION

This document contains information affecting the National Defense of the United States within the meaning of the Espionage Laws, Title 18, U.S.C., Sections 793 and 794, the transmission or revelation of which in any manner to an unauthorized person is prohibited by law.

Group 3
Downgraded at 12-year intervals;
not automatically declassified.

DISTRIBUTION OF THIS DOCUMENT UNLIMITED

MARTIN MARIETTA CORPORATION
BALTIMORE, MARYLAND 21203

~~DISTRIBUTION OF THIS DOCUMENT IS UNLIMITED~~

~~CONFIDENTIAL~~

LEGAL NOTICE

DISTRIBUTION LIST

Addressee	No. of Copies
AEC Albuquerque Operations Office	1
AEC Canoga Park Area Office	1
AEC Chicago Patent Group	1
AEC Library, Washington	6
AEC New York Operations Office	1
AEC Oak Ridge Operations Office	2
AEC Patent Office	1
AEC Sandia Area Office	1
AEC Savannah River Operations Office	1
Aerojet-General Corporation (NASA)	2
Aerojet-General Corporation	1
Aerojet-General Nucleonics (NASA)	1
Aeronautical Systems Division	2
Aerospace Corporation	1
Air Force Headquarters	1
Air Force Surgeon General	1
Air Force Technical Applications Center	1
Air Force Weapons Laboratory	3
Air University Library	1
AiResearch Manufacturing Company, Los Angeles	1
Argonne National Laboratory	1
Army Reactors Field Group	1
ARO, Inc.	1
Atomics International	2
Battelle Memorial Institute	1
Battelle-Northwest	5
Bendix Corporation (NASA)	1
Brookhaven National Laboratory	1
Director and Defense Research and Engineering	1
DuPont Company, Aiken	2
DuPont Company, Wilmington	1
Electro-Optical Systems, Inc.	1
General Atomic Division	1
General Dynamics/Fort Worth	1
General Electric Company, Cincinnati	1
General Electric Company (FPD)	1
General Electric Company (MSVD)	2
General Electric Company, San Jose	1
Hittmann Associates, Inc.	1
Hughes Research Laboratories	1
Institute for Defense Analyses	1
Jet Propulsion Laboratory	1
Johns Hopkins University (APL)	1
Lockheed Missiles & Space Company (SAN)	1
Los Alamos Scientific Laboratory	1
Martin Marietta Corporation	1
Martin Marietta Corporation, Denver Division	1
Massachusetts Institute of Technology (Evans)	1
Minnesota Mining & Manufacturing Company	1
Mound Laboratory	1
NASA-Goddard Space Flight Center	4
NASA-Langley Research Center	2
NASA-Lewis Research Center	7
NASA Manned Spacecraft Center	1
NASA-Marshall Space Flight Center	5
NASA, Washington	2
National Reactor Testing Station (Inc.)	4
Navy Air Development Center	1
Navy Air Systems Command	1
Navy Marine Engineering Laboratory	1
Navy Missile Center	1
Navy Office of the Chief of Naval Operations	1
Navy Ordnance Systems Command	3
Navy Radiological Defense Laboratory	1
Navy Research Laboratory	1
Navy Ship Systems Command Headquarters	1
Navy Weapons Laboratory	1
Nuclear Materials & Equipment Corp.	2
Pratt & Whitney Aircraft Division (NASA)	1
Radio Corporation of America (NY)	1
Radio Corporation of America, Cranbury	1

DISTRIBUTION LIST (continued)

Addressee	No. of Copies
Rand Corporation	1
Republic Aviation Division	1
Sandia Corporation	5
Thermo Electron Engineering Corporation	1
Tracerlab, Richmond	1
TRW Systems	1
TRW Systems (SAN)	1
Union Carbide Corp. (ORNL)	2
University of California, Livermore	1
Westinghouse Electric Corp., Lima (AF)	1
Westinghouse Electric Corp. (NASA)	1
Westinghouse Electric Corp. (WAL)	1
AEC Division of Technical Information Extension	10

FOREWORD

This report presents a detailed summary of the technical effort performed to develop a radioisotope thermoelectric generator using a short half-life fuel. The work described was accomplished by the Martin Marietta Corporation for the U.S. Atomic Energy Commission under Contract AT(30-1)-2952 during the period of February 1962 through January 1967.

The technical information is presented in two volumes: Volume 1 contains a summary of the entire program and Volume 2 provides the details of the design, analysis and testing of the various generator systems and components. Results of the post-test diagnostic examination of the radioisotopic heat source utilized for the fueled demonstration test generator will be reported separately by the Oak Ridge National Laboratory.

BLANK

CONTENTS

		Page
	Legal Notice	ii
	Distribution List	iii
	Foreword	v
	Contents	vii
I.	Introduction	I-1
II.	Generator Design Development	II-1
	A. Initial Configuration and Design Constraints	II-1
	B. Material Selection and Evaluation	II-6
	C. Generator Testing and Configuration Changes	II-14
III.	Second Generation Generators	III-1
	A. Q/N-1 Modified Generator	III-2
	B. Q/N-3 Generator	III-25
	C. Q/N-4 Generator	III-42
IV.	Heat Source Development	IV-1
	A. Electrical Heat Source	IV-1
	B. Radioisotopic Heat Source	IV-9
V.	Generator Fueling and Demonstration Test	V-1
	A. Radioisotopic Heat Source	V-1
	B. Prefueling Effort	V-36
	C. Fueling Effort	V-51
VI.	Thermoelectric Development Program	VI-1
	A. Analytical Comparison of 2N-2P and 2N-3P Couples	VI-2

CONTENTS (continued)

		Page
	B. Thermoelectric Couple Evaluation Program. . . .	VI-8
VII.	DC-to-DC Converter	VII-1
	A. Design.	VII-1
	B. Dynamic and Environmental Tests	VII-5
	C. Temperature, Partial Load and Short Circuit Protection Tests	VII-11
	D. Vacuum Test	VII-12
	E. Generator S/N-2 and Converter S/N-3 Marriage Test	VII-14
	F. Conclusions	VII-14
VIII.	Generator Field Test Kit.	VIII-1
IX.	Nuclear Safety.	IX-1
	A. Safety Philosophy and Design Criteria.	IX-1
	B. Safety Aspects of Generator Design	IX-3
	C. Analysis Summary.	IX-6
	D. Summary of Safety Tests	IX-39
	E. Safety Application to New Design	IX-49
	F. Future Safety Analysis	IX-50
	Appendices	
	A. Fuel Block Thermal Analysis	A-1
	B. Fuel Block Stress Analysis	B-1
	C. List of Drawings for Model 431D: Q/N-1M, Q/N-3 and Q/N-4	C-1
	D. List of Reports and Manuals	D-1

I. INTRODUCTION

This volume of the SNAP 11 Final Report contains a detailed discussion of the generator development activities encompassing:

(1) Generator component development

(2) Heat source development, including both electrical and radioisotopic sources

(3) Thermoelectric materials studies

(4) Prototype generator testing.

The discussion logically culminates in a detailed discussion of: the final design generator performance in air; thermal vacuum and dynamic environments; fabrication of a radioisotopic heat source specifically designed for a laboratory demonstration test; and, performance of a 90-day fueled generator demonstration test at ORNL. Primary emphasis in presenting the technical accomplishments of the SNAP 11 program was placed on the relatively recent efforts, which are of greater interest, rather than on those efforts which have been superceded. Additional information on any technical aspect of the program can be found in the reports listed in Appendix D.

Principal design modifications resulting from development studies and testing on earlier units were:

(1) The replacement of 2P with 3P thermoelements in the thermocouple design to obtain stable generator operation at anticipated beginning-of-life hot junction temperatures (~1000° F).

(2) The replacement of the 100% tin solder at the cold end thermocouple/terminal strap solder joint with a PbIn alloy to permit higher cold junction operating temperatures during lunar day periods.

(3) Redesign of the electrical heater block to more closely simulate the materials, configuration and emissivity coating of the demonstration test fuel block assembly.

(4) Incorporation of radiation foils to control the hot junction temperature gradient.

(5) Increase in fin length to compensate for removal of a heat-conducting aluminum grease in the cold junction spring and piston hardware, believed to contribute to generator internal contamination.

A listing of the final design drawings is presented in Appendix C.

Three final design generators were fabricated and tested as described herein prior to delivery to the respective agencies. Generator designations and ultimate dispositions were as follows:

Q/N-1M Generator: Power output at end-of-life (EOL) design condition (lunar night) was 20.9 watts. The generator was subsequently fueled with a curium-242 heat source at ORNL and completed a 90-day demonstration test in a simulated lunar environment; power output at end-of-life condition was ~20 watts. The generator was subsequently shipped to Sandia Corporation for further air testing.

Q/N-3 Generator: Power output at EOL design condition (lunar night) was 21.3 watts. The generator was shipped to Jet Propulsion Laboratory for further air, vacuum and dynamic testing.

Q/N-4 Generator: Power output at EOL design condition (lunar night) was 20.9 watts. The generator was shipped to NASA-Manned Spacecraft Center/Houston for further air and vacuum testing.

II. GENERATOR DESIGN DEVELOPMENT

The generator development presented in this chapter is grouped by major areas of development and test efforts, as opposed to a continuous discussion of events in strict chronological order. Starting with the initial concept, each modification or addition is identified and described, and the experimental work which led to the modification is summarized. Specific data and analytical results have been omitted in most cases in the development review. Emphasis has been placed on those actions which changed the design configuration.

A. INITIAL CONFIGURATION AND DESIGN CONSTRAINTS

1. General Description

The initial conceptual design of the SNAP 11 generator to be discussed in this subsection is illustrated in Figs. II-1 and II-2. Externally, it consists of a cylindrical shell approximately 8-1/4 inches in diameter and 9-1/2 inches long, with 6 tapered fins attached to provide adequate radiating surface area. Internally, heat is produced in a capsule (containing the radioisotopic fuel) located in the center of the heat source assembly. Heat flows through this assembly to its surface and, from there, is radiated to the inner shell. (The inner shell, in conjunction with the outer shell, hermetically isolates the internal generator environment.) The heat is then conducted through the thermoelectric converters, consisting of thermoelements and thermal insulation, to the outer shell, from which it is radiated to space. Electrical power is produced by the heat flow through the thermoelements.

Because of the short half life of the curium-242 isotope used as the fuel, a significant decrease in the isotope heat production rate is experienced during the generator life. To compensate for this decay, the isotope inventory is deliberately oversized, and the excess energy at the beginning-of-life is discarded by radiation directly from the heat source assembly to prevent excessive generator operating temperatues. The rate at which heat is dumped is controlled by the opening of the shutter, which exposes one end of the heat source assembly to the lunar environment. The door position is controlled by the hot junction temperature through expansion and contraction of a liquid metal system. The entire generator outer shell is coated with a high-temperature oxide which has a high emissivity to infrared radiation but a low absorptivity to solar radiation of a shorter wave length. This combination produces a radiator of minimum size and high effectiveness.

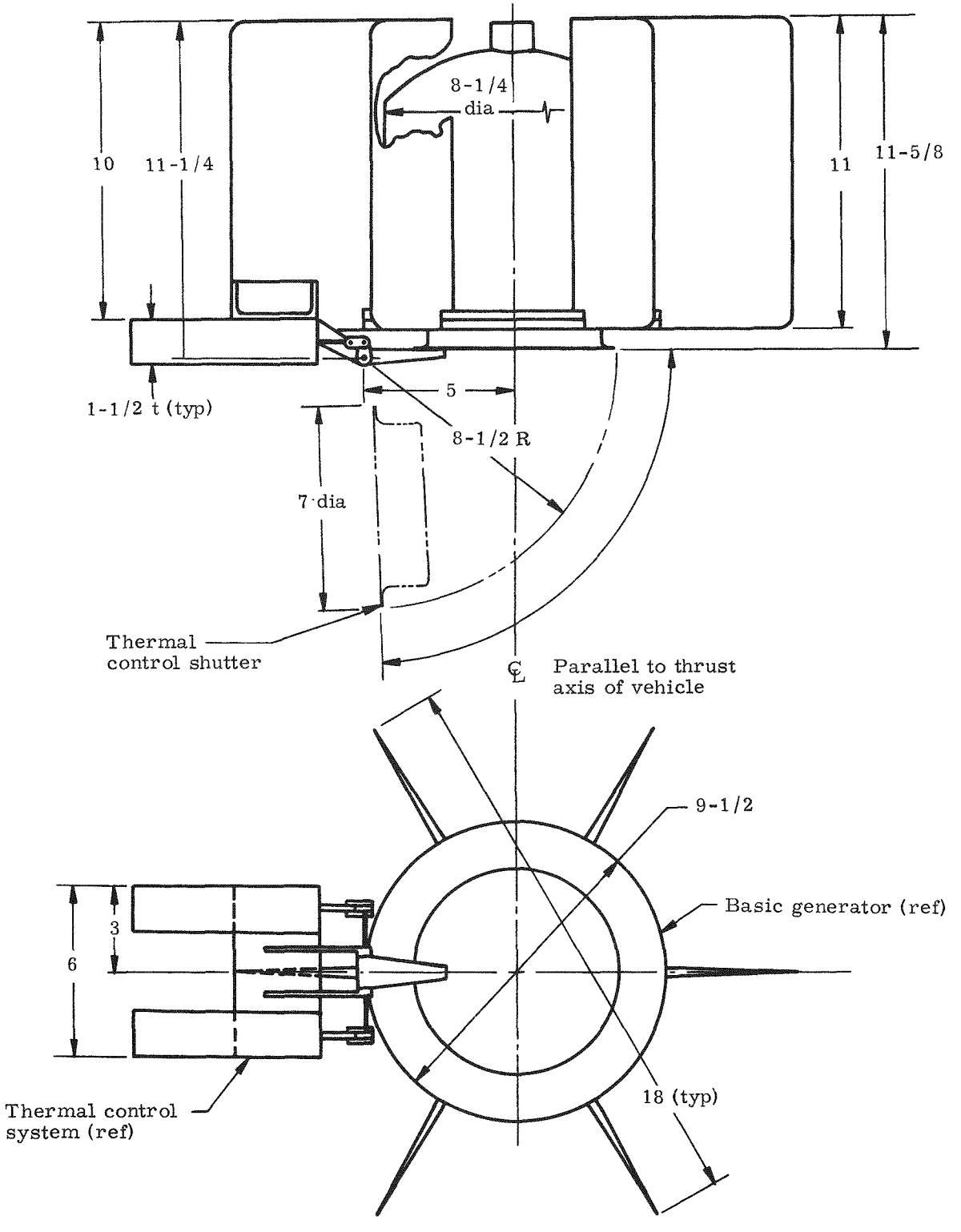

Fig. II-1. Initial Generator Conceptual Design

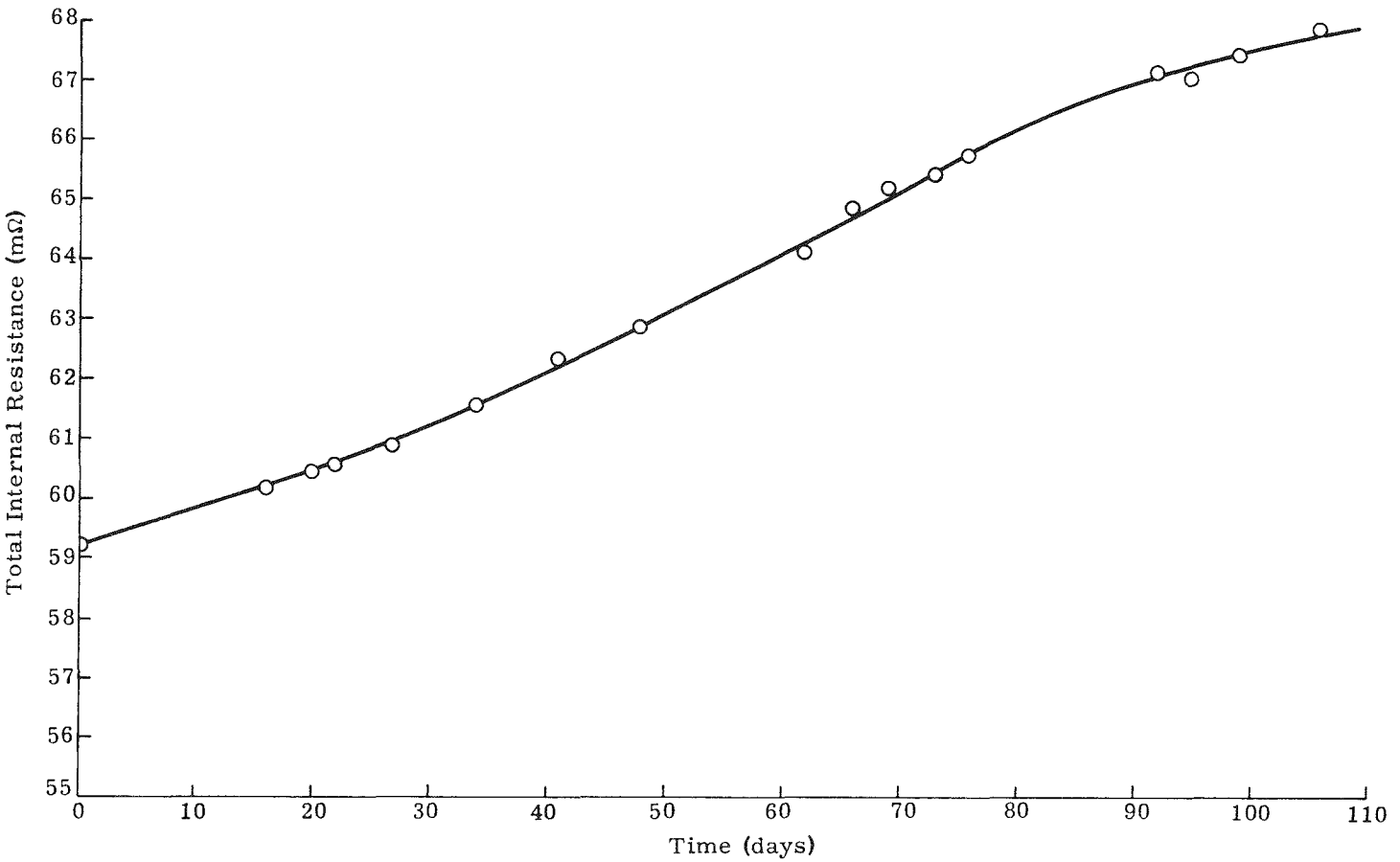

Fig. II-2. Module Test Fixture No. 2--Total Internal Resistance History

2. Thermoelectric Converter Configuration

Conversion of heat to electricity is effected in 12 module assemblies, each containing 6 thermoelectric couples. The space between the elements is filled with Johns-Manville Type 1301 Min-K insulation to minimize heat losses. The modules and associated hardware are hermetically sealed within the argon-filled annular cavity between the outer and inner shells. The cold end hardware consists of a spherical washer, a piston, a spring, and a cold sink bar, as shown in Fig. II-2. This arrangement compensates for axial, lateral and angular misalignments while applying an axial load to each thermoelement. In order to improve system reliability, the couples are arranged in parallel pairs, and these pairs are connected in series. Diameters computed for the P- and N-type elements are 0.348 and 0.343 inch, respectively. Both elements are 0.50 inch long.

The N and P elements are bonded to iron shoes at the hot and cold ends to form a couple assembly. Six couples are subsequently installed in Min-K insulation, and copper conductor straps are soldered to the cold iron discs to form a module assembly. Each of the 12 module assemblies is affixed to the inner shell by means of a retainer screw and the cold end hardware previously described. Following installation of the outer shell, the retainer screws are removed through 12 access holes in the outer shell. This removal permits the cold sink bars to be displaced outward to contact the outer shell, thus spring-loading the modules into position. Each access penetration is subsequently sealed with an O-ring, cap and threaded plug.

3. Radiation Shield Configuration

The radiation shield, which encircles the fuel capsule, attenuates the gamma radiation in certain critical zones, while maintaining the ability of the heat source to transfer heat to both the inner shell of the generator and the upper surface of the heat source for radiation of excess heat to the lunar environment. The material initially selected for more than half of the cylindrical section of the block was a tungsten alloy. Subsequently, tantalum, tantalum alloy (Ta-10W), gold, beryllium and platinum were considered as shield materials. Initial shielding requirements were difficult to meet, and selective shielding in critical areas was considered to reduce weight. When shielding requirements were relaxed as a result of introducing physical separation of the generator from other parts of the spacecraft, these elaborate designs were discarded. Initial studies revealed that platinum appeared to be the best container and radiation shield material based on both the melting point and compatibility (see Figs. V-1 and V-2).

4. Temperature Control Mechanism Configuration

The rate at which heat is dumped from the heat source is a function of the shutter door position. This, in turn, is a function of the generator hot junction temperature. In the initial configuration, door positioning

was accomplished by a mercury vapor pressure actuator system consisting of a sensing bulb sandwiched between the inner shell and a supporting strap, a capillary connecting tube and a bellows actuator. Initially, the system is completely filled with mercury, and a spring which reacts against the bellows is preloaded to produce system pressurization equal to the mercury vapor pressure corresponding to a selected hot junction operating temperature. Dual independent actuation systems are provided, each capable of positioning the door independently.

5. Reflector Configuration

The reflector assembly consists of the support bracket and reflector. The reflector, like the shutter cap, is faced with gold foil and mechanically assembled by electron beam spot welding. The reflector prevents a direct heat path that would result in radiation losses from the heat source shield, liquid metal reservoir and the inner shell; it also prevents temperature gradients which would disrupt the correlation between the liquid metal reservoir and hot junction temperatures required for calibration. At the time of assembly, the void formed by the diaphragm and reflector is packed with AA glass fiber insulation to minimize heat losses.

6. Inner Shell Configuration

The inner shell provides the inner support for the spring-loaded thermoelectric couples, helps maintain the thermoelectric cavity hermetic seal and provides the means for mounting the fuel source assembly. Stable metal oxide coatings are flame-sprayed on its inner periphery to provide a highly emissive surface that assures a low thermal resistance path between the heat source and thermoelectric converter during lunar operation.

7. Design Operating Temperature Limitations

Generator maximum hot junction operating temperatures are limited primarily by the thermoelement material while cold junction temperatures are limited by the melting temperature of the cold strap-to-element solder material. The hot junction temperature limitation for the lead telluride elements was set at 975° F for the most stringent operating condition; i.e., beginning-of-life, lunar day. A hot junction temperature of 925° F at end-of-life lunar night was selected on the basis of generator efficiency and the requirement for a 50° F hot junction temperature increase to cause full opening of the shutter door at the beginning-of-life condition. A cold junction temperature of 350° F was selected for the end-of-life operating point, considering thermoelectric efficiency, required radiator area for heat rejection from the generator during vacuum operation and the melting temperature of the 95% lead-5% tin cold strap solder.

B. MATERIAL SELECTION AND EVALUATION

1. Thermal Control System

a. Working fluid and reservoir materials

As discussed in Chapter II-A, the initial generator concept utilized a mercury working fluid in the thermal control system. In this system, the position of the shutter door was determined by the mercury vapor pressure; as the hot junction temperature rose, the adjacent sensing bulb vapor pressure would increase and, by means of an actuator piston and associated linkage, would increase the shutter opening for greater heat rejection from the heat source.

To reduce weight and simplify construction, a sodium-potassium mixture (78% potassium, 22% sodium by weight) was subsequently chosen as the thermal control system working fluid. Since the NaK remains in the liquid phase for the intended operating temperature range due to its low vapor pressure, the inherent problems of very accurately determining frictional forces and spring pressures as required for a vapor system are somewhat minimized. Also, the complexity of designing redundant control is minimized, since doubling of the load on a vapor-controlled system would completely disrupt the initial calibration point, whereas in a liquid system, the low compressibility of the working fluid would maintain the calibration point.

Series 300 stainless steel was chosen for all components in direct contact with the liquid NaK due to previously established compatibility at intended operating temperatures. Filling of the stainless steel reservoir and actuator system is accomplished in the following sequence:

(1) Complete evacuation of system at room temperature

(2) Heatup of system to operating temperature while under continuous evacuation

(3) Hydrogen cleaning of system while hot

(4) Backfilling of system at temperature with liquid NaK

(5) Seal-welding of system after stabilization at the desired temperatures.

b. Linkage and shutter door lid materials

The initial shutter door design utilized a titanium arm and lid, due to weight considerations. To minimize heat losses from the generator at the end-of-life point, when the shutter door is fully closed, gold

foil was spot welded to both sides of the lid to provide surfaces with a low emissivity. However, due to spot weld failures at temperature caused by oxidation of the titanium, an electroless nickel coating was applied to the titanium prior to spot welding. Subsequently, the nickel-coated titanium single lid was replaced by two 300-series stainless steel lids which sandwiched thermal insulating felt. In this configuration, the gold was spotwelded to the stainless steel lids.

To simplify construction, attempts were made to gold plate the stainless steel lids in lieu of spotwelding the gold foil. However, plating was demonstrated to be unsatisfactory, due to diffusion of the gold into the stainless steel. A process was then developed using a ceramic diffusion barrier between the stainless steel and gold surfaces. This barrier, commercially known as Solaramic, is fired onto the preoxidized stainless steel surface at 1750° F in air. A liquid bright-gold solution is then brushed on the ceramic coated surface and fired in air at 1000° F.

To further reduce parasitic heat losses through the shutter door lid, Min-K insulation, contained in a Refrasil* bag, replaced the felt previously used. In addition, gold-coated insulation foils were incorporated between the Min-K and the gold-coated upper and lower lids.

To prevent galling of the linkage components, dissimilar metals and/or platings are used at all sliding surfaces. Testing demonstrated that a lubricant was needed at critical sliding points in the linkage due to the hysteresis effect on the hot junction temperature noted upon cycling the thermal shutter, i.e., the hot junction temperature was lower for the same shutter opening during door closing than in opening. Thus, Molykote X-15 lubricant was incorporated at all critical sliding points.

2. Thermoelectric Converter

a. Thermocouple materials

From its inception, the SNAP 11 program was to utilize technology and experience derived from the SNAP 9A program. This included employing identical thermoelements and couple fabrication techniques to minimize thermoelectric development effort. The SNAP 11 program retained the basic 2N-2P thermocouple design of the SNAP 9A generator. The common hot junction connecting strap of the thermocouple was FerroVacE iron with FerroVacE iron cold caps used as diffusion barriers at the cold junction of each element. The 2P element of the thermocouple was mechanically bonded to the FerroVacE shoes at both the hot and cold junctions with 100% tin, which combined with the tellurium in the element to form a tin telluride bond upon heating to bonding temperatures; the 2N element was diffusion bonded to the FerroVacE iron shoes with nickel (bonding temperature is 1450° F)

* High temperature woven fiberglass cloth manufactured by H. I. Thompson Fiber Glass Company.

The basic couple design described above was retained through the Q/N-2 generator. Due to generator performance degradation associated with the 2N-2P couple (15 to 20% decrease in power output in 2000 to 3000 hours, the decision was made to evaluate 3P material for replacement of the 2P by comparison testing of these materials in modules. Since the 2N leg exhibited relatively stable performance, this material was retained. To minimize test variables, the existing hot and cold shoe configurations and material (FerroVacE iron) were retained.

Eight six-couple modules, contained in four test fixtures, were fabricated and placed on test. Table II-1 summarizes the major characteristics of each module and its operating characteristics. Each test module contains six couples connected electrically in series. Couples to be compared are contained in the same module test fixture, but each module output is connected across its own external load resistance to allow monitoring of the individual module outputs. In addition, instrumentation allows monitoring of the performance of the individual couple legs in each module.

As shown in Table II-1, modules are being tested at 900°, 1000° and 1100° F hot junction temperatures. In the 1100° F test fixture, only 2N-3P couples are utilized, since the operation of 2P was expected to be limited to temperatures below 1000° F. 2N-3P couple performance with bonded and pressure contacts at the 3P hot junction is evaluated in the 1100° F fixture, with three knurled and three plain pressure contacts being incorporated in the six couples of the pressure contact module.

In Test Fixture No. 1 (1000° F hot junction), the effect of spring pressure on leg performance is also being evaluated; element contact pressures of 70, 140 and 210 psi are employed. As of this November 30, 1966, total test times of 8673, 7916, 1830 and 7577 hours have been accumulated on Test Fixtures No. 1, 2, 3 and 4, respectively. All test fixtures with the exception of No. 3 are remaining on test under the SNAP 19 program; Test Fixture No. 3 was discontinued after 1830 hours due to repeated heater failures. (See Chapter VI for a detailed discussion of the testing summarized in this section.)

Pertinent conclusions from testing performed to date are as follows:

(1) The 3P material is more stable than the 2P material at all hot junction temperatures investigated.

(2) The superior performance of 3P over 2P is evident at hot junction temperatures of 1000° F and higher; the superiority of 3P over 2P at a 900° F hot junction temperature is not quite as evident as at the 1000° F hot junction temperature.

(3) Plain pressure contacts appear to be more stable at the 1100° F than either knurled or bonded contacts, although still exhibiting a higher resistance than bonded legs.

TABLE II-1

SNAP 11 Module Test Data
$D_n = D_p = 0.375$ inch; $L = 0.500$ inch

Module	Material	T_H (°F)	T_C (°F)	Hot Bond and Process P Leg	Hot Bond and Process N Leg	Spring Pressure (psi)	Comments
1	2N-2P	1000	350	SnTe-HP(1)	Ni-FB(2)	70, 140, 210	2 couples at 70, 2 at 140, 2 at 210
2	2N-3P	1000	350	SnTe-HP(1)	Ni-FB(2)	70, 140, 210	2 couples at 70, 2 at 140, 2 at 210
3	2N-2P	900	350	SnTe-HP(1)	Ni-FB(2)	140	
4	2N-3P	900	350	SnTe-HP(1)	Ni-FB(2)	140	
5	2N-2P	1000	350	SnTe-HP(3)	Ni-FB(2)	140	
6	2N-3P	1000	350	SnTe-HP(3)	Ni-FB(2)	140	
7	2N-3P	1100	400	SnTe-HP(3)	Ni-FB(2)	140	
8	2N-3P	1100	400	No Bond(4)	Ni-FB(2)	140	

NOTE:
(1) HP = hot pressed
(2) FB = furnace bond
(3) Two couples (2 and 4) are furnace bonded
(4) Pressure contacts, 3 knurled and 3 plain shoe surfaces at P hot junction

(4) Operation of 2N-3P material at hot junction temperatures as high as 1100° F appears feasible.

(5) The spring pressures evaluated, i.e., 70, 140 and 210 psi appear to have no effect on performance.

Based on the above test results, the Q/N-1M, Q/N-3 and Q/N-4 generators were fabricated with 2N-3P thermocouple materials in lieu of 2N-2P. Since the test results revealed no preference, the 140 psi spring pressure used in previous generators was retained. Since no comparison of bonded versus pressure contacts was run at the SNAP 11 hot junction temperature (<1000° F), bonding of couples was selected because of the lower resistance and, therefore, higher performance provided. At the 1100° F test temperature, couple stability is greater for pressure contacts than for bonded elements; also element seating is enhanced at higher temperatures. At the SNAP 11 hot junction temperature, the anticipated stability and seating advantages are reduced, thereby favoring the selection of bonded couples.

b. Module construction

The basic module design again made full use of SNAP 9A technology. A SNAP 11 module assembly is composed of six thermocouple assemblies and the necessary thermal insulation and connector straps for extraction of the couple power outputs at maximum thermal efficiency. In fabricating a module assembly the six-couple assemblies are inserted into holes in the thermal insulating material and the electrical connector straps are soldered to the FerroVacE iron cold caps on each couple leg. N and P terminal straps emanate from opposite ends of the module assembly; 12 modules are electrically connected in series to form a generator circuit.

Initially, a 95% lead, 5% tin alloy was used to solder gold-plated copper connector straps to the FerroVacE cold caps. However, due to the high lead content of the solder, problems were incurred in wetting both the connector straps and the FerroVacE iron cold caps. Thus, a material change to a 100% tin solder was made which exhibited excellent wetting characteristics. Subsequent generator testing revealed, however, that the low melting point of tin (460° F) would not allow operation of the generator at beginning-of-life power input during lunar day periods. Diagnostic disassembly of the Q/N-1 generator showed that 96 of the 144 copper terminal strap bonds had unbonded from the cold shoe of the thermoelectric couples during 1950 hours of operation. (This was the first generator assembled without the use of aluminum grease on the cold end hardware, used on previous generators to decrease the ΔT from the thermoelectric cold junction to the generator fins. Comparison with the S/N-4 generator disassembly results, in which aluminum grease was used on the cold end hardware, showed that none of the S/N-4 generator terminal straps had unbonded during its operation.) Unbonding of the pure tin solder joints was due to excessive cold junction temperatures during operation under lunar day conditions. Marginal cold junction operating conditions were also observed during the testing of Q/N-2, which incorporated increased

fin area over that of the Q/N-1 to compensate for removal of the aluminum grease.

To overcome this problem, an evaluation effort was initiated with the objective of identifying a solder that melted between 550° and 650° F, that was compatible with the thermoelectric cold junction and that could be used in the module bonding operation to achieve a low electrical resistance joint.

Of 14 solders identified by a literature survey, 10% In - 90% Pb solder was selected after exposure to wetting tests, shear tests, thermal cycling, aging tests and compatibility tests. Subsequent evaluation in a prototype module bonding operation showed that bonding could not be achieved in the standard bonding fixture. Thus, a hand soldering technique was developed and incorporated for bonding of modules in the Q/N-1M, Q/N-3 and Q/N-4 generators.

c. Thermal insulation

Johns-Manville Type 1301 Min-K insulation, identical to that used in the SNAP 9A, was chosen as the thermal insulating material in the thermoelectric converter cavity because of its excellent thermal insulating properties, low contamination level when properly baked out and outgassed, and known operating characteristics from SNAP 9A experience. Due to the complexity of the module insulation configuration, Johns-Manville supplies these components in cast form. Other Min-K insulation (used in the lower dome and above the modules) is received in block form and machined to shape.

Initially the Min-K insulation was baked out in both air and vacuum at 950° F and generator assembly performed in air. However, for generators subsequent to the S/N-4, all Min-K insulation was baked out in both air and vacuum at 1050° F to assure adequate removal of organic binders and other volatile substances which might contaminate the generator during operation. In addition, after the final bakeout in the vacuum furnace, the Min-K insulation components were sealed in argon and were never again exposed to air, as generator assembly was performed in a dry box with an argon atmosphere.

d. Electrical insulation

Mica was chosen as the electrical insulating material between the thermocouple hot shoes and inner can. This material was proven to be satisfactory by the SNAP 9A application. Prior to fabrication of the Q/N-1 and Q/N-2 generators, an evaluation was performed on five different types of mica:

(1) Muscovite India ruby

(2) Phlogopite light

(3) Muscovite Brazilian ruby

(4) Grade C (muscovite)

(5) Phlogopite dark.

Resistivity of the mica was evaluated as a function of time and temperature; and results indicated that all types were acceptable, with the phlogopite micas showing slightly lower resistivity than the muscovite micas being used in the generators. Since the difference in resistivity was negligible, muscovite mica was retained in the generator.

e. Cold end hardware

The cold end hardware components are composed of the pistons with mating alignment caps, heat sink bars and springs. All components, with the exception of the stainless steel springs, are fabricated from aluminum for both lightweight and good thermal conductivity. To prevent electrical shorts, the aluminum components are coated with aluminum oxide to a thickness of ~0.001 inch; thus, between the module terminal straps and the aluminum heat sink bar, a total of five aluminum oxide interfaces is imposed.

On generators prior to the Q/N-1, the spring pressure (element compressive load) was 70 psi. In addition, an aluminum-based grease was incorporated at all interfaces in the cold end hardware, i.e., at the terminal strap/alignment cap, alignment cap/piston and piston/heat sink bar interfaces. However, on the Q/N-1 and subsequent generators, the aluminum grease was removed as a possible contaminant; and the spring pressure was increased to 140 psi in an effort to decrease element contact resistances and to prevent alignment caps from becoming dislodged during vibration testing as had been noted on several previous generators.

Prior to assembling the cold end hardware for the Q/N-1 modified and subsequent generators, a diamond-base polishing paste was used in conforming the alignment cap/piston interface to assure that a low ΔT would be maintained at this interface; previously, an aluminum oxide base paste had been used, but the diamond paste resulted in a more uniform contact surface.

3. Inner Can

The inner can is constructed from Type 316 stainless steel to take advantage of this material's high temperature strength characteristics. As previously mentioned, the 12-sided can shell is explosively formed with the lower head and other details subsequently welded to the formed part.

Efforts to select a suitable emissivity coating for the inner can were initiated by evaluating silicate-bonded zirconium oxide. This coating spalled off the stainless steel inner can surface after operation at 1200° F. Apparently, the coating had vitrified, becoming more brittle, and flaked off on cooling because of the difference in expansion between it and the stainless steel.

Two porcelain enamels and two organic coatings were evaluated. Neither porcelain enamel was satisfactory in a vacuum. A butyl titanate-bonded aluminum paint (Pratt and Lambert No. 91-1524) deteriorated when tested in both air and vacuum. A silicate-bonded titania (Vita Var No. 15966-PV100) was tested on stainless steel at 1200° F in air. Flaking was observed in some areas.

Finally flame-sprayed aluminum oxide and chromium oxide coatings were evaluated and were shown to be stable at simulated operating conditions under thermal cycling. Subsequently, an examination of the Al_2O_3 and Cr_2O_3 coatings applied to the inner can assembly of the S/N-4 generator disclosed poor adherence and spalling.

A study program which examined the surface preparation was undertaken. Three methods of preparation were investigated:

(1) Vapor blast uses No. 1250 Al_2O_3 grit and water, sprayed under pressure; imparts a smooth, uniform finish.

(2) Sand blast uses No. 121 grit Al_2O_3. Finish is rough to medium.

(3) Grit blast uses No. 16 iron grit (Al_2O_3 may be substituted). Finish is coarse to rough.

Evaluation of samples resulted in the requirement that all inner can assemblies be grit blasted with No. 16 iron prior to flame spraying for maximum adherence.

Emittance values obtained for flame-sprayed coatings were:

Coating	Temperature 900° F	Temperature 1100° F
Flame-sprayed Cr_2O_3	0.89	0.89
Flame-sprayed Al_2O_3	0.66	0.63

4. Outer Housing

A magnesium-thorium alloy, identical to that utilized on the SNAP 9A, was selected for the outer skin to take advantage of its high strength-to-weight ratio. The outer housing surface is coated with a zirconium oxide, sodium silicate mixture also developed under the SNAP 9A program. The composition is 25.6% Treopax, 10.5% sodium silicate Brand D and 63.9% water. Treopax is 92% zirconium oxide and 5% silica. Sodium silicated Brand D has a ratio of silica to sodium oxide of 2 to 1. This coating composition was chosen because of its high surface emissivity (0.8) in conjunction with its low solar absorptivity (0.2).

C. GENERATOR TESTING AND CONFIGURATION CHANGES

1. Thermal Mockup Testing

Initial performance data for evaluation of the thermal control system was obtained from a generator thermal mockup containing no active thermoelectric elements. It differed from a prototype generator in that Inconel rods were employed to simulate thermal effects of the thermoelectric elements. The Inconel rods were sized in a separate assembly, the module test fixture, as follows: Inconel rods were assembled in one fixture and thermoelectric couples in a second fixture. Input power and cold junction temperature were approximately matched, and the size and number of Inconel rods were determined to duplicate the hot junction and element ΔT. Experiments revealed that 6 Inconel elements 0.50 inch in length and 0.156 inch in diameter simulated the thermal effects of the 12 elements in the SNAP 11 strip thermoelectric module. Naturally, this was an approximation, since Peltier cooling in active elements changes with external load.

The performance of the thermal mockup was determined by setting the manually operated thermal shutter to a desired position prior to installation in the thermal vacuum chamber (see Fig. II-3). After installation in the chamber, the electrical power input was varied incrementally and steady-state temperatures were measured for each preset shutter position. Results indicated that an average drop of 150° F occurred between the inner can (adjacent to the hot junction) and the NaK reservoir cavity. The heat dissipation capability of the fuel block with the shutter completely open was 460 watts, which compared favorably with the analytically determined 435 watts required. The results also indicated that the mockup outer housing or radiator dissipated thermal energy at temperatures approximately 30° F lower than the design temperature of 320° F.

The manually actuated thermal shutter in the thermal mockup was replaced with the NaK actuated shutter, and performance in a vacuum environment was observed. The data indicated a very small response

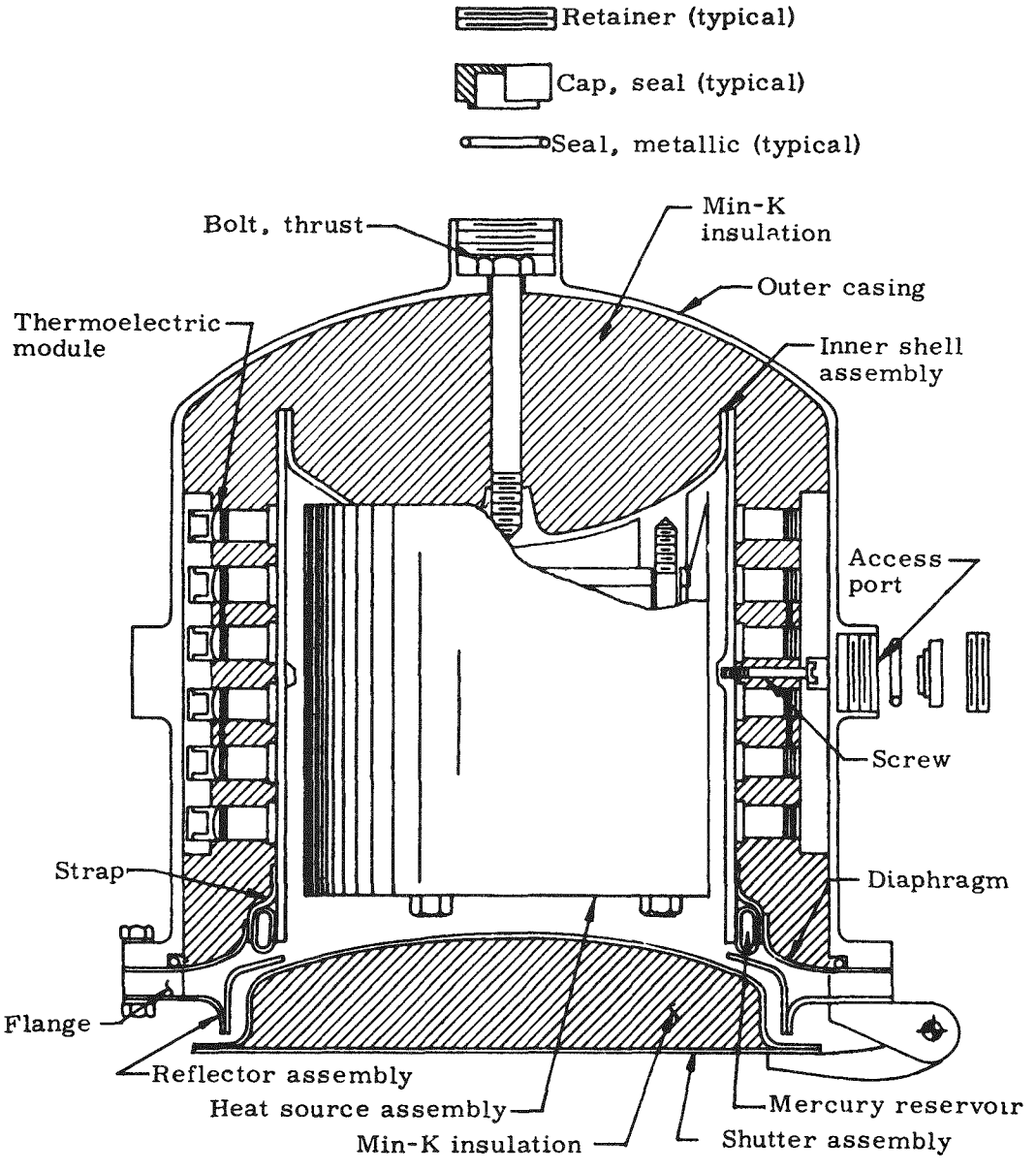

Fig. II-3. Proposed SNAP 11 Generator--Cross Section

in reservoir temperature to changes of inner skin temperature, implying that design modifications were necessary. The response of the NaK-actuated thermal shutter during a transition from an atmospheric environment to space conditions was observed. As the environmental change was effected, the shutter almost closed before starting its upward (opening) swing. The NaK reservoir temperature decreased while other component temperatures increased, due to loss of convective heating of the reservoir and the low volumetric heat capacity of the NaK. Shutter door response to reservoir temperature changes agreed with design requirements.

Conclusions from the thermal mockup testing were:

(1) Additional testing would be required on an operating generator to solve thermal control problems.

(2) A configuration change was required for the lower head of the inner shell from a dished head to a flat head to permit the entire fuel block assembly to be moved closer to the base of the inner shell so as to reduce the thermal gradients associated with the thermoelectric elements.

2. Initial Prototype Testing (Generators S/N-1 and S/N-3)

a. Dynamic testing of prototype Generator S/N-1

Generator S/N-1 was subjected to vibration, acceleration and shock tests to determine its mechanical and electrical capabilities under these critical environments.* The generator was operated at a stabilized input during all tests, and its output was monitored throughout the test program. A cast aluminum test fixture was used to mount the generator for all environmental tests and was constructed to duplicate the 30-degree mounting angle of the generator on the Surveyor vehicle. To avoid spontaneous ignition of the sodium-potassium material used to activate the shutter of operational generators, isopropyl Santo wax was substituted in the thermal control system as the operating fluid. The electrically heated block employed in S/N-1 for dynamic testing differed from those used for performance tests in that it simulated the calculated fuel block weight of 8.5 pounds and the center of gravity.

Oscillograph recordings made during each dynamic test showed no power failures or intermittencies. Problems occurred in obtaining proper shutter position which were attributed to the substituted Santo wax. The gold foil covering the shutter plate and surrounding the heater block was lost. Remedial action was designed into Prototype Generators S/N-2 and S/N-4.

* Dynamic environments for the S/N generator series were essentially identical to those for the Q/N series (see Table III-11).

b. S/N-3 performance testing

Vacuum testing at lunar day environmental conditions was performed during the first 15 days of generator operation. For a 655-watt power input, maximum power output was 17.1 watts. After the 15 days of simulated lunar testing, the generator was put on life test for 130 days. Test results are shown in Figs. II-4 and II-5. Approximately 20% decrease in output power was noted during the first 40 days and 7% during the remainder of the test period.

c. Diagnostic disassembly of Prototype Generator S/N-3

The S/N-3 generator was disassembled and inspected to determine the effects of long-term performance testing. Dimensional and resistance measurements were made on selected components. Results indicated:

(1) Inward deflection of the center of the inner can of approximately five to seven mils as compared to the ends. Deflection of the base of the inner can was negligible. The top of the polygon section of the inner can deflected approximately five mils radially outward when the modules were removed.

(2) Resistance measurements, made between the power outlets at the electrical plug and the outer housing, resulted in a reading of 70,000 ohms.

(3) Resistance measurements made across the leads of each module indicated a substantial increase in module resistance.

Inspection of the cold junction hardware indicated good thermal contact between all components, i.e., cold straps, buttons, pistons, heat sink bars and outer housing.

The electrical degradation in both N and P bonds appeared to be associated with the formation of void areas in the element near the bond, which may contain a crystallizing phase. Metallographic evidence indicated that the parting was through the PbTe element and not at the bond.

d. Design modifications after initial prototype testing

Results from subcomponent testing and operation of Prototype Generators S/N-1 and S/N-3 indicated the need for several design modifications:

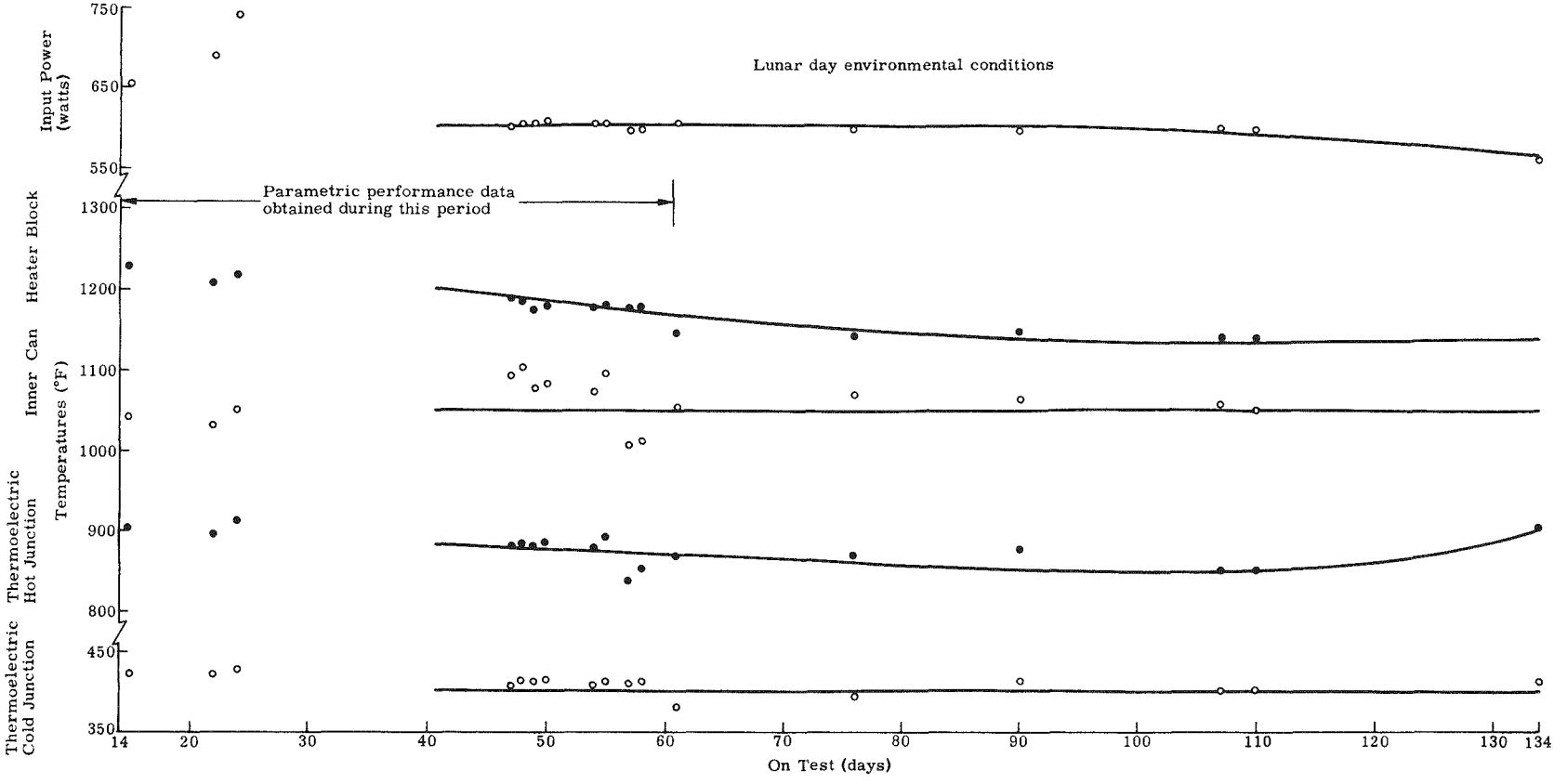

Fig. II-4. Prototype Generator S/N 3 Life Test--Operational Parameters

CONFIDENTIAL

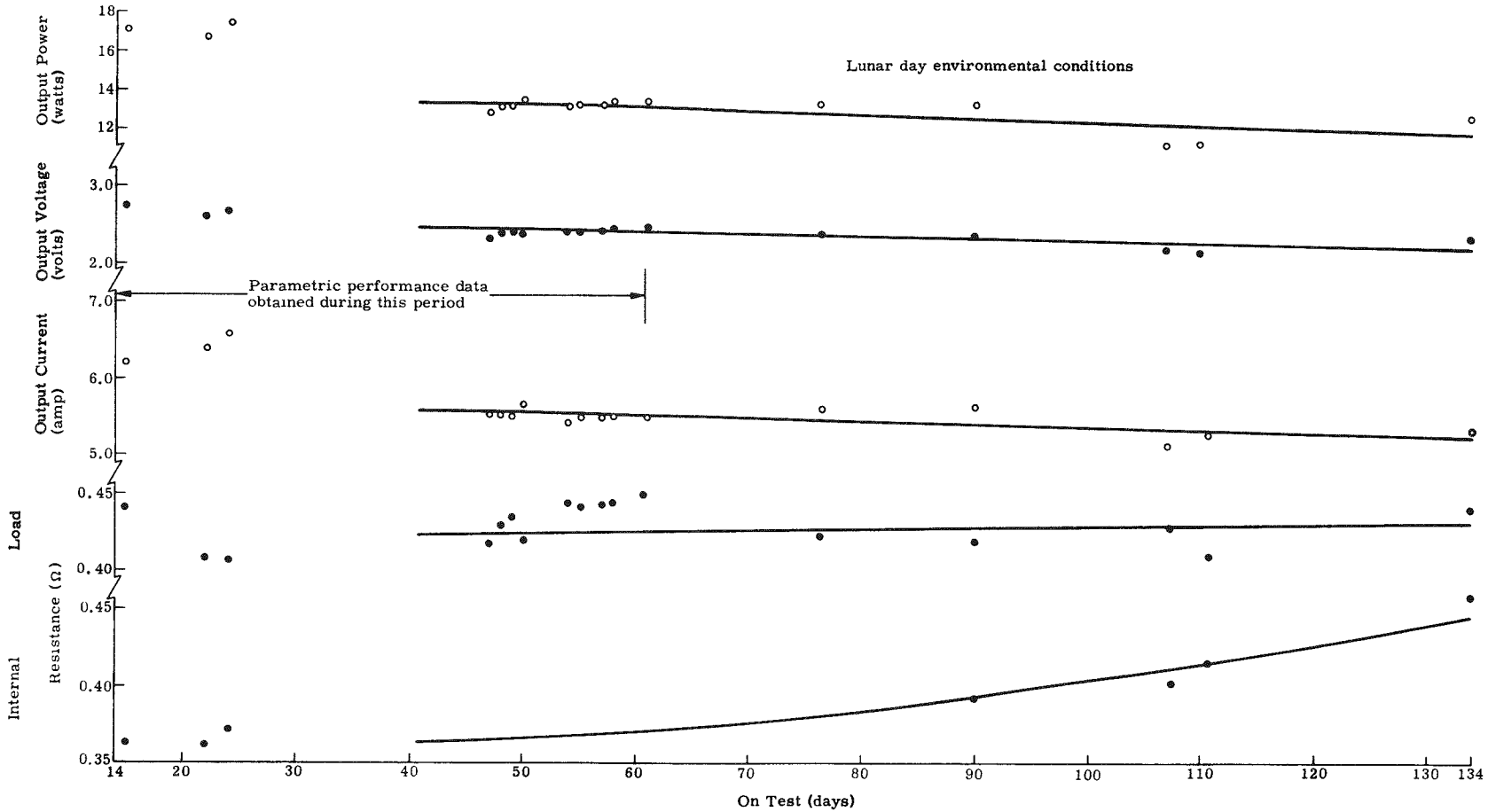

Fig. II-5. Prototype Generator S/N 3 Life Test--Operational Parameters

(1) The generator outer housing weld configuration was redesigned to eliminate all weld penetrations of the outer housing, because leak testing of the weld joints between the radiator fins and the outer housing showed that these welds were porous.

(2) The closure between the inner and outer housings was redesigned to include two independent Viton O-ring seals in place of the aluminum O-ring.

(3) The thermal control system was modified to provide improved alignment for actuator components.

(4) The thermal shutter heat dump door was redesigned to incorporate 3/8 inch of AA fiberglass insulation, and an electrolytic gold foil reflector was employed to reduce heat losses.

(5) The 12 thermoelectric module ports were modified to permit more uniform loading of the O-ring seals. (Four studs were used at each module port to replace the two previously used.)

(6) The NaK reservoir support diaphragm was redesigned to take up the differential thermal expansion between the inner and outer housings.

(7) A provision was incorporated in both the inner and outer housings to enable a three-point fuel block suspension system to be employed should dynamic tests indicate a need for more support.

(8) The tubes extending from the thermal control system bellows to the reservoirs were relocated to fit between the adjacent fins without fin alteration.

(9) The top surface of the heater block was coated with chromium oxide to increase the heat rejection capability of the heat source.

(10) The lower section of the inner shell inner periphery was coated with aluminum oxide while the upper half was coated with chromium oxide to reduce the axial temperature gradient experienced along the inner shell during performance testing.

The parasitic heat loss was determined for Generator S/N-3 at end-of-life under lunar day conditions, i.e., hot junction temperature of 925° F and the thermal shutter closed. This was accomplished by making a series of steady-state, open-circuit runs at different input power levels, corresponding to near design point hot junction temperatures. The parasitic heat loss is the total heat input minus that conducted

through the elements. The measured heat loss at a hot junction temperature of 925° F was 206.5 watts, which was higher than the calculated 118 watts. Three modifications were made to reduce parasitic heat losses:

(1) The thermal heat dump shutter door was redesigned to a sandwich construction to permit the addition of Min-K insulation and thus reduce conductive heat loss.

(2) A chromium oxide coating was selectively incorporated on the surface of the fuel block and inner shell opposite the shutter to increase emissivity and thereby reduce temperature gradients.

(3) The thermoelectric hot junction faces of the inner shell were lapped to reduce gaps at the hot shoe interface.

3. Testing of Prototype Generators S/N-2 and S/N-4

a. Performance testing

Performance testing indicated that the design changes incorporated in Prototype Generators S/N-2 and S/N-4 substantially improved generator thermal characteristics over Prototype Generator S/N-3. Power output for both generators was ~ 20 watts with an ~ 650-watt input (lunar day), a 20% increase over that determined for the S/N-3. The axial temperature differences on the inner shell and hot junctions were reduced by inner shell emissivity coatings of chromium and aluminum oxide. The radial temperature difference between the inner shell and hot junctions was reduced. Generator heat losses were reduced by employing insulation and a gold-plated reflector on the thermal shutter. Also, heat losses were reduced by employing emissivity coatings on the heater block to reduce temperature. The reduction in heat losses was accompanied by an increase in overall generator efficiency of ~20%. After initial checkout at Martin Marietta, the S/N-2 generator was shipped to JPL for further evaluation.

During initial testing, difficulties were experienced in the thermal control system of S/N-4. Improper filling techniques caused poor shutter door operation. The entire thermal control system was replaced with the system previously used in Generator S/N-3 after parametric performance data were collected with the shutter door closed (end-of-life) for atmospheric and vacuum conditions.

Extensive room temperature electrical parametric and thermal vacuum tests at lunar day and night conditions were conducted on the S/N-4 prototype generator. Prior to performance tests, an outgassing

sequence consisting of a series of evacuation and backfill cycles at elevated temperatures was implemented. A parametric test in room temperature air was run, followed by lunar day and lunar night simulations. During lunar night simulation, the shutter door was fully open at a hot junction temperature of 647° F and a power input of 500 watts. The test was continued with the shutter door secured in the closed position. The premature opening of the thermal control system (taken from the S/N-3 generator) was attributed to a combination of an improperly installed linkage and a rigid adjustment bellows which produced false indications of initial settings.

Additional tests were performed at controlled hot and cold junction temperatures by regulating the amount of convective cooling around the generator. Test results indicated a maximum power output of 29.15 watts for room temperature air test with 820 watts input. For lunar night simulation, the data indicated that, at a hot junction temperature of 925° F, the cold junction would operate at 370° F, approximately 20° F higher than design. Similarly, the power input to maintain the hot junction at the end-of-life value was approximately 680 watts, considerably in excess of the 556 watts available, based on the anticipated curium-242 fuel inventory.

Tests performed under lunar night conditions at a hot junction temperature of 925° F and a 350° F cold junction temperature, using the instantaneous E-I method, indicated a maximum power output of 23.48 watts at matched load.

Subsequent to initial generator checkout, the S/N-4 generator was subjected to life testing. The generator electrical output showed a 16% decrease over the 2300-hour test period, believed partially due to extensive thermal cycling and inadvertent overheating of the generator cold junction early in the lunar day test series.

The S/N-4 generator was subsequently reworked to incorporate the design modifications required. All internal components, i.e., insulation, thermoelectric modules and circuitry, were renewed. The thermal control shutter door and brackets, internal heat shields and heat transfer fins were modified.

b. Design modifications from S/N-2 and S/N-4 testing

Design changes incorporated to eliminate problems incurred during testing included the following:

(1) The adjustment bellows was tack-welded at its highest position in the casing.

(2) A positive attachment of the adjustment screw to the bellows was provided, permitting deliberate expansion as well as compression.

(3) Linkage sliding parts were chrome plated to reduce friction.

(4) An actuator link was modified to provide better operational control of the shutter.

(5) An eye bolt was added to the spring for control of spring tension to provide a significant degree of adjustment.

(6) The length of the fins was increased from 4.5 inches to 5.5 inches to provide the required cooling capacity.

(7) The mounting lugs at the base of the generator were eliminated, since dynamic testing indicated that they were not necessary.

(8) The shutter bracket was revised to include a box-shaped section with an overlapping extrusion. This increased the stiffness of the shutter bracket and provided a method of latching the door during launch.

(9) An examination of the coatings applied to the inner shell assembly of the S/N-4 prototype generator indicated poor adherence and spalling of the Al_2O_3 and Cr_2O_3 material. A study which examined the effect of surface preparation indicated that the surfaces should be grit blasted with No. 16 iron or Al_2O_3 prior to flame spraying for maximum adherence.

The following modifications were incorporated to reduce heat losses through the shutter:

(1) Microfibers felt was replaced with Min-K 1301 to decrease the thermal conductance by a factor of two.

(2) A connecting member between the upper and lower envelope was removed, thus reducing heat transfer to the external surface.

(3) Polished dimpled nickel foil was sandwiched between the lower dome and Min-K insulation so that the reflectivity of the lower dome would be maintained in case the lower dome gold plating emissivity increases during operation.

(4) The upper dome was gold plated to decrease heat transfer from the top surface of the shutter.

(5) A heat shield was changed to include a more effective radiation baffle, limiting the loss of heat from the blocks through the gap between the upper portion of the block and the inner shell.

Figure II-6 shows a cross-sectional view comparing the original S/N-4 with the modified version.

4. S/N-4 Modified Testing

The modified S/N-4 generator was tested in air and in a thermal vacuum chamber capable of simulating lunar night conditions. The thermal control system did not operate properly because of a general system softness, which, in turn, caused sluggish door operation. The softness was attributed to argon gas entrapped while a previously used system was being salvaged from the initial S/N-4 generator. Because the thermal control system would not operate properly, a mechanical linkage with a rotary feedthrough was used to adjust the door position during the vacuum testing. Power output, at lunar night conditions, normalized to design hot and cold junction temperatures of 925° and 350° F, respectively, ranged between 25 and 26 watts at a power input of 620 watts.

Test results indicated that heat lost through the shutter door was 22.8 watts, compared to 80 watts for the original S/N-4 door design. Insufficient heat was dissipated with the door open, primarily because the heater block upper hold-down ring was not coated with high emissivity chromium oxide. A second factor which reduced the effectiveness of the shutter assembly was the deterioration of the gold coatings on the inner surface of the door and the inner cavity heat shields.

Analysis of thermal data from the control system indicated that, if a properly operating thermal control system had been used in the S/N-4 modified generator, the hot junction would have undergone an excursion of approximately 165° F for a change in power input of 270 watts under lunar night conditions, considered to be in excess of that required for a properly operating thermal control system.

5. Investigation of Thermal Control System

Due to the repeated failures of thermal control systems to perform satisfactorily, an extensive investigation of the thermal control system was performed toward the end of 1964. Individual system components were evaluated and the NaK filling procedure reviewed. As a result of this investigation, it was determined that the large adjustment bellows was unsuitable for accurate calibration of the thermal control system, and should be removed before system calibration in a vacuum chamber by means of the small auxiliary adjustment bellows at the lower

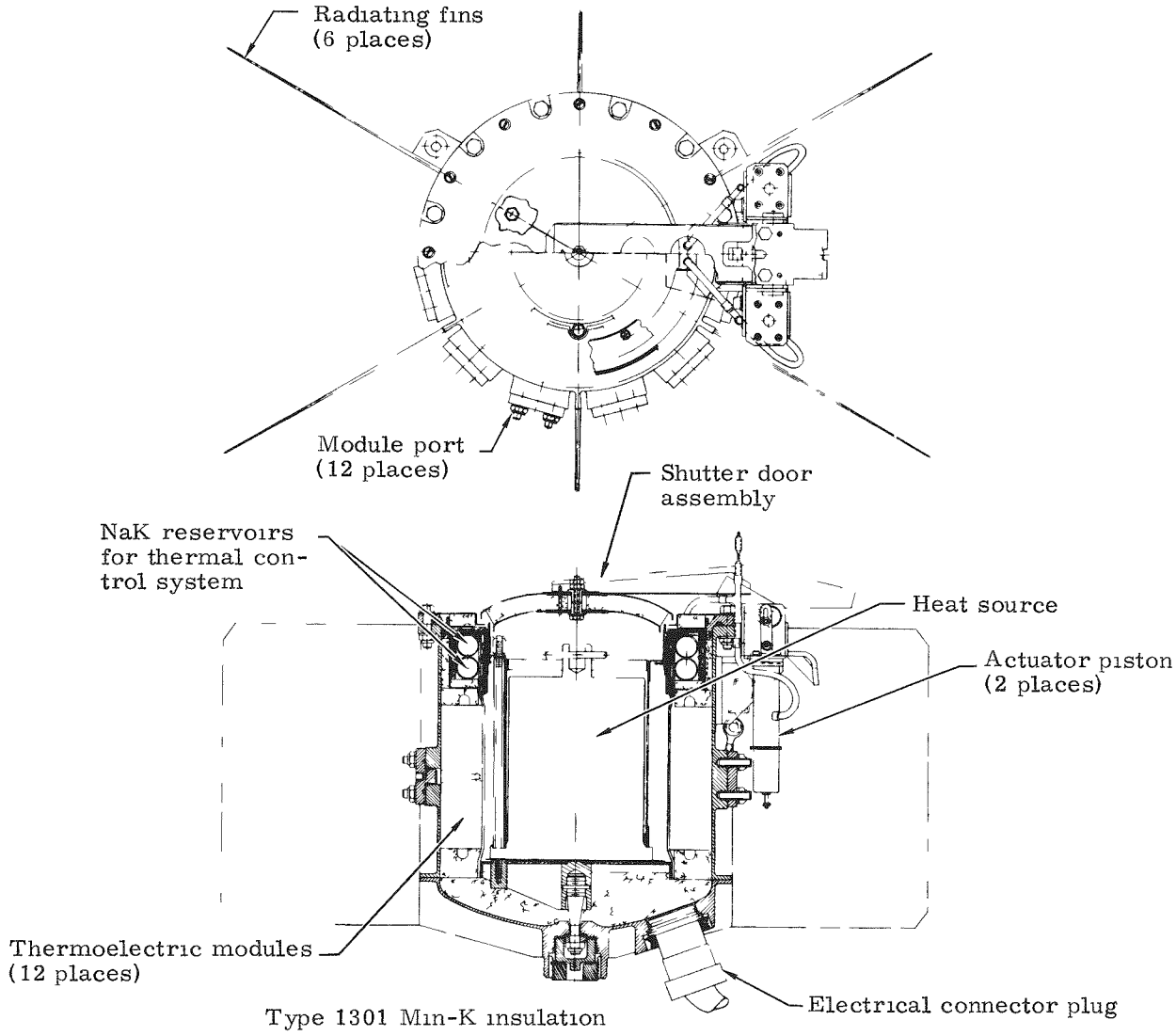

Fig. II-6. SNAP 11 Generator Cross Section

end of each piston assembly. In addition, modifications to the filling procedure were made to minimize the possibility of gas becoming entrapped in the system during NaK filling.

6. Initial Improvement in Thermal Coupling Between Hot Junction and NaK Ring

An effort was made to reduce the hot junction ΔT associated with the NaK ring ΔT required to activate the shutter door. Three tests were performed with a reworked S/N-1 generator in a lunar day vacuum environment.

a. Test No. 1

The S/N-1 generator, with a new thermal control system calibrated and filled according to the experience gained from the study discussed in the previous subsection, was tested. In addition, the inner heat shield and shutter door gold surfaces were plated by the process used on all previous generators (gold plated directly on the stainless steel surfaces, without any intermediate barrier coating).

b. Test No. 2

Test No. 1 was repeated, with an intermediate ceramic layer between the gold and the surface being coated.

c. Test No. 3

Test No. 1 was repeated, with 14 layers of gold-coated, one-mil stainless steel foil installed around the inner periphery of the heat shield.

The results of these tests were:

Test No.	ΔT Hot Junction (°F)	ΔT NaK Ring (°F)	Power Dumped (watts)
1	162	28	320
2	101	32	320
3	64	30	320

It is readily apparent that the ceramic-fired gold coating, which exhibited excellent stability during 1000° F vacuum testing, and the gold-coated foil resulted in improved thermal coupling.

7. Additional Testing of the S/N-4 Modified Generator

a. Performance testing

With the completion of the investigations of thermal coupling discussed in the previous subsection, the S/N-4 modified generator was reworked by installing a new thermal control system and replacing components gold plated by the old process with components gold coated by the newly developed process.

A series of thermal tests was performed on 14 configurations of this reworked generator in an attempt to improve thermal coupling between the hot junction and the NaK reservoir. The initial configuration required a 95° F change in hot junction temperature to open the shutter door 12.5 degrees, whereas the last configuration required approximately 30° F, an improvement in thermal coupling by a factor of three.

During air and vacuum testing of the S/N-4 modified generator at lunar night and day conditions, the ability of the generator to operate at beginning-of-life power inputs at lunar night temperatures was demonstrated. At 950 watts input, the door was open 51 degrees. The average hot junction was 1011° F and the average cold junction was 413° F. The generator was also able to dump beginning-of-life power with the thermal control system adjusted for lunar day and night operation. Final calibration of the thermal control system at the desired operational temperature under lunar night conditions, using vacuum tank mechanical penetrations, proved feasible.

b. Dynamic testing

Upon completion of the thermal coupling investigations and thermal vacuum tests, the S/N-4 modified generator was subjected to dynamic test environments at both flight acceptance and qualification levels. At the completion of flight acceptance level vibration tests, the generator shutter door motion was judged too stiff for repeatable and smooth shutter motion; 38 ounces of force, applied at the center of the shutter door, were needed to open the shutter during this inspection. The door shafts and bushings were lubricated with rose oil as a temporary fix, reducing the force necessary to open the shutter door to 26 ounces. A decision was made to lubricate all future door shafts with Molykote X-15 prior to assembly of the thermal control system.

During qualification level testing, it was demonstrated that the shutter door would remain in calibration at operating temperature with the shutter door in the unlatched position.

c. Design modifications from S/N-4 modified generator testing

Based on the results obtained from this series of tests, the following modifications were incorporated into the thermal control system area of the Q series of generators:

(1) Reflective surfaces of the generator were gold coated, using the gold coating ceramic process previously described.

(2) Gold-coated stainless steel foils were positioned around the inner and outer peripheries of the inner heat shield to minimize the cooling effect of door opening on NaK ring temperature.

(3) A thin asbestos spacer was positioned between the inner heat shield and the inner shell bolt ring to minimize conductive heat transfer between the heat shield and NaK rings.

(4) The NaK rings were brazed to the inner shell to ensure a good thermal path between the inner shell and NaK rings.

(5) A nickel-plated copper conducting ring was brazed to the inner periphery of the shell adjacent to the NaK rings to decrease the thermal resistance between the NaK rings and the adjacent hot junction.

(6) The gold-coated inner heat shield was shortened to allow more heat to be radiated to the NaK rings directly from the fuel block.

Refer to Fig. II-7 for these configuration changes.

Additional design modifications incorporated for the Q series generators include:

(1) The use of a fuel block with a 19/32-inch greater height than the electrically heated block required relocation of the heat baffle on the heat shield.

(2) Silver-soldered intermodule connections were replaced with mechanically crimped joints, using a modified and gold-plated Nicropress sleeve.

(3) The 0.002-inch thick dimpled reflective foil insulation was replaced with an improved gold-coated reflective foil consisting of 0.001-inch gold-coated, stainless steel foil with 0.006-inch dimples evenly spaced over its surface.

Existing Q/N 1

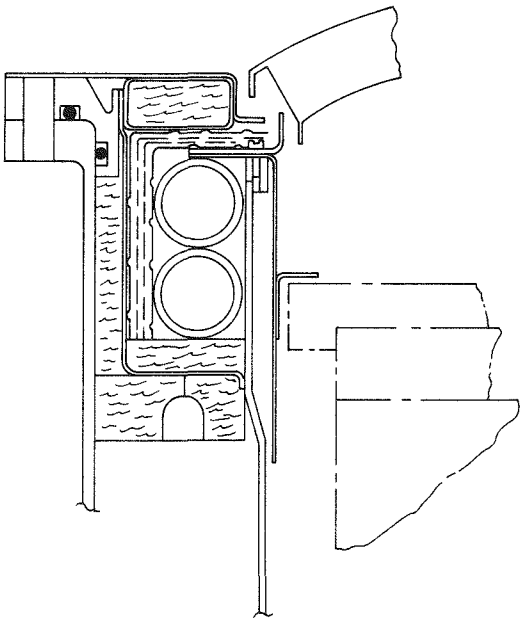

Revised Q/N 1

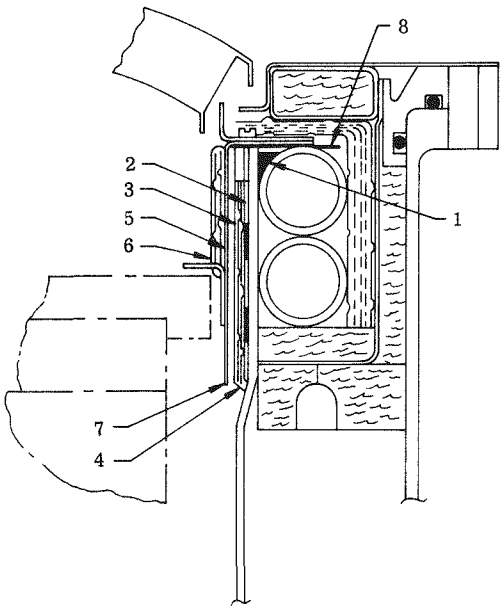

1 NaK tube silver soldered to housing around entire circumference

2 0.062-inch thick x 1.5-inch wide OFHC copper strap added to inside of housing (plug solder at center and flow silver solder at both edges)

3 0.001 SS dimpled foil (fired-gold coated) approximately 5 wraps added between housing and heat shield

4 Holding straps (6) 0.005 x 0.187 wide, tack welded to housing

5 0.001 SS dimpled foil (fired-gold coated) approximately 12 to 14 wraps added on inside of heat shield

6 Holding straps (6) 0.005 x 0.187 wide, tack welded to heat shield

7 Approximately 0.50 inch removed from bottom of heat shield

8 0.050-inch asbestos ring added between NaK tube and heat shield

Fig. II-7. Comparison of Existing Q/N-1 and Revised Q/N-1 Generators

(4) To further reduce hysteresis in shutter door motion, the chrome-plated 17-4PH shutter shaft bushings were replaced with uncoated SAE 660 bronze bushings. The shaft control slotted links were lubricated with Molykote X-15.

(5) Alumina shutter door lid spacer bushings were replaced with titanium to lessen the probability of breaking during dynamic testing.

(6) To remove the contact resistance of the electrical outlet male-female cannon plug, the female end of the electrical connector was removed, the external power leads were soldered to the terminals and the exposed end of the male electrical connector was potted with RTV-501.

Testing of the S/N-4 modified generator showed an increase in internal resistance and resultant decrease in power output. It was suspected that impurities contained within the internal components of the generator may adversely affect the thermoelectrics. Fabrication processes, assembly procedures and components of the Q series generators were modified to reduce internal resistance increases and eliminate potential sources of contamination. The major changes included:

(1) Bakeout of the Min-K insulation in air at 1050° F to remove organic binders and water, in lieu of the 950° F used in the past. This temperature is higher than the operating temperature of the generator. After bakeout in air, the insulation is transferred to a vacuum fixture and reheated to 1050° F, evacuated to 50 microns and backfilled with cold trapped argon at temperature. The insulation, along with other components is subsequently transferred to an inert dry box, where generator assembly is performed.*

(2) Aluminum grease, used as a heat transfer medium for conduction of heat between the module cold shoe heat sink and the outer shell, was eliminated.

---

*The Q/N-1 generator thermoelectric module insulation was fabricated earlier in the program, using the 950° F bakeout temperature; then module assembly was performed in air. However, the inner can assembly, with attached modules, was heated to an intermediate temperature and evacuated prior to dry box final assembly. The Q/N-2 generator was fabricated by outgassing all insulations, including modules prior to the bonding operations. Module bonding and generator final assembly used inert gas-dry box procedures.

(3) The cold shoe piston springs were replaced to increase the element contact pressure from 70 psi to 150 psi.

8. Testing of the Q/N-1 Generator

The Q/N-1 generator was dynamically tested successfully at the flight acceptance levels of acceleration and vibration, and at the qualification levels of shock, acceleration and vibration. Initial power output was 24.2 watts, approximately 10% less than that obtained on previous generators during initial checkout. Thermal vacuum testing at lunar conditions showed that the cold junction temperature became excessive during lunar day simulation and that the generator was unable to dump excess thermal input at beginning-of-life conditions (900 watts power input, lunar day). Operating time accumulated on the generator totaled 1942 hours with the low electrical output evident throughout testing; power decrease of 2.89 watts was observed during the total test time.

9. Diagnostic Disassembly of Generator Q/N-1

Operation of the Q/N-1 generator demonstrated that the electrical performance was poorer than that obtained from the S/N-4 modified generator (see Section 6 of this chapter). The initial power output was less than for the S/N-4 generator, and the power degradation rate and rate of increase in internal resistance were higher. Performance testing of the Q/N-1 generator was terminated on September 29, 1965 for diagnostic disassembly.

Prior to disassembly, resistance measurements, shown in the table below, were made and the values compared with those taken just after generator assembly. (Also included are the S/N-4 generator values for comparison.)

Resistance Measurements
(room temperature)

	After Assembly		At Disassembly	
	Q/N-1	S/N-4	Q/N-1	S/N-4
Circuit internal resistance (ohms)	0.061	0.058	0.103	0.104
Circuit-to-generator housing resistance (megohms)	4.5	0.020	2.5	0.001

On disassembly, the major cause of increase in generator internal resistance was found to be due to degradation of the 2P-leg hot junction bonds and deterioration of the cold strap-to-cold cap bonds caused by

overheating of the cold junction during testing. No significant change in th the N-leg room temperature properties was noted.

10. Q/N-2 Testing

Initial tests on the Q/N-2 generator under lunar day conditions revealed that extraction of a portion of NaK from the thermal control system was required to allow opening of the shutter door at the design hot junction temperature (~925° F). After removal of the NaK and calibration of the system in the vacuum chamber, tests demonstrated that the shutter door opened at a hot junction temperature of ~925° F as desired. However, the generator was capable of operating with only a 775-watt power input under lunar day conditions, due to insufficient heat dump capability, without exceeding an average hot junction temperature of 1000° F. Power output at the door "just closing" point, lunar night conditions, was 24.3 watts with a 600-watt input.

After thermal vacuum testing under lunar day and lunar night conditions, the Q/N-2 generator was subjected to flight acceptance dynamic tests. No mechanical failures were observed and no indication of functional degradation was observed during testing. The longer fins installed on this generator had the effect of lowering the natural frequencies and increasing the resonant response.

A comparison of the Q/N-2 and Q/N-1 air performance data revealed that:

(1) The Q/N-2 generator normalized power was approximately four watts higher than that of the Q/N-1 unit.

(2) The calculated contact resistivity of the Q/N-2 generator was less than that of Q/N-1 generator.

(3) The Seebeck coefficient calculated for the Q/N-2 generator was uniformly higher than that of the Q/N-1 unit.

To gain an optimum distribution of hot junction temperature and an increase in heater block operating temperature, a test program involving operation of the Q/N-2 generator with oxidized dimpled nickel foil applied to the heater block was begun. Various radiation foil configurations were tested in conjunction with a carbon steel heater block, and at the maximum power input capability without exceeding a hot junction temperature of 1000° F. Additional tests with a nonsealed graphite heater block replacing the carbon steel block resulted in 925 watts input, with an average hot junction of 1001° F and a hot junction axial gradient of 14° F. This test series with the nonsealed graphite heater block showed that there were definite advantages in operating with a heater block thermally similar to a fuel block.

Load voltage, power output and door position versus current curves were obtained for the Q/N-2 generator with a power input of 700 watts under lunar day conditions for different external resistive loads. These data are presented in Fig. II-8. The curves demonstrate that the shutter door will adjust as the generator external load is varied.

A new heater block, shown in Fig. II-9, was fabricated of graphite and clad with 0.020 inch of oxidized Haynes-25 to improve its ability to radiate heat. It was designed to provide a more accurate simulation of the fuel block. Tests were performed to determine the foil configuration in combination with this heater block which would reject sufficiently decay heat through the shutter door opening while maintaining a limit of 1000° F on the average hot junction temperature. Secondary objectives were to determine the NaK ring temperature at which the door opened and to estimate the parasitic heat losses for the Q/N-2 generator. The location of foils used around the heater block in this test series is shown in Fig. II-10. Results indicated that the graphite-Haynes heater block with foils only at the lower face of the heater block provided a significant reduction in the axial hot junction temperature gradient and permitted operation at the maximum power input (under lunar day conditions) anticipated for the ORNL demonstration test.

Based on the test results, the decision was made to use no side foils on the subsequent generators. The maximum isotope fuel loading (925 watts at encapsulation) for the demonstration test will have decayed to approximately 813 watts at the time of insertion into the generator. Although it was demonstrated that the generator could operate at higher power inputs by adding foils around the heater block, this resulted in increased parasitic heat losses.

11. Q/N-1M, Q/N-3 and Q/N-4 Generators

For a detailed discussion of these generators, refer to Chapter III. Emphasis is placed on these generators, since they are considered to be the SNAP 11 final design and are the evolution of the component testing and material selections which have been discussed in this section.

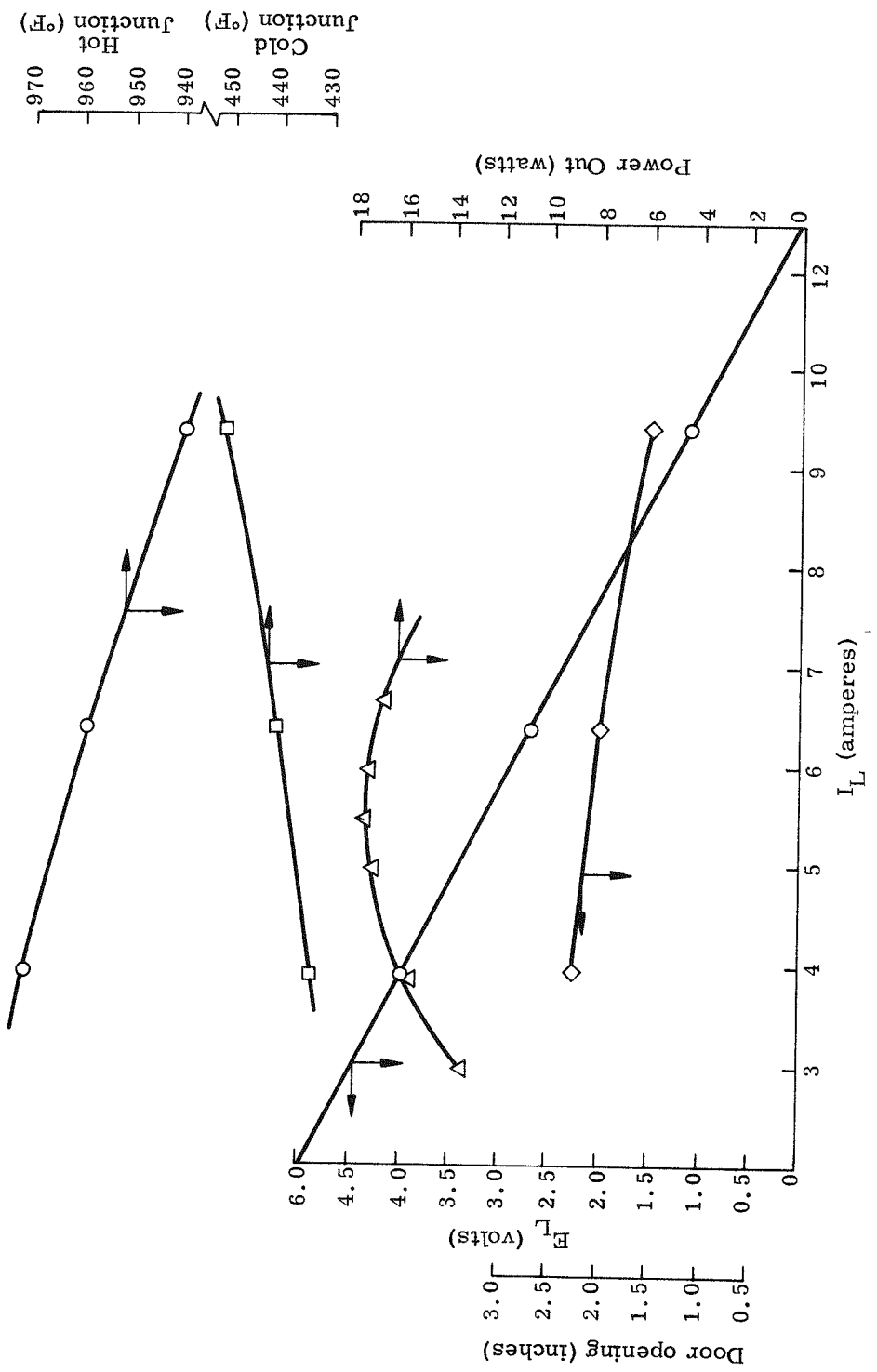

Fig. II-8. Q/N-2 Electrical Performance Lunar Day-Constant Power Input

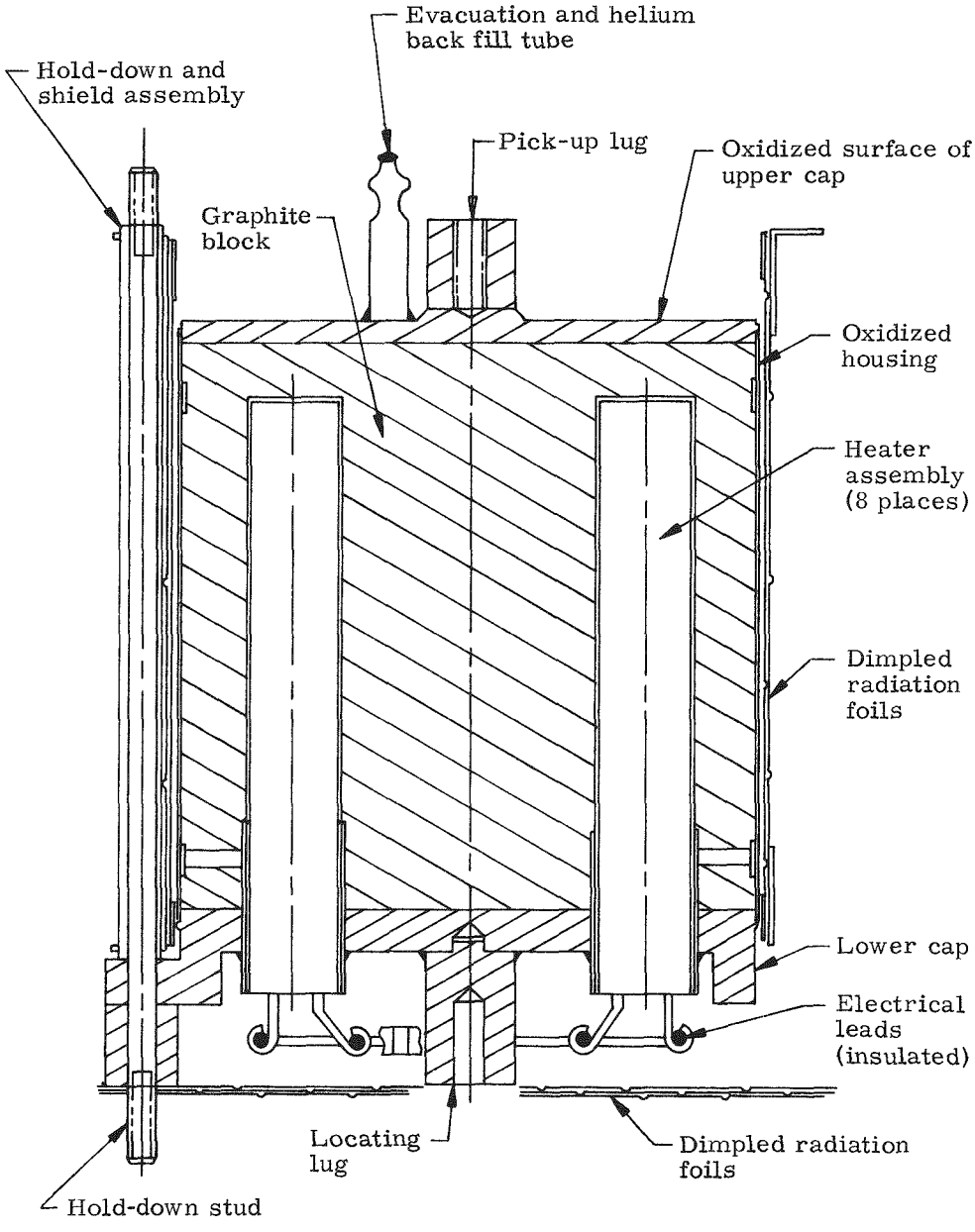

Fig. II-9. Heater Block Assembly

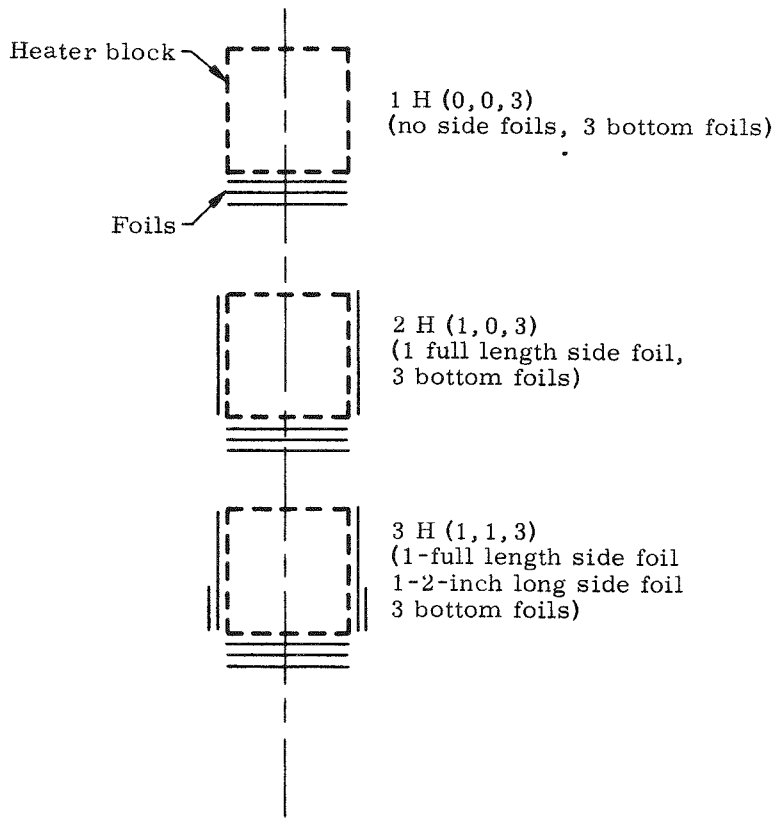

Fig. II-10. Q/N-2 Foil Configurations (Haynes clad graphite heater block)

III. SECOND GENERATION GENERATORS

The Q/N-1 modified, Q/N-3 and Q/N-4 units are considered to be a second generation of SNAP 11 generators due primarily to the fact that 3P thermoelectric elements are incorporated in place of the 2P-type used in previous units; the 2N elements were retained. With the exception of the redesigned heater block, these generators are similar in configuration to the Q/N-1 and Q/N-2 generators. The following is a list of the principal design changes made in the second generation units and the reason for each change:

(1) The nickel-plated copper ring on the inner can was replaced with a silver ring furnace brazed onto the inner can assembly. The nickel plating used previously did not provide adequate oxidation protection for the copper ring when operated for long periods in air, as evidenced during the Q/N-1 generator disassembly. The function of the ring is to assure adequate heat distribution around the circumference of the thermal control system NaK rings.

(2) A 0.020-inch thick, gold-coated ring was incorporated on the inner circumference of the inner heat shield radiation foils to provide additional support during vibration testing and protection from damage during heater block (or fuel block) removal or installation.

(3) Nuclear process and engineering specifications required for couple and module production and generator outgassing were revised.

(4) An improved process was instituted for lapping the hardcoat interface between the alignment buttons and thermoelement hold-down pistons to assure adequate contact area for heat transfer.

(5) A new heater block was designed to more closely simulate the configuration and thermal interfaces of a fuel block.

(6) The 3P thermoelectric elements were used in the P leg of the thermocouple assembly. Based on the module test program discussed in Chapter VI, the 3P material exhibited performance stability superior to the 2P material at the maximum anticipated hot junction operating temperatures (~1000° F) without apparent sacrifice in output performance for long term operation.

(7) An increase in external fin length from 4.85 to 8.00 inches was required to compensate for the increase in temperature drop through the cold end hardware caused by removal of the

aluminum grease. This need became apparent after initial vacuum testing of the Q/N-1 unit; the fin length increase was first incorporated on the Q/N-2 generator.

(8) The 100% tin solder used in joining the gold-plated copper terminal straps to the thermocouples at the cold end was replaced with a 90% Pb-10% indium alloy to permit higher cold junction operating temperatures during lunar day periods.

A. Q/N-1 MODIFIED GENERATOR

1. Fabrication

The Q/N-1M generator designation is derived from the fact that the outer shell and shutter door parts from the Q/N-1 generator were salvaged for use in its assembly. The remainder of the components were new. Since the Q/N-1M was the first generator of the SNAP 11 series using 3P thermoelectric elements, development of a couple fabrication process was performed and a revised process for module assembly was developed for bonding with the 90% Pb-10% indium alloy. Figure III-1 illustrates assembly of the T/E conversion system components from couple bonding to the module assembly.

Generator assembly was performed in a dry box under an argon atmosphere. Although this operation encumbers generator assembly, the elimination of air exposure minimizes generator contaminants and is an asset in the final generator outgassing. Figure III-2 shows the inner can with modules attached. The subassembly is shown in the dry box prior to installation of the outer housing.

After completion of the generator assembly and before initiating outgassing, the thermoelectric circuit room temperature resistance of the Q/N-1M generator was measured to be 0.084 ohm.

A controlled outgassing of the generator assures maximum removal of volatile contaminants in a manner which minimizes adverse effects on the thermoelectric components. The generator heatup rate is controlled to minimize the effect of differential thermal expansion and thermal shock on the generator components. Figure III-3 shows the generator outgassing station. The generator is shown out of its outgassing tank (at left) used to envelop the generator in argon during outgassing, thus minimizing seepage of air into the generator during evacuated periods.

The fabrication techniques outlined above were incorporated in fabricating the Q/N-3 and Q/N-4 generator discussed later in this chapter.

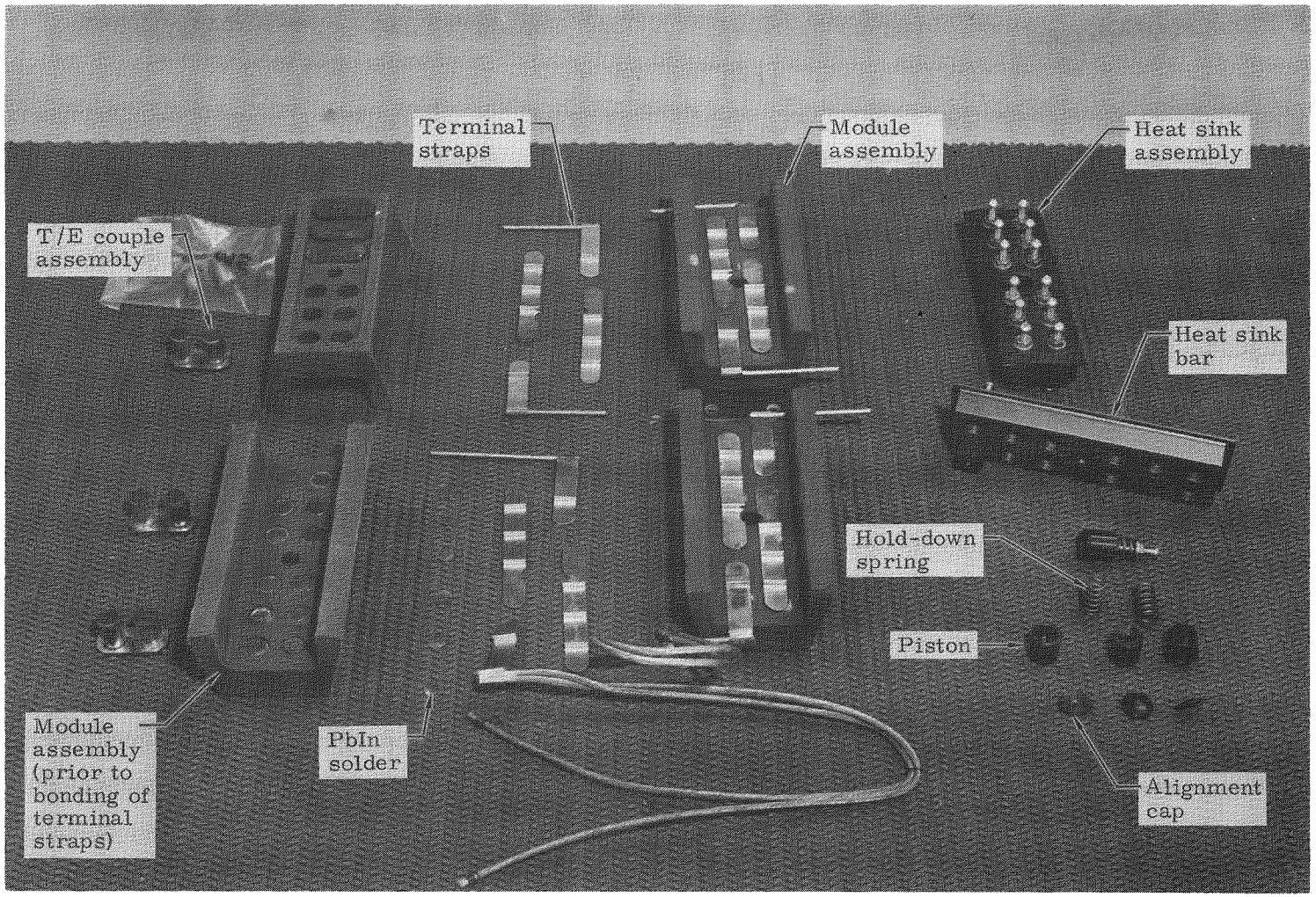

Thermoelectric module assembly

Heat sink hardware

Fig. III-1. Thermoelectric Converter Assembly Sequence

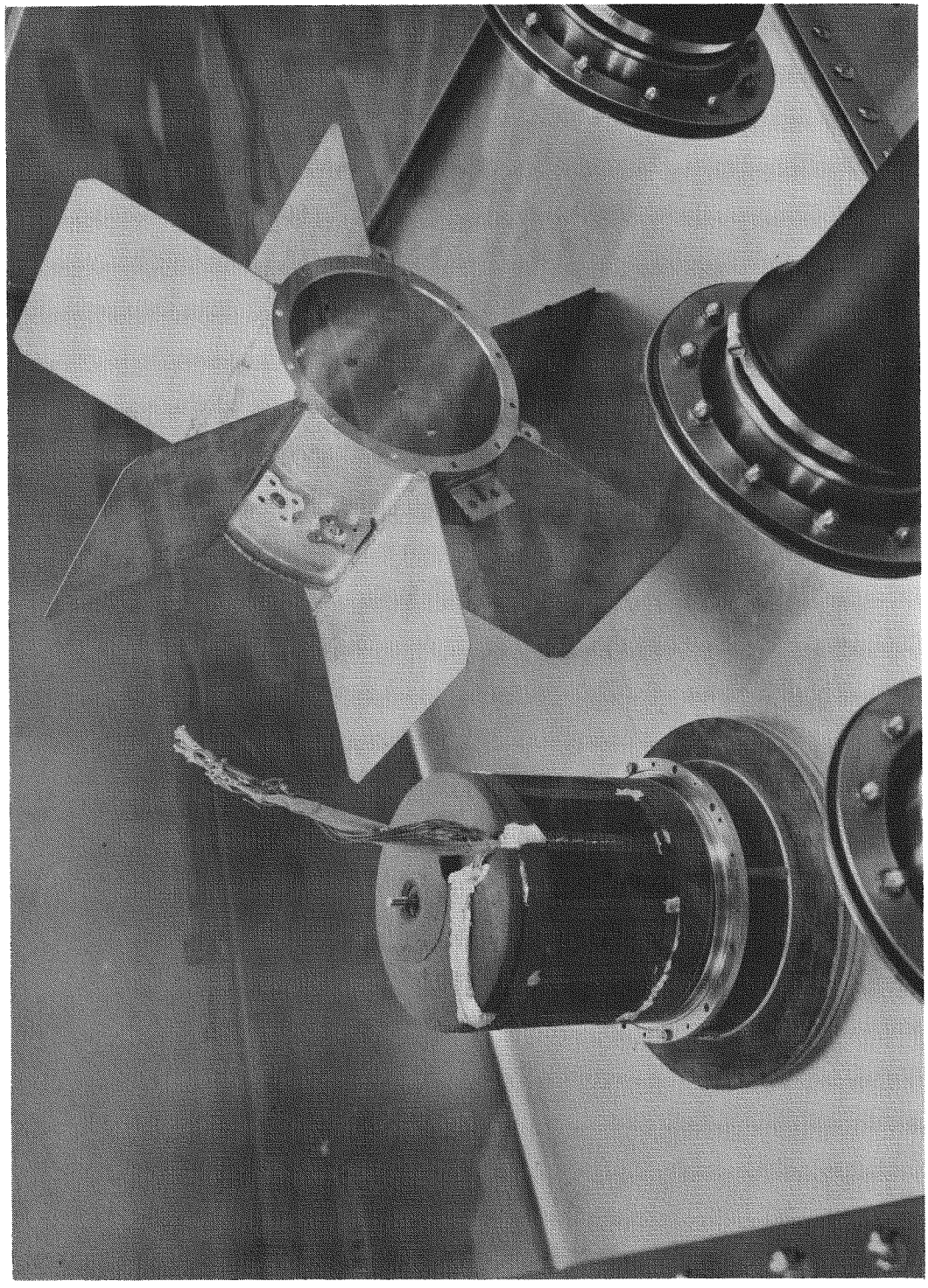

Fig. III-2. Final Dry Box Assembly Operation

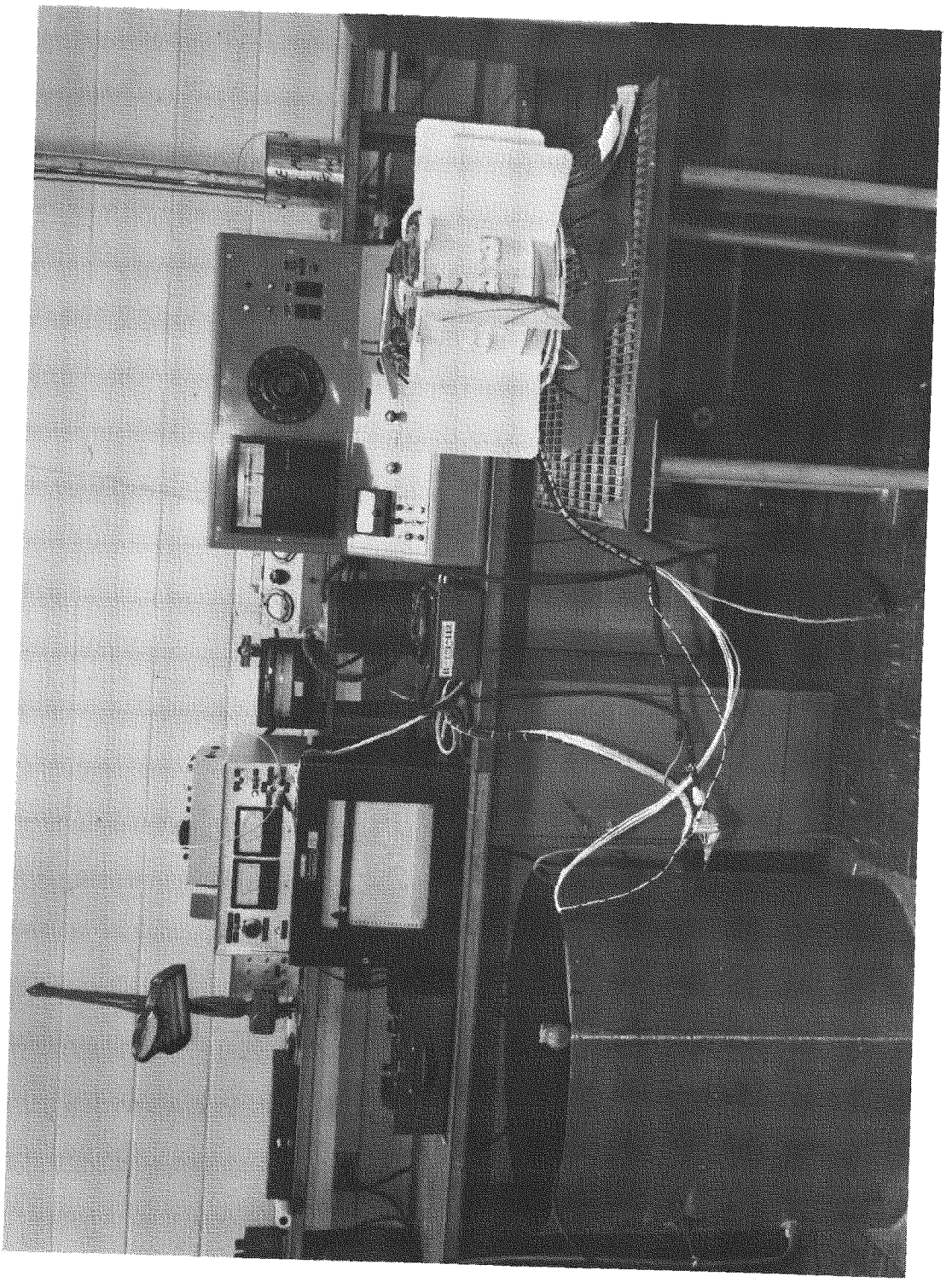

Fig. III-3. Generator Outgassing Station and Generator Installation

2. Generator Testing

The testing discussed in this section was performed to determine the electrical and thermal performance of the Q/N-1M generator, and to assure the integrity of the generator and shipping container under anticipated shipping loads. The vacuum and air testing performed were of particular interest since the Q/N-1M was the first SNAP 11 generator utilizing 2N-3P couples.

(a) Thermal vacuum testing

The principal objectives of the thermal vacuum testing were as follows:

(1) To adjust the thermal control system shutter for closure at the end-of-life power input under lunar night conditions.

(2) To determine the optimum generator load for maximum efficiency at EOL conditions. (The optimum load point thus determined was used for the ORNL demonstration test.)

(3) To determine the thermal and electrical performance characteristics of the generator at simulated lunar day and night conditions.

The environmental chamber used in testing the Q/N-1M generator is shown in Fig. III-4. The chamber, designed and built by Consolidated Vacuum Corporation, measures three feet in diameter by four feet long (inside shroud dimensions). Vacuum capability is in the 10^{-9} torr range; pumping capability is provided by a mechanical pump and 6- and 20-inch diffusion pumps. A 20-inch elbow with chevron baffles, cooled with liquid nitrogen (LN_2), minimizes backstreaming into the chamber. Accessible shroud temperatures range between +250° to -300° F and are automatically controlled. Shroud temperatures between +250° and -250° F are maintained with gaseous nitrogen (GN_2); below -250° F temperatures are attained with LN_2. A six-inch diameter view port allows observation of the generator during operation.

As shown in Fig. III-4, the generator is suspended in the chamber in the horizontal position so the plane of motion for the shutter door is horizontal. This orientation minimizes the effect of gravity on the shutter door operation and thereby closely simulates space conditions.

Figures III-5 and III-6 present the electrical circuitry and instrumentation used for measuring generator output and for supplying power to the electrically heated block. Most generator data, both air and vacuum, were taken with the generator connected to the test instrumentation through the chamber penetrations as shown. Generator volt-

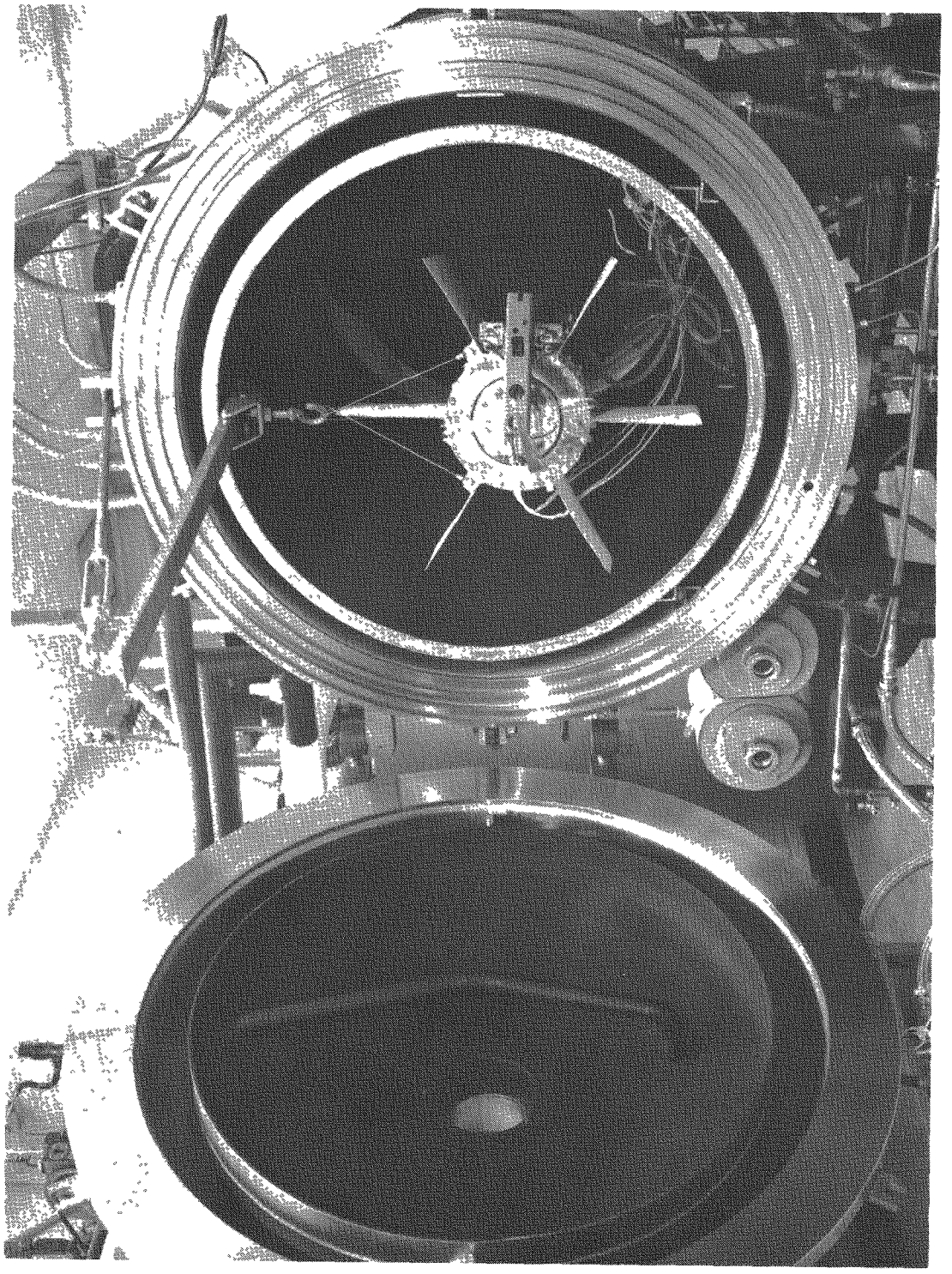

Fig. III-4. Generator Installation in Environmental Chamber

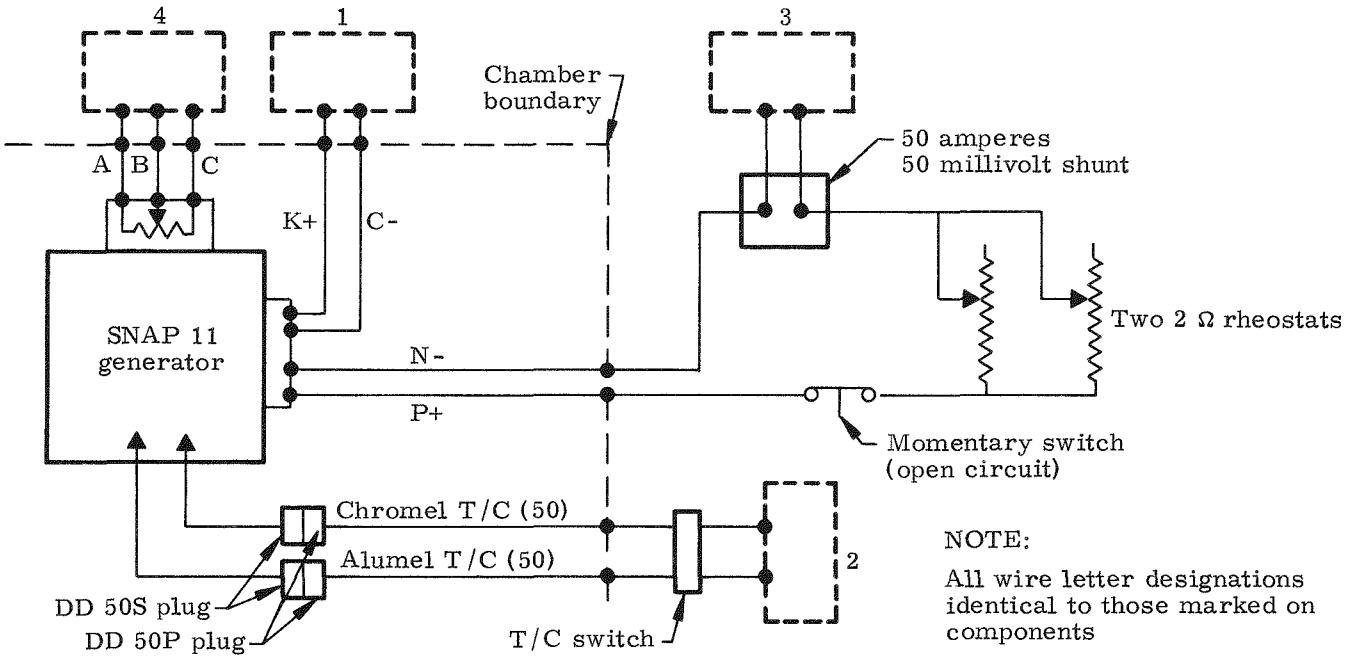

Equipment List

1 D-C digital voltmeter, E-I Model 840MB
2 Rubicon potentiometer, Model 2745
3 Leeds & Northrup potentiometer
4 Wheatstone bridge

Fig. III-5. Test Instrumentation and Circuitry

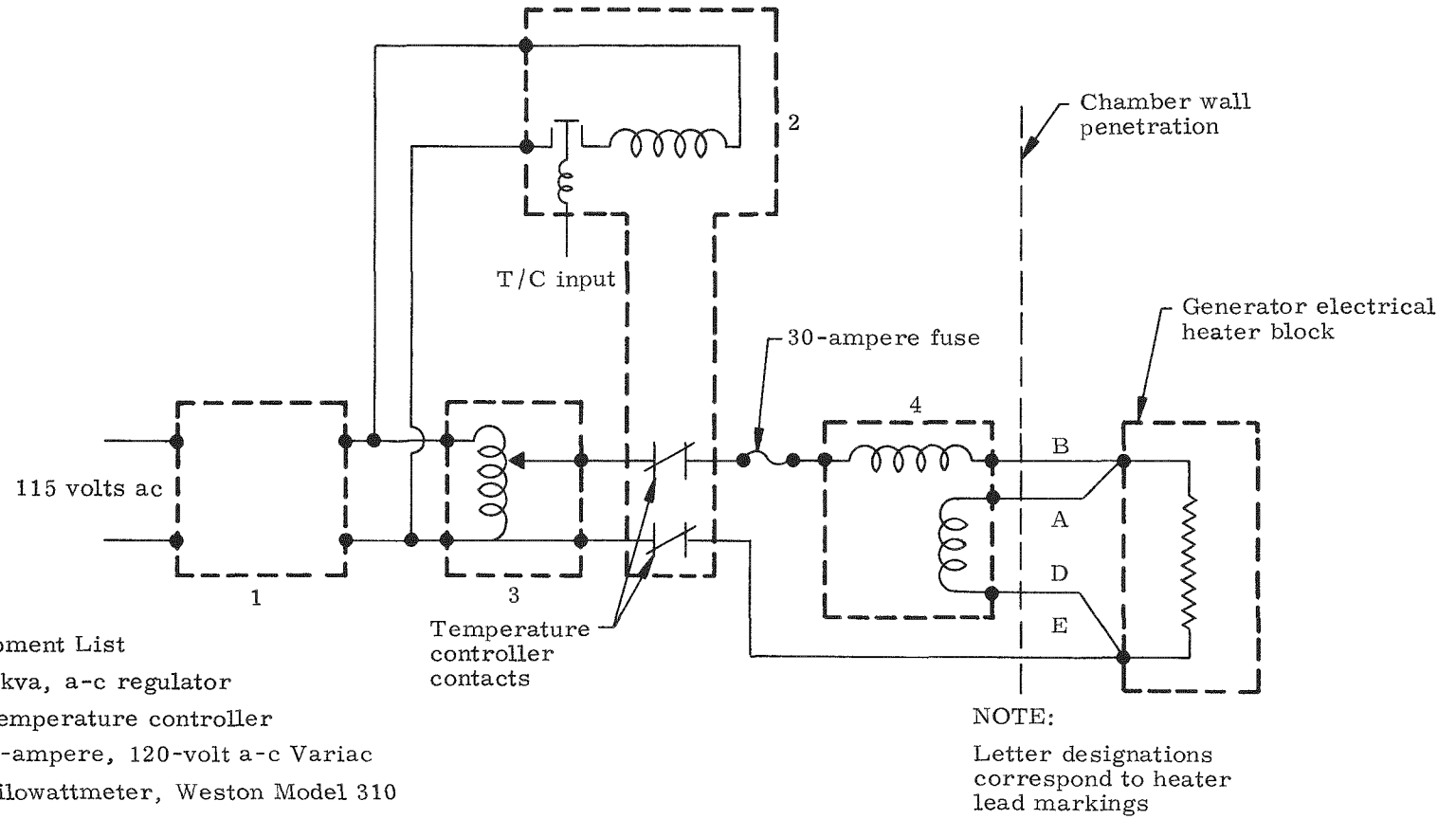

Fig. III-6. Instrumentation for Power Input

age was measured with a digital voltmeter; load current was determined by measuring the voltage drop across a calibrated 50-ampere, 50-millivolt shunt. A momentary-type open circuit switch in the output line allowed determination of the generator instantaneous open circuit voltage. Two, two-ohm rheostats provided the flexibility for varying load resistance over the desired range.

The regulated power input to the electrical heater block was controlled by an a-c Variac with a 20-ampere rating. Power input was determined by a Weston Model 310-kilowatt meter with voltage taps connected near the electrical heater as shown. A temperature controller, activated by a hot junction temperature input, assured generator operation within design limitations during unattended periods. (Alternately, an isolation transformer may be employed at the output of the a-c regulator to preclude interference of the a-c and d-c characteristics to be monitored.

Table III-1 summarizes the testing performed on the Q/N-1M generator. The first run in the vacuum chamber was performed at EOL, lunar night (LN) conditions to check the point at which the door opened. This point was based on the requirement of a minimum power output of 20 watts at EOL with approximately 600 watts(e) power input. After adjustment of the door and with the door in the position where it was just closing, the generator produced 20.36 watts output at an input power of 590 watts. The corresponding temperature of the NaK ring was 975° F. The NaK system on the Q/N-1M unit was filled at 958° F, the value established by thermal vacuum tests on the Q/N-2 generator. The NaK systems on the other generators to be discussed in this chapter (Q/N-3 and Q/N-4) were filled at 975° F on the basis of the Q/N-1M generator test.

TABLE III-1

Summary of Q/N-1M Generator Performance Tests

Run	Environment	Input Power (watts)
1(1)	LN (-235° F, 10^{-5} torr)	930, 810(2), 715, 590(2)
2	LD (+235° F, 10^{-5} torr)	810, 720, 635, 590(2)
3	+100° F, 10^{-5} torr	812, 716, 632, 592
4(3)	LN (-235° F, 10^{-5} torr)	591
5	Air (room temperature)	808

NOTE:

(1) During this run, door was adjusted to open at 975° F (T_{NaK}).

(2) E-I data generated at these power levels.

(3) Run was made to check data obtained at 590 watts in Run 1.

Pertinent data for the point at which the door opened at LN are listed in Table III-2. This table also includes corresponding data for lunar day (LD) conditions. The presence of heater and instrumentation leads through the door opening prevented the door from closing completely at the lunar night condition. As a result, the actual input power at which the door closes must be determined by extrapolating test results. This value is estimated to be between 550 and 570 watts.

TABLE III-2

Q/N-1M Generator Data with Door Open

	Environment	
Parameter	Lunar Night	Lunar Day
P_{in} (watts)	590	590
P_{out} (watts)	20.36	15.17
Door opening (in.)	1/8	1
$T_{NaK\ ring}$ (°F)	975	944
$\overline{T}_{HJ}$ (°F)	919	937
$\overline{T}_{CJ}$ (°F)	365	452
Q_{EL} (watts)(1)	355	312
Q_D (watts)(2)	38	108
Q_P (watts)(3)	175	154

NOTE:

(1) Q_{EL} = estimated heat to elements at $\overline{T}_{HJ}$ and $\overline{T}_{CJ}$.

(2) Q_D = estimated heat dumped through door opening.

(3) Q_P = estimated parasitic heat losses through the generator.

$$P_{in} = Q_{EL} + Q_D + Q_P + P_{out}$$

Performance results for the Q/N-1M generator at LN conditions are illustrated in Fig. III-7. This figure shows how the principal parameters vary with the input power and provides an indication of trends that will occur during normal operation. Maximum and minimum temperatures of the hot and cold junctions were included to illustrate the

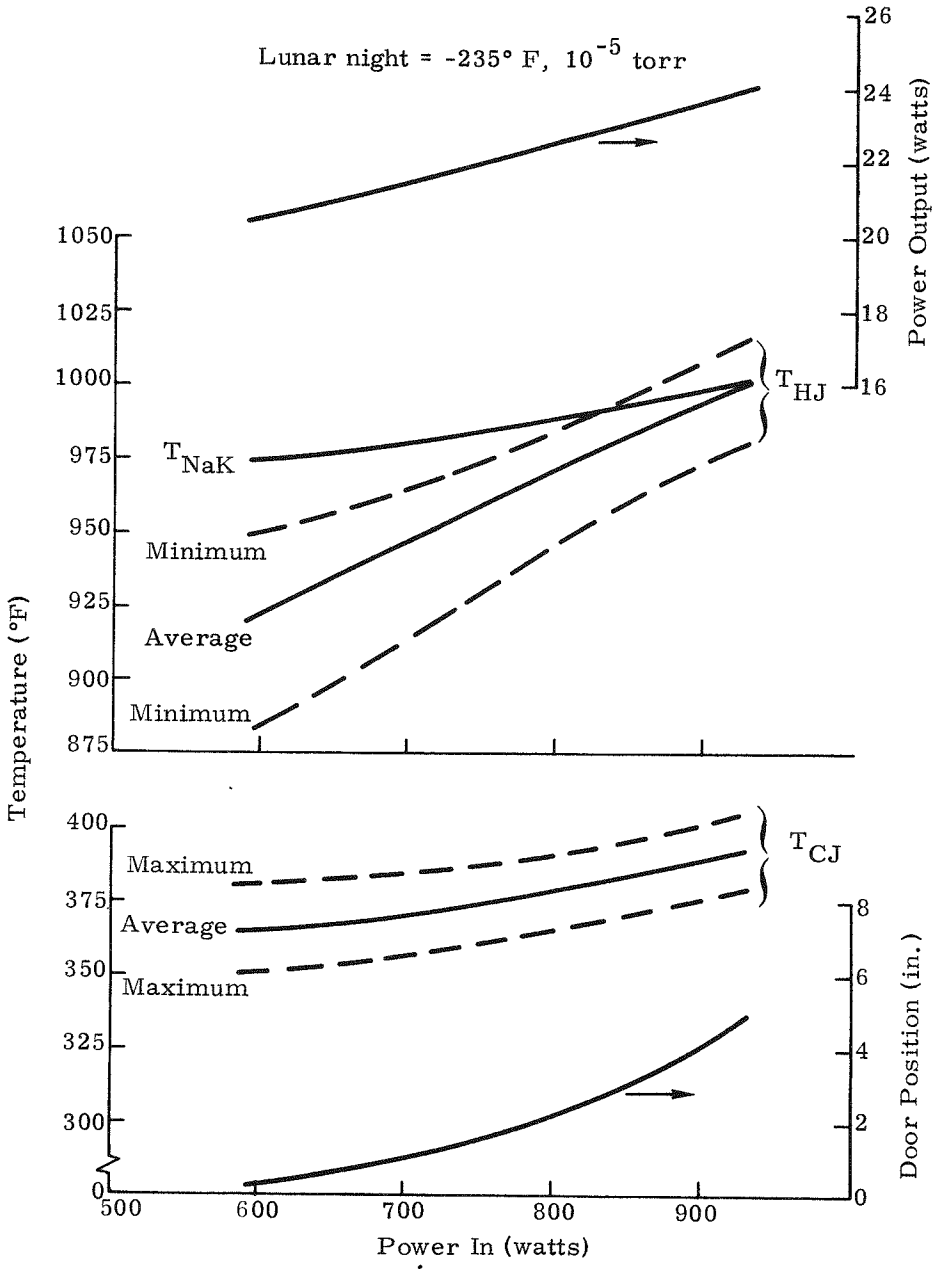

Fig. III-7. Q/N-1M Generator Performance

magnitude of the axial temperature gradient and its dependence on the input power. While operating at LN, the hot junction gradient varied from a maximum of 65° F at 590 watts power input to a minimum of 37° F at 930 watts power input. The input power range was extended to 930 watts in order to determine the maximum power which could be put into the generator under LN conditions. This limit is established as the point at which the average hot junction temperature reaches 1000° F. The cold junction temperature gradient was reasonably constant (25° to 30° F) throughout the range tested.

Figure III-7 also shows the generator output power at LN conditions. This parameter varied from 22.7 watts at the estimated BOL input power (810 watts) to 20.4 watts at the estimated EOL input power (590 watts).* These BOL and EOL values are based on a 90-day mission and a curium-242 fueled generator.

Figures III-8 and III-9 show the lunar night E-I and power curves for BOL and EOL, respectively. Data for the peak power point in each case are listed in Table III-3 which also includes similar data for the E-I and power curves at BOL, LD conditions.

TABLE III-3

Summary of Peak Power Data for the Q/N-1M Generator

Environment	P_{in} (watts)	$P_{out\ (max)}$ (watts)	E_L (volts)	I_L (amp)	$\overline{T}_{HJ}$ (°F)	$\overline{T}_{CJ}$ (°F)
Lunar night	810	22.9	2.83	8.0	975	380
Lunar night	590	20.4	2.50	8.0	921	363
Lunar day	590	15.2	2.40	6.5	937	452

Performance of the Q/N-1M unit at LD as a function of the input power is illustrated in Fig. III-10. The output power of the generator in this environment varied from 17.5 watts at BOL to 15.2 watts at EOL. The average hot junction temperature limit (1000° F) for this environment occurred at an input power of approximately 810 watts. Both hot and cold junction axial temperature gradients are nearly constant throughout the input power range tested. The hot junction gradient (25° to 30° F) is a maximum at the midpoint and a minimum at the ends. The gradient along the cold junction is 15° to 20° F throughout the range tested.

* Equivalent to 550 to 570 isotope watts on a flight generator. The 1/8-inch door opening on electrical prototype generators for instrumentation feedthroughs increases losses at EOL, LN condition.

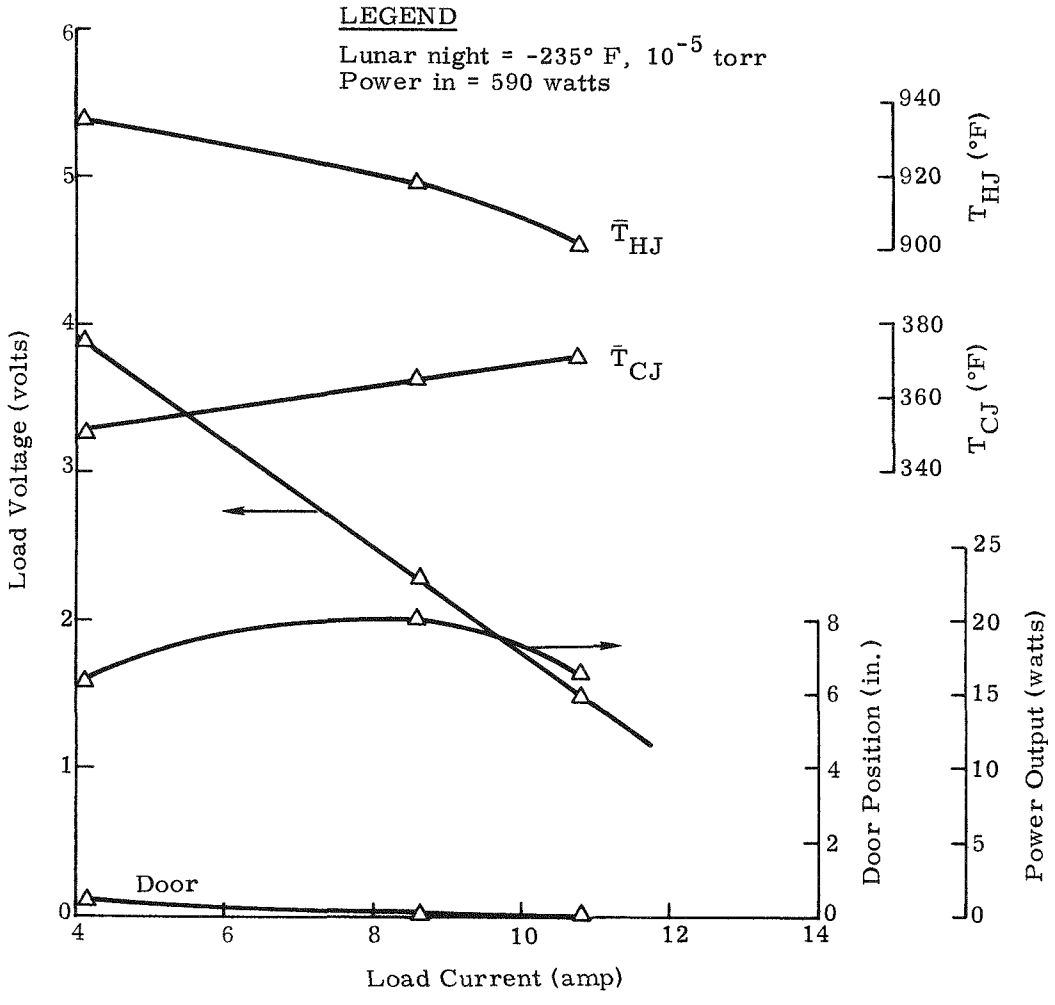

Fig. III-8. Q/N-1M Generator Parametric Performance

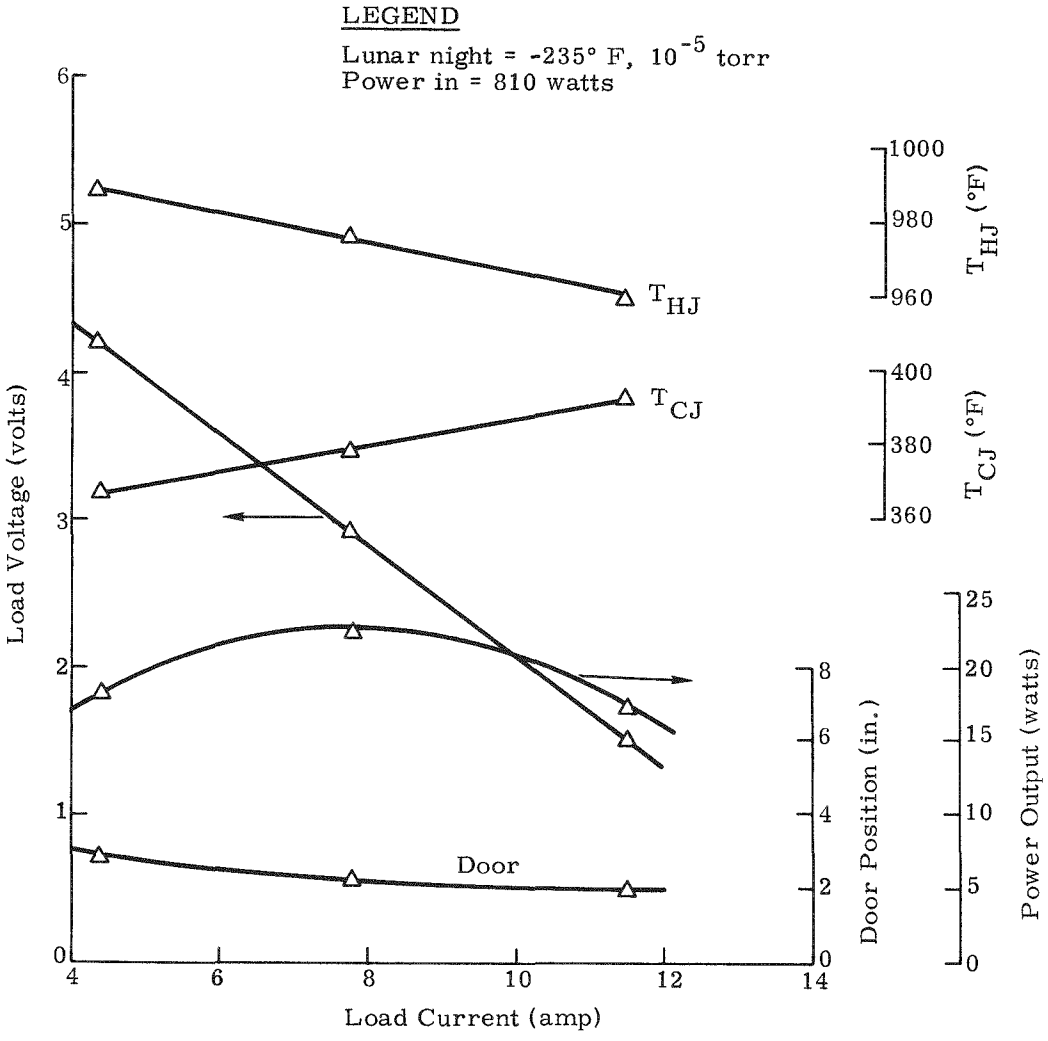

Fig. III-9. Q/N-1M Generator Parametric Performance

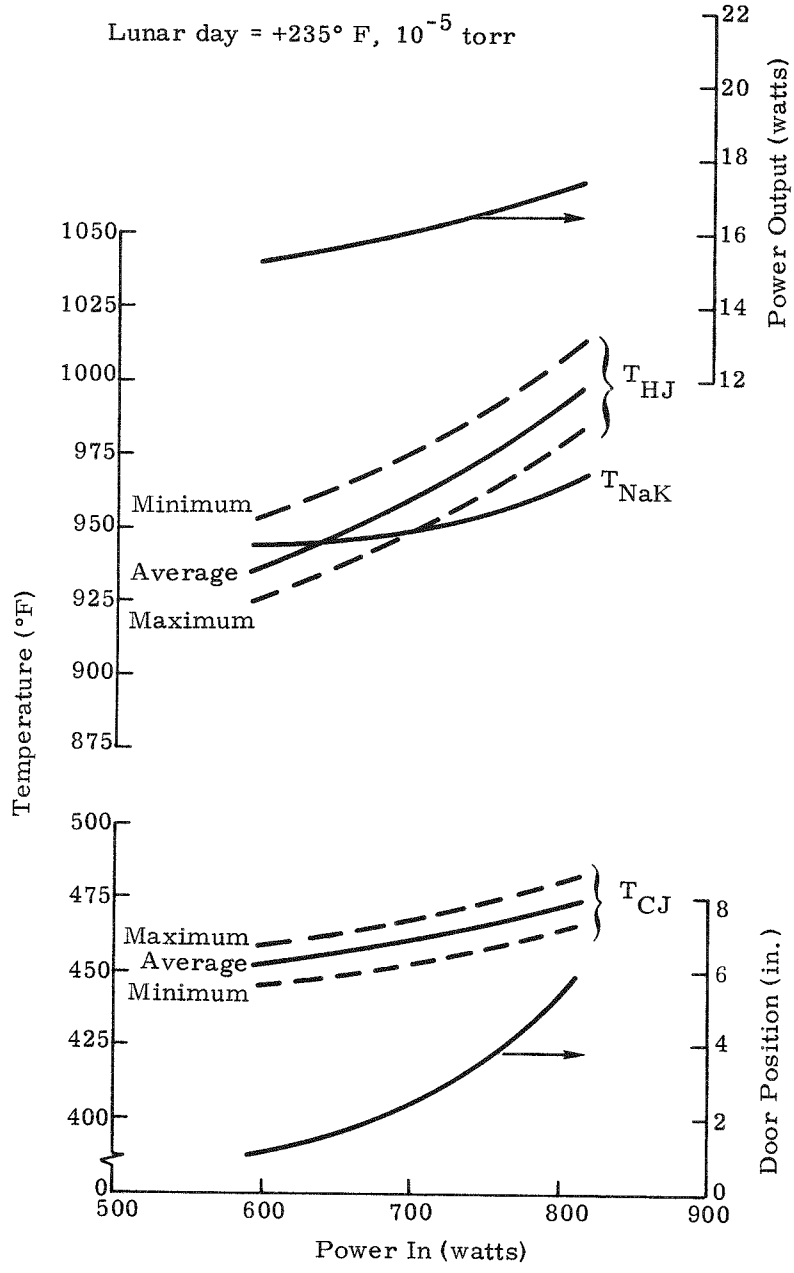

Fig. III-10. Q/N-1M Generator Performance

Figure III-11 presents the E-I and power curves for the Q/N-1M unit at EOL lunar day conditions. Data for the peak power point are included in Table III-3 for comparison with the EOL data at lunar night conditions. This comparison shows a decrease in the peak from 20.4 watts at lunar night to 15.2 watts at lunar day.

Figure III-12 presents a special set of performance data for this generator with the cryowall temperature at +100° F and a vacuum of ~10^{-5} torr. These data were taken in the event that facility failure at ORNL resulted in vacuum testing at an ambient tank wall temperature estimated to be ~100° F. This graph shows that the generator power output will vary from 20.7 watts at BOL to 18.3 watts at the EOL condition. Both hot and cold junction temperature gradients are comparatively constant throughout the range of input power investigated.

b. Air performance

Upon completion of the thermal vacuum tests, the generator was placed vertically in air and performance tested. These tests were run to obtain a set of steady-state data which would serve as a reference for future performance testing of the generator. Input power was set at 810 watts, and a matched load condition was employed ($R_L = R_i$).

Results of Q/N-1M generator performance in air are summarized in Table III-4. The power output was measured at 25.7 watts at hot and cold junction temperatures of 974° and 343° F, respectively. The generator contact resistivity at this time (~300 hours total operating time) was determined to be ~750 $\mu\Omega$-cm^2.

c. Transportation testing

Transportation testing was performed on the Q/N-1M generator to demonstrate that the SNAP 11 shipping container was adequate for protection of the generator against the shock and vibration environments anticipated during transportation.

The shipping container consists of an inner box (wood and Tekwood) and an outer box (plywood). The outer box is eight inches larger in all dimensions than the inner box, and the intervening space is filled with rubberized horsehair. The inner box contains padded supports, into which the fins of the generator are placed. The padding on these supports was originally a paper composition material, but the fins of the generator gradually wore through this material during the testing. The paper composition padding was subsequently replaced by a felt material, and the transportation tests were successfully completed, thereby qualifying the shipping container and generator for shipment by commercial carrier.

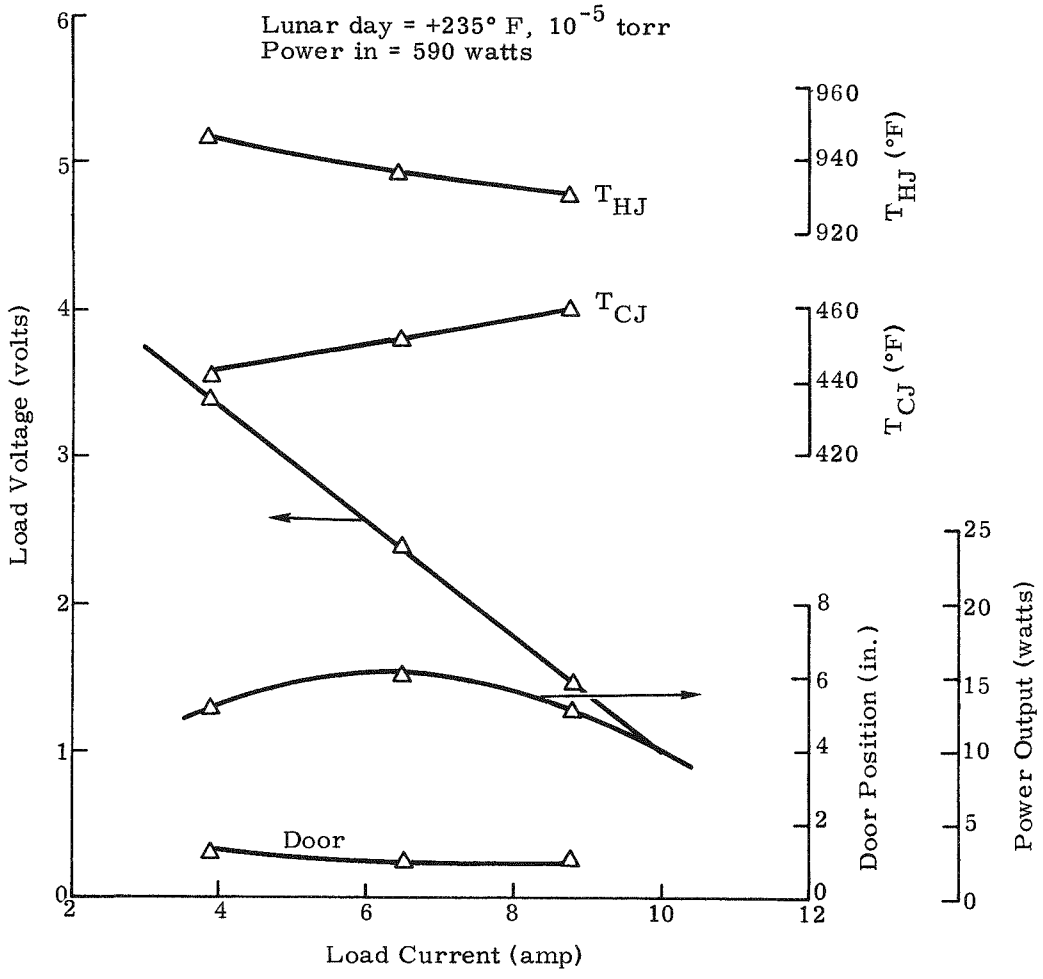

Fig. III-11. Q/N-1M Generator Parametric Performance

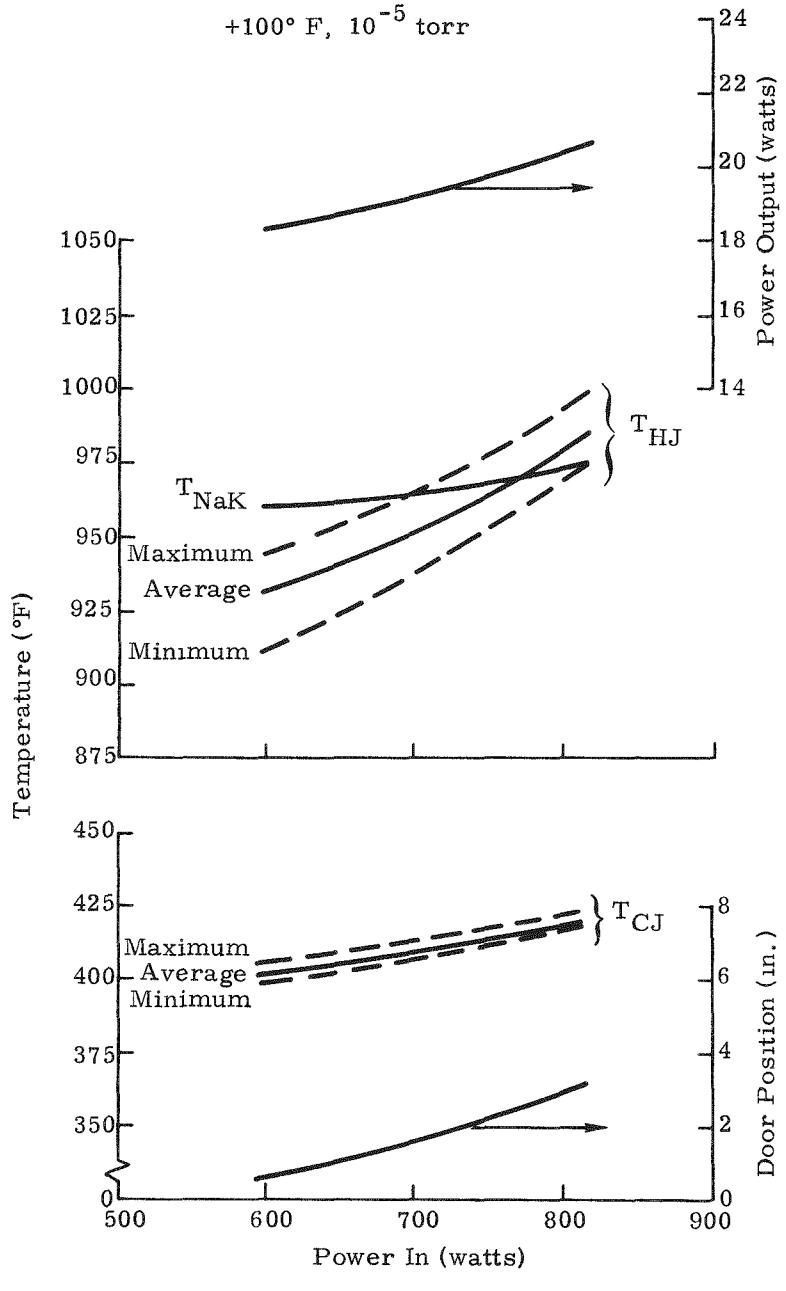

Fig. III-12. Q/N-1M Generator Performance

TABLE III-4

Summary of Q/N-1M Generator Performance in Air

Date	6/1/66
Average junction temperature (° F)	
Hot	974
Cold	343
Resistance (ohms)	
Internal	0.288
Load	0.284
Door position (in.)	Closed (~1/8)
Power (watts)	
In	808
Out	25.65
Open circuit voltage (volts)	5.439
Contact resistivity ($\mu\Omega$-cm^2)	~750
Accumulated operating time (hr)	~300

Shock testing. Each of the four lower edges of the shipping container was raised 12 inches from a concrete floor and allowed to fall freely. Figure III-13 shows the sequence of these 12-inch drops. The entire container was then raised three inches from the floor (with its lower surface parallel to the floor) and allowed to fall freely. Table III-5 lists the pressure, internal resistance and temperature measurements that were taken before and after the shock testing.

Vibration testing. After allowing more than eight hours for the unit to achieve temperature stabilization, a series of vibration tests was run. Figure III-14 shows the equipment setup, with the shipping container positioned for vertical vibration. The container was clamped to a base plate, and the entire assembly was then suspended from a low-frequency overhead suspension system. The system was adjusted to nullify the static load of the container and base plate, and the base plate was then attached to a vibrator.

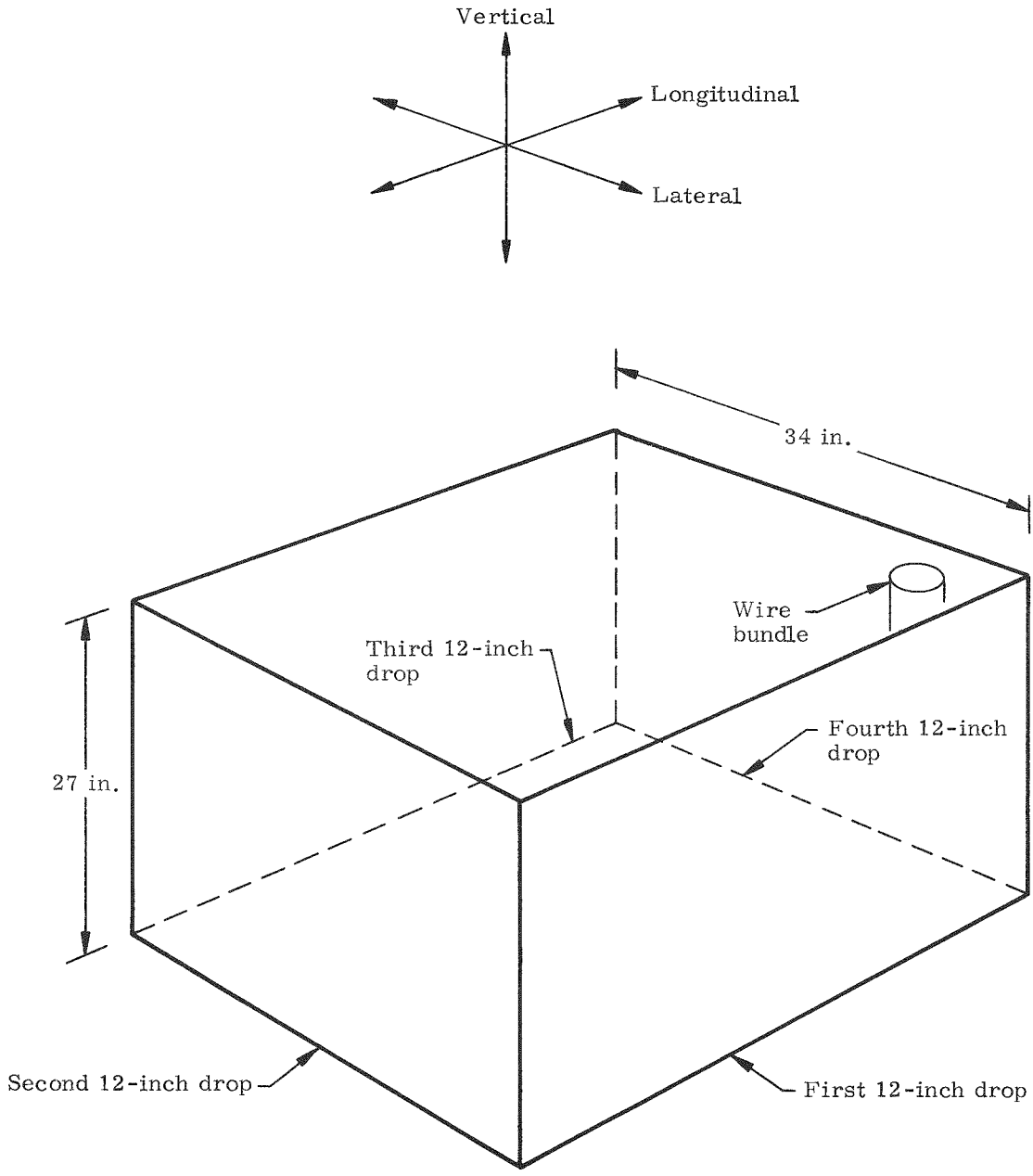

Fig. III-13. Transportation Testing, Axis Designation and Sequence of 12-Inch Drops

Fig. III-14. Equipment Setup for Vertical Vibration Testing

TABLE III-5

Q/N-1M Generator Transportation Testing Data

	Pressure (psia)	Internal Resistance (ohms)	Temperature inside box (°F)
Shock			
Before shock testing	9.57	0.087	73
After shock testing	9.48	0.079	76
Vibration			
Before vibration test	9.51	0.088	72
After first axis, vertical	9.63	0.090	82
After second axis, longitudinal	9.66	0.093	88
After first run of third axis, lateral	9.69	0.091	85
After second run of third axis, lateral	9.54	0.091	82

	Peak Acceleration Responses Noted			
	Frequency (cps)	Input (g)	Output (g)	Magnification Factor*, Q
Vertical	8.5	±1.3	±7	5.38
	190	±5	±5	1.0
	195	±5	±6	1.2
Longitudinal	8	±1.3	±17	13.07
Lateral (Run 1)	8	±1.3	±30	23.07
Generator Repackaged				
Lateral (Run 2)	8	±1.3	±5	3.84

*Magnification factor = Q = output/input

The following vibration spectrum was applied:

cps	
5 to 8	0.4 inch peak-to-peak displacement
8 to 26	±1.3 g
26 to 52	0.036 inch peak-to-peak displacement
52 to 360	±5 g

The frequency range from 5 to 360 to 5 cps was swept at a logarithmic rate, with a complete sweep up and down requiring 13 minutes. Three such sweeps were performed in the vertical axis. The frequencies which produced peak acceleration responses of the system were noted, and the system was vibrated at each of these frequencies for 30 minutes.

During these 30-minute dwell periods, the pressure and internal resistance of the generator were checked every five minutes. (Pressure and internal resistance were checked once each minute during periods of frequency sweeping.) Temperature inside the box was checked at random intervals throughout the vibration tests. Table III-5 lists the pressure, internal resistance and box temperature measurements recorded at the conclusion of each vibration test. Also listed are the frequencies which caused peak acceleration responses in each of the three axes.

The system was then subjected to vibrations in the longitudinal axis. The same frequency spectrum was employed, and the same measurements were recorded.

The system was then subjected to vibrations in the lateral axis. Testing was discontinued at this point when a large increase in the response of the generator was noted. When the container was disassembled, the paper composition material used for padding the supports was found to be worn through. This was replaced by felt material, and the test system was reassembled.

Complete frequency sweeps were then repeated for the lateral axis. The system was also retested for 30-minute periods using vertical vibrations at the resonant frequencies of the vertical axis. With the mofidied container, the magnification factor, Q, in the lateral axis was reduced to 3.84, and the Q in the vertical axis was also low. The modified container and generator were then considered acceptable for shipment.

Upon concluding the tests, the Q/N-1M generator was shipped to ORNL, fueled with a curium-242 heat source and subjected to a 90-day test at simulated lunar conditions. Details of the fueling operation are in Chapter V of this report.

B. Q/N-3 GENERATOR

In this section the results of electrical and dynamic testing performed on the Q/N-3 generator are discussed. Fabrication techniques and test instrumentation were as discussed for the Q/N-1M generator (see Section A). Prior to initiation of generator heatup and outgassing, the room temperature generator internal resistance was measured as 0.077 ohm.

Table III-6 summarizes the electrical testing sequence to be discussed in Subsections 1, 2 and 3.

TABLE III-6

Summary of Air and Vacuum Testing Performed on Q/N-3 Generator

Air tests (ambient room conditions)

Load voltage versus load current (E-I) maps generated at power inputs of 810, 716 and 590 watts ± 5 by varying load resistance.

Vacuum tests

Lunar night: -235° F shroud temperature, 10^{-5} torr maximum pressure

1. Shutter door calibrated with 590 watts ± 15 input
2. E-I map generated for 590 watts ± 5 input
3. Performance determined at power inputs of 590, 634, 716 and 810 watts ± 5
4. E-I map generated with 810 watts ± 5 input
5. Determined maximum allowable power input into generator at lunar night conditions without exceeding a maximum hot junction temperature of 1025° F or a shutter door opening of 7 inches

For all performance points discussed (both lunar night and lunar day), the load resistance used was the optimum resistance (that for maximum efficiency) determined in Item 2.

Lunar day: +235° F shroud temperature, 10^{-5} torr maximum pressure

1. Performance determined at a power input of 810 watts ± 5
2. Determined maximum allowable power input to generator noting limitations in Item 5
3. Performance determined at power inputs of 716, 634 and 590 watts ± 5
4. E-I map generated at power input of 590 watts ± 5

Lunar night: -235° F shroud temperature, 10^{-5} torr maximum pressure.

1. Repeated 590 watts ± 5 power input point

1. Air Performance

To evaluate performance in air, the generator was positioned upright (shutter door up) in a location which permitted free air circulation around the generator. Generator air performance with an 810 watt ± 5 input at a matched-load condition ($R_L = R_i$) is given in Table III-7. Power output was 27.9 watts at average hot and cold junction temperatures of 995° and 349° F, respectively. This matched-load point was used as a reference point for checking performance after subsequent vacuum and dynamic testing to be discussed later in this section.

TABLE III-7

Q/N-3 Generator Air Performance at Matched-Load Condition

Power (watts)	
Input	812
Output	27.9
Average junction temperature (°F)	
Hot	995
Cold	349
Open circuit voltage (volts)	5.58
Load voltage (volts)	2.78
Load current (amp)	10.04
Resistance (ohms)	
Load	0.277
Internal	0.278
Internal pressure (psia)	16.1
Door position	Closed

Air performance E-I maps were generated for power inputs of 810, 716 and 590 watts ± 5. The E-I curves generated are shown in Figs. III-15, III-16 and III-17; peak point performance parameters determined from the curves are summarized in Table III-8.

2. Lunar Night Performance

After completing air parametric testing, the generator was tested at simulated lunar night conditions. The shutter door was calibrated at the end-of-life power input, 590 watts ± 5, and subsequently, an

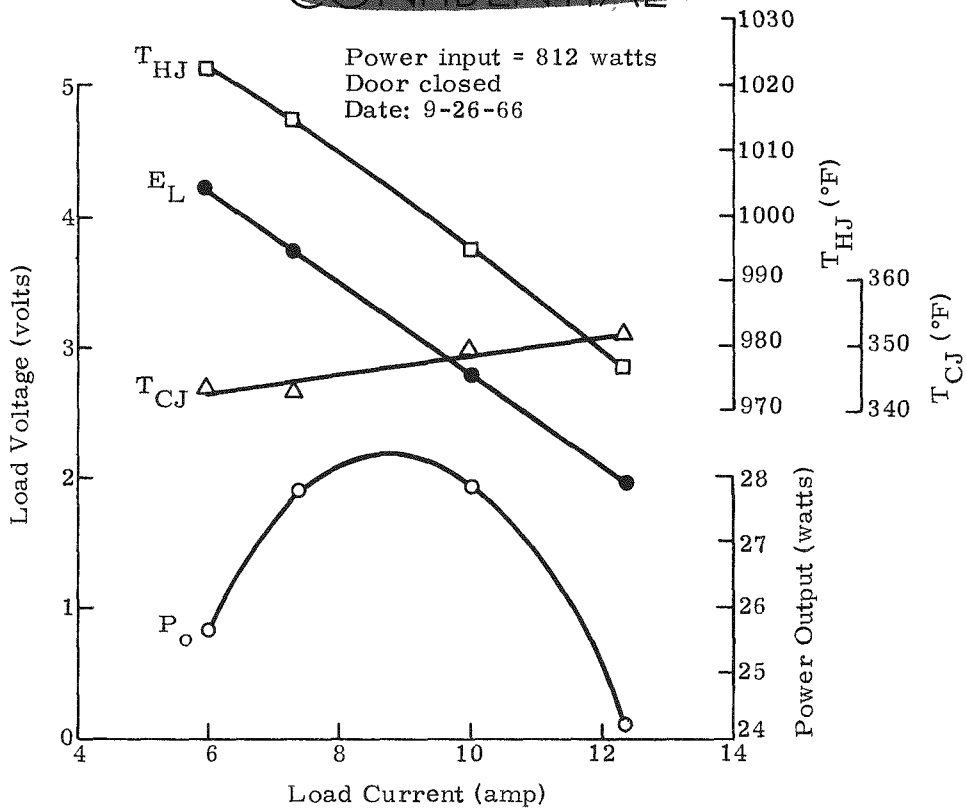

Fig. III-15. Q/N-3 Generator Air Parametric Performance

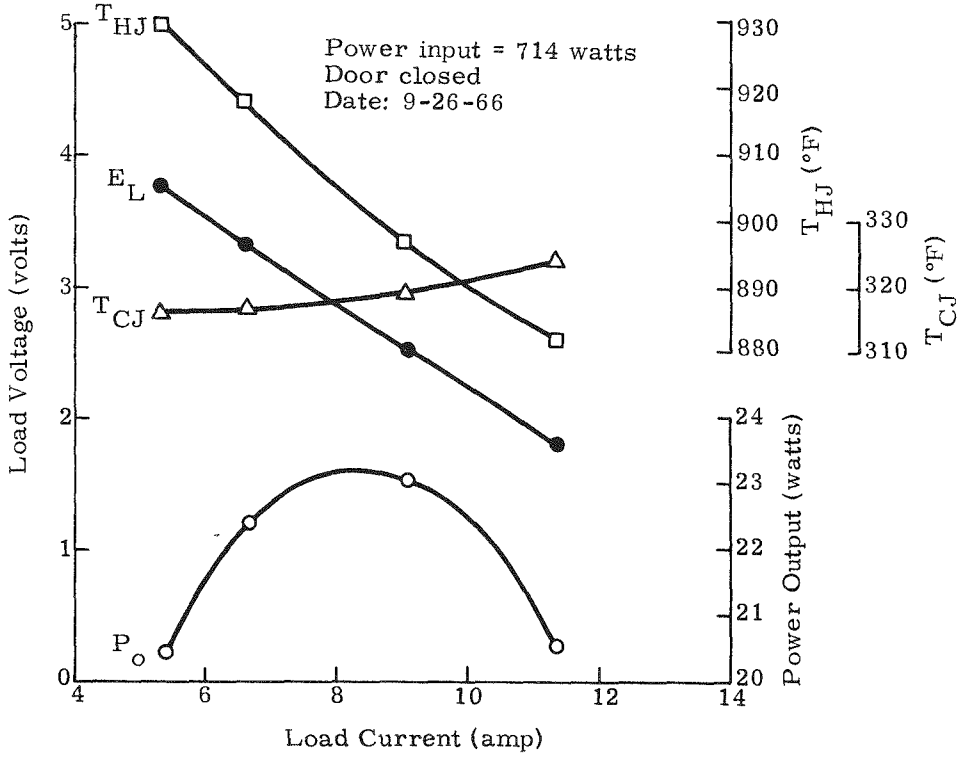

Fig. III-16. Q/N-3 Generator Air Parametric Performance

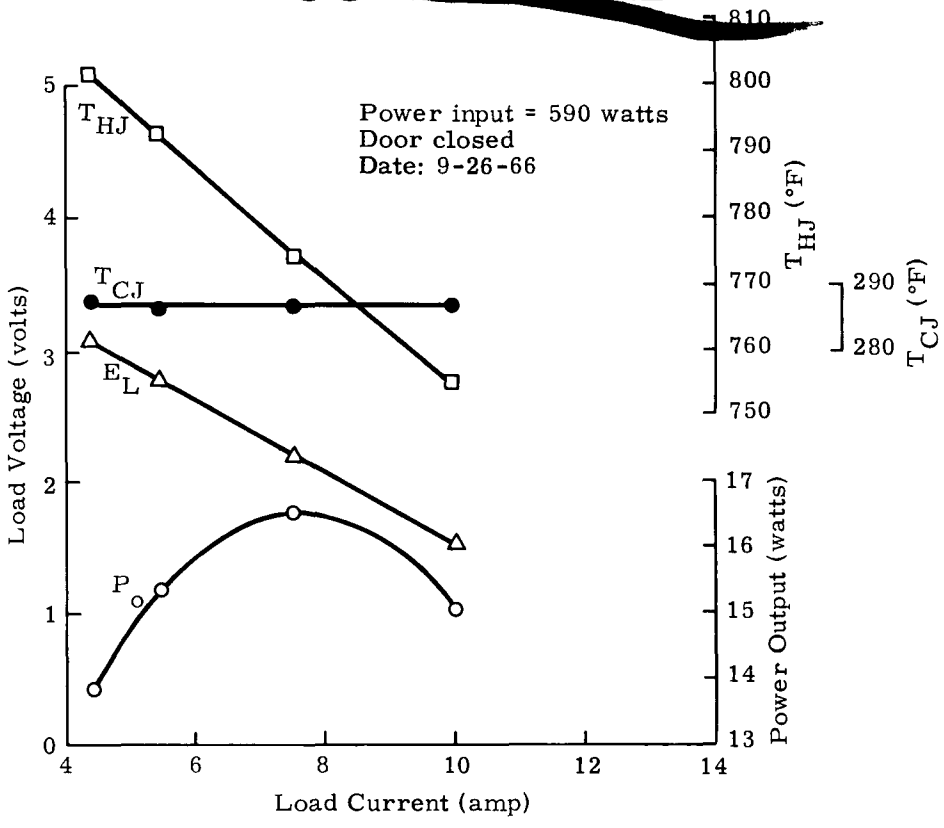

Fig. III-17. Q/N-3 Generator Air Parametric Performance

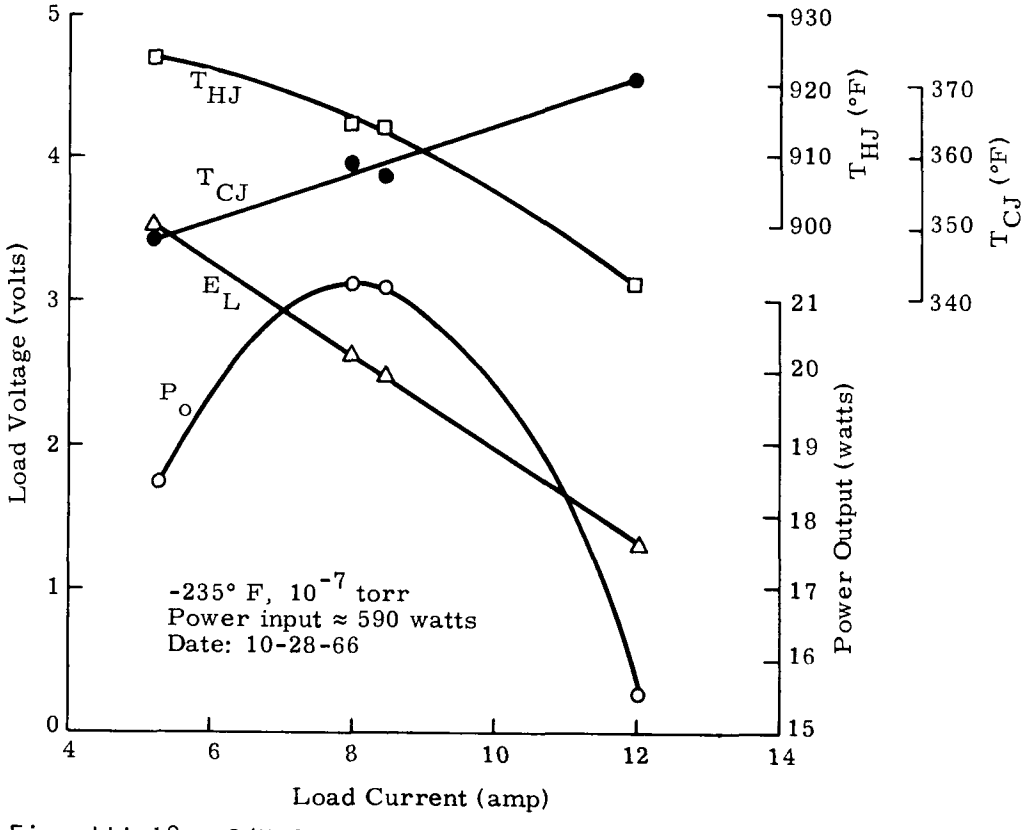

Fig. III-18. Q/N-3 Generator Lunar Night Parametric Performance

TABLE III-8

Summary of Q/N-3 Generator E-I Air Performance Maps

Power input (watts)	812	714	590
Maximum power output (watts)	28.4	23.2	16.5
Average junction temperature (°F)			
Hot	1006	904	775
Cold	347	318	287
Load current (amp)	8.70	8.30	7.52
Load voltage (volts)	3.26	2.81	2.20
Load resistance (ohms)	0.375	0.339	0.293

E-I curve was generated with this power input. Generator performance was then determined at power inputs of 634, 716 and 810 watts ± 5. At the 810 watt ± 5 beginning-of-life power input, an E-I curve was generated. The maximum electrical power which could be put into the generator heater block without exceeding design limitations was then determined. After completion of testing at lunar night conditions, lunar day conditions were established and generator performance determined at electrical power inputs similar to those outlined for lunar night conditions. Table III-6 summarizes the tests performed.

Lunar night test results are shown in Figs. III-18, III-19 and III-20. Figure III-18 presents the E-I map generated with a 590 watt ± 5 power input; EOL maximum power output for the Q/N-3 generator was 21.3 watts; the load resistance for maximum power was 0.33 ohm. Shutter door opening was initiated at a NaK ring temperature of approximately 974° F.

Figure III-19 shows the Q/N-3 generator lunar night performance at power inputs between 590 and 964 watts. The latter was determined to be the maximum allowable power input without exceeding a maximum hot junction temperature of 1025° F. The door opening for this maximum point was 6-1/2 inches. All performance parameters shown in Fig. III-19 were determined with the load resistance which yielded maximum power output at the EOL design condition of ~0.33 ohm. The hot junction temperature gradient ranged from 76° (590 watts) to 30° F (964 watts).

Figure III-20 is an E-I map generated at a power input of 810 watts ± 5. Maximum power output was 23.9 watts.

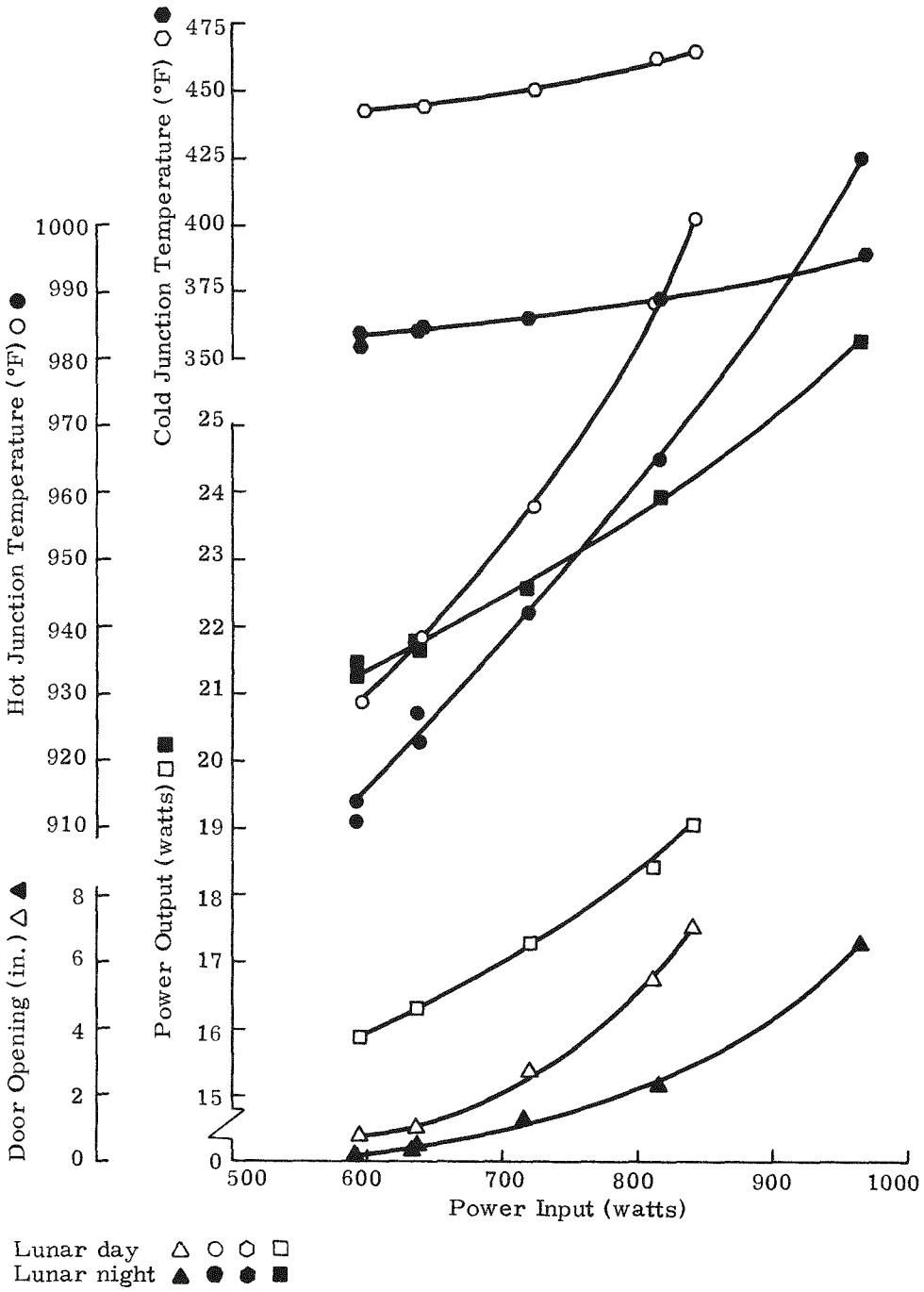

Fig. III-19. Q/N-3 Generator Vacuum Performance

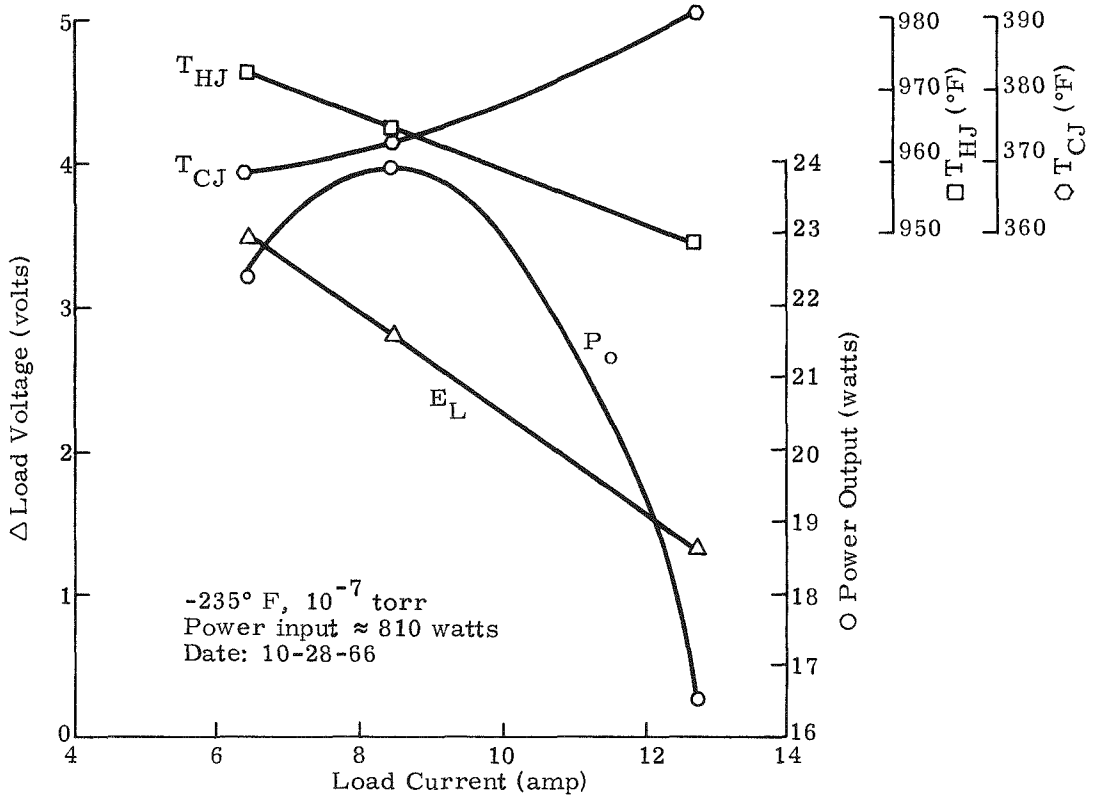

Fig. III-20. Q/N-3 Generator Lunar Night Parametric Performance

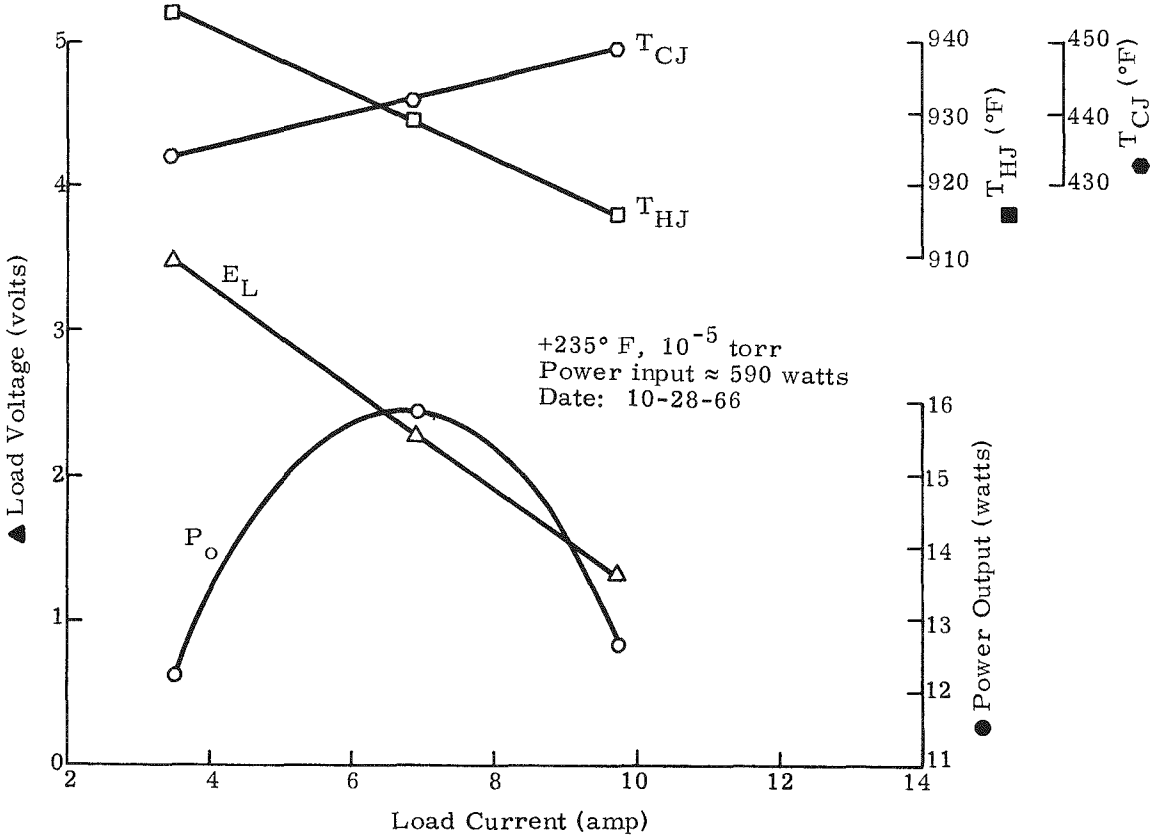

Fig. III-21. Q/N-3 Generator Lunar Day Parametric Performance

3. Lunar Day Performance

After completion of lunar night testing, simulated test conditions were changed to lunar day. Test results are shown in Fig. III-19. The maximum allowable power input at lunar day conditions was determined to be 840 watts, at which point the seven-inch door opening limitation was reached. The hot junction temperature gradient ranged between 24° (590 watts) and 29° F (840 watts). Subsequently, generator performance was determined at power inputs of 810, 716, 634 and 590 watts ± 5 as shown. At the 590-watt point, an E-I map shown in Fig. III-21 was generated; maximum power output was determined to be 15.9 watts.

After completing lunar day testing, the point for maximum power output at EOL (590 watts, lunar night) as determined from Fig. III-18 was rerun. Power output was 21.5 watts comparing closely with the 21.3-watt value previously determined. (This point is included on the E-I map in Fig. III-18.) After removing the generator from the vacuum chamber, an air performance check with an 810 watt ± 5 input and matched external load resulted in a power output of 27.9 watts, comparing identically with the 27.9-watt point obtained during initial air parametric testing.

Table III-9 summarizes the lunar day and lunar night test results.

4. Additional Testing Performed

During the Q/N-3 generator final inspection, a definite discoloration of the gold-coated surfaces inside the heat source cavity and on the lower lid of the shutter door was noted. This occurrence was unexpected since four previous generators with gold surfaces coated by the same process had exhibited excellent stability during both air and vacuum operation. Based on subsequent experimental investigations, it was determined that the discoloration of the gold-coated surfaces was attributable to the presence of an excess amount of halogen-bearing flux used to solder the NaK ring to the inner can.

Accessible gold surfaces inside the heat source cavity and the lower lid of the shutter door were replaced with new components. To determine if any change in generator performance had resulted from replacing these parts, generator operation in both air and vacuum was compared with initial points discussed in the previous subsections. Generator performance in air at matched load with 810-watt input was determined. Subsequent performance points were taken at power inputs of 590, 716 and 810 watts in both simulated lunar night and day environments. As is evident by the retest values, compared in Table III-10, higher power outputs were noted in most cases as a result of the rework performed. The change in power output in air was less than 1%.

TABLE III-9

Summary of Q/N-3 Generator Vacuum Test Results

	Lunar Night (-235° F, 10^{-5} torr)				
Power (watts)					
Input	590 (EOL)	634	716	814 (BOL)	964**
Output	21.3	21.8	22.6	23.9	26.3
Average junction temperature (°F)					
Hot	914	927	942	965	1010
Cold	360	361	365	373	388
Voltage (volts)					
Open circuit	4.75	4.83	4.98	5.17	5.54
Load	2.64	2.69	2.75	2.82	2.94
Load current (amp)	8.06	8.10	8.22	8.50	8.94
Resistance (ohms)					
Load*	0.327	0.332	0.334	0.331	0.329
Internal	0.262	0.264	0.272	0.277	0.291
Door position (in.)	Closed (~1/8)	3/8	1-1/8	2-1/4	6-1/2
	Lunar Day (+235° F, 10^{-5} torr)				
Power (watts)					
Input	594 (EOL)	636	720	810 (BOL)	840**
Output	15.9	16.3	17.3	18.4	19.1
Average junction temperature (°F)					
Hot	929	938	958	988	1001
Cold	442	444	450	462	464
Voltage (volts)					
Open circuit	4.29	4.38	4.55	4.79	4.89
Load	2.29	2.32	2.39	2.46	2.51
Load current (amp)	6.92	7.02	7.23	7.49	7.62
Resistance (ohms)					
Load*	0.331	0.330	0.330	0.328	0.329
Internal	0.289	0.293	0.299	0.311	0.313
Door position (in.)	7/8	1	2-3/4	5-1/2	7

* Load resistance is value for maximum power output at EOL design point.

** Maximum allowable power input determined from imposed generator operating limitations.

CONFIDENTIAL

TABLE III-10

Q/N-3 Generator Performance Comparison After Rework

Air Performance

	Before* Rework	After Rework
Power (watts)		
Input	812	810
Output	27.9	28.1
Average junction temperature (°F)		
Hot	995	999
Cold	349	351
Voltgage (volts)		
Open circuit	5.58	5.59
Load	2.78	2.80
Load current (amp)	10.04	10.06
Load resistance (ohms)	0.277	0.278
Internal pressure (psia)	16.1	15.46
Door position (in.)	Closed	Closed

Vacuum Performance

Power Input (±5 watts)	Initial Power** Output	Retest Power Output	Difference (%)
590 lunar night	21.3	21.5	<1
716 lunar night	22.6	22.9	1.1
810 lunar night	23.9	24.1	<1
590 lunar day	15.9	16.3	2.5
716 lunar day	17.3	17.6	1.7
810 lunar day	18.4	18.9	2.7

* Ref. Table III-7.
** Ref. Table III-9.

5. Dynamic Testing

The SNAP 11 generator is designed to withstand the anticipated launch, flight and landing loads of the Surveyor and its Atlas-Centaur launch vehicle. Dynamic test requirements include vibration, acceleration and shock at a qualification level, and vibration and acceleration at a flight acceptance level. Test requirements for these two levels are presented in Table III-11. Qualification level testing qualifies the final generator design for flight. Due to the severity of the qualification level requirements, actual flight generators would be accepted for flight to the less

TABLE III-11

SNAP 11 Dynamic Test Requirements

QUALIFICATION LEVEL TEST REQUIREMENTS

Acceleration--Steady-state acceleration of 10 g applied for 4 minutes along the thrust axis of the generator (Fig. III-22). This test shall be followed by seven minutes at 5 g along the same generator axis.

Vibration--The generator shall be subjected to the following vibration requirements, applied for the duration and cycles noted, in each of three orthogonal axes.

Sine wave sweeps from:

5 to 26 cps at 0.5 inch double amplitude

26 to 1500 cps at ±18 g

Sweep rate logarithmic from 5 to 1500 cps over 2 minutes. Random gaussian noise of 4.5 g rms, band limited from 100 to 1500 cps, shall be superimposed on the sinusoidal vibration. Combined sinusoidal and random loads repeated 5 more times for a 6-cycle total, except random noise may be reduced to 2.0 g rms for 5 additional cycles.

Shock--Four, 25 g shocks of 5^{+2}_{-0} msec duration applied parallel to the thrust axis of the generator. Wave form of shock shall be half-sine wave.

Test will be repeated at 15 g with shock load applied in 1 direction along each of 2 mutually perpendicular axes at right angles with the direction of the initial shock load.

FLIGHT ACCEPTANCE LEVEL TEST REQUIREMENTS

Acceleration--A steady-state acceleration of 6 g applied for 5 minutes along the thrust axis of the generator (Fig. III-22).

Vibration--The generator shall be subjected to the following vibration requirements, applied for duration and cycles noted, in each of 3 orthogonal axes.

Sine wave sweeps from:

5 to 20 cps at 0.3 inch double amplitude

20 to 150 cps at 6.0 g peak

150 to 1500 cps at 2.0 g peak

Each sweep rate logarithmic from 5 to 1500 cps in a 2-minute period and repeated twice for a total of 6 minutes in each axis.

Shock--(not required)

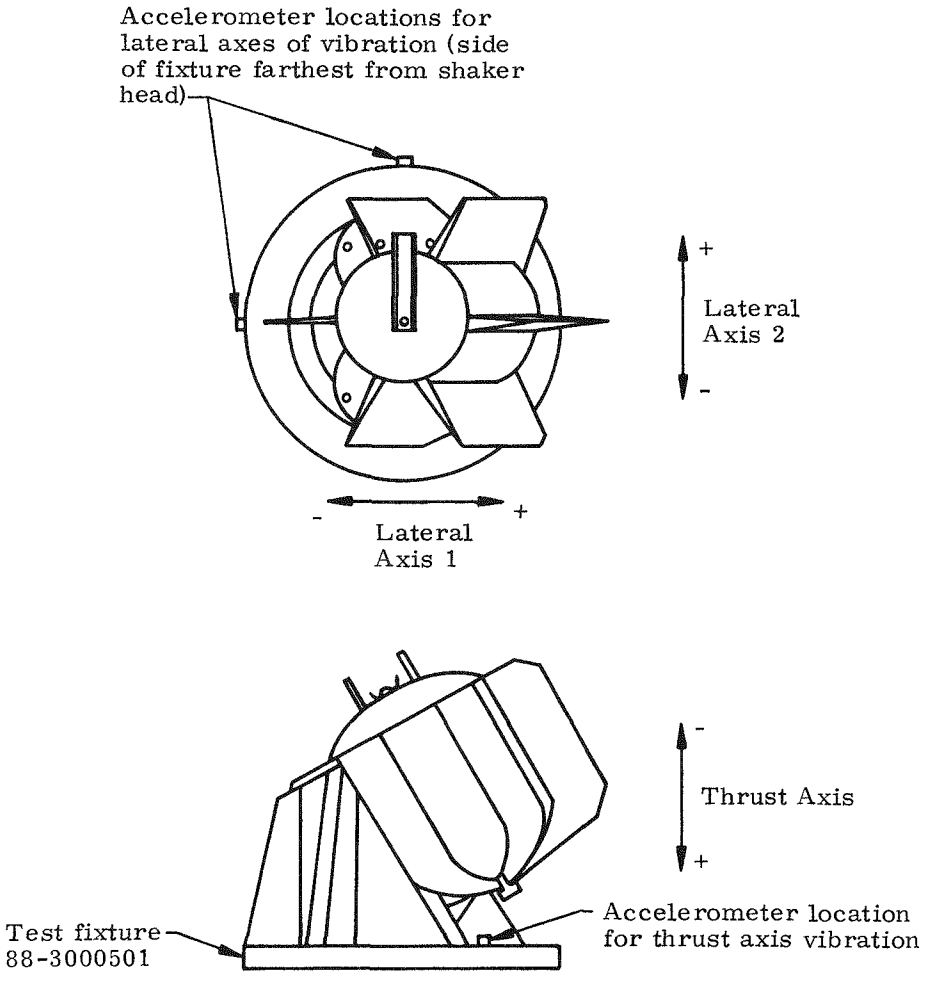

Fig. III-22. SNAP 11 Reference Axes and Accelerometer Locations for Acceptance Vibration Tests

severe flight acceptance level. To date, the 2N-2P (see Chapter II) generator series has successfully completed both qualification level and flight acceptance level testing. However, the 2N-3P series with their longer fins and redesigned heater block have not been qualified. At present, excepting transportation level dynamic tests on the Q/N-1M and Q/N-4 generators, the Q/N-3 is the only generator of this design to be dynamically tested to the flight acceptance level.

For dynamic testing, instrumentation and circuitry were as shown in Fig. III-23. Instrumentation for monitoring generator output and input power was similar to that shown in Fig. III-5.

Prior to dynamic testing, generator parameters to be monitored by oscillograph galvanometers during testing were attached as shown in Fig. III-23. Functions monitored were:

(1) Hot junction, cold junction, heater block and NaK ring temperatures

(2) The a-c input voltage and current

(3) The d-c output voltage and current.

Use of oscillograph galvanometers allowed a visual evaluation of any intermittent output during testing of any function being monitored.

The generator was electrically heated during testing with a power input of 810 watts ± 5 and the power output leads connected to a matched-load resistance for simulation of launch conditions.

Figure III-24 shows the generator installed in the test fixture prior to vibration in a lateral axis. The generator was mounted for all tests on the test fixture (Drawing 88-3000501) and an adapter-spacer plate. The spacer provided additional clearance for the larger generator fins which extend beyond the base of the test fixture.

The test axes and the accelerometer locations for vibration tests were as shown in Fig. III-22. The fixture and adapter plate were mounted directly to a MB Company C25H shaker for vibration in the thrust axis. Vibration in the lateral axes was performed with the generator, fixture and adapter plate attached to an auxiliary horizontal slide plate which was in turn attached to the shaker.

For the acceleration test, the generator was mounted to a Genisco Corporation 1230-1 centrifuge by means of two adapter plates and a T fixture (Fig. III-25).

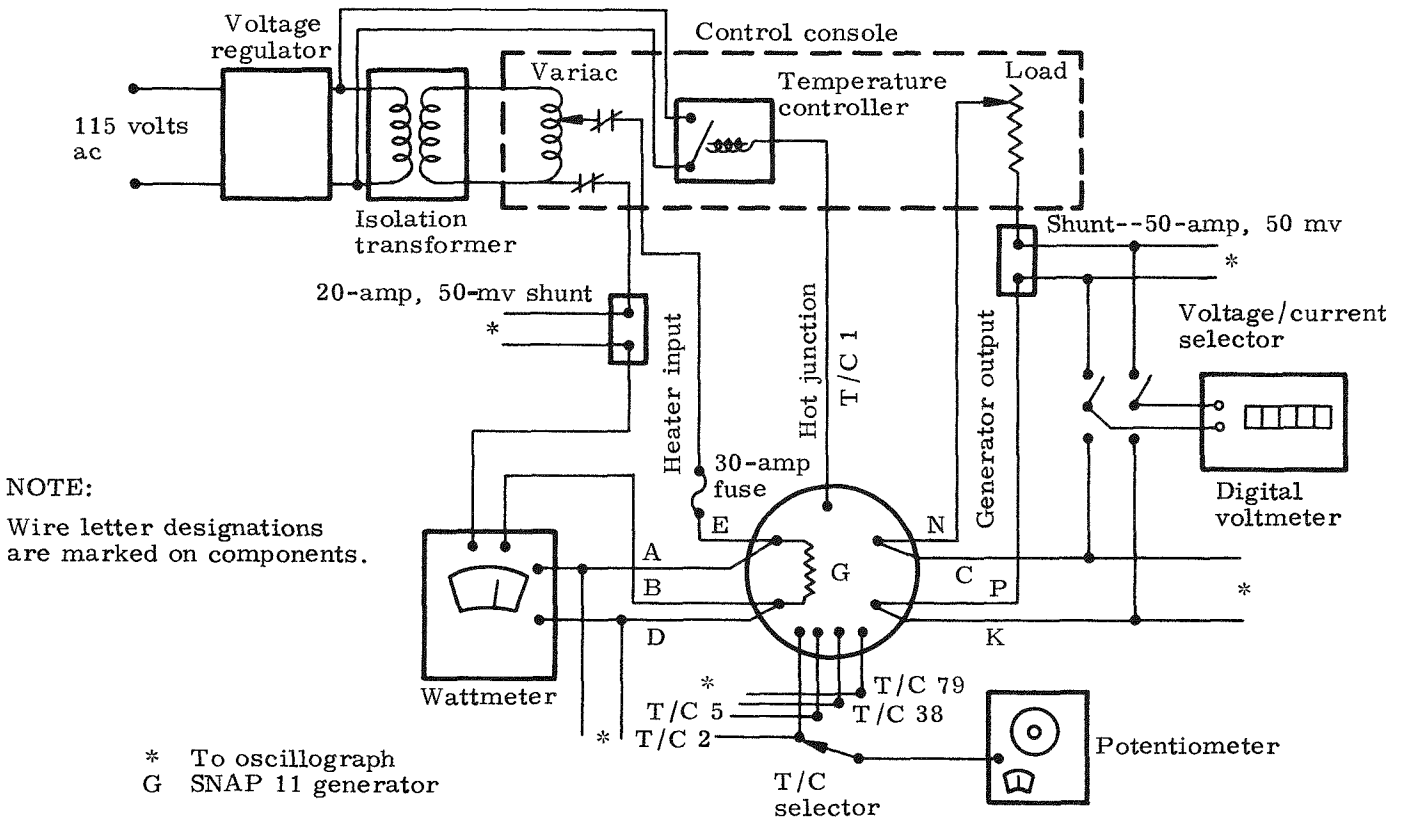

Fig. III-23. Schematic of Operation and Instrumentation Circuitry for Dynamic Tests

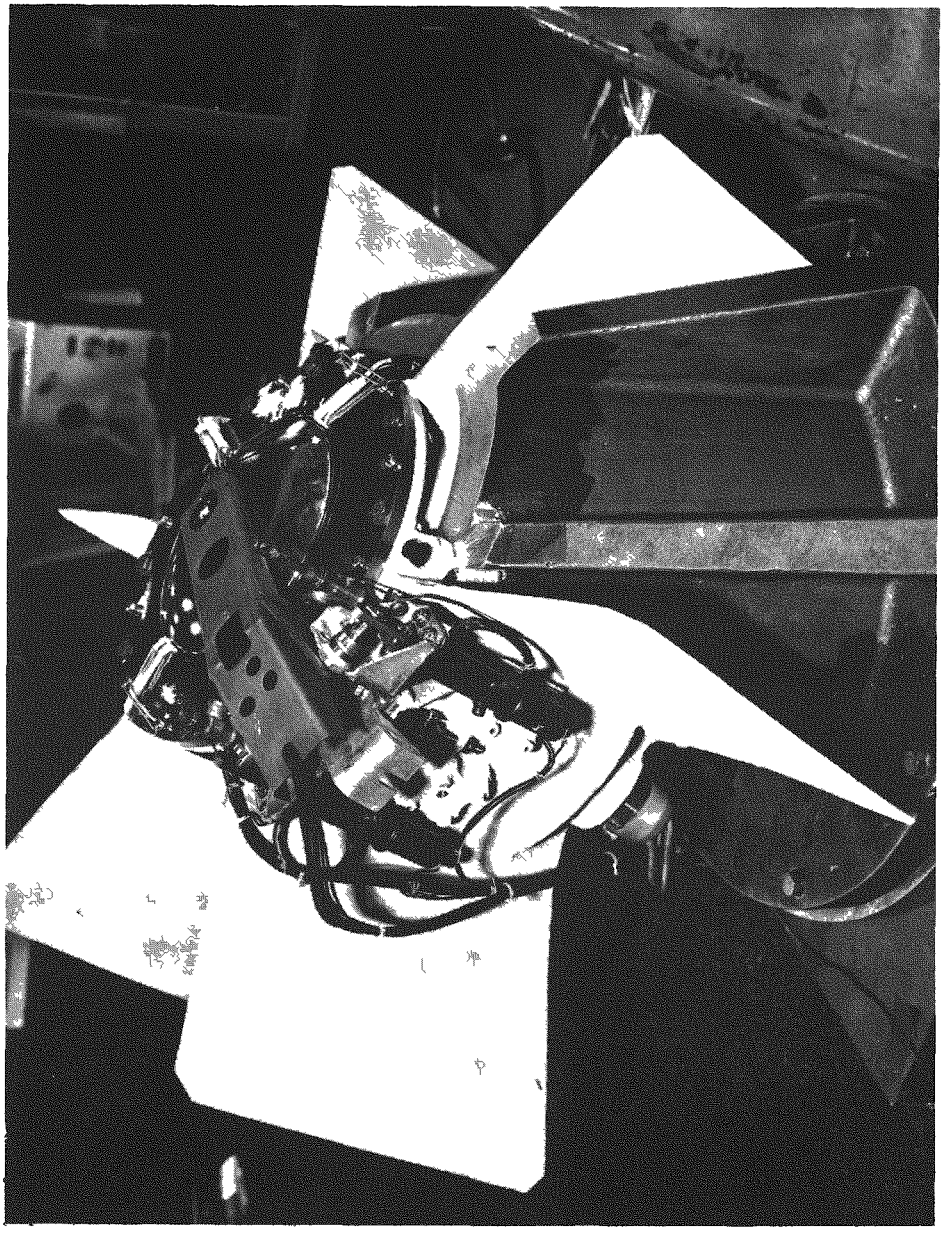

Fig. III-24. Generator Mounted in Test Fixture

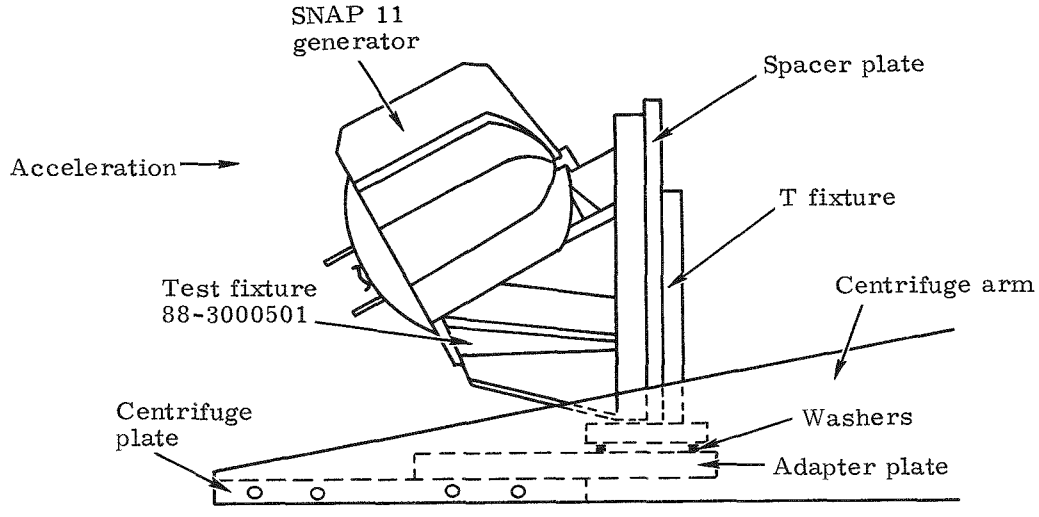

Fig. III-25. Generator Mounting for Acceleration Test

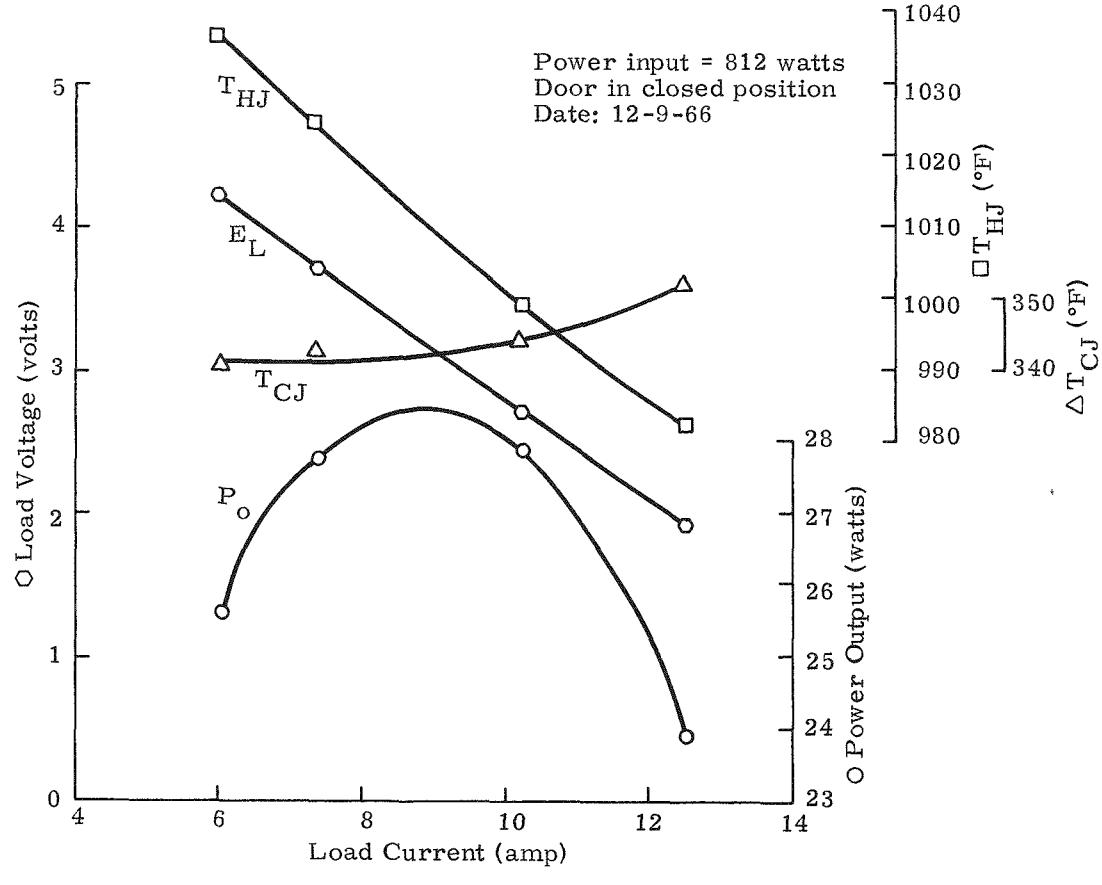

Fig. III-26. Q/N-4 Generator Air Parametric Performance

The only apparent damage to the generator during testing was the loss of noncritical thermocouples which feed through the shutter door opening. These thermocouples are considered noncritical in that they would not be included on a flight generator. During vibration, door movement crushed the ceramic insulation on these thermocouples, causing them to short or be severed. These thermocouples were subsequently repaired and the shutter door notched to minimize thermocouple damage in subsequent dynamic tests.

Table III-12 compares generator air performance before and after dynamic testing. As is evident, power output was virtually unchanged.

TABLE III-12

Comparison of Q/N-3 Generator Air Performance Before and After Dynamic Testing

	Before Testing*	After Testing**
Power (watts)		
Input	812	810
Output	27.9	28.0
Average junction temperature (°F)		
Hot	989	989
Cold	350	346
Voltage (volts)		
Open circuit	5.52	5.55
Load	2.78	2.75
Load current (amp)	10.05	10.17
Resistance (ohms)		
Load	0.277	0.270
Internal	0.273	0.275

* Performance point taken just prior to initiating dynamic testing.
** Performance point taken after dynamic and hot leak testing just prior to generator cooldown.

6. Hot Argon Leak Test

Starting with the Q/N-3 generator, a leak test was performed on the generator while it was operating in a LN_2 cooled hot leak test chamber. A Veeco Model GA-4 gas analyzer was used to determine the argon leak rate for the generator while at operating temperature (1000° F hot junction, 450° F cold junction). First, a background scan of the clean, dry, empty test chamber was made. The heated generator was then installed in the chamber and the leak test performed. The maximum leak rate determined was 2.88×10^{-5} cm^3/sec argon. After removal of the generator from the vacuum chamber, another background scan was made of

the empty chamber to demonstrate that no significant change in chamber background had occurred.

After completion of the Q/N-3 generator testing, the unit was shipped to the Jet Propulsion Laboratory for further evaluation in air, vacuum and dynamic environments. The Q/N-3 generator, when delivered to JPL, had an accumulated operating time of approximately 2260 hours, and had been subjected to two thermal cycles (from room to operating temperatures) at controlled heatup and cool-down rates. Measured generator room temperature internal resistance was 0.082 ohm prior to shipment. All generator performance and operating data including a generator description and operating instructions were summarized in the operating manual.*

C. Q/N-4 GENERATOR

Electrical testing performed on the Q/N-4 generator was essentially identical to that discussed previously for the Q/N-3 unit (see Table III-6). Comparison of the resulting data revealed the Q/N-3 and Q/N-4 generators to be virtually identical in performance. Qualification level dynamic testing initially scheduled for the Q/N-4 unit was forfeited after an inadvertent shaker malfunction, and a transportation level test was substituted. Prior to initiation of heatup and outgassing, the Q/N-4 generator room temperature internal resistance was 0.077 ohm.

1. Air Performance

Generator performance (upright in air) with an 810 watt ± 5 input and matched-load condition ($R_L = R_i$) is given in Table III-13. Power output was 27.9 watts at average hot and cold junction temperatures of 999° and 344° F, respectively. This matched-load point was used as a reference for checking performance after subsequent vacuum and dynamic testing that is discussed later in this section.

Air performance E-I maps were generated for power inputs of 810, 716 and 590 watts ± 5. The E-I curves generated are shown in Figs. III-26, III-27 and III-28; peak point performance parameters determined from the curves are summarized in Table III-14.

2. Lunar Night Performance

After completing the air parametric testing, the generator was tested at simulated lunar night conditions. The shutter door was calibrated at the end-of-life power input, 590 watts ± 5, and, subsequently, an E-I

* MND-2952-65, Operating Instructions Manual for the SNAP 11 Q/N-3 Generator, November 1966.

TABLE III-13

Q/N-4 Generator Air Performance at Matched-Load Condition

Power (watts)	
Input	810
Output	27.9
Average junction temperature (°F)	
Hot	999
Cold	344
Voltage (volts)	
Open circuit	5.52
Load	2.72
Load current (amp)	10.25
Resistance (ohm)	
Load	0.265
Internal	0.273
Door position	Closed

TABLE III-14

Summary of Q/N-4 Generator E-I Air Performance Maps

Power (watts)			
Input	812	714	588
Maximum output	28.4	23.2	16.5
Average junction temperature (°F)			
Hot	1014	915	788
Cold	344	318	291
Load current (amp)	8.7	8.3	7.5
Load voltage (volts)	3.28	2.82	2.20
Load resistance (ohms)	0.377	0.340	0.293

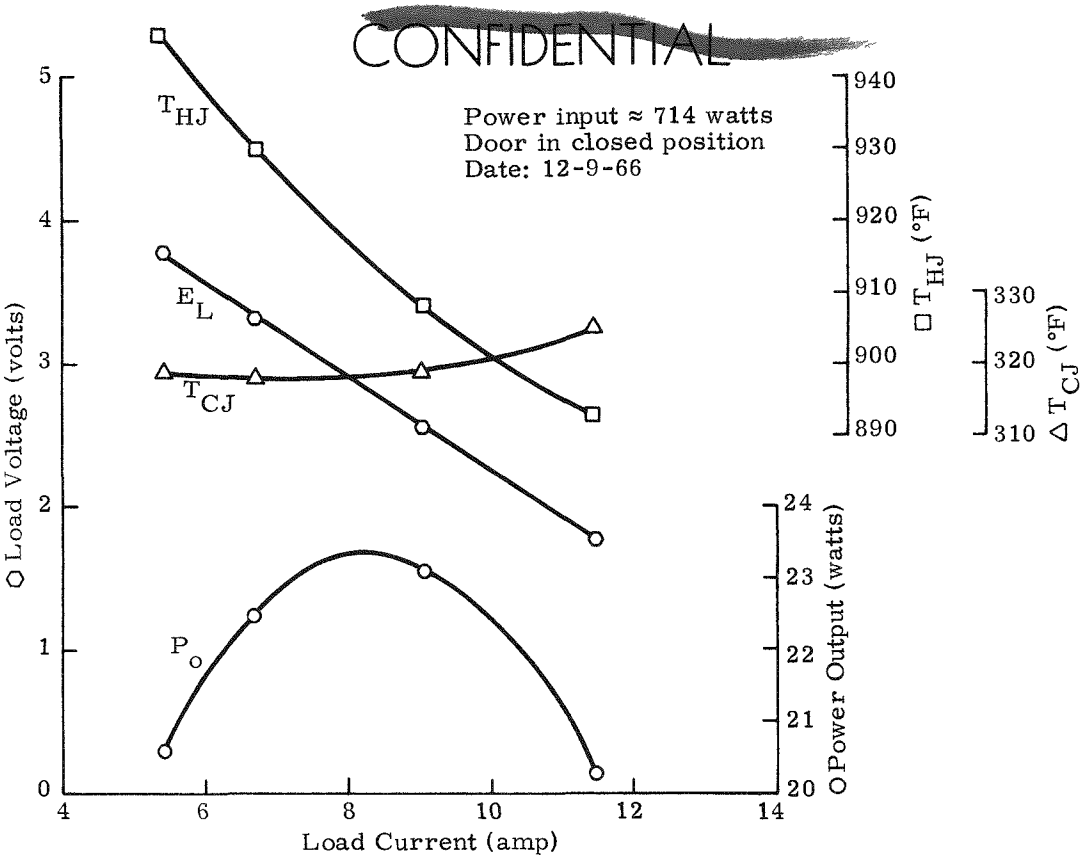

Fig. III-27. Q/N-4 Generator Air Parametric Performance

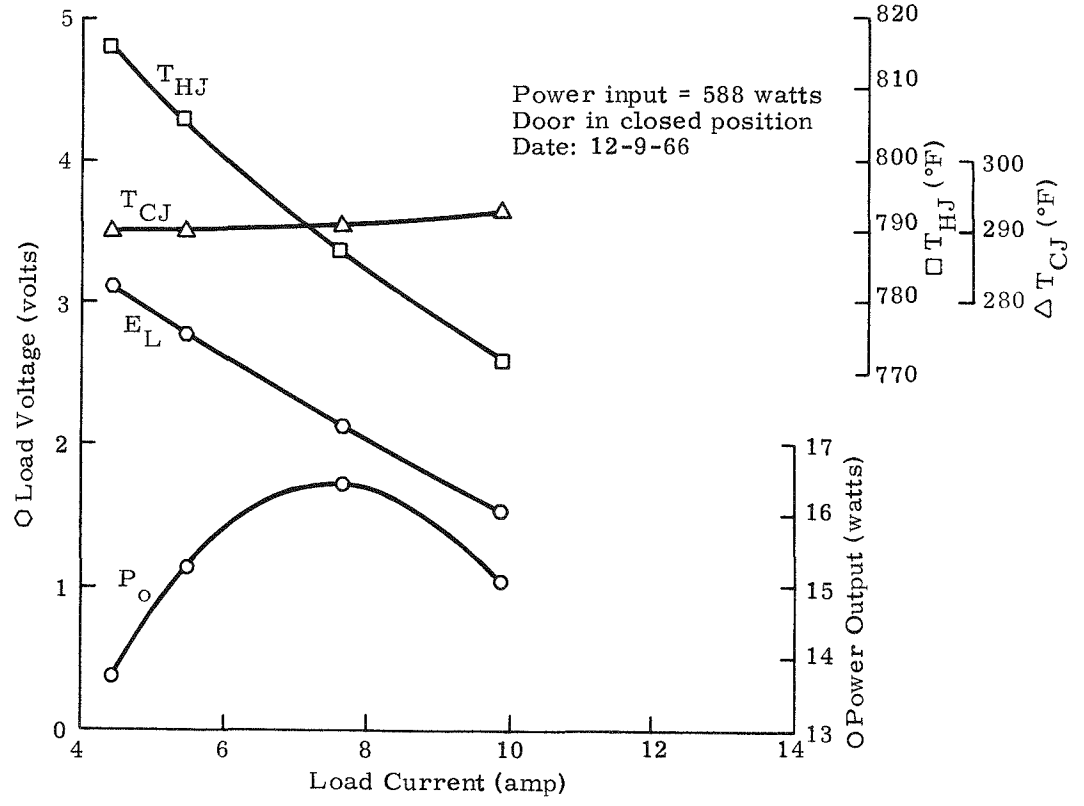

Fig. III-28. Q/N-4 Generator Air Parametric Performance

curve was generated with this power input. Generator performance was then determined at power inputs of 634, 716 and 810 watts ± 5. At the 810-watt ± 5 beginning-of-life power input, an E-I curve was generated. The maximum electrical power which could be put into the generator heater block without exceeding design limitations was then determined. After completion of testing at lunar night conditions, lunar day conditions were established and generator performance determined at electrical power inputs as outlined for the lunar night conditions.

Lunar night test results are shown in Figs. III-29, III-30 and III-31. Figure III-29 presents the E-I map generated with a 590-watt ± 5 power input; EOL maximum power output for the Q/N-4 generator was 20.9 watts. The load resistance for maximum power was 0.33 ohm. A shutter door opening was initiated at a NaK ring temperature of approximately 981° F.

Figure III-30 shows the Q/N-4 generator lunar night performance at power inputs between 590 and 944 watts, the latter determined to be the maximum allowable power input without exceeding a maximum hot junction temperature of 1025° F. Door opening for this maximum point was 5-3/4 inches. All performance parameters shown in Fig. III-30 were determined with the load resistance which yielded maximum power output at the EOL design condition, ~0.33 ohm. The hot junction temperature gradient ranged between 82° F (590 watts) and 43° F (944 watts).

Figure III-31 is an E-I map generated at a power input of 810 watts ± 5. Maximum power output was 23.7 watts.

3. Lunar Day Performance

After completion of lunar night testing, simulated test conditions were changed to lunar day. Test results are shown in Fig. III-30. The maximum allowable power input at lunar day conditions was determined to be 840 watts, at which point the seven-inch door opening limitation was reached. The hot junction temperature gradient ranged between 33° F (590 watts) and 18° F (840 watts). Subsequently, generator performance was determined at power inputs of 810, 716, 634 and 590 watts ± 5, as shown. At the 590-watt point an E-I map, shown in Fig. III-32, was generated; maximum power output was determined to be 15.5 watts.

After completing lunar day testing, the point for maximum power output at EOL (590 watts, lunar night) as determined from Fig. III-29 was rerun. Power output was 20.9 watts, identical to the 20.9-watt value previously determined. (This point is included on the E-I map in Fig. III-29.) After removal of the generator from the vacuum chamber, an air performance check with an 810-watt ± 5 input and matched external load resulted in a power output of 27.6 watts, comparing with the 27.9-watt point obtained during initial air parametric testing.

Table III-15 summarizes the lunar day and lunar night test results.

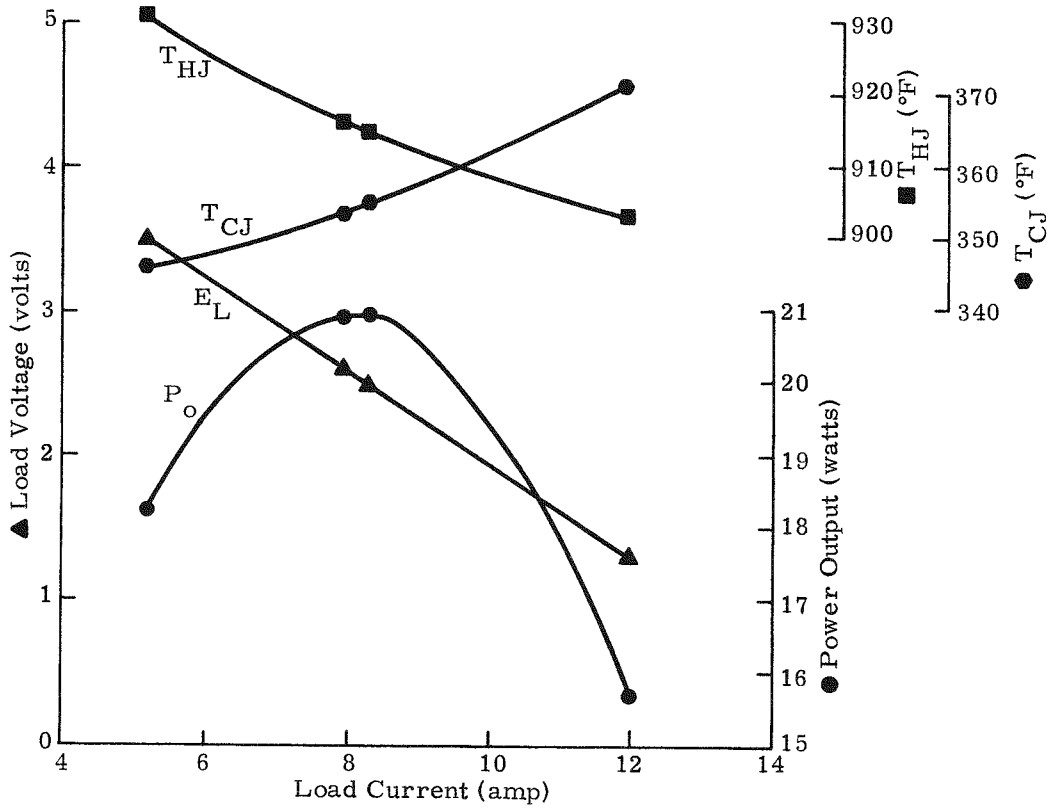

Fig. III-29. Q/N-4 Generator Lunar Night Parametric Performance

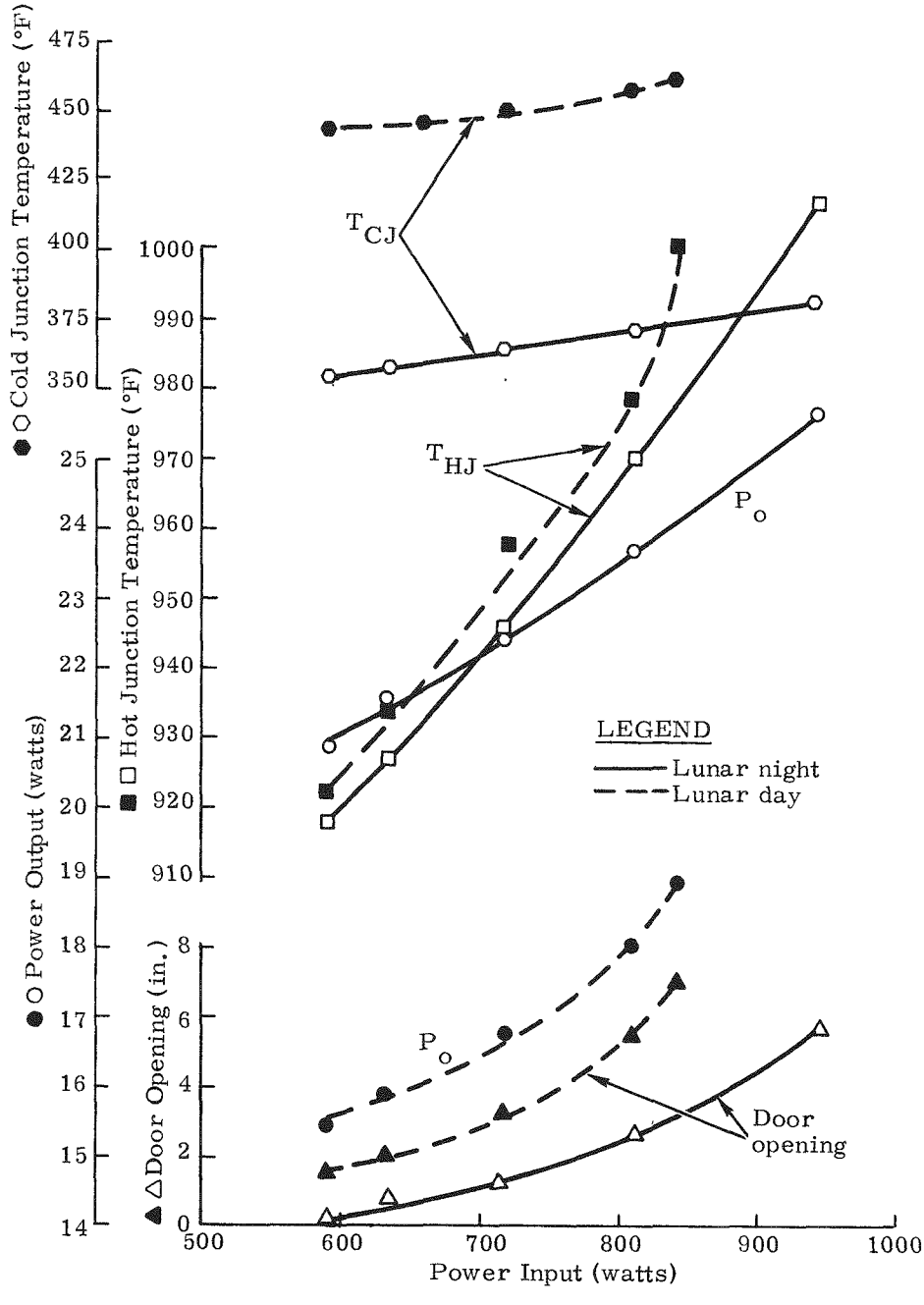

Fig. III-30. Q/N-4 Generator Vacuum Performance

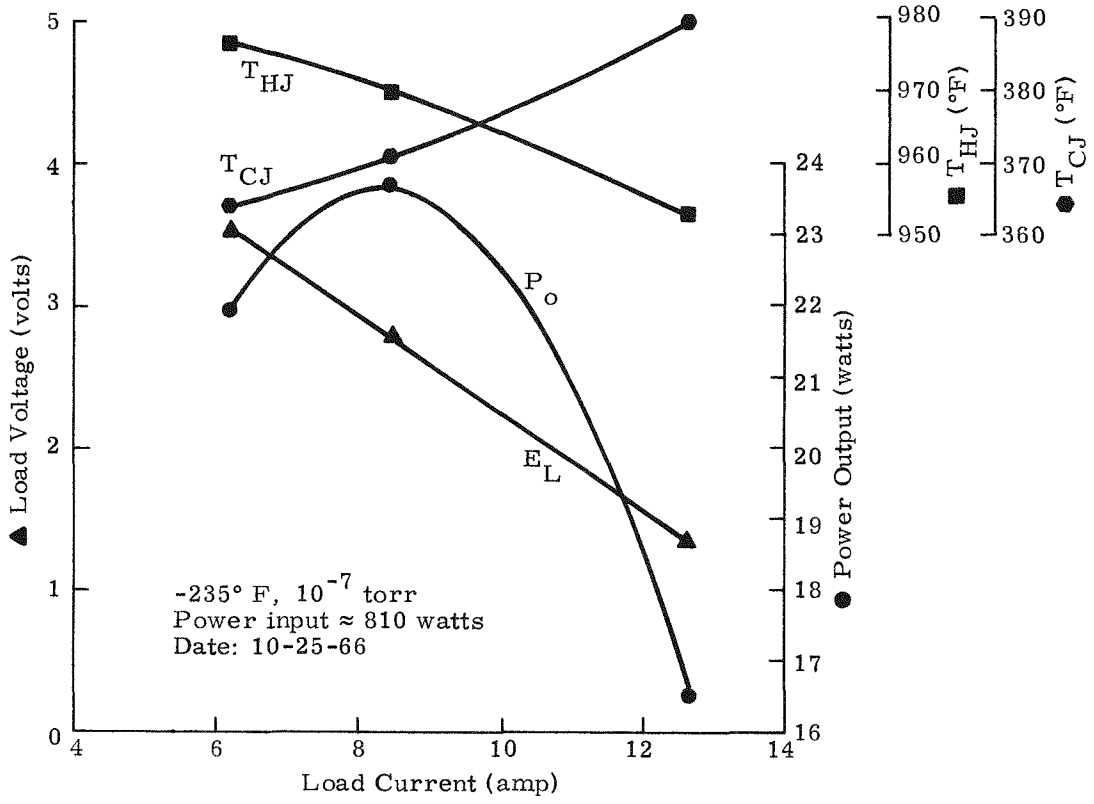

Fig. III-31. Q/N-4 Generator Lunar Night Parametric Performance

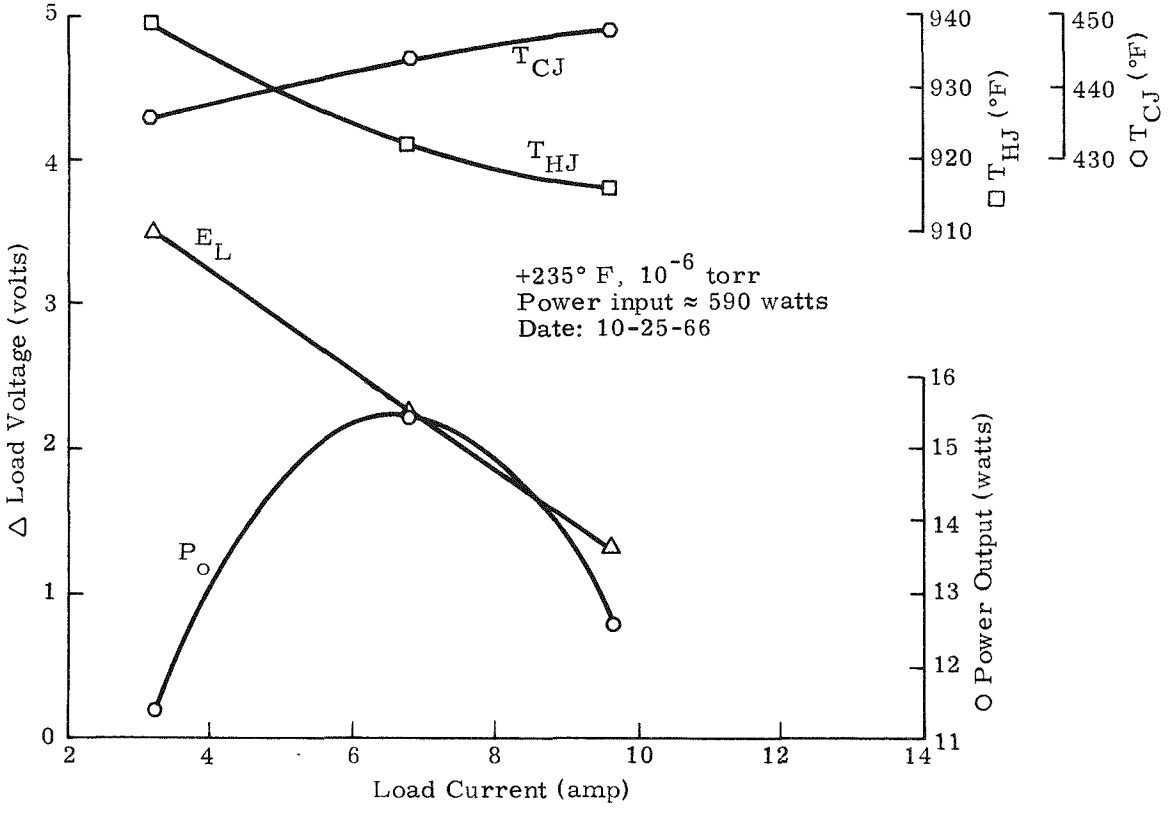

Fig. III-32. Q/N-4 Generator Lunar Day Parametric Performance

TABLE III-15

Summary of Q/N-4 Generator Vacuum Test Results

	Lunar Night (-235° F, 10^{-5} torr)				
Power (watts)					
Input	590	634	716	810	944**
Output	20.9	21.5	22.4	23.7	25.6
Average junction temperature (°F)					
Hot	918	927	946	970	1007
Cold	353	358	366	371	381
Voltage (volts)					
Open circuit	4.61	4.76	4.89	5.09	5.38
Load	2.61	2.64	2.71	2.79	2.90
Load current (amp)	8.00	8.15	8.28	8.49	8.84
Resistance (ohms)					
Load*	0.326	0.324	0.326	0.328	0.328
Internal	0.250	0.260	0.264	0.270	0.280
Door position (in.)	1/16	7/8	1-1/4	2-3/4	5-3/4
	Lunar Day (+235° F, 10^{-5} torr)				
Power (watts)					
Input	590	632	716	808	840**
Output	15.5	15.9	16.8	18.0	18.9
Average junction temperature (°F)					
Hot	922	937	958	979	1001
Cold	444	444	451	456	460
Voltage (volts)					
Open circuit	4.19	4.27	4.43	4.65	4.78
Load	2.25	2.29	2.35	2.43	2.49
Load current (amp)	6.86	6.96	7.16	7.42	7.60
Resistance (ohms)					
Load*	0.329	0.328	0.328	0.327	0.328
Internal	0.283	0.285	0.290	0.299	0.300
Door position (in.)	1-1/2	2	3-1/4	5-1/2	7

* Load resistance is value for maximum power output at the EOL design point.

** Maximum allowable power input determined from imposed generator operating limitations.

4. Dynamic Testing

Following the completion of both air and vacuum testing on the Q/N-4 generator, dynamic testing at the qualification level was planned. However, a malfunction in the shaker during instrumentation checkout subjected the generator to a dynamic shock (or shocks) estimated to be in excess of 50 g. The spurious pulse or pulses, the number at present being unknown, imposed on the generator were of such magnitude as to shear the mechanical stops in the vibrator which limit armature travel. Mechanical damage to the generator included shearing of the bottom mounting lug from the generator housing, cracking and deformation of the two upper mounting lugs and breakage of a fin. Up to the time of the malfunction on the MB C25HB shaker, a total of 7470 hours of vibration had been performed without any damage to a specimen. During that time, individual components and subsystems for Mace, Titan I, Titan II, Gemini-Titan II, PRIME and other nuclear devices were tested without incident. The built-in safety devices in the instrumentation were designed primarily to protect the exciter from damage when a malfunction occurred in the shaker system or an error was made by the operator.

After several specimen damages due to shaker malfunction within the industry (e.g., one occurring to the Nimbus satellite at NASA, several at GE and RCA), there is a growing trend toward providing protection for the specimen in addition to the shaker equipment. NASA-Goddard is presently installing a specimen protector on its shakers, but none of them are operational at the present time.

The high loading imposed on the Q/N-4 generator is at present believed to be the result of an electrical pulse which introduced a large g spike into the shaker head, thereby actuating the shaker armature and the Q/N-4 generator installed on it. The electrical pulse originated from either or both of the following sources: while switching the input to the shaker head from a random to sine mode; or a fuse failure, discovered after the incident, in the displacement limiter power supply.

The scheduled leak test with the generator at operating temperature (~1000° F hot junction, 450° F cold junction temperatures) was performed to determine the argon leak rate from the generator. The measured leak rate was 4.6×10^{-5} cm^3/sec argon, falling below the 5×10^{-5} cm^3/sec maximum allowable value. Thus, the shock did not cause any apparent structural damage which may have resulted in loss of the thermoelectric cavity hermetic seal.

As a result of this incident, qualification level dynamic testing of the Q/N-4 generator was deleted from the program. The revised test plan and results are discussed in the following section.

5. Electrical and Dynamic Retesting

After the hot leak test, the generator was retested in both air and vacuum environments to determine if generator performance was changed as a result of the shock. Subsequently, the generator was dynamically tested at a level to assure generator integrity against shipping loads.

a. Electrical retest

Generator performance in air, at matched-load with an 810-watt input, was determined. Subsequent performance points were taken at power inputs of 590, 716 and 810 watts in both simulated lunar night and lunar day environments. As is evident by the retest values, compared in Table III-16, lower power outputs were noted during vacuum retesting in most cases. No change in power output in air was apparent. Comparing with initial test values in Table III-15, the maximum percent differences in vacuum performance was less than 3%.

b. Transportation level dynamic test

After completing the electrical retest, the generator was cooled down and the room temperature resistance of the thermoelectric circuit was determined to be 0.077 ohm, indicating no generator internal damage had occurred.

Generator rework required was then performed and the generator installed in its shipping container for a transportation level dynamic test as discussed for the Q/N-1M unit in Section A At the conclusion of this test the generator was removed from its shipping container. The room temperature internal resistance was measured as 0.079 ohm.

To determine if any generator damage had been incurred during the transportation level test, the generator was heated up to operating temperature with an 810-watt ± 5 power input, and data taken at a matched-load condition for comparison with previously measured values. Results are compared in Table III-17; the percent difference in the power outputs was 2.6%

Resistance measurements at temperature revealed the thermoelectric circuit-to-case resistance to be very low, <1 ohm, with the low resistance occurring near the positive terminal of the thermoelectric circuit. The heater circuit-to-case resistance at temperature was measured to be 100 ohms. After generator cool-down, the room temperature internal resistance was determined to be 0.081 ohm, showing a slight increase. Circuit-to-case resistance was 1600 ohms, considered low compared to previous generators; the Q/N-3 generator circuit-to-case resistance was 13 kilohms prior to delivery to JPL.

TABLE III-16

Comparison of Q/N-4 Generator Before and After Shock

Air Performance

	Before* Shock	After** Shock
Power (watts)		
Input	808	814
Output	27.6	27.6
Average junction temperature (°F)		
Hot	991	998
Cold	349	342
Voltage (volts)		
Open circuit	5.39	5.42
Load	2.69	2.72
Load current (amp)	10.25	10.13
Resistance (ohms)		
Load	0.262	0.269
Internal	0.263	0.266
Door position	Closed	Closed

Vacuum Performance

Power Input (+ 5 watts)	Initial Power*** Output (watts)	Retest Power Output (watts)	Difference (%)
590 lunar night	20.9	20.3	2.9
716 lunar night	22.4	21.9	2.3
810 lunar night	23.7	23.1	2.6
590 lunar day	15.5	15.2	1.9
716 lunar day	16.8	16.6	1.2
810 lunar day	18.0	17.9	0.6

* Performance point taken just prior to dynamic testing.
** Performance point taken after the shock and hot leak tests.
*** Reference Table III-15.

TABLE III-17

Q/N-4 Generator Power Output at Matched Load Before and After Transportation Test

	Before* Test	After Test
Power (watts)		
Input	805	808
Output	27.2	26.5
Average junction temperature (°F)		
Hot	986	987
Cold	338	342
Voltage (volts)		
Open circuit	5.35	5.31
Load	2.64	2.73
Load current (amp)	10.28	9.69
Resistance (ohms)		
Load	0.258	0.282
Internal	0.263	0.266
Door position	Closed	Closed

* Point taken after hot leak test. Data differ from those shown in Table III-16 because these were taken on a different test console (at hot leak chamber) while those in Table III-16 were taken on vacuum chamber test console.

The effect on future performance of the low T/E circuit-to-case resistance at temperature is not known as its cause cannot be determined without generator disassembly. Since this is considered as a floating circuit, the low resistance path will not affect performance unless other circuit low resistance paths occur during future electrical testing.

The Q/N-4 generator was subsequently shipped to NASA-MSC/Houston, for further air and vacuum testing. When delivered to NASA an operating time of approximately 1415 hours had been accumulated, and the generator had been subjected to two thermal cycles (between room and operating temperatures) at controlled heatup and cool-down rates. All generator performance and operating data including a generator description and operating instructions were summarized in the operating manual.*

* MND-2952-68, Operating Instructions Manual for the SNAP 11 Q/N-4 Generator, December 1966.

BLANK

IV. HEAT SOURCE DEVELOPMENT

Because of the obvious inherent hazards and considerations of cost and availability, an electrical heat source was designed for use in the SNAP 11 program for prototype generator testing. The function of the electrical heat source was to simulate the isotopic heat source during air performance, thermal vacuum and dynamic tests. Specific simulation was desired with respect to power input capability, mass and center of gravity, operating temperature and heat rejection surfaces. In addition, the capability of heater block operation in both air and vacuum environments was required. The design and development of the electrical heat source is presented in this chapter.

The primary considerations in the design of the nuclear heat source involved not only the requirements imposed for proper generator performance, but also conformance to the safety philosophy and criteria established for the Surveyor mission. The analytical and test programs conducted to demonstrate that the safety requirements were met are presented in Chapter IX. The fuel block design development is discussed in this chapter. It should be noted that the design presented herein is not the design used for the fueling demonstration test (see Chapter V), but is the initial flight design on which extensive safety studies were performed.

A. ELECTRICAL HEAT SOURCE

1. Orginal Design

The original SNAP 11 electrical heat source design is shown in Fig. IV-1. It consisted of a carbon steel block, cartridge heaters and a stainless steel holddown ring which were sized to simulate the mass, center of gravity and external dimensions of the isotopic heat source described in Section B of this chapter. Eight cartridge heaters, connected in a parallel circuit, were used to simulate the power from the isotopic heat source. The heaters were sized such that their rated power was approximately twice the required power. This provided a margin of safety in case of individual heater failures and also allowed heater operation at reduced power, hence increasing their life expectancy. Emissive coatings for the heat rejection surface to the thermoelectric and the excess heat rejection surface were chosen to provide optimum heat rejection conditions.

This heater block design was used in all SNAP 11 test generators prior to the Q/N-1M. During those tests, it became apparent that a heater block redesign was desirable to eliminate the following problem areas:

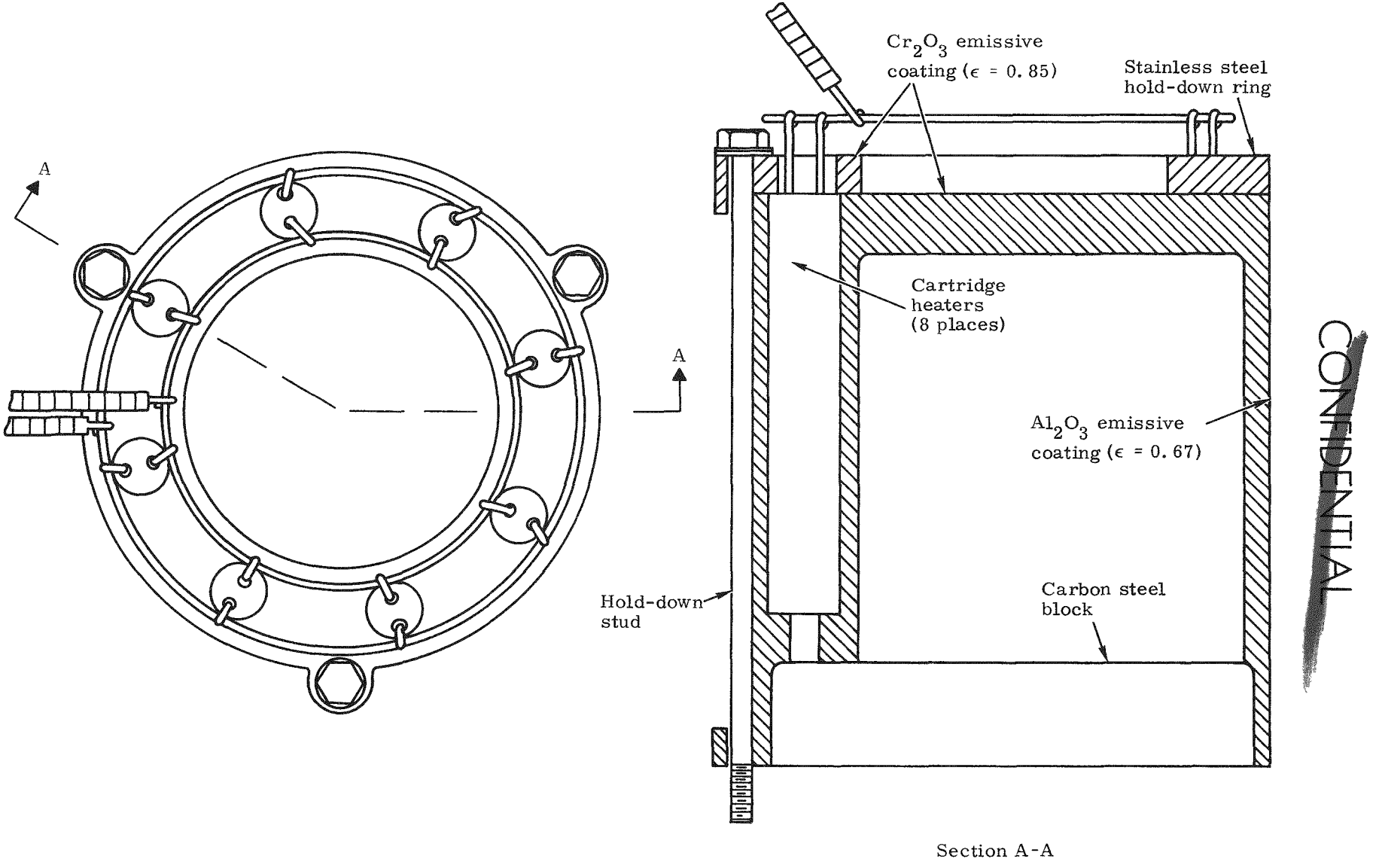

Fig. IV-1. Fuel Block Assembly

(1) Severe oxidation of the carbon steel block after prolonged operation (see Fig. IV-2). As a result of oxidation, severe deterioration of the emissive coatings resulted.

(2) Cartridge heater positions at the top of the heater block and the stainless steel holddown ring prevented good simulation of the fuel block heat rejection surface.

(3) In order to more accurately simulate the redesigned fuel block (demonstration test), an electrical source to simulate the oxidized Haynes-25 emissivity coating and materials was desirable.

2. Final Design

As a result of these heater block problems, the heater block was redesigned. The final design is shown in Figs. IV-3 and IV-4. The heater block consists of an ATJ graphite heat distribution block sealed in a helium gas atmosphere by Haynes-25 cladding. The Haynes-25 emitting surfaces (circumferential surface which radiates to the T/E conversion modules, and the top of the block which radiates excess thermal heat through the shutter door opening) are stably oxidized to provide highly emissive surfaces (emissivity = 0.8 to 0.9). The heater block is retained in the generator by means of a Haynes-25 holddown structure, which precludes torquing loads from being imposed on the thin heater block shroud. The new heater block configuration provides view factors and thermal interfaces which are more representative of a fuel block than obtained with the carbon steel electrical heater block previously used for the fuel block mockup. Power is supplied to the block through eight cartridge-type electrical heaters connected in parallel.

Structurally, the heater block is designed to operate with a 15-psi maximum differential pressure across the Haynes-25 shroud at operating temperature. Therefore, to allow operation in a vacuum, the block must be backfilled with helium while at operating temperature. In heating from room temperature to the anticipated operating temperature, the pressure inside the heater block increases by a factor of approximately 3.7. Before the final helium backfill, the graphite block is outgassed by evacuating at operating temperature, thus minimizing pressure buildup and cover gas contamination during heater block operation.

a. Coating stability study

The Haynes-25 oxide emissive coating was selected because of its high emissivity, vacuum stability and inherent mechanical compatibility with the Haynes-25 substrate material as reported in literature and evidenced by Martin Marietta testing. Several emissivity coatings were subjected to vacuum stability testing in support of the heater block/fuel block design programs. Emissive surfaces tested were as follows:

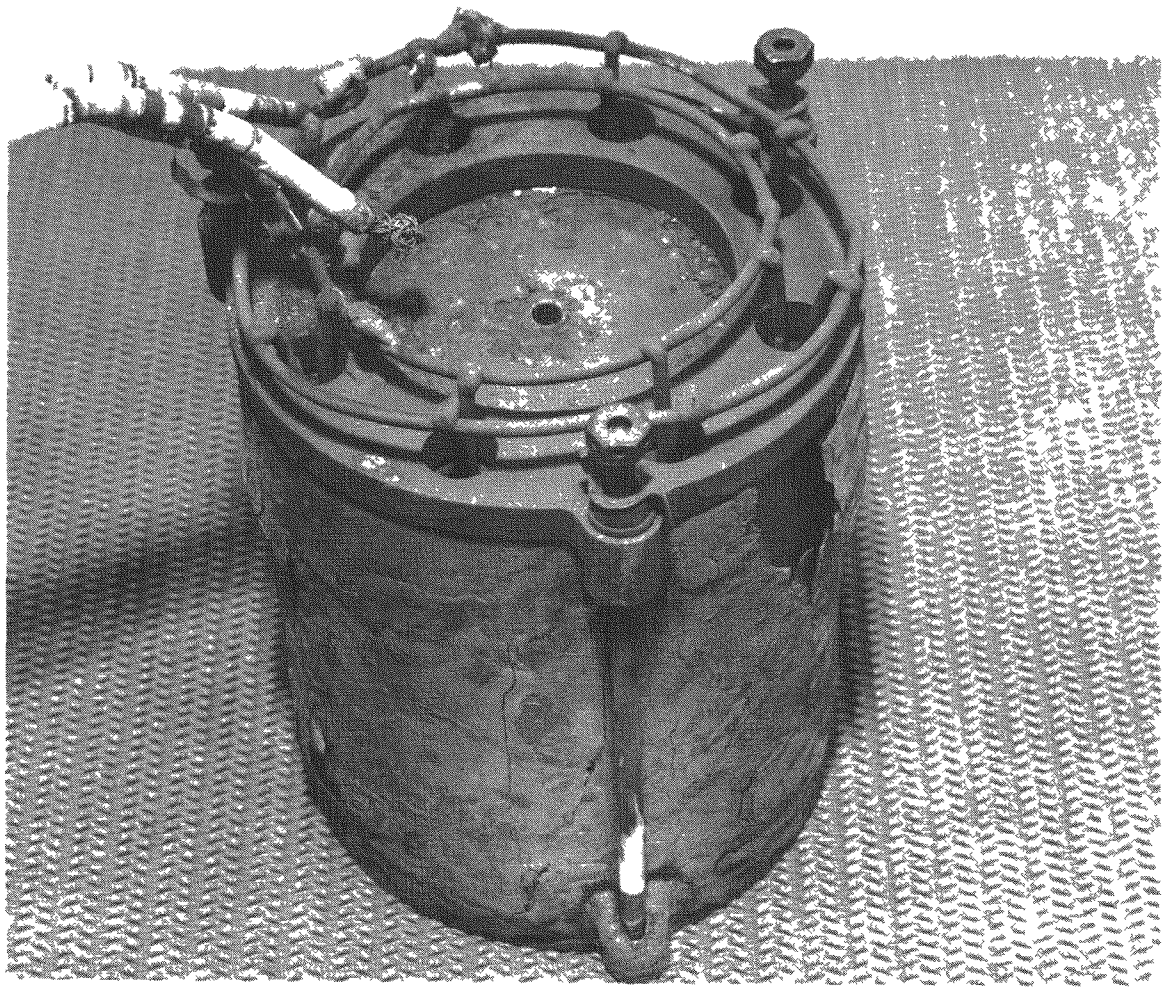

Fig. IV-2. SNAP 11 Q/N-1 Generator Heater Block

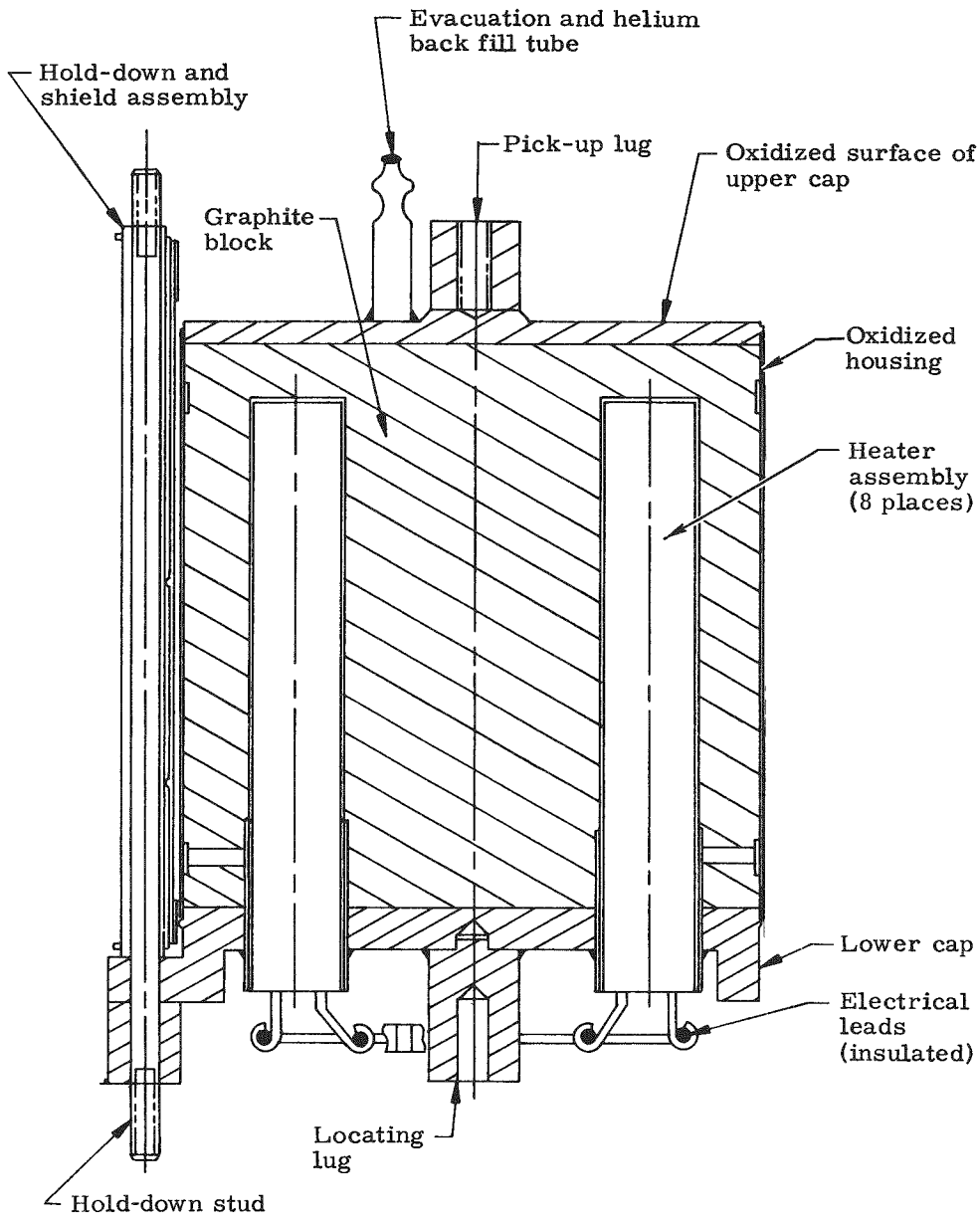

Fig. IV-3. Heater Block Assembly--Final Design

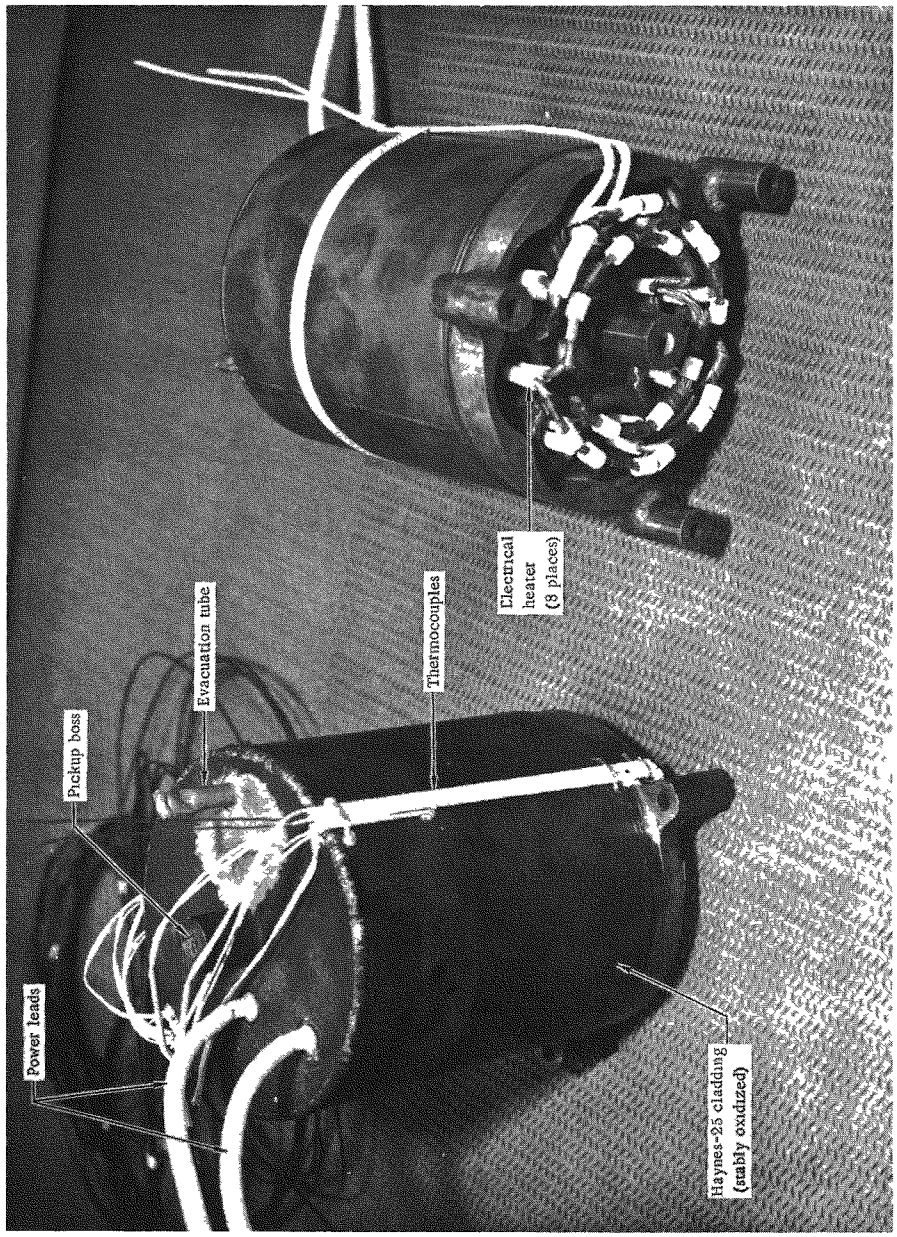

Fig. IV-4. Electrical Heater Assembly

(1) Fused ceramic coating, Solaramic

(2) Flame-sprayed aluminum oxide (Al_2O_3)

(3) Flame-sprayed chromium oxide (Cr_2O_4)

(4) Oxidized Haynes-25

(5) Oxidized nickel.

Testing was performed in a vacuum furnace at 1450° F, the maximum anticipated fuel block surface operating temperature. Test results were as follows:

(1) Fused ceramic coating, Solaramic. This commercial coating was applied over a 1 x 2 x 0.025 inch Haynes-25 panel by dipping, drying and firing at 1750° F in air for three minutes. The coated panel was tested for three hours at 1450° F in a vacuum of 2 to 2.5 x 10^{-5} torr. Surface blistering occurred and testing on the coating was discontinued.

(2) Flame-sprayed Al_2O_3 coating. The Al_2O_3 coating was applied by flame-spraying on a 1 x 2 x 0.062 inch (iron grit blasted) Type 316 stainless steel panel. The coating was tested for 18 hours at 1450° F in a vacuum environment (2.4 to 4.3 x 10^{-5} torr). A weight loss of 0.0003 gm/in.^{2} was obtained for this test period.

(3) Flame-sprayed Cr_2O_4 coating. This coating was applied and evaluated in the same manner as the Al_2O_3 coating. A weight loss of 0.0001 gm/in.^{2} was obtained for the test panel after the 18-hour test period.

Testing on Samples 2 and 3 was discontinued when the chromium oxide began to contaminate other test samples and the aluminum oxide exhibited a high weight loss when compared with the oxidized Haynes-25 panels.

(4) Oxidized Haynes-25. Two Haynes-25 test panels were prepared by sandblasting with 120 mesh grid, oxidizing in air at 2250° F for 10 minutes, and air quenching. The resulting surface was a bluish-black oxide layer. Each sample had a surface area of approximately 2 in.^{2}. The samples were tested for a total of 527 hours at 1450° F and 2 to 2.7 x 10^{-5} torr. Average weight loss of the two samples for this period was 0.0003 gm/in.^{2}.

(5) Oxidized nickel. Two nickel foil samples (0.002 in. thick) were stably oxidized in air at 1650° F for 30 minutes and air quenched, resulting in the characteristic greenish oxide layer. Test time was 527 hours in the same environment with the Haynes-25. Evaluation after this period showed an average weight loss of 0.0003 gm/in.^{2}.

The following conclusions were reached as a result of the stability study. Use of Coatings 2 and 3 at 1450° F in a vacuum environment appeared to be undesirable when compared with the stability and ease of conditioning the Haynes-25 material. Oxidized nickel appears to be stable, but does not possess sufficient strength at the high temperatures required for the heater block material.

b. Emissivity measurements

After completion of the vacuum testing, the emissivity of a Haynes-25 vacuum aged panel was determined and compared with a panel oxidized by the same process but which was not subjected to vacuum testing. The purpose of the test was to determine any significant change in the total normal emittance (at 1350° F) of the vacuum aged test sample due to extended vacuum testing. The reflectance of each sample was determined in a Gier-Dunkel reflectometer using a single beam monochromator. The reflectance from 0.295 to 2.7 micron wavelengths was measured in an integrating sphere in 2% increments of the Johnson curve. With the sample transferred to the heated cavity, measurements of reflectance were made from 1.4 to 25 microns. The sample was maintained at room temperature in a water-cooled holder. This technique acts to prevent the sample from emitting stray energy of its own above the reference level of room temperature. The reflectance curve thus produced was integrated for emittance in 2-micron increments according to the Planckian distribution of energy for a black body at 1350° F.

The results are presented as total normal emittance, which is an average emittance perpendicular to the surface over the principal wavelength band at 1350° F.

At 1350° F, The surfaces under consideration would be emitting principally at approximately 2.5 microns; while 2.5 microns represent the approximate point at which energy would peak, considerable energy would be emitted between 2.5 and 18 microns. In addition, some energy would still be emitted down to 1.6 microns, with insignificant amounts emitted beyond both these limits.

Test results, shown in Table IV-1, revealed that the total normal emittance of the oxidized Haynes-25 panel which had undergone vacuum testing retained its high emissivity property. An emissivity value for the aged specimen larger than that for the control or unaged specimen was noted, but was due to possible differences in initial oxidized condition and experimental error.

TABLE IV-1

Emissivity of Oxidized Haynes-25 Panels

Specimen Condition	Total Normal Emittance at 1350° F
Vacuum aged (527 hr)	0.86
Unaged	0.80

c. Thermal analysis

The eight electrical heaters for power input are designed to operate up to a maximum centerline temperature of 1600° F. At this temperature, heater life is a minimum of one year. Above this temperature, the heater life decreases sharply. To assure adequate heater life would be obtained with the existing heater block design, a thermal analysis was performed assuming worst case dimensions and a heater block surface temperature of 1400° F. In addition, only conductive heat transfer was considered. With the maximum anticipated heater block power input (925 watts), the heater centerline temperature was calculated to be 1670° F. With the conservative assumptions made and assuming no radiative heat transfer, the heaters are considered to be adequate for the application. In addition, the heater block will be operated with 925 watts power input only in simulating beginning-of-life power conditions. Most thermal testing will be performed at less than this value.

B. RADIOISOTOPIC HEAT SOURCE

1. Design Objectives

A short half life, high power density radioisotope, curium-242, was chosen for the Surveyor mission by the President's Scientific Advisory Council. The purpose was to avoid contaminating the lunar surface with large quantities of naturally occurring radioisotopes which could inhibit future scientific studies and investigations of the lunar surface.

The basic design philosophy of the SNAP 11 fuel block was to ensure that the design would not, under all credible operational and accidental conditions, permit intractable contamination of populated areas and unnecessary contamination of the lunar surface. To conform to this basic design philosophy, the following criteria for the system were developed:

(1) Fuel must be compatible with the fuel containment material.

(2) The fuel capsule must maintain its integrity during helium pressure buildup.

(3) The fuel capsule must maintain its integrity during possible abort re-entry and during subsequent impact.

(4) The fuel capsule must maintain its integrity under lunar impact conditions.

(5) The fuel capsule will not melt down under any credible accidental or operational conditions.

(6) Radiation hazards must be minimized to allow personnel to work around the generator.

2. Fuel Description

The characteristics of the fuel form chosen for the SNAP 11 generator, curium-242 oxide, are summarized in Table IV-2. Production of Cm-242 is accomplished by neutron irradiation of Am-241 in a nuclear reactor until the optimum content of Cm-242 is achieved. After irradiation, the target capsule contains a mixture of isotopes of americium, plutonium and curium, and fission products resulting from fissioning of all these isotopes. Most of the plutonium isotopes and the fission products are then removed by chemical separation. Separation of the americium was not planned primarily because of the low dose rate involved and because processing costs do not make americium recovery economically desirable.

TABLE IV-2

Fuel Characteristics*

Fuel form	Diluted Cm_2O_3
Melting point (°F)	4081
Power density of fuel form (watts/cm^3)	150
Weight density of fuel form (gm/cm^3)	11.75
Specific activity of Cm-242 (watts/Kcurie)	36.7
Shielding requirements	Moderate

*These were best estimates at time of the original fuel block design and were based on preliminary information. More accurate properties were obtained from fueled demonstration test (see Chapter V).

Curium-242 decays by alpha emission to Pu-238 according to the decay scheme shown in Fig. IV-5. The complete decay chain of Cm-242 is given in Tables IV-3 and IV-4. The growth of the first three daughters is given in Fig. IV-6. After about one half-life of Cm-242 (162.5 days), there is

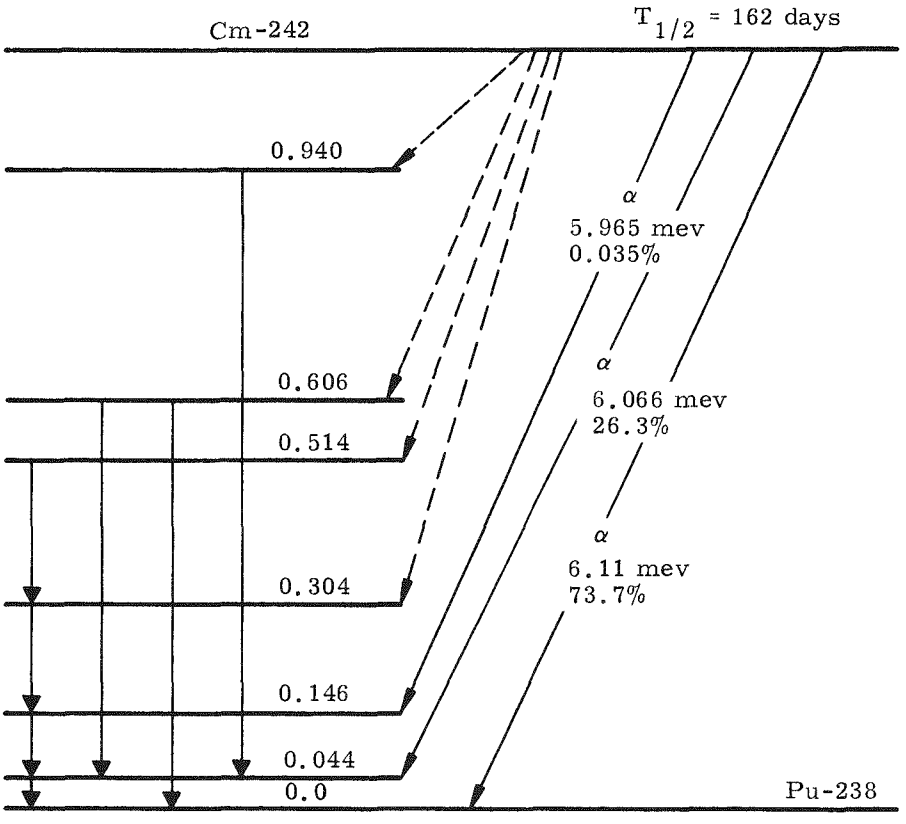

Fig. IV-5. Decay Scheme of Curium-242

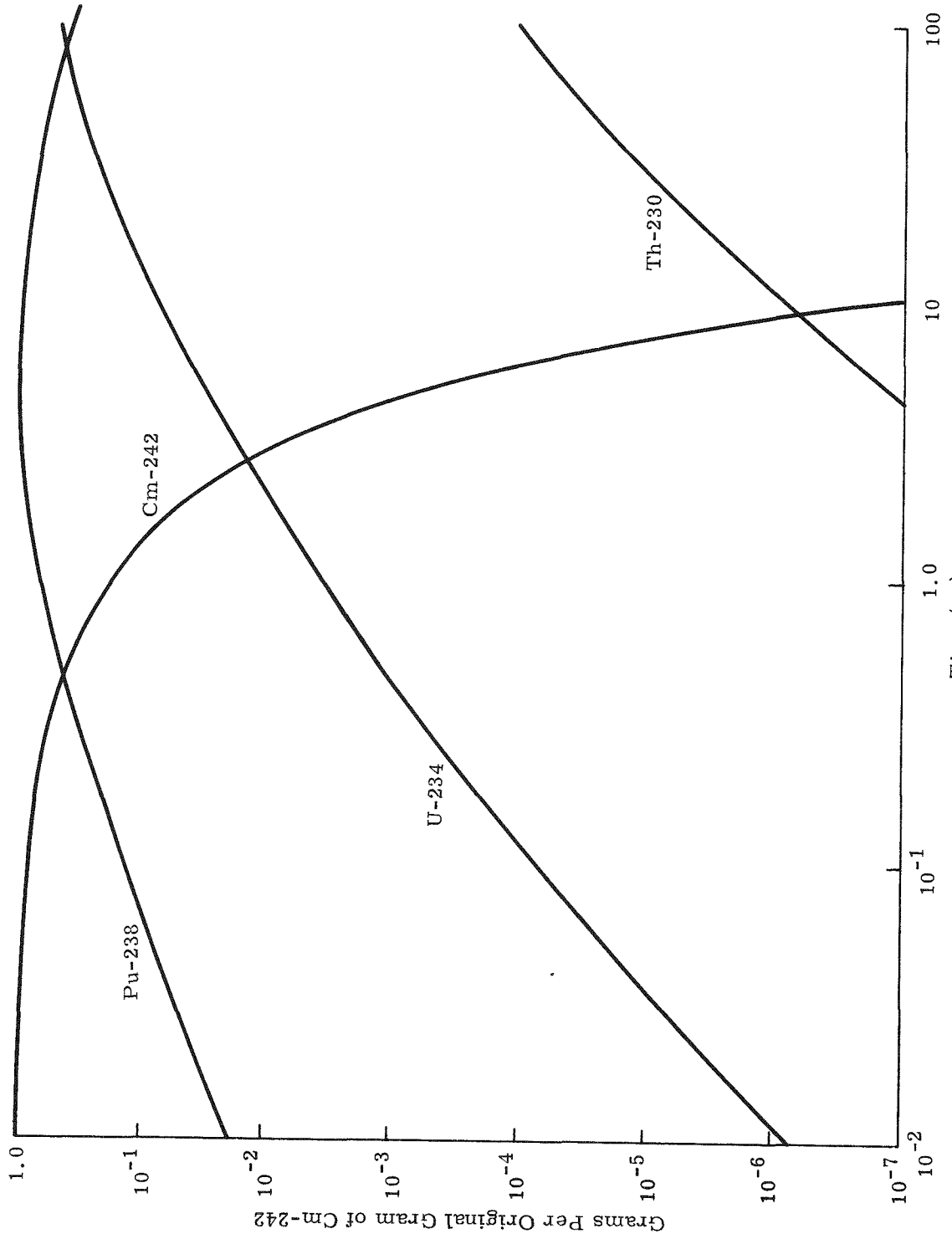

Fig. IV-6. Decay of Cm-242 and Growth of Decay Products

TABLE IV-3

Decay Products of Cm-242 and Pu-238

Isotope	Gamma Rays: Energy (mev)	Gamma Rays: Fraction of Disintegrations Producing X-ray	Neutrons/sec/gm from Spontaneous Fissioning
Cm-242	0.044	4.1×10^{-4}	2.013×10^{7}
	0.102	6.0×10^{-5}	
	0.158	2.7×10^{-5}	
	0.210	2.0×10^{-7}	
	0.562	1.8×10^{-6}	
	0.606	1.4×10^{-6}	
	0.896	0.9×10^{-7}	
Pu-238	0.0438	3.8×10^{-4}	4.4×10^{3}
	0.099	8.0×10^{-5}	
	0.150	1.0×10^{-5}	
	0.203	4.0×10^{-8}	
	0.760	5.0×10^{-7}	
	0.810	$\sim 1.0 \times 10^{-7}$	
	0.875	2.0×10^{-7}	
U-234	0.050	0.283	7.08×10^{-3}
	0.118	0.003	
	0.450	2.0×10^{-7}	
	0.500	1.0×10^{-7}	
Th-230	0.068	0.0059	9.6×10^{-4}
	0.110	1.0×10^{-6}	
	0.142	7.0×10^{-4}	
	0.184	1.4×10^{-4}	
	0.206	5.0×10^{-8}	
	0.235	5.0×10^{-8}	
	0.253	1.78×10^{-4}	
Ra-226	0.184	0.012	
	0.260	7×10^{-5}	
	0.420	2×10^{-6}	
	0.610	2×10^{-6}	
Rn-222	0.510	0.0007	
Po-218		None listed	
Pb-214	0.241	0.115	
	0.294	0.258	
	0.350	0.450	
Bi-214	0.607	0.658	
	0.766	0.065	
	0.933	0.067	
	1.120	0.206	
	1.238	0.063	
	1.379	0.064	
	1.761	0.258	
	2.198	0.074	
Po-214		None listed	
Pb-210	0.0465	0.040	
Bi-210		None listed	
Po-210	0.803	1.8×10^{-5}	

TABLE IV-4

Decay Products of Cm-242 and Pu-238

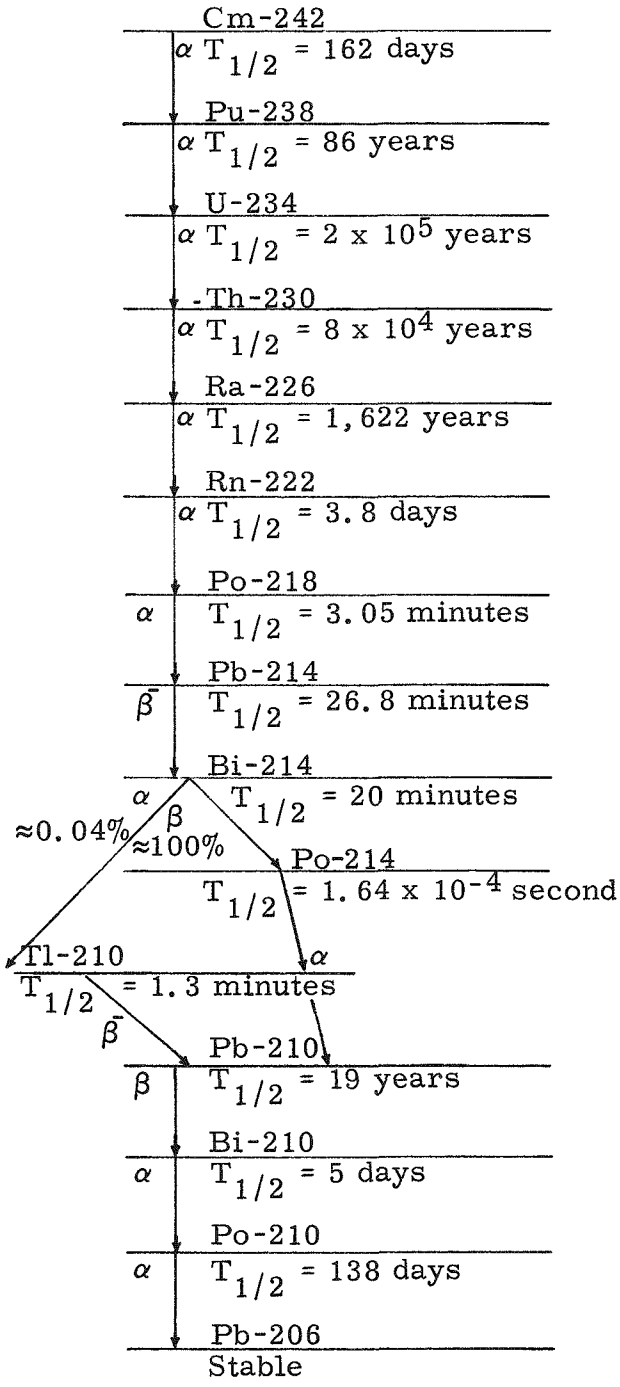

as much Pu-238 present in the fuel as there is curium; and after about two years, more than 90% of the original curium has decayed to plutonium. Plutonium compatibility with materials must, therefore, be considered along with that of curium.

As Cm-242 decays, the resultant Pu-238 nucleus is left in various excited states. As the nucleus returns to its normal state, gamma radiation is released. Other gamma radiation inherent with Cm-242 results from spontaneous fissioning. These additional gammas are prompt fission gammas, which are released instantaneously when fission occurs, and delayed gammas resulting from accumulated fission products. Other fission products originating during the neutron irradiation of Am-241 cannot be separated in the purification process and remain with the final product. The energy and abundance of each of these (spontaneous fissioning) gamma emissions are given in Table IV-5.

Although Cm-242 has many successive decay products, or daughters, these do not affect shielding requirements. Dose rates reach a minimum after 300 to 400 years of decay. After this time, the gamma radiation from the daughters causes the dose rate to increase until a maximum is reached after about 200,000 years. Approximately 15,000 years are required for the gamma dose rate to build up to the original value.

In addition to alpha and gamma radiation, neutrons are also emitted by Cm-242. Neutrons result from spontaneous fissioning of the curium and from (α, n) reactions if the fuel form contains light elements. The half-life for spontaneous fissioning is given as 7.2×10^6 years, and the average number of neutrons per fission is 2.65. These yield a production rate of 1.65×10^5 neutrons/sec/watt. If the oxide (Cm_2O_3) is used as the fuel form, neutron production from (α, n) reactions has been calculated to be 7.77×10^3 neutrons/sec/watt.

3. Description of Heat Source

The fuel block assembly, shown in Figs. IV-7 and IV-8, is comprised of the encapsulated fuel in a radiation shield and ablative material. The fuel is encased in a molybdenum base alloy (TZM consisting of 0.5% Ti, 0.07% Zr, balance Mo) liner with hemispherical end caps. The liner also serves to isolate the fuel form and to contain the helium resulting from the fuel decay. Within the TZM liner is a 72.8-gram fuel disc and a void volume of 0.376 $in.^3$. The fuel disc is placed in the capsule liner by remote means in a hot cell operation, and supplies approximately 925 watts(t) at the time of encapsulation. Experience has shown that special attention must be given to the diameter of the fuel disc, following pressing and sintering. The fuel disc expands due to the higher temperature of the compacted pellet and may result in an assembly problem when being inserted into the liner.

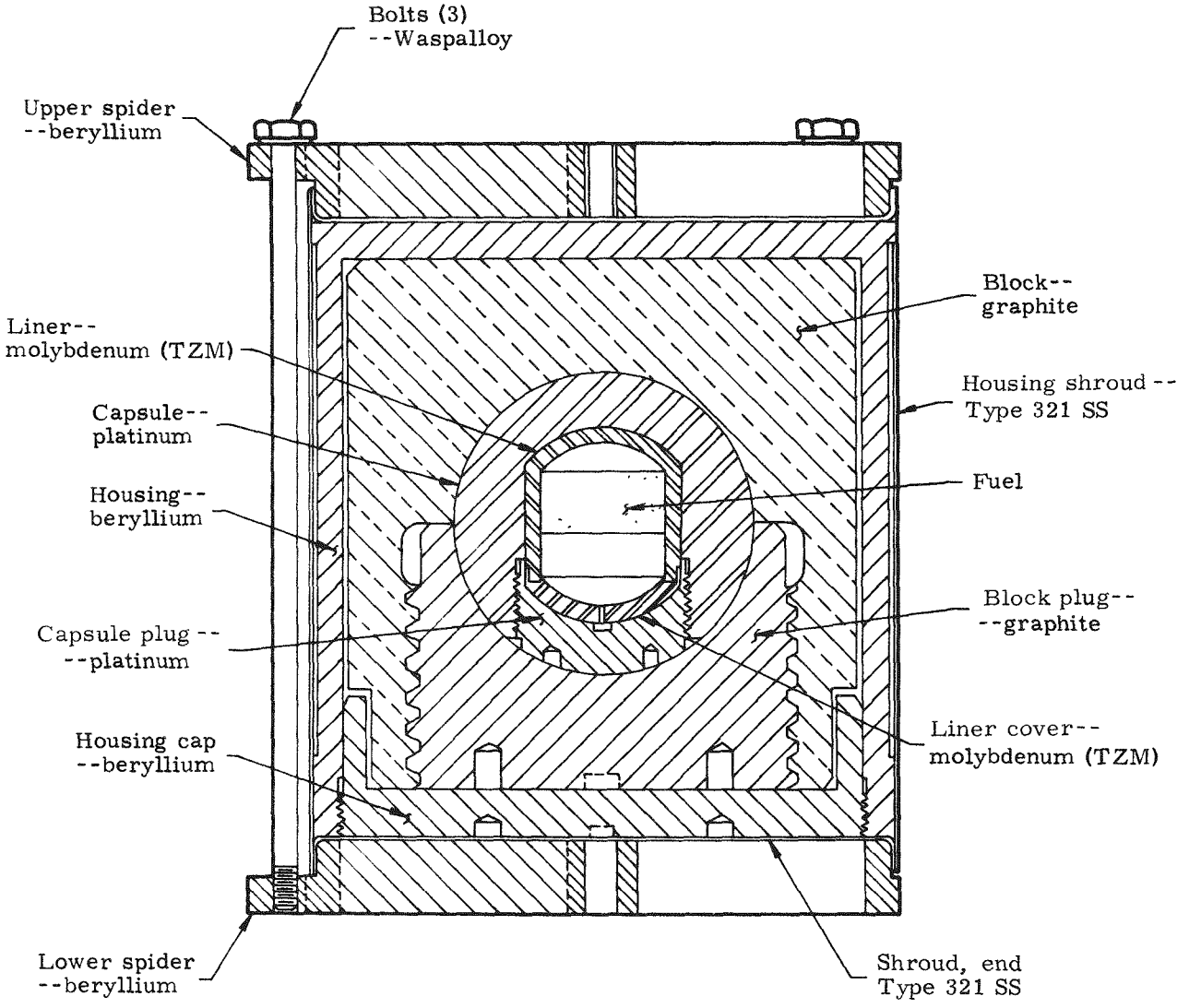

Fig. IV-7. Fuel Block Assembly

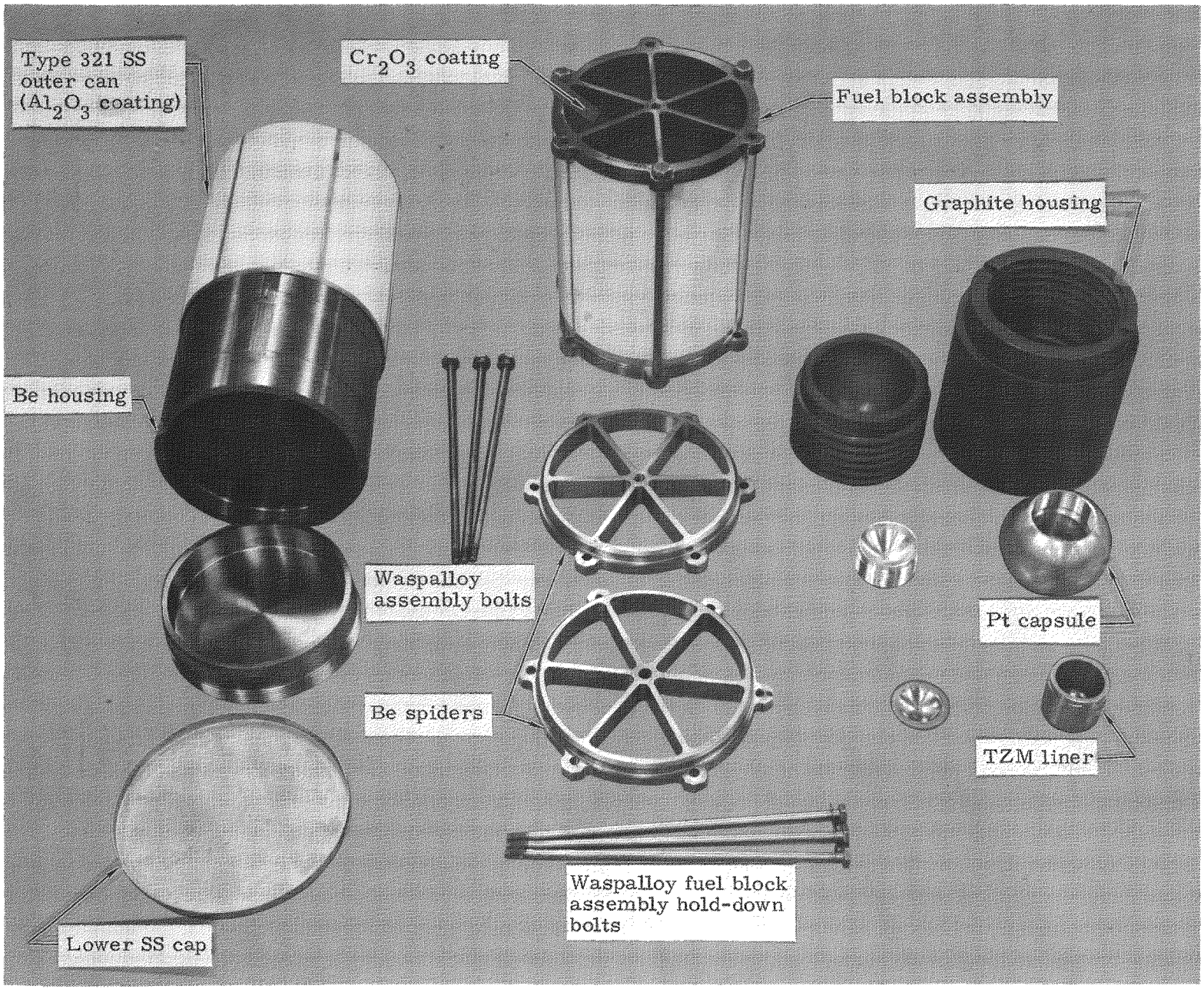

Fig. IV-9 Fuel Block Components and Assembly

TABLE IV-5

Gamma Radiation Associated with Cm-242

Decay		Prompt Fission		Fission Products	
Gamma Energy (mev)	Gammas/ sec-gm	Gamma Energy (mev)	Gammas/ sec-gm	Gamma Energy (mev)	Gammas/ sec-gm
0.044	3.6×10^{10}	0.5	2.36×10^{7}	0.15	2.05×10^{6}
0.102	5.05×10^{9}	1.0	1.44×10^{7}	0.75	2.16×10^{7}
0.158	2.22×10^{9}	1.5	6.78×10^{6}	1.2	4.61×10^{6}
0.210	1.85×10^{7}	2.0	4.18×10^{6}	1.6	3.05×10^{6}
0.562	2.22×10^{8}	2.5	2.20×10^{6}	2.2	7.1×10^{5}
0.606	1.72×10^{8}	3.0 up	2.58×10^{6}	2.4	4.8×10^{5}
0.896	1.06×10^{8}			2.7	2.8×10^{5}

CONFIDENTIAL

Closure of the liner is also performed within a hot cell in a helium atmosphere by a fusion method with no filler metal. A helium atmosphere will be used throughout the assembly of the generator to ensure against a large temperature drop through the void areas. The finished weld outer envelope does not exceed the outside diameter of the cylindrical section of the container and a 100% weld penetration is achieved.

After welding the cap to the liner, the assembly is allowed to soak until temperature equilibrium is reached, at which time the center vent hole in the cap is seal-welded in a helium atmosphere using the protrusion for filler material. The sealed liner assembly is then inserted into the platinum sphere which provides required shielding and impact protection. The assembly is allowed to reach steady state temperature, and then the platinum plug is tightened to a snug fit.

The same type of seal weld as was performed on the liner is repeated on the platinum plug-sphere junction. The sealed fuel container is then transferred to and installed in the fuel block. Graphite and beryllium surrounding the platinum sphere afford the thermal protection necessary for intact re-entry. A stainless steel shroud of Type 321 stainless steel encases the graphite and beryllium ablative material and is seal welded with end caps to prevent oxidation of the graphite during terrestrial operation and loss of the helium atmosphere during vacuum operation.

The selection of platinum as the capsule material represents a compromise between depleted uranium and Haynes-25 alloy. Depleted uranium possesses favorable shielding but unfavorable impact characteristics, whereas the Haynes-25 is a good energy absorption material with poor shielding characteristics. Platinum possesses excellent seawater corrosion resistance, comparable to Haynes-25 (less than 1 mil/yr), and has an oxidation rate of 4.7×10^{-3} mils/day in still air at 1700° F. Although TZM is brittle at room temperature, it exhibits excellent high temperature structural properties. The more important physical and mechanical properties of platinum and TZM are presented in Table IV-6.

Graphite was chosen for earth re-entry heating protection because of its capability to survive aerodynamic heating. This is due to its high sublimation temperature. However, during the most severe abort conditions, heat can be transmitted through the graphite in sufficient quantities to melt the platinum sphere. Therefore, a beryllium shield has been included to absorb and dissipate sufficient heat by the ablation mechanism to eliminate the possibilities of melting the platinum.

As previously mentioned, a fuel block redesign was performed for the fueled generator demonstration tests, and is described in detail in Chapter V-A.

TABLE IV-6

Physical Properties of Platinum and TZM

Physical Properties	Platinum	TZM
Density (lb/in.^{3})	0.775	0.369
Melting point (°F)	3217	4730
Thermal conductivity (Btu/hr/ft^2/°F/ft)	42 (212° F)	56 (2000° F)
Coefficient of thermal expansion per °F	4.9×10^{-6}	3.0×10^{-6}
Specific heat (Btu/lb/° F)	0.031	0.07
Mechanical Properties		
Modulus of elasticity (psi)	25×10^6	47×10^6
Tensile strength, 10^3 (psi)	18 to 21 annealed 28 to 30 cold rolled	85.5 at 1800° F SR 41.7 at 1800° F R
Yield strength, 10^3 (psi)	2 to 5.5 annealed 27 cold worked	-- 17.9 at 1800° F R
Elongation in 2 in. (%)	30 to 40 annealed 2.5 to 3.5 cold worked	18 at 1800° F SR 35 at 1800° F R
Hardness (Vickers)	40 annealed 100 cold worked	172 at 70° F

All data at room temperature unless otherwise noted.
SR--stress relieved
R--recrystallized

CONFIDENTIAL

4. Nuclear Safety Study Summary

In order to establish compliance with the criteria established for the fuel block design, a nuclear safety study was performed. This study included investigations of the following areas:

(1) Fuel form investigation (material compatibility)

(2) Re-entry evaluation (plasma jet testing)

(3) High velocity impact tests of the fuel capsule against granite to demonstrate fuel containment for the terminal velocity earth abort condition, and containment of fuel within the impact crater for lunar impact conditions.

(4) Helium pressure buildup analysis.

(5) Air dispersion analysis

(6) Radiation analysis.

The results of these investigations are discussed in detail in Chapter IX. Summarized, they are as follow:

(1) Fuel form compatibility--test results, utilizing a simulated curium fuel form (Gd_2O_3) and a molybdenum (TZM contains over 99% Mo) capsule, revealed that no attack occurred up to 2000° F.

(2) Radiation dose rates--the calculated dose rates indicate that a person could safely work around the generator for short time increments.

(3) Helium pressure buildup analysis and tests show that the fuel capsule will maintain its integrity when exposed to maximum expected pressure buildup.

(4) Creep due to pressure buildup--dimensional measurements of the fuel capsule at maximum pressure buildup showed that the capsule material will not creep.

(5) Fuel capsule meltdown--an analysis was performed which showed that under the most severe credible conditions meltdown would not occur.

(6) Explosion overpressures--calculations have shown that a Centaur fuel explosion would produce a maximum pressure of 375 psi; the steel inner casing will withstand a pressure of 1400 psi.

(7) Dropping of the fuel block--analyses have shown that the generator will contain the fuel when dropped from a height of 125 feet. A half-scale impact test program showed that containment was also maintained for impact against a granite block for velocities up to 3356 fps.

(8) Fire--the generator outer housing will not fail when exposed to the temperatures resulting from the Centaur fireballs, or continuing fires.

V. GENERATOR FUELING AND DEMONSTRATION TEST

Concurrent with prefueling activities, a new fuel block was designed for the SNAP 11 generator to assure a safe and successful encapsulation of the fuel form and fabrication of a fuel block assembly. No attempt was made to flight-optimize the design. In addition, Martin Marietta worked with the Oak Ridge National Laboratory in establishing requirements and procedures to assure an on-schedule fueling and generator test considered critical because of the inventory decay associated with a radioisotopic heat source. The task of fueling and testing the SNAP 11 demonstration generator was accomplished in three phases: the prefueling effort; the fuel encapsulation and generator fueling effort; and, the fueled generator test effort.

These efforts culminated in a successful encapsulation of the curium-242 isotope heat source on July 1, 1966. A 10-day shelf test was then performed to gain further assurance of isotope containment. The assembly of the fuel block was subsequently completed and the fuel block was inserted into the Q/N-1M SNAP 11 test generator on July 12, 1966. This was followed by the scheduled 90-day demonstration test under simulated lunar environmental conditions.

At the conclusion of the fueled demonstration test, the Q/N-1M generator was defueled and shipped to Sandia Corporation for additional endurance testing using an electrical heater block. Diagnostic disassembly and inspection of the fuel block will be performed by ORNL and will be the subject of a separate report.

A. RADIOISOTOPIC HEAT SOURCE

1. Radioisotopic Heat Source Demonstration Test

a. Design criteria and summary

At the end of 1965 the decision was made to redesign the SNAP 11 fuel block to enhance the chances for a successful fueling operation and generator demonstration test. This decision was based on the results from a joint meeting between the AEC, Oak Ridge National Laboratory and Martin Marietta. Since the unprocessed isotope fuel sources (a mixture of americium and curium dioxides) were already committed for removal from the reactor, it was necessary to schedule the fueling operation for mid-1966.

The joint meeting revealed that the isotope fuel source could not be prepared in the previously planned form and power density (curium-242 in an iridium matrix at 150 watts/cm^3). Further, the previously manufactured fuel block, as shown in Fig. V-1, was considered marginal

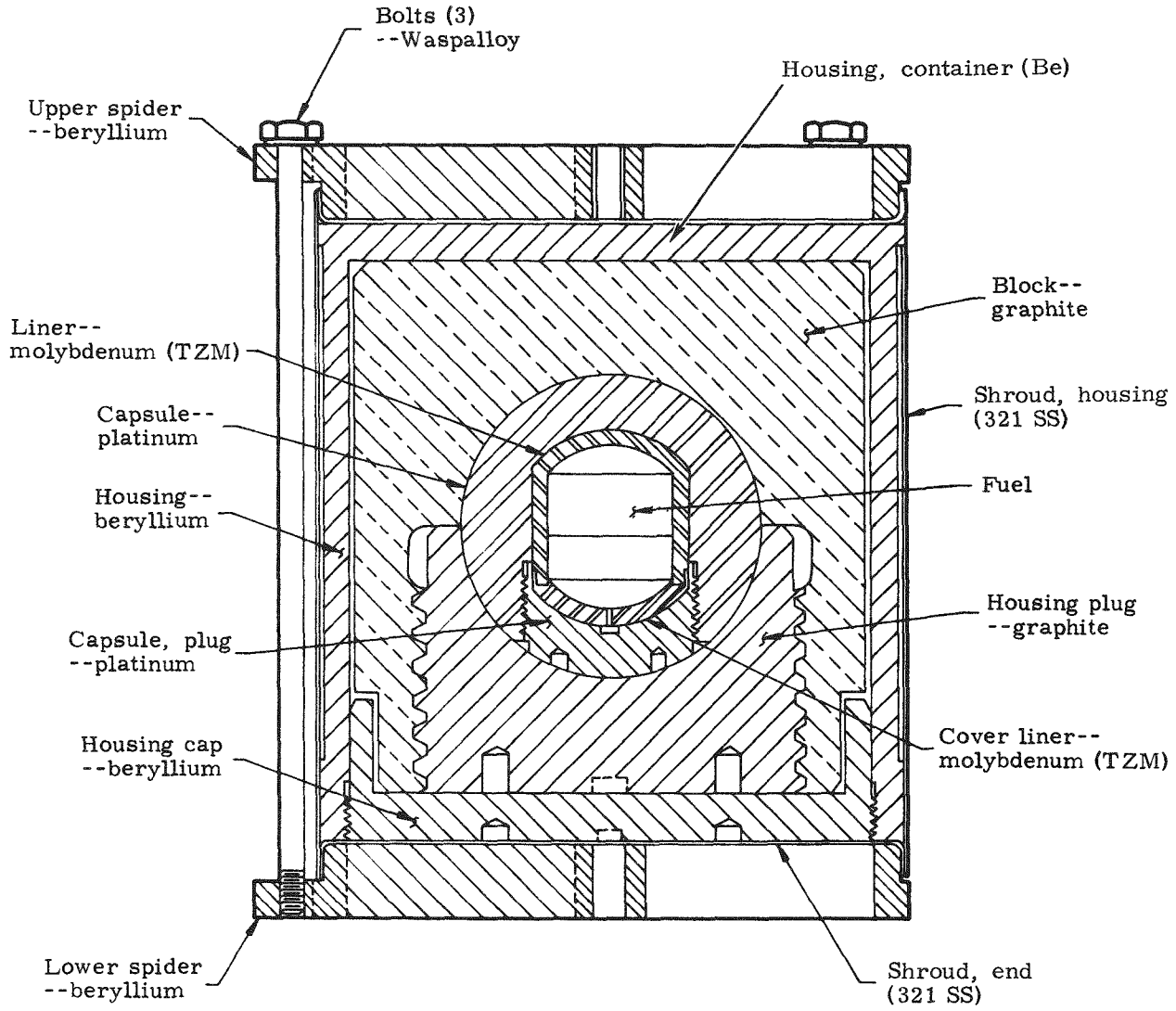

Fig. V-1. Fuel Block Assembly (original design)

due to anticipated problems in welding in pure helium (rather than argon), and due to anticipated higher fuel block surface temperatures during operation. Table V-1 is a summary of a thermal analysis for this fuel block, and leads to the conclusion that there may be a fuel release for the case where the fuel block is sealed with an argon gas fill or if the shroud is ruptured and vacuum gaps are developed at the heat transfer interfaces. This conclusion was based on a maximum recommended operating temperature for the TZM capsule of 2000° F.

TABLE V-1

Fuel Block Temperature Distribution
(original design)

	Temperatures		
	Door Open (normal)		
Location	Vacuum(1)	Argon(1)	Helium(1)
Fuel block surface	1300	1300	1300
Outer surfaces (°F)			
Be	1628	1540	1361
Graphite	1840	1760	1422
Platinum	2960	1910	1508
TZM	4490	3060	1840
Inner surfaces (°F)			
Platinum	3022	1970	1570
TZM	4520	3090	1870

(1) Interfacial atmosphere

As a result of this review, a change in the fuel block design and the original approach to encapsulating the isotope heat source was initiated to enhance the chance for successful fueling. The AEC allowed the additional degree of freedom, i.e., that the resultant block no longer had to meet the original requirements for flight safety. Rather, the revised goal for SNAP 11 was to fuel a system oriented toward demonstrating safe operation in a controlled laboratory environment.

For demonstration purposes, the following ground rules were established for the design:

(1) The envelope dimensions were limited to previous values for compatibility with the existing generator design.

(2) Materials were limited to those established in the previous fuel block with the exception that the fuel block housing would be changed from a Type 321 stainless steel shroud (with Be holddown spiders) to an all Haynes-25 enclosure.

(3) The general fuel block configuration was retained. That is, the block was comprised of a TZM primary capsule contained within a platinum capsule followed by enclosures of graphite, beryllium and Haynes-25.

(4) Double containment, if possible, was to be provided to reduce the possibility of a fill gas leak from the fuel block.*

Objectives established for the design effort were to:

(1) Make provisions for remote handling and assembly of the fuel block components in the hot cell.

(2) Develop satisfactory weld joint designs for remote welding of the TZM, platinum and Haynes-25.

(3) Develop radial interface gaps consistent with the remote assembly of components and nominal temperature operation of the fuel block in the generator.

(4) Establish structural integrity at operating temperatures and pressures.

(5) Provide about 24 cm^3 internal volume in the TZM capsule (previous capsule was only 12 cm^3).

Based on the ground rules and objectives, the SNAP 11 fuel block was redesigned. This new fuel block design is shown in Fig. V-2. Briefly, the revised fuel block consists of a TZM capsule, platinum capsule, graphite and beryllium housings and a Haynes-25 sealed container. The tapered TZM capsule is the prime fuel container but requires protection from air to prevent oxidation. This protection is pro-

* The concept was later changed to a single shroud machined from a single piece of bar stock. This is discussed later.

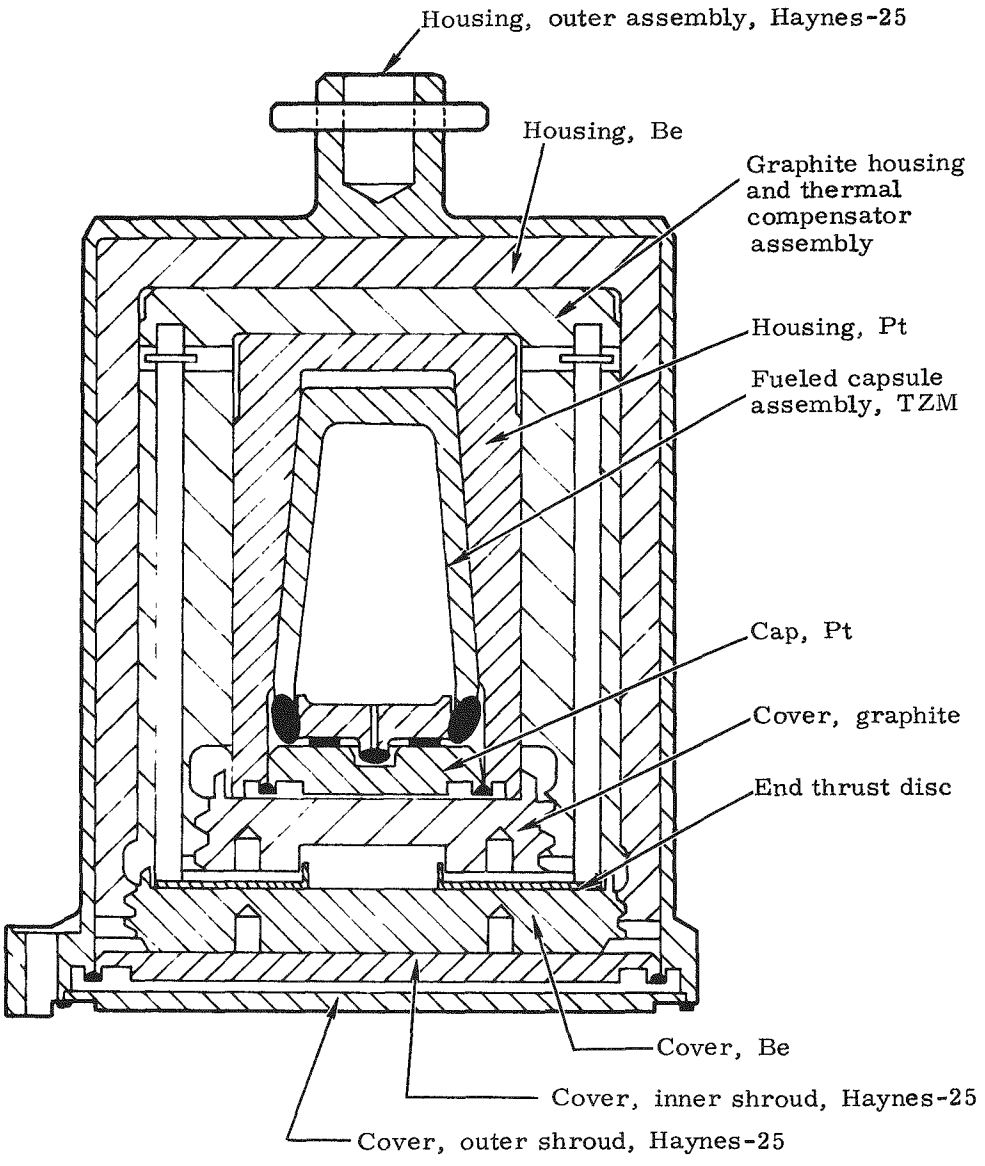

Fig. V-2. Redesigned Fuel Block Assembly

vided by the platinum secondary capsule which was originally designed into the system for impact, radiation shielding and corrosion protection. The graphite and beryllium housings were required in the original fuel block for intact earth re-entry purposes and have been retained in this design as specified by the ground rules. The Haynes-25 outer container maintains an inert gas fill during system vacuum operation to reduce thermal drops across the several interfaces. Further, the Haynes-25 provides a seal and prevents oxidation of the beryllium and graphite during operation in air. The surfaces of the Haynes-25 are stably oxidized in air during component fabrication to achieve a highly emissive surface. For the demonstration fuel block, redundant covers are welded in place as a guard against loss of the inert fill gas.

Two important concepts were introduced in the fuel block redesign to achieve the desirable radial gaps for minimum thermal drop. First, a taper was introduced at the TZM-platinum interface. Second, to eliminate a large gap at the graphite-beryllium interface, it was decided to preheat the Haynes-25-beryllium housing to ~1300° F during assembly. The graphite-platinum-TZM subassembly could then be inserted into an already expanded beryllium housing and thus the gap between the graphite and the beryllium would be minimized. At the remaining two interfaces (i.e., beryllium-Haynes-25 and platinum-graphite), the inner material expands faster than the outer material. This means that, with proper dimensioning at ambient conditions, a minimal gap can be attained at all interfaces. Using an iterative process between thermal and thermal expansion analyses, a set of nominal gaps were established together with a corresponding temperature profile. Those values were used to determine the feasibility of the conceptual fuel block design. Subsequently a set of maximum-minimum axial gap conditions was established corresponding temperature profiles calculated and a thermal expansion analysis performed to determine fabrication dimensions and tolerances. A summary of this final iteration is given later in this section. Once the radial gaps and temperatures were established, corresponding axial thermal expansions were calculated. This established the required axial dimensions and tolerances.

From the thermal and thermal expansion analyses, it was determined that the fuel block and its components will be subjected to a number of temperature cycles during the assembly (see Fig. V-3). Because of differential thermal expansion, interferences between fuel block components will occur during a number of phases of the hot cell fueling operation. The effects of temperature cycling on the fuel block assembly and subassemblies were investigated and it was determined that the most adverse temperature cycle would be experienced between the completion of fuel block assembly until the time the fuel block reaches temperature equilibrium inside the generator. Therefore, only the temperature cycling of the total fuel block was investigated in detail.

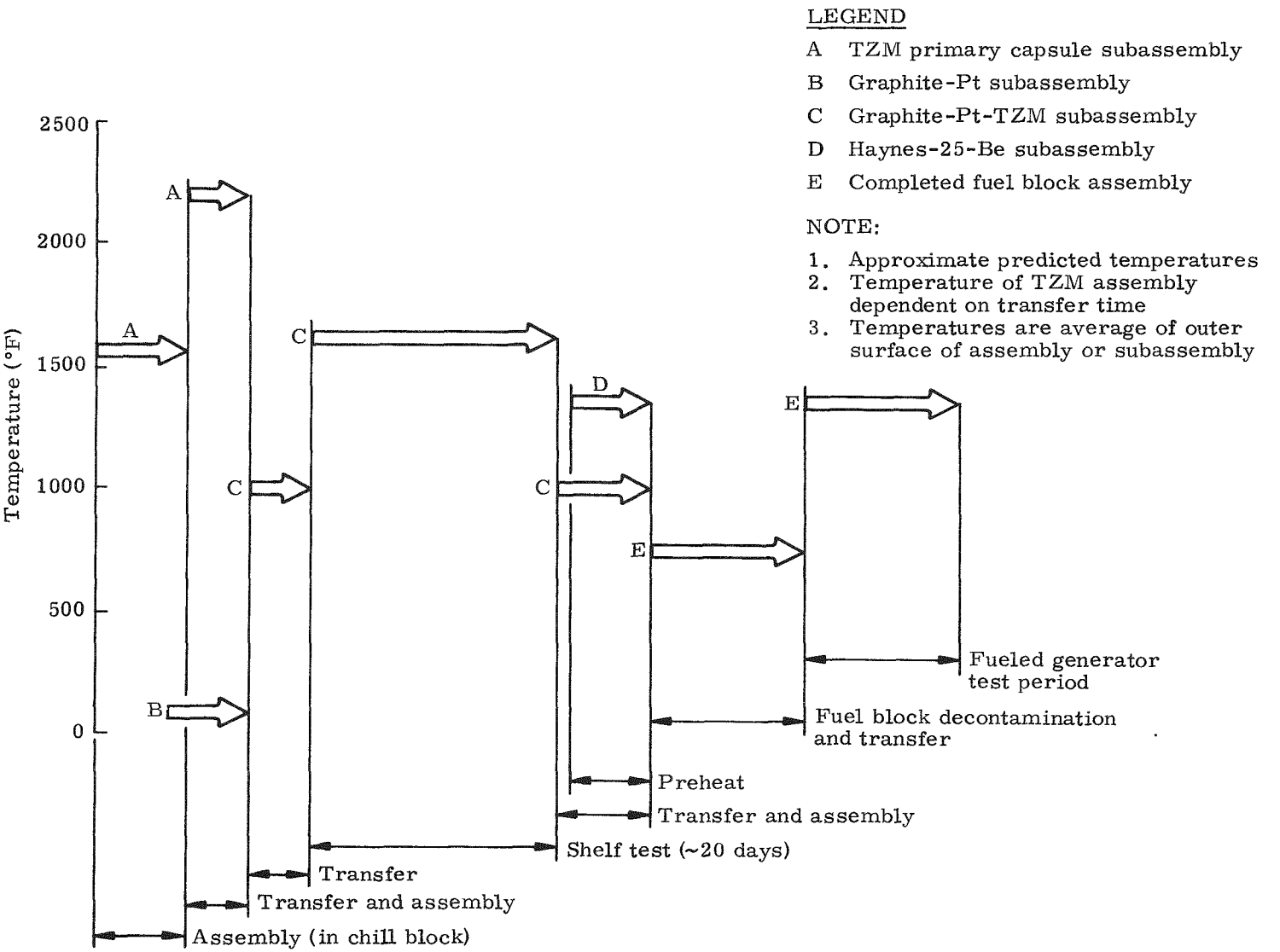

Fig. V-3. Anticipated Temperature Cycle Flow Chart for Fuel Block Components

The thermal cycling of the fuel block assembly was found to cause no adverse effect except at two interfaces. At the radial TZM-platinum interface, deformation of the platinum will occur as a result of lowering the fuel block temperatures during decontamination and transfer operations. Once the fuel block is brought back to operating conditions, a gap results between the TZM and platinum. It was determined that this gap will not be too severe as long as the fuel block is not allowed to cycle below 800° F on the Haynes-25. The other area where an undesirable interference would occur is at the beryllium-Haynes-25 axial interface. To eliminate this problem, a thermal compensator was designed into the graphite block. The operating principle of the thermal compensator is described later in this section.

Another area requiring considerable design effort was the Haynes-25 shroud. Originally, a concept which utilized a double-walled container was contemplated. This concept was changed in favor of a single heavy wall shroud machined from a single piece of bar stock. This approach was used to eliminate as many welds as possible and to simplify the manufacturing operations. The concept of using a final redundant weld was retained.

Other areas which were investigated and designed accordingly were: TZM primary capsule weld; handling and assembly of the fuel block into the generator; material compatibility; and, structural integrity of the fuel block components. The following is a list of the design efforts in these areas:

(1) A TZM primary capsule weld joint design was generated jointly with ORNL. Weld overhang and weld penetration were the primary considerations.

(2) Handling and assembly problems were discussed with ORNL and the fuel block components were designed and sized so that only minimum difficulties would occur during hot cell operation.

(3) Material compatibility was considered and proper cleaning of all fuel components was specified. Where two incompatible materials (e.g., TZM-Pt) exist in the fuel block, additional material thickness was allowed.

(4) A stress analysis was performed and the fuel block components were sized accordingly.

(5) Consideration was given to the transfer of the fuel block from the hot cell and its assembly into the generator. The fuel block handling tool was reviewed and simplified; the hexagonal nuts used to hold the electrical heater block in the generator were deleted and replaced by special nuts which could be handled with a remote tool.

The new fuel block design was then reviewed. The following comments represent a general evaluation of the design prior to the fueled generator demonstration test:

(1) Lack of compatibility data on the fuel source and TZM was perhaps the weakest point in the fuel block design. Although some data on Cm-244 (oxide) was available before fueling, the fueled SNAP 11 generator itself was to provide the first meaningful study of compatibility of the Cm-242 (oxide) fuel with the TZM primary capsule.

(2) The present fuel block design is oriented toward laboratory use only and is not satisfactory for an intact re-entry flight article. Numerous changes would be necessary for this system to be launched successfully and for intact re-entry. To make the fuel block flight worthy would require redesign of the platinum cap, beryllium plug and Haynes-25 cap in order that the fuel block could withstand launch and re-entry conditions.

(3) This revised block basically reflects the state-of-the-art in re-entry that existed near the commencement of the SNAP 11 program (~1962) and as such is somewhat antiquated. If the block were redesigned for actual flight purposes, a different design approach would be investigated using current analytical techniques and test data.

(4) The thermal analysis of the block in the event of total weld failures, i.e., the vacuum condition, was considered conservative to the extent that conduction heat transfer between mating parts was not taken into account.

(5) The TZM primary capsule was shown to be structurally adequate for a 120-day life if the capsule temperature does not exceed 2000° F and full penetration at the cover-to-body weld joint is obtained. For normal operating conditions, the Haynes-25 shroud was also shown to be adequate.

(6) In the event of abnormal operating conditions, the following conclusions were made as a result of the stress analysis:

    (a) Haynes shroud--the analysis indicated that if the TZM capsule fails, the Haynes-25 cylindrical section should not rupture during the 120-day test (30-day shelf test 90-day performance test in generator). The analysis also indicated that high stresses are induced in the flat cover plates and at the cylinder-to-cover weld junction. Since these stresses are highly localized and exist in the

weld area, failure of the Haynes-25 shroud was assumed upon failure of the TZM capsule. This condition was assumed because the weld characteristics (efficiency, ductility, etc.) could not be defined and, hence, could not be structurally accounted for.

(b) Fuel capsule--later in this section, times-to-rupture for the TZM capsule are approximated for a condition which assumed loss of the Haynes-25 shroud (loss of gas fill and therefore a higher temperature). This evaluation accounted for loss of the shroud at various times after fuel block assembly and for several assumed TZM temperatures.

Although, in most instances, a reasonable theoretical period of time was shown to be available before TZM failure after loss of the shroud, from a safety standpoint loss of the TZM capsule was assumed to occur at the time of shroud failure. It was felt that this approach must be taken because of the following undefined areas which could not be accounted for in the theoretical analysis:

(1) TZM temperature after shroud failure could not be accurately predicted though believed to be conservative.

(2) The Larson-Miller stress-rupture parameter for TZM was questionable because of the limited number of test data points used to develop same.

(3) The actual cover-to-cylinder weld characteristics (efficiency, penetration, ductility, etc.) were not known and, hence, could not be accounted for. Those weld characteristics were, however, specified and determined in the weld development effort.

(4) TZM compatibility with fuel at the anticipated elevated temperatures if the Haynes-25 should fail was not known.

b. Final fuel block design

The overall concept of the fuel block is shown in detail in Fig. V-4. As was previously pointed out, the ground rules for the redesign of the fuel block specified that the envelope dimensions be limited to previous values and the materials limited to those established in the previous fuel block with the exception that the outer housing was changed from a Type 321 stainless steel shroud and beryllium spiders to a Haynes-25 enclosure. The design of each fuel block component is discussed.

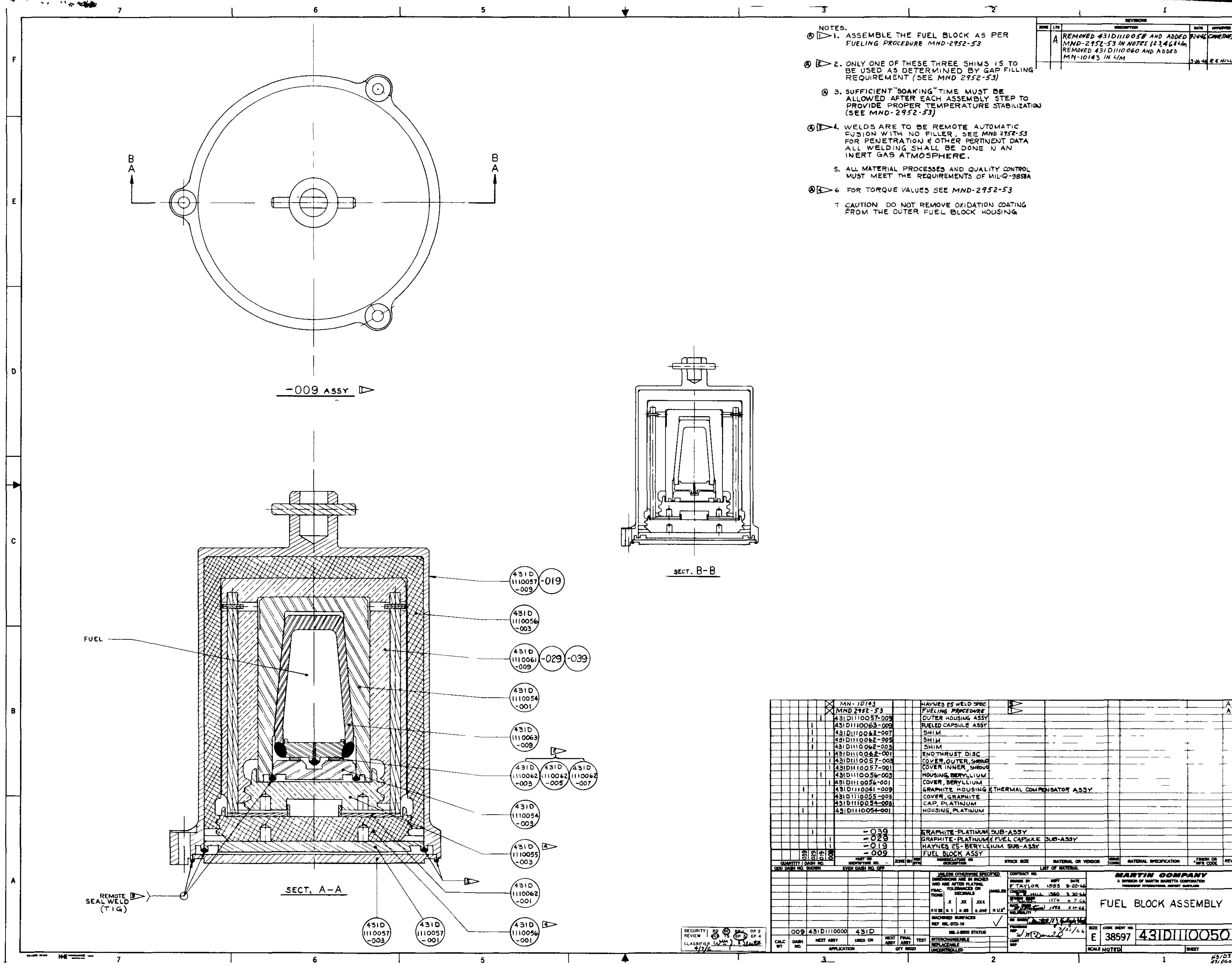

039	029	019	009	PART OR IDENTIFYING NO.	NOMENCLATURE OR DESCRIPTION	STOCK SIZE	REV
			X	MN-10143	HAYNES 25 WELD SPEC	5	A
			X	MND 2952-53	FUELING PROCEDURE	1	A
		1		431D1110057-009	OUTER HOUSING ASSY		
	1			431D1110063-009	FUELED CAPSULE ASSY		
	1			431D1110062-007	SHIM		
	1			431D1110062-005	SHIM		
	1			431D1110062-003	SHIM		
			1	431D1110062-001	ENDTHRUST DISC		
			1	431D1110057-003	COVER, OUTER, SHROUD		
			1	431D1110057-001	COVER INNER, SHROUD		
		1		431D1110056-003	HOUSING, BERYLLIUM		
			1	431D1110056-001	COVER, BERYLLIUM		
1				431D1110061-009	GRAPHITE HOUSING & THERMAL COMPENSATOR ASSY		
	1			431D1110055-003	COVER, GRAPHITE		
	1			431D1110054-003	CAP, PLATINUM		
1				431D1110054-001	HOUSING, PLATINUM		
	1			-039	GRAPHITE-PLATINUM SUB-ASSY		
			1	-029	GRAPHITE-PLATINUM & FUEL CAPSULE SUB-ASSY		
			1	-019	HAYNES 25-BERYLLIUM SUB-ASSY		
				-009	FUEL BLOCK ASSY		

Fig. V-4. Fuel Block Layout

TZM primary capsule. The TZM, a molybdenum base alloy (0.5% Ti, 0.07% Zr, balance Mo), serves as the prime barrier for the Cm_2O_3 fuel source. As such, it is mandatory that reliable welds be developed, and that all reasonable steps be taken to maintain the capsule below 2000° F during normal operating. In working toward the latter objective, a tapered TZM-to-platinum interface was established which serves to minimize the radiant gap for heat transfer purposes as well as enhance the ease of remote assembly. To accommodate this taper, the capsule geometry was changed from spherical to cylindrical. This taper would eliminate any large gaps which would have caused an excessive temperature drop, and would facilitate the insertion of the hot (fueled) primary capsule into the platinum while using remote operation. For analytical purposes, a one-mil average gap was assumed at the tapered interface although it was believed a tighter fit was attained by seating the TZM into the platinum.

The TZM cap and body have been designed for a full penetration tungsten inert gas weld. Because of the high melting point of TZM, a vent hole has been provided in the cap to prevent a blowout of the main weld during the welding operation. This vent is then sealed by inserting a tapered pin and making a fusion weld. Since the final seal weld was considered the weakest point in the TZM primary capsule from a fuel compatibility standpoint, it was desirable to obtain at least 40 to 60 mils penetration. For this reason, the pin concept with a locking taper was introduced to allow sufficient time to obtain the minimum desired weld penetration.

In addition to the change in geometry, the TZM primary capsule has also been increased in size. A 24-cm^3 internal volume has been provided in anticipation of the possibility of low power density fuel and to provide additional void volume for helium gas pressure buildup. In light of the new size, and an operating temperature close to 2000° F, the capsule design was stress analyzed. Sufficient capsule wall and cap thicknesses have been allowed to provide a conservative design under normal operating conditions. In addition, 20 mils of material have been allowed both inside and outside of the capsule for material compatibility.

Platinum secondary capsule. The three functions of the platinum surrounding the TZM are to provide a gamma shield for the fuel, impact protection on re-entry and an oxidation barrier for the primary refractory capsule. Since the fuel block was intended for fueling demonstration purposes, the re-entry impact protection criteria was relaxed to ensure successful fueling. Therefore, during the redesign effort, the original concept of a threaded platinum cap was eliminated to reduce the complexity of the fueling operation. Instead a cap was substituted with provisions for a fusion seal weld. This weld would not possess sufficient strength for impact purposes but served to seal the TZM primary capsule against an oxidizing atmosphere in the event the Haynes-25 outer shroud failed.

To accommodate the new size and geometry of the TZM primary capsule, the platinum body was designed with a taper on the inside, was increased in size and was changed externally from a sphere to a right circular cylinder. The inside bottom surface has a relief to prevent the TZM from bottoming out as it mates to the taper. A TZM shim is provided between the platinum and TZM caps for height control. This provides alignment between the platinum cap and body for proper seal welding.

Graphite housing. The graphite was basically unchanged from the previous design except for new dimensions and the addition of thermal compensator rods. The purpose of the compensator rods is to minimize the adverse effects of temperature cycling of the fuel block during decontamination and transfer operations. Since graphite has a much lower coefficient of expansion than beryllium or Haynes-25, it was found that a severe temperature cycle (from ~1300° F assembly condition to ~750° F transfer operation, Haynes-25 ref.) would cause sufficient interference at the Haynes-25 cap-beryllium plug interface to cause a failure of the Haynes-25 seal weld. For this reason, the graphite housing was designed undersized. Thermal compensator rods were then chosen with a thermal expansion coefficient which closely matched the coefficient of beryllium. Thus, the compensators, by expanding and contracting at almost the same rate as the beryllium housing, maintained the graphite-beryllium interface gap at the heat rejection end of the fuel block to a minimum. At the same time the compensators contracted sufficiently during temperature cycling to avoid any stressing of the Haynes-25 weld joints.

Beryllium housing. The only change in the beryllium housing, other than geometrical and dimensional changes to accept the new graphite housing, is that the 4-inch diameter 16 UN-2A thread has been changed to a 60-degree stub thread similar to the one used on the graphite housing. This thread makes the assembly of the in-cell beryllium plug much easier.

Haynes-25 shroud. In addition to the change of materials (Type 321 SS to Haynes-25), an effort was made to provide double containment at the outer shroud to ensure against loss of the gas fill during operation in the thermal vacuum chamber. In the double containment concept (Fig. V-5), a set of concentric (20 mils) shrouds welded to two end members (plus provisions for redundant welds at final closure) provides the enclosure for gas fill containment. It was found that this concept would require intricate machining of the two end members to make the welding of the thin concentric shrouds possible. In addition to difficult machining operations, there would have been a need to develop, test and qualify all the welds required for the fabrication of the container. Finally, it was found that differential thermal expansion between the inner and outer concentric walls would stress the weld areas sufficiently

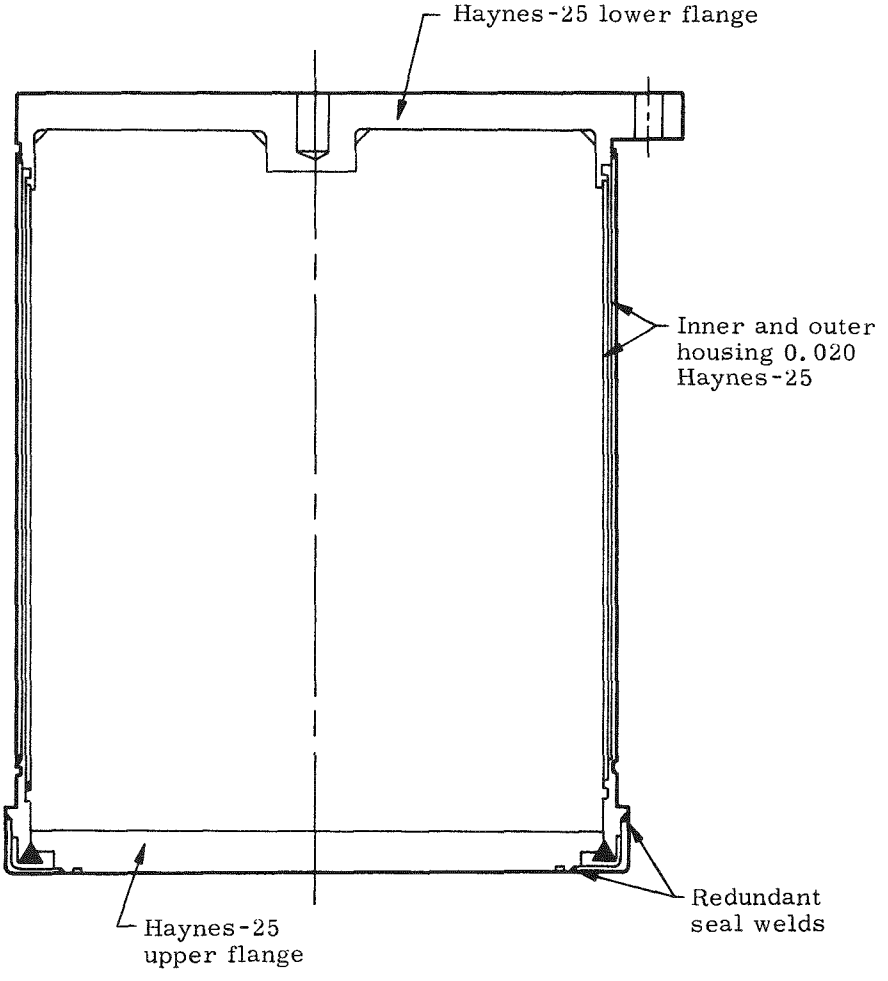

Fig. V-5. Haynes-25 Shroud--Double Containment Concept

to cause a failure. Therefore, it was decided that a double-walled container would not provide sufficient reliability and would actually compromise gas fill containment. Instead, the double shroud and top end member were replaced by an integral container (Fig. V-6) which was machined from a single piece of bar stock. The machined piece was then inspected to ensure that no cracks, inclusions or defects of any kind existed. For a closure after fueling, two end caps were welded for redundancy. Finally, instead of the double 20-mil concentric shrouds, the machined Haynes-25 shroud was made 100 mils thick, thus providing some additional strength in the event of a TZM rupture.

c. Thermal analysis

In designing the fuel capsule and other fuel block components for normal operating conditions, it was necessary to determine the temperature profile in the fuel block at beginning-of-life conditions (see Appendix A). These calculations were performed with argon* as the fill gas at all interfaces, with a thermal inventory of 813** watts, and for the following two cases:

(1) Maximum design gaps at all interfaces

(2) Minimum design gaps.

For these calculations it was assumed that the outer surface of the fuel block was 1400° F, a necessary requirement to radiate the excess heat through the generator shutter door opening.

A layout of the new fuel block was made, and nominal dimensions were established and used in this thermal analysis.

Maximum and minimum gaps (at temperature) as follows were used:

Interface	Radial Gaps (mils) Minimum	Maximum
Haynes 25-beryllium	1	5
Beryllium-graphite	16	20
Graphite-platinum	0.5	4
Platinum-TZM (tapered fit)	1	1

*Some helium was included since it was used for welding purposes and to allow detection of a leak during operation in a vacuum chamber. Since argon has the lower thermal conductivity, the calculations are conservative.

**For this analysis the capsule was assumed to be loaded with ~925 watts, and the generator fueled upon completion of the capsule shelf test and fuel block assembly (~30 days).

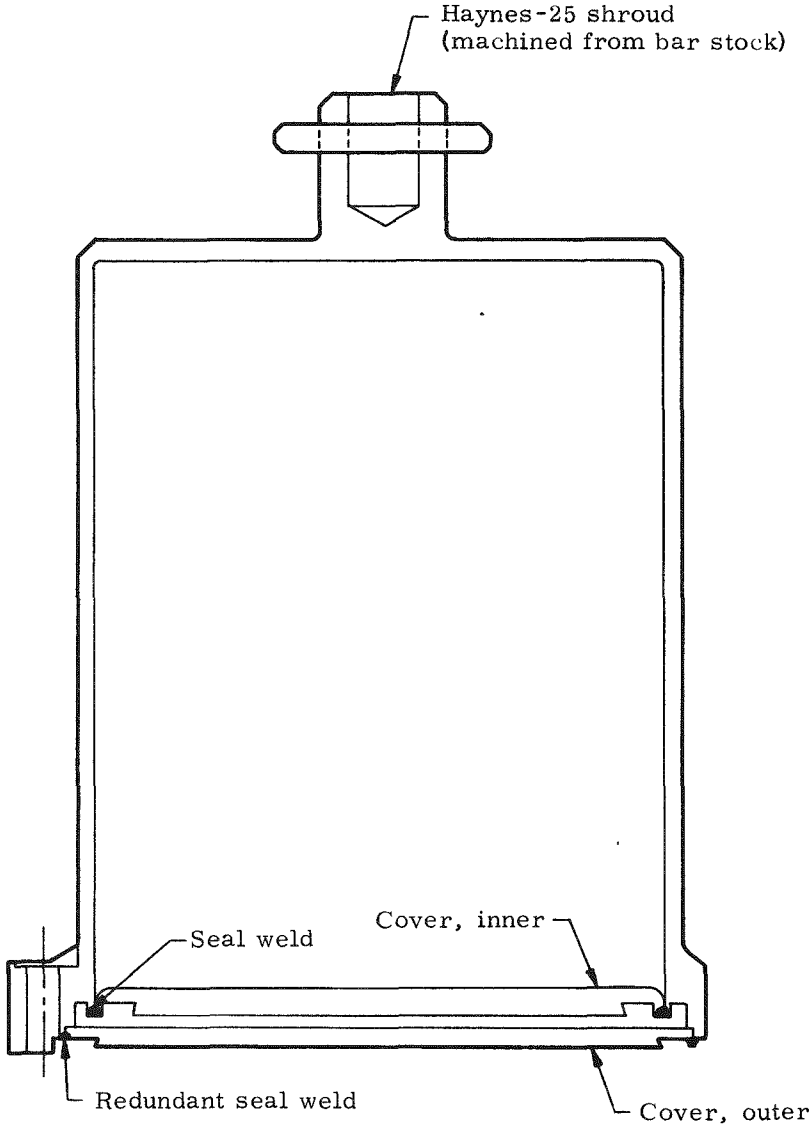

Fig. V-6. Haynes-25 Shroud--Alternate Concept

These gaps were derived by an iterative process between thermal analysis and thermal expansion analysis coupled with tolerances defined on each part at room temperatures.

Table V-2 presents the resulting fuel block temperature profile at beginning of life (813 watts inventory) for the two cases with argon as the gas fill:

(1) Maximum at-temperature intercomponent gaps

(2) Minimum at-temperature intercomponent gaps.

TABLE V-2

Thermal Analysis of Fuel Block in Generator*
Normal Operation at Beginning of Life

	Hot Gaps (in.)		Temperature (°F)**	
Material	Maximum	Minimum	With Maximum Gap	With Minimum Gap
Haynes-25			1400	1400
	0.005	0.001		
Beryllium				
Outer			1478	1446
Inner			1483	1451
	0.020	0.016		
Graphite				
Outer			1634	1594
Inner			1656	1616
	0.004	0.0005		
Platinum				
Outer			1886	1648
Inner			1919	1681
	0.001	0.001		
TZM				
Outer			2041	1813
Inner			2054	1826

*q = 813 watts; argon gas fill in all gaps
**Average

For normal operation with maximum gaps, the temperatures derived are conservative for the following reasons:

(1) Argon was assumed to be the fill gas. A certain percentage of helium was used by ORNL during welding. The effect of a helium additive was favorable.

(2) It is unlikely that maximum gaps could occur simultaneously at all interfaces.

(3) The maximum gaps used provide for a ± 10% variation in the expansion coefficients of TZM, platinum and graphite, a ± 5% variation in beryllium, and a ± 2% variation in that of Haynes-25. It is unlikely that the expansion coefficients varied this much and even more remote that the errors stacked up in the worst possible way considering the number of materials involved.

(4) No credit was made for heat transfer between adjacent materials because of direct contact between the materials.

(5) The outer surface temperature of the fuel block (Haynes-25) was assumed to be 1400° F, a maximum temperature necessary to dump the excess heat out of the shutter. The actual temperature was much lower and, as a result, all internal temperatures were also lower.

During fuel block assembly, it was necessary to know the surface temperature of several of the components as they reached equilibrium in the argon environment of the hot cells. These temperatures were computed for the Haynes-25 shroud, the graphite enclosure and the platinum* capsule. The results are summarized in Table V-3 and were used to determine the effects of temperature cycling during successive assembly steps in the hot cell. All component temperatures have been computed under the assumption that the components are suspended in the argon and are not exposed to additional cooling by contact with a water-cooled hot cell floor or other solid objects.

TABLE V-3

Component Surface Temperatures During Successive Hot Cell Assembly Steps

	(°F)
TZM capsule	2800
Platinum capsule	2170
Graphite housing	1050
Haynes-25 shroud	785

*Surface of platinum is normally not directly exposed for free convection but housed inside graphite. This calculation was of interest in the event the graphite was dropped during fuel block assembly and exposed the platinum.

Since the final fuel block assembly at equilibrium in the hot cell represented the worst temperature cycle for all components, the temperatures of the other components inside the fuel block were also computed for both maximum and minimum gap cases. Those results are summarized in Table V-4.

TABLE V-4

Thermal Analysis of Fuel Block During Assembly*

	Hot Gaps (in.)		Temperature (°F)	
Material	Maximum	Minimum	With Maximum Gap	With Minimum Gap
Haynes-25			785	785
	0.006	0.002		
Beryllium				
Outer			900	830
Inner			905	835
	0.010	0.006		
Graphite				
Outer			1100	975
Inner			1122	997
	0.0057	0.0017		
Platinum				
Outer			1602	1153
Inner			1635	1186
	0.001	0.001		
TZM				
Outer			1786	1370
Inner			1799	1383

*q = 813 watts; argon gas fill for all gaps

Finally, a thermal analysis was performed to examine possible failure modes which could result in the loss of fuel containment during operation of the fuel block inside the generator. Two possible conditions were considered. First, the effects of a vacuum condition inside the fuel block (total failure of both welds on the Haynes-25 shroud and failure of the platinum seal weld) were investigated. Second, an analysis was performed to determine the generator temperatures in the event of a generator open circuit condition.

Calculations for the internal vacuum condition were performed both at the beginning-of-life condition (813 watts(t)) and at the end of life (555 watts). The results are presented in Table V-5. The vacuum thermal analyses must be considered conservative since no allowance was made for contact between the parts. In particular, at the platinum-graphite interface, the drop is greater than 1000° F. However, after

only a few hundred degrees increase in the platinum temperature, an interference fit would occur and enhance the heat transfer. If excessive temperatures were encountered on the TZM (such as are predicted by the vacuum analysis), the TZM would yield and the resulting elongation would produce a favorable contact pressure at the Pt-TZM interface.

TABLE V-5

Thermal Analysis of Fuel Block in Generator* for Vacuum Condition With Door Open

Material	Emissivity	Temperature (°F)** q = 813 Watts	Temperature (°F)** q = 555 Watts	Melt Temperature (°F)
Haynes-25	0.90 (oxidized)	1400	1400	2425 to 2570
Beryllium				
Outer	0.60	1584	1550	2341
Inner	0.60	1589	1555	
Graphite				
Outer	0.70	1795	1710	--
Inner	0.70	1817	1725	
Platinum				
Outer	0.16 to 0.20	2860	2600	3217
Inner	0.16 to 0.20	2893	2623	
TZM				
Outer	0.20	4040	3640	4730
Inner	--	4053	3649	

*No allowance for contact conduction between fuel block components.
**Average.

A thermal investigation of the generator open circuit condition was performed which indicated that the temperature of the fuel block would be approximately 1440° F on the Haynes-25 shroud. This small rise from the normal design operating temperature (1444° F maximum) would result in a further opening of the generator thermal shutter to reject the additional heat energy. In addition, it is extremely unlikely that an internal open circuit would occur since the generator employs T/E couples in a series-parallel array. Either two adjacent elements would both have to fail, or the internal wiring would have to fail. A more likely type of open circuit is an opening in the generator external circuit. It was concluded, therefore, that this failure mode would have no appreciable effect on fuel containment.

d. Thermal expansion analysis

In the redesign of the fuel block, particular attention has been given to the thermal expansion analysis. There are two reasons why this was done. First, the change in component geometry and dimensions, and the change of the outer shroud materials required that new ambient temperature dimensions be calculated. Second, the initial fuel block temperature profile analysis revealed that the temperature of the TZM primary capsule was at best marginal for the desired 120-day life. As can be seen from Fig. V-7, the expansion coefficients for each material in the fuel block are spaced over a wide range and are temperature dependent. The changes of geometry, dimensions and temperature profile together with the thermal expansion characteristics of the materials prompted a detailed thermal and expansion analysis.

The effort was initiated by making a layout of the redesigned fuel block which reflected the desired changes (i.e., increased TZM primary capsule volume, Haynes-25 shroud, etc.). This layout was used to establish nominal dimensions at operating conditions. Through an iterative process between thermal analysis and thermal expansion analysis, together with tolerances which had been established on the previous fuel block, a set of nominal radial gaps was derived. Those gaps were reviewed and maximum-minimum desirable gap conditions were established. The maximum-minimum gaps were then used to establish maximum-minimum fuel block temperature profiles.

Using those two temperature profiles, an average anticipated temperature profile was obtained and from this profile nominal ambient temperature dimensions were established. Next, using machining tolerances and a ± 10% allowance for analytical and thermal coefficient of expansion errors, actual maximum-minimum gaps were calculated on the basis of the average temperature profile. The dimensions and tolerances were then judged acceptable if the minimum calculated gap was larger than the desired minimum gap and if the maximum calculated gap was smaller than the desired maximum gap. Table V-6 summarizes the result of the radial expansion analysis. As can be seen, the only gap which does not meet this requirement is the Haynes-25-beryllium radial gap. Since the temperature drop across the gap is small compared to the other gaps and the deviation from the requirement was not too great, it was concluded that further iterations would not be necessary.

Once radial gaps were established and the corresponding temperature profile calculated, an analysis of the axial thermal expansion was made. This was found to be considerably easier to perform since no iteration process was required. Nominal dimensions of the components were established for assembly condition (1300° F on the Haynes-25 shroud) and thermal expansions were calculated. From this, ambient temperature dimensions and tolerances were established. The only criteria imposed

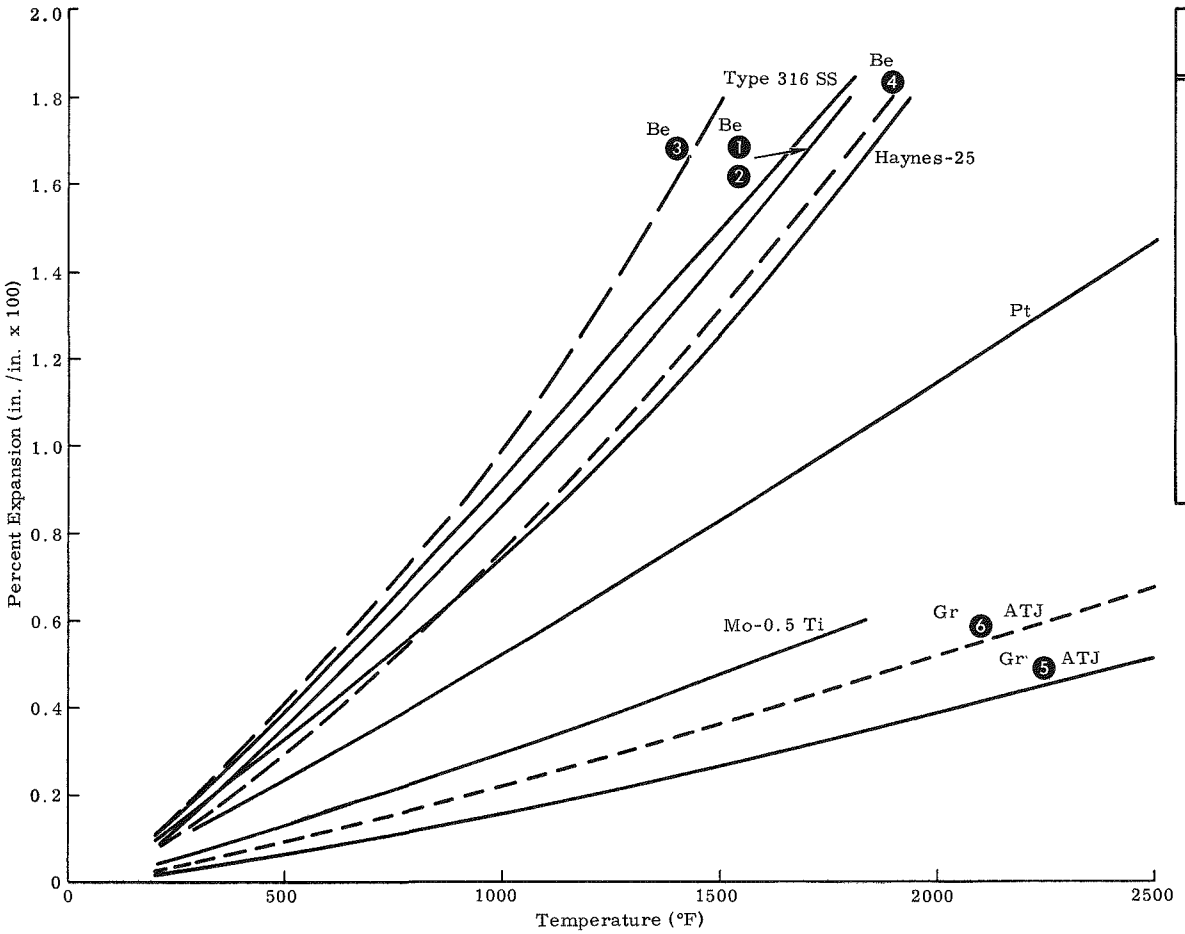

	Alloy	Base Temperature (°F)	Grain Direction	Ref.
1	Be as-cast and hot extruded	77	With grain	1
2	Be hot pressed	77	With grain	1
3	Be hot pressed	77	Against grain	1
4	Be as-cast and exit	77	Against grain	1
5	Gr (ATJ)	70	With grain	2
6	Gr (ATJ)	70	Against grain	2
	Haynes-25	70	-	3
	Pt	40	-	5
	Mo-0.5 Ti	68	-	4
	Type 316 stainless steel	70	-	6

References

1. Reactor Handbook
2. The Industrial Graphite Engineering Handbook, National Carbon Co., April 1964
3. "Haynes Alloy No. 25," Haynes Stellite Company, March 1959
4. "The Engineering Properties of Molybdenum and Molybdenum Alloys," DMIC Report 190
5. "High-Temperature Structure and Thermal Expansion of some Metals as Determined by X-ray Diffraction Data," J. Appl. Phys., Vol. 22 (4), pp 424-428
6. Aerospace Structural Metals Handbook, ARDC TR 59-66, March 1963

Fig. V-7. Percent Thermal Expansion per Linear Inch from Base Temperature to Indicated Temperature

TABLE V-6

Radial Gaps--Operating Condition

Interface	Desired Gap (in.) Maximum	Desired Gap (in.) Minimum	Nominal Desired Gap (in.)	Nominal Average Material Temperature (°F)	Computed Ambient Dimensions (radius)	Computed Gap (in.) Maximum	Computed Gap (in.) Minimum
Haynes-25 to Be	0.005	0.001	0.003	1400	1.937 +0.001 -0.000	0.008	-0.004 (interference)
				1465	1.930 +0.001 -0.000		
Be to Graphite	0.020	0.016	0.018	1465	1.643 +0.001 -0.000	0.020	0.017
				1625	1.645 +0.001 -0.000		
Graphite to Pt	0.004	0.000	0.002	1625	1.000 +0.001 -0.000	0.004	0.000
				1784	0.991 +0.001 -0.000		
Pt to TZM	0.001	0.000	0.0005	1784	Tapered fit	--	--
				1934			

CONFIDENTIAL

on those dimensions was that the worst possible tolerance and analysis error stackup could not result in more than a ± 0.020 inch mismatch at the inner Haynes-25 cap weld area. Allowing a ± 10% analysis error, it was found that the mismatch requirement could be met. Finally, axial differential expansions from assembly to operating conditions were investigated. The rise in temperature from one condition to the other was found to be too small to have any effects.

The final area which was investigated in the thermal expansion analysis was the effects of temperature cycling on the fuel block assembly and the graphite-platinum-TZM shelf test* subassembly. Temperature cycling conditions occur as a result of natural cooling during transfer operations, decontamination, etc. In analyzing the fuel block and shelf test subassembly, it was found that an almost identical set of temperature cycling conditions existed for the graphite platinum and TZM during the shelf test as during transfer and decontamination in the fuel block. Therefore, only the temperature cycling of the total fuel block was investigated.

Only two adverse conditions were found to exist in the fuel block for a temperature cycle from assembly conditions to natural cooling condition (~750° F on the outer shroud) and back to operating condition. First, it was found that, when cooled, the platinum would shrink onto the TZM and deform itself. Then, as the temperature is brought back to operating condition, a gap would result at the platinum-TZM tapered interface. It was computed that this gap will be 0.0013 inch maximum. Since this is very close to the 0.001 inch gap used in the thermal analysis, it was decided that a cycle down to 800° F on the Haynes-25 is tolerable and that any cycling below this temperature will have adverse effects. A second area of concern was found to exist at the Haynes-25 cap-beryllium plug interface. During temperature cycling the graphite shrinks at a much slower rate than the Haynes-25 shroud. The result would be stresses in the Haynes-25 seal welds that would cause the welds to fail and, most probably, the gas fill would be lost. To eliminate this problem, a thermal compensator has been designed into the graphite housing. With this compensator, a maximum interference of 0.001 inch has been estimated under cycled conditions, thus eliminating any detrimental effects on the seal weld.

In this thermal expansion analysis, a conservative approach has been taken. It is very unlikely that maximum tolerance stackup, together with maximum analytical errors, would occur simultaneously. In addition, the system for the most part is self-compensating. That is, an increase in temperature of the internal materials will cause them to expand, reduce the gaps, reduce the interface temperature drops and thus reduce the temperature of the internal materials. The major conclusion which was drawn from the thermal expansion analysis was that

*Shelf test was 10-day hold period during which the TZM capsule was maintained at operating temperature to determine whether containment was achieved and whether severe incompatibility existed.

the fuel block should not be allowed to go below 800° F on the Haynes-25 (after fueling) and, correspondingly, the graphite-platinum-TZM subassembly should not be allowed to go below 1050° F (based on the graphite temperature).

e. Stress analysis

For design of the TZM capsule, a pressure-temperature study was performed to determine the variation of these properties with time for normal operation. The fuel investigated was curium-242. Using the ideal gas relation, pressure versus time curves were generated (Appendix B) and are shown in Fig. V-8. From the curves, it was found that the maximum pressures occur at a time equal to 1.025 years. After a period of 10 years, the pressure remains constant. The fuel capsule structural analysis was based on the requirements of temperature and pressure predicated by the proposed 90-day generator test. It was assumed that the RTG thermal control shutter maintains the capsule temperature at 2000° F for a period of 120 days after fuel encapsulation. It was also assumed that the capsule internal pressure buildup follows the isotope helium release, based on normal decay, with adjustment for the higher temperature condition imposed by the shutter. A plot of capsule temperature, T, and internal pressure, P, versus time, t, after encapsulation is shown as Fig. V-9. This plot is based on: 930-watt fuel inventory at encapsulation, capsule void volume of 20 cm^3, and a capsule temperature of 2000° F from time of encapsulation to 120 days, whereupon, a normal isotope temperature decay occurs.

A detailed stress analysis of the capsule is presented in Appendix B. Maximum capsule stresses (σ), given as a function of capsule internal pressure, p_c, are summarized as follows:

σ_{b_2} = maximum bending stress = 6.705 p_c in cover (at center)

σ_{h_1} = circumferential stress = 5.68 p_c in cylinder

σ_{b_1} = maximum combined stress = 11.25 p_c in cylinder (at junction).

These stress magnitudes reflect a fuel-to-capsule and platinum-to-capsule material compatibility allowance. Specifically, a 0.020-inch allowance was made on the inside and outside surfaces of the capsule (i.e., assumed both cover and cylinder thicknesses were reduced 0.040 inch from actual values). A plot of the listed stresses versus time after encapsulation is shown as Fig. V-10. The capsule pressure history used corresponds to that shown in Fig. V-9. All stress magnitudes start at 0 psi at encapsulation and build up to a maximum at the end of the test (120 days). The peak stresses at 120 days are:

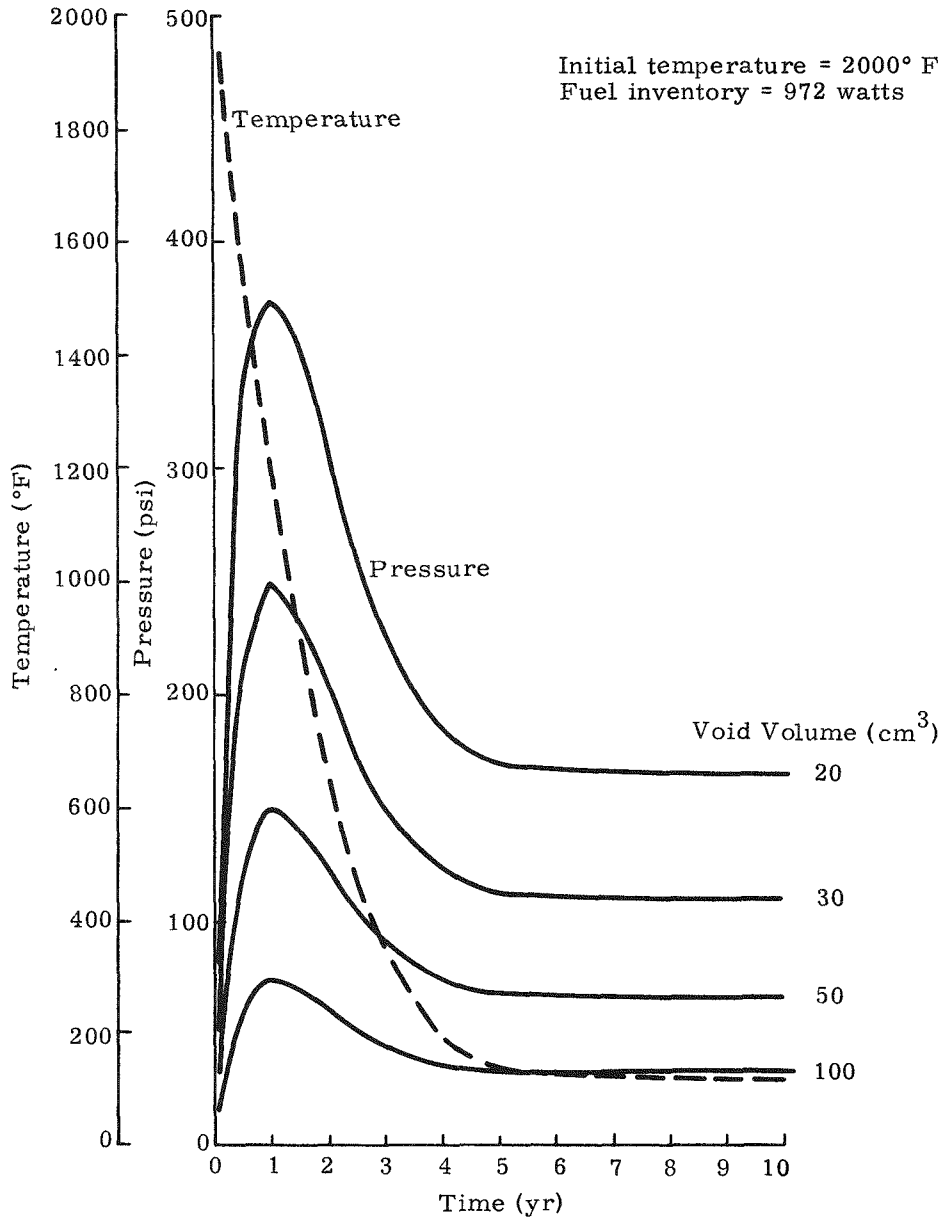

Fig. V-8. Pressure, Temperature Versus Time Curves for Curium Fuel

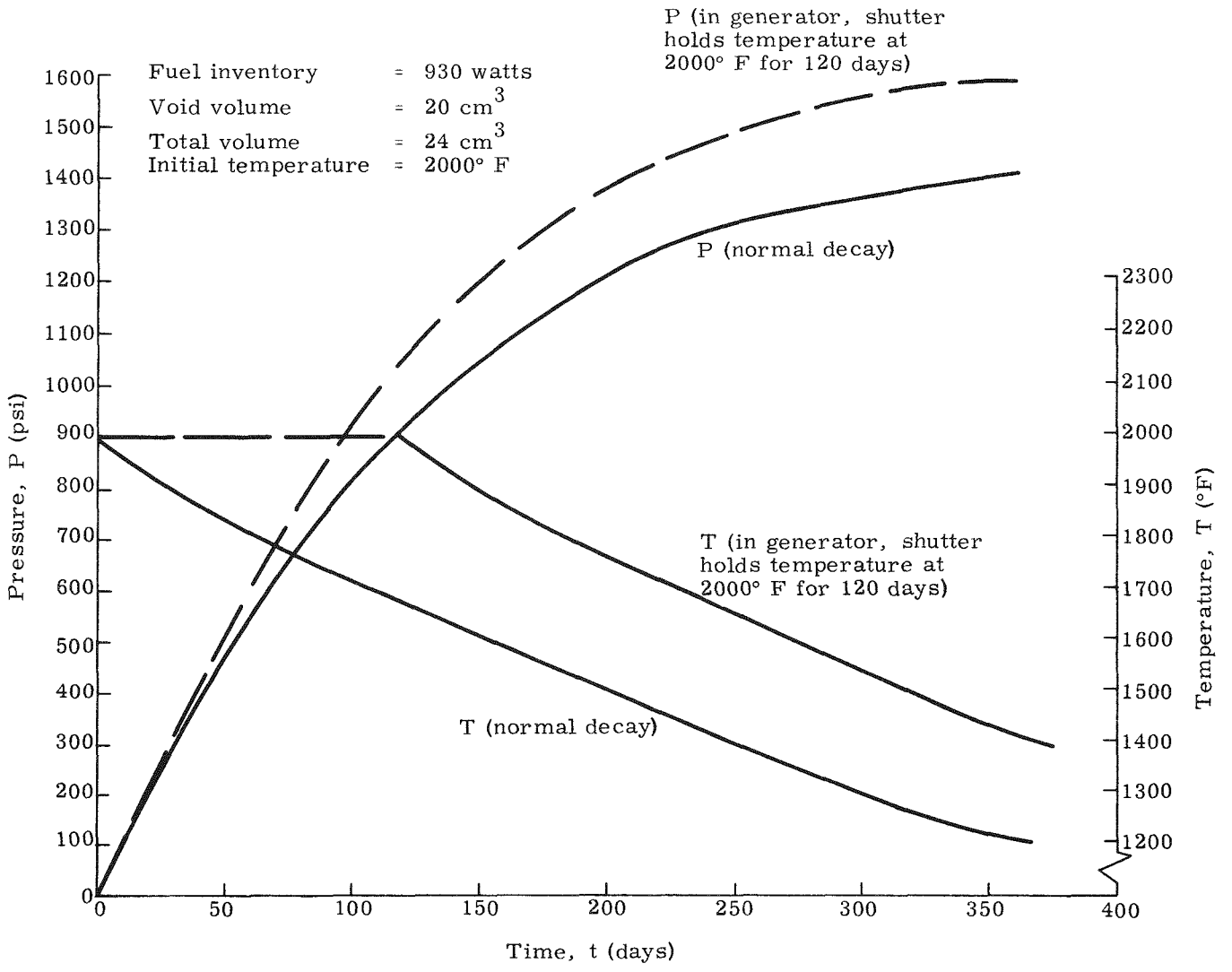

Fig. V-9. Pressure and Temperature Versus Time

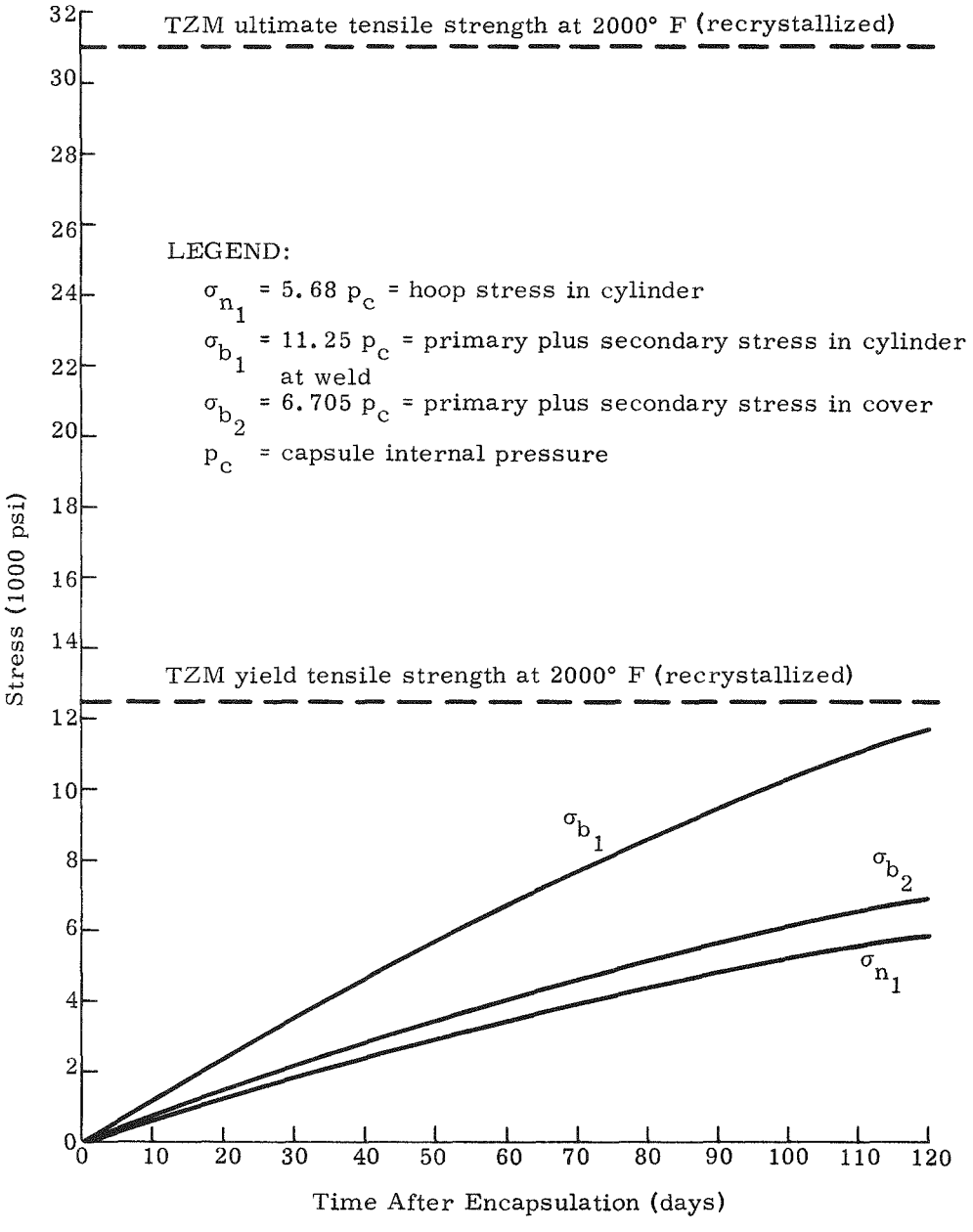

Fig. V-10. Capsule Stress Versus Time After Encapsulation

σ_{b_1} = 11,700 psi, σ_{h_1} = 5910 psi, and σ_{b_2} = 6970 psi.

The fuel capsule is made from the molybdenum alloy, TZM. Since the cover was welded to the cylinder, it was assumed that the material would be in a recrystallized condition.* A plot of ultimate and yield tensile stress versus temperature for recrystallized TZM material is presented in Fig. V-11.

In the literature (Ref. 1, Appendix B), tensile test data for recrystallized TZM is given at only two temperatures: 1800° and 2400° F. To establish strength values at intermediate temperatures linearity was assumed. An upper and lower limit was established for both ultimate and yield strengths by connecting the maximum and minimum stress values with straight lines. For design purposes, the lower limit curves were used; the minimum values of yield and ultimate at 2000° F are shown in Fig. V-10. A Larson-Miller parameter (Ref. 2, Appendix B), which relates temperature, stress, and time to rupture was used for evaluating stress rupture. This parameter is presented as Fig. V-12.

From Fig. V-11 it was concluded that the capsule membrane and secondary stresses would be well below the material ultimate strength at 2000° F and would not exceed the material yield strength at 2000° F over the 120-day period considered. In the literature (Ref. 3, Appendix B), yield strengths as high as 43,000 psi are reported for TZM material in the as-welded condition for stress-relieved 0.040-inch thick specimens automatically fusion welded with no filler material at 2000° F. This is substantially higher than the 12,500 psi yield stress predicted in this analysis (as per Ref. 1 for recrystallized TZM).

At 2000° F, recrystallized TZM is well into the creep range of the material (the threshold for creep occurs at about 1600° F). Hence, it was felt that comparison of stress magnitude with short time materials properties above 1600° F would be misleading and of little practical value since stress rupture could be critical. Stress rupture data are developed from tensile test procedures, hence, only membrane stresses were compared with rupture data. In the TZM capsule, the maximum membrane stress occurs in the cylinder side wall at the large diameter end and was computed to be 5910 psi at 120 days after encapsulation. For pressure vessel design, the maximum allowable stress, based on rupture, was taken as 60% of the average stress necessary to produce rupture over the vessel design life. For this design, a life of 120 days was assumed and the maximum temperature (2000° F) and pressure (1040 psi) were conservatively considered to act over the entire period. For these conditions, the rupture stress was calculated by use of the Larson-Miller parameter (see Fig. V-12) as follows:

*Capsule material is initially in stress-relieved condition and would be subject to recrystallization in area of weld. It was conservatively assumed that the entire capsule would be in a recrystallized state.

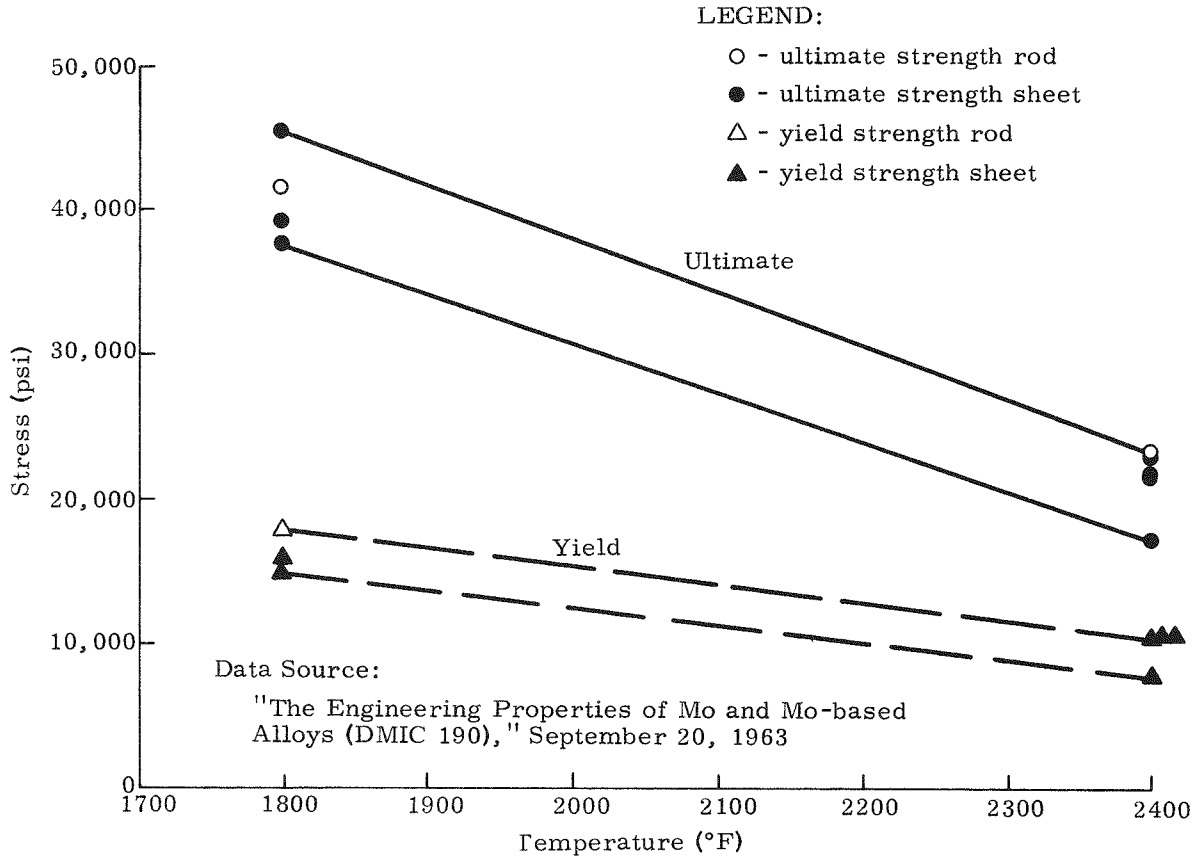

Fig. V-11. Ultimate and Yield Tensile Strength of Recrystallized TZM

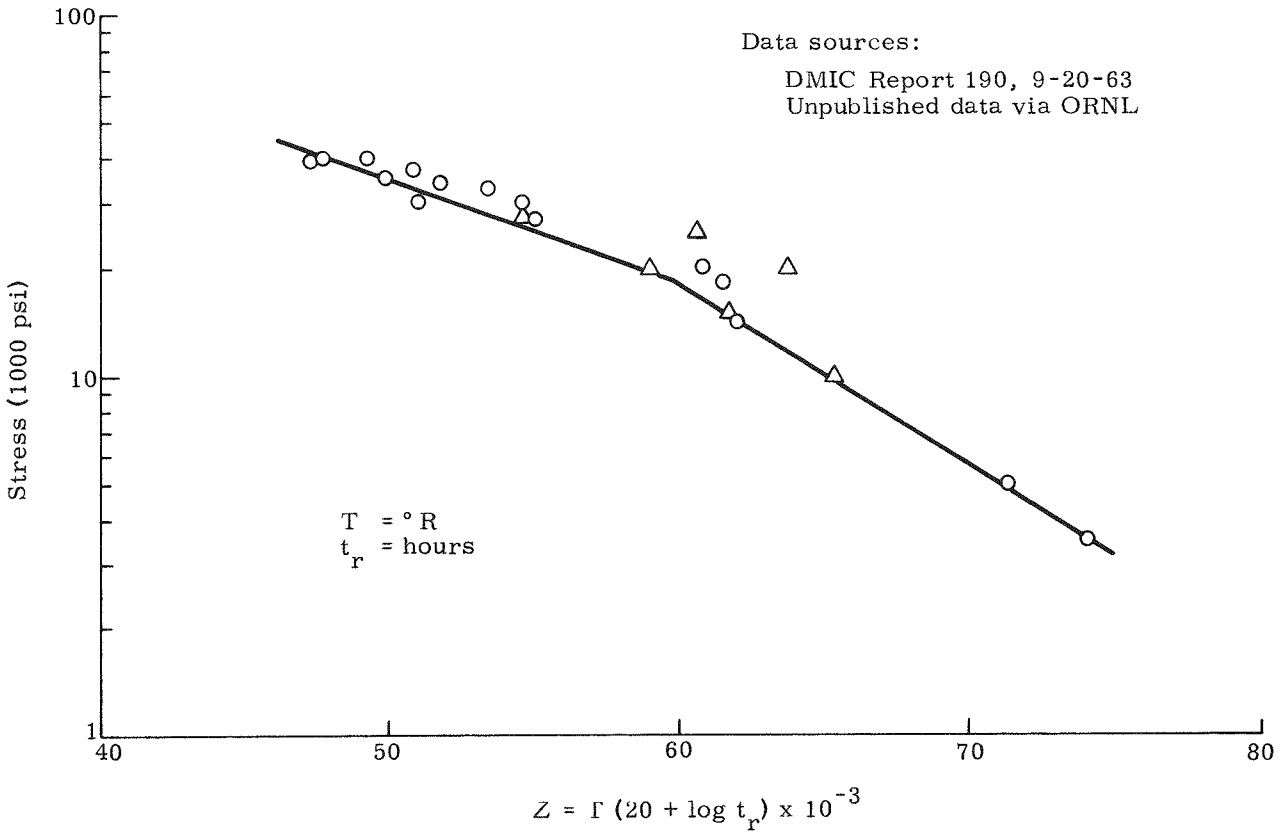

Fig. V-12. Larson-Miller Master Rupture Curve for Recrystallized TZM (Mo-0.5 Ti-0.08 Zr-0.03c)

CONFIDENTIAL

$$Z = \text{parameter value} = T\,(20 + \log t) \times 10^{-3}$$

where:

T = absolute temperature = 2460° R

t_r = time = 120 days = 2880 hours

thus:

$$Z = 57.6$$

From Fig. V-12 a stress-to-rupture value of 21,000 psi was found. Based on 60% of stress-to-rupture, an allowable stress of 12,600 psi was obtained. It was felt that the capsule would meet the rupture criteria.

Since the maximum combined membrane plus secondary stress at the cover-to-cylinder junction approaches the TZM yield stress at 2000° F at the end of life, it was felt that, based on creep, local yielding would occur. Since these stresses are highly localized and consist primarily of bending stresses, the TZM material should allow local yielding and subsequent load redistribution and lowering of stress levels due to its relatively high ductility at 2000° F (minimum elongation, as per Ref. 3, for recrystallized bar at 2000° F is 24%).

In this analysis no allowance was made for stress concentrations. The possibility that a stress raiser could occur at the cover-to-cylinder weld junction was considered. Since this is in the vicinity where the highest local stress occurs, it was felt that the presence of a stress raiser could result in a local weld failure at relatively low pressure and corresponding stress level. It was therefore recommended that this weld be fully qualified in the weld development program to show that full penetration would be achieved. If full penetration could not be achieved, it was further recommended that a short time test to failure be conducted. This would require pressurizing a capsule at 2000° F until failure. As a minimum this test would show at what pressure and calculated stress level failure occurred, where failure occurred, and the magnitude of deformation the capsule experiences during failure.

For design operating conditions of the Haynes-25 shroud, an internal pressure of 17.9 psia was assumed (based on 1400° F maximum shroud temperature). Based on a cylindrical side wall thickness of 0.1 inch and a 4-inch diameter, a cover plate thickness of 0.150 inch, and a cover-to-cylinder weld penetration (inner cover) of 0.060 inch, the following stress values were obtained:

$\sigma_{h_{sw}}$ = hoop stress in side wall = 370 psi

σ_{b_c} = maximum bending stress in cover = 4200 psi

σ_{s_w} = shear stress in weld = 300 psi

At 1400° F the typical ultimate tensile strength and yield strength of Haynes-25 (0.109 inch sheet) is 66,000 and 37,700 psi, respectively (Ref. 5, Appendix B). Since the calculated stress values were well below the material available strength, the design was considered structurally sound for normal operating conditions.

In addition to the stress analysis for normal operation, a failure analysis was performed. For the analysis of the effect of TZM failure on the Haynes-25 shroud, a failure of the TZM capsule was postulated, whereupon, the Haynes-25 shroud assembly would be required to contain the released helium pressure. The void volume existing at the internal fuel block radial interface gaps is approximately 22.2 cm^3, and since the capsule void volume is 20 cm^3, the internal pressure on the Haynes-25 (L-605) after TZM failure was obtained from the equation:

$$p_{L-605} = p_c \left(\frac{20}{42.2}\right) = 0.475\, p_c$$

where p_c is the capsule internal pressure. For quantitative purposes, a TZM failure at 90 days after encapsulation was assumed. The capsule pressure, p_c, at this time is 840 psi, hence, the Haynes-25 pressure becomes, $p_{L-605} = 17.9 + 0.475\,(840) = 418$ psi or $418/17.9 = 23.4$ times greater than normal operating pressure. Based on this pressure and the shroud geometry, the following stresses were found:

$\sigma_{h_{sw}}$ = 8650 psi (hoop stress in side wall)

σ_{b_c} = 98,250 psi (bending stress in cover)

σ_{s_w} = 7000 psi (shear stress in weld).

Qualitative evaluation of these stress levels led to the following conclusions: the cylinder side wall should not rupture for an extended period; the inner cover weld (neglecting secondary stresses due to constraint) should be structurally adequate; and, the cover plates would yield.

The calculated cover plate stress was above the yield point of the material, hence, it was concluded that permanent deformation would result. Since the plate stresses are flexible in nature, a stress-rupture analysis was not considered to be valid (stress rupture is based on tensile tests). Hence, all that could be done analytically was to assume a deflected shape for the cover and determine if the deflected shape reduced cover stress levels to acceptable limits, and the plate material could assume the deflected shape without failing. Having met both these conditions would not necessarily prove structural adequacy because the cover plate-to-cylinder weld secondary stresses have been neglected. To achieve gross deformation of the cover, large rotations are imposed on the weld joint connecting the cylinder and cover. Calculating stress magnitudes in this joint due to rotation would produce fictitiously high values (much higher than the ultimate strength of the material), but, since these stresses would be primarily flexure, it was felt that local yielding and redistribution of load would result in considerably lower real stress values. To determine analytically if the weld will resist the required local yielding without failing was all but impossible because of the variables involved. Some of these variables are:

(1) Weld efficiency, loss of strength relative to that of the parent material and depth of weld penetration.

(2) Stress raisers (local irregularities present)

(3) Weld material ductility.

To determine the effect of gross deformation on cover plate stress levels, an evaluation was performed and is presented in Appendix B. Assuming a 1/4-inch deformation of the cover at its center, the stress was found to be 10,700 psi which is considerably lower than the 98,250 psi flexure stress found for the undeformed flat plate. A check was then made to determine whether this is attainable (see Appendix B). The percent elongation, e, was found to be 1.155%. The elongation of Haynes-25 (at failure) at 1400° F is 12%; hence, it was concluded that the assumed deformation of the cover could be attained without fracture.

Finally, for the failure analysis of the Haynes-25 shroud, an approximate upper limit failure temperature was found to be 2000° F. This temperature was based on rupture of the side wall in a 150-day period assuming, at assembly, one atmosphere internal pressure present at 1300° F. This is discussed in Appendix B.

Finally, the possibility of a failure of the Haynes-25 shroud at various times after beginning of life was determined. For this case it was assumed that the Haynes-25 shroud develops a leak at some time after the beginning of life. Upon shroud failure, the internal fuel block

interface gaps are again subject to a vacuum condition. In this analysis, four shroud failure times were considered: 30, 60, 90 and 120 days. In addition, four TZM temperatures were assumed: 2200° , 2500° , 2800° and 3000° F.

As in the previous case, the TZM failure was predicted based on stress-rupture of the capsule side wall. The results of this study are presented in Table V-7.

TABLE V-7

Time to Rupture After Shroud Failure

TZM Temperature (°F)	Time After Beginning of Life When Vacuum is Imposed (days)			
	30 Days	60 Days	90 Days	120 Days
2200	365	365	365	365
2500	90	65	40	20
2800	28	3	10 hr	3 hr
3000	4	4 hr	1 hr	1 hr

To determine the failure condition for the TZM at the beginning of life, it was assumed that the Haynes-25 shroud is not leak free at the time of assembly. Hence, the inert gas mixture is lost at all internal fuel block interfaces and heat transfer across interface gaps is by radiation only. With existing gaps it was found that the TZM capsule can attain a theoretical temperature of 3600° F and the platinum 3450° F. In reality, the platinum will grow into the graphite and the TZM will grow into the platinum and these interface gaps will be eliminated or at least minimized. Due to the inability to predict final gaps, the TZM is evaluated for four assumed temperatures: 2200° , 2500° , 2800° and and 3000° F. For this analysis, it was assumed that an internal vacuum condition is imposed at the beginning of life and the time required to rupture the TZM capsule (based on hoop stress in side wall) is determined. Due to the variable pressure and corresponding stress, the capsule history was segmented into reasonable time periods to afford a more realistic evaluation. For each time period considered, the percent of TZM rupture life used was calculated based on the maximum temperature and pressure occurring during the period. A Larson-Miller stress-rupture parameter (see Fig. V-12) for TZM is used for determining the percentage of rupture life used. The predicted total life available is established when the cumulative percent of rupture life reaches 100%.

The results of this study are presented in Table V-8. A sample calculation for determining available life for a specific temperature is presented in Table V-9.

TABLE V-8

Total Rupture Life

TZM Temperature (°F)	Time to Rupture TZM From Time of Encapsulation (days)
2200	>365
2500	120 to 130
2800	40 to 50
3000	25 to 30

B. PREFUELING EFFORT

The primary objective of the SNAP 11 prefueling effort was to establish requirements and procedures to assure a successful, on-schedule fueling. To accomplish this objective, Martin Marietta assisted ORNL in the following areas:

(1) Fueling requirements and procedures

(2) Fuel block weld development

(3) Fueling procedure and facilities checkout

(4) Generator and test facilities checkout.

1. Fuel Processing*

In preparation for the fueling of the SNAP 11 generator, the ORR and MTR reactors were utilized to irradiate 77.4 grams of Am-241, etc., contained in 21 capsules. Five of the capsules were prepared by Martin Marietta Corporation for irradiation in the Materials Test Reactor (MTR); 16 capsules were fabricated by ORNL for irradiation in

*Information used in preparing this section was provided by E. Lamb, ORNL

TABLE V-9

Time After Encapsulation to Rupture TZM Assuming a Constant TZM Temperature of 2500° F

t	Δt	Δt	T_1	T_2	R_1 (1)	R_2		Z (2)	t_r	Rupture Life Used (%)	Cumulative Life Used
		② x 24		④ + 500		⑥ x ⑤/④	5.73 x ⑦			⑩/③ x 100	⑪
(days)	(days)	(hr)	(°F)	(°F)	(psi)	(psi)	(psi)	--	(hr)	(%)	(%)
①	②	③	④	⑤	⑥	⑦	⑧	⑨	⑩	⑪	⑫
0											
	30	720	2000	2500	310	373	2140	78.5	$3.16(10)^6$	0.023	0.023
30											
	10	240	2000	2500	420	506	2900	75.75	$3.98(10)^5$	0.060	0.083
40											
	10	240	2000	2500	515	620	3550	74	$(10)^5$	0.24	0.323
50											
	10	240	2000	2500	600	722	4140	72.7	$3.55(10)^4$	0.677	1.000
60											
	10	240	2000	2500	680	819	4700	71.5	$1.41(10)^4$	1.70	1.700
70											
	10	240	2000	2500	765	921	5275	70.5	$6.3(10)^3$	3.82	5.52
80											
	10	240	2000	2500	840	1010	5790	69.7	$3.16(10)^3$	7.60	13.12
90											
	10	240	2000	2500	915	1100	6300	68.9	$1.995(10)^3$	12.05	25.17
100											
	10	240	2000	2500	980	1180	6760	68.25	$1.26(10)^3$	19.07	44.24
110											
	10	240	2000	2500	1040	1253	7200	67.75	$7.95(10)^3$	30.20	75.45
120											
	10	240	2000	2500	1100	1325	7600	67.3	$4.47(10)^2$	53.75	128.19
130											

t = time after encapsulation
Δt = time increment considered
R_1 = pressure at operating conditions
R_2 = pressure adjusted for increased temperature
= capsule circumferential side wall stress
Z = Larson-Miller stress rupture parameter = $T\ (20 + \log t_r) \times 10^{-3}$
t_r = time to rupture

(1) Ref. Fig. V-9
(2) Ref. Fig. V-12

the Oak Ridge Research Reactor (ORR). After an integrated flux exposure of 1.2×10^{21} nvt in an average effective flux of 1.84×10^{14} n/cm^2-sec, the resultant composition was 35 moles of Cm-242, 35 moles of Am-241, 17 moles of plutonium (Pu-238, Pu-239 and Pu-242), 3 moles of Am-243, and 10 moles of fission products for each original 100 moles of Am-241. The target material was then processed chemically in Cell 1 of the Source Fabrication Facility (SFF). Chemical composition analysis, fuel melting point determination and simulated fuel compatibility with TZM were also performed. Fuel batches were then stored in Cell 2 of SFF for subsequent pressing and encapsulation.

At the time of discharge from the reactor, the targets contained 30 grams of Cm-242 with an equal quantity of Am-241 and several grams of fission products. After the targets were dissolved in hydrochloric acid, a combination of Dapex and Tramex solvent extraction cycles was used to effect a gross gamma decontamination factor of 3.4×10^3. The resultant Cm-242 product was contained in four batches having the composition shown in Table V-10.

The radiochemical purity of the product is shown by a typical gamma ray spectrum in Fig. V-13. The only gamma emissions other than those from curium isotopes are from Ru-103, Ce-144 and Nb-95. The emissions of the predominant gamma impurity, Ru-103 are less than 10% of those from Cm-242. Following the Tramex cycle, the Cm-242 product solution was converted from the chloride to the nitrate form and oxalate precipitations were performed to separate curium from the lithium introduced in the Tramex process and to prepare curium oxide. The Cm-242-Am-241 oxalate precipitate was filtered in several batches containing approximately two grams of Cm-242 each and was calcined to the oxide form by self-heating.

Determination of the fuel melting point and fuel compatibility tests with TZM were also made. The melting points of samples from each batch of the oxide ranged from 1594° to 1760° C. Compatibility couples of TZM and a mixture of 29 wt% Cm_2O_3, 57 wt% CmO_2, and 14 wt% PuO_2, simulating the SNAP 11 fuel mixture 80 days after encapsulation, exhibited no interaction after exposure to 1100° C for 1000 hours.

2. Fueling Requirements and Procedure

The primary goal for the fueling of the SNAP 11 was to establish a system oriented toward safe operation in a controlled laboratory environment. Three basic requirements were established for the fueling operation:

TABLE V-10

Curium-242 Product Ionic Impurities

	MTR Targets		ORR Targets	
	Batch 1	Batch 2	Batch 3	Batch 4
Cm-242 (gm/liter)	0.503	0.50	0.603	0.526
HNO_3 M	6.9	5.0	7.04	5.0
Cl^- (gm/liter)	<0.1	<0.1	<0.1	<0.1
Ni (gm/liter)	0.25	0.26	0.2	0.32
Bi (gm/liter)	--[a]	--	--	--
Pb (gm/liter)	0.1[b]	--	--	--
Ca (gm/liter)	<0.01	<0.1	0.02	0.018
Si (gm/liter)	--	--	--	--
Li (gm/liter)	4.7	6.7	8.65	5.6
Al [b] (gm/liter)	0.033	~0.1	0.1	--
Cr (gm/liter)	0.05	0.042	0.07	0.084
Cu (gm/liter)	0.24[b]	0.005	0.03	0.022
Fe (gm/liter)	--	--	--	--
La (gm/liter)	--	--	--	--
Mn (gm/liter)	--	--	--	--
Mo (gm/liter)	0.01	--	0.045	0.018
Ti (gm/liter)	--	--	--	--
Zr (gm/liter)	0.003	0.021	0.02	0.019
Volume (liter)	11.3	11.75	9.7	11.95
Total Cm-242 (gm)	5.7 (3/9/66)	5.87 (4/2/66)	5.84 (5/5/66)	6.29 (5/23/66)
Decay time since reactor discharge (mo)	~2.5	~2.0	~2.0	~2.0

[a] Dash indicates sought but not found (below detection limit).

[b] Probably sample contamination.

[c] Volume was adjusted to give 0.25 to 0.30 gm/liter of Cm-242.

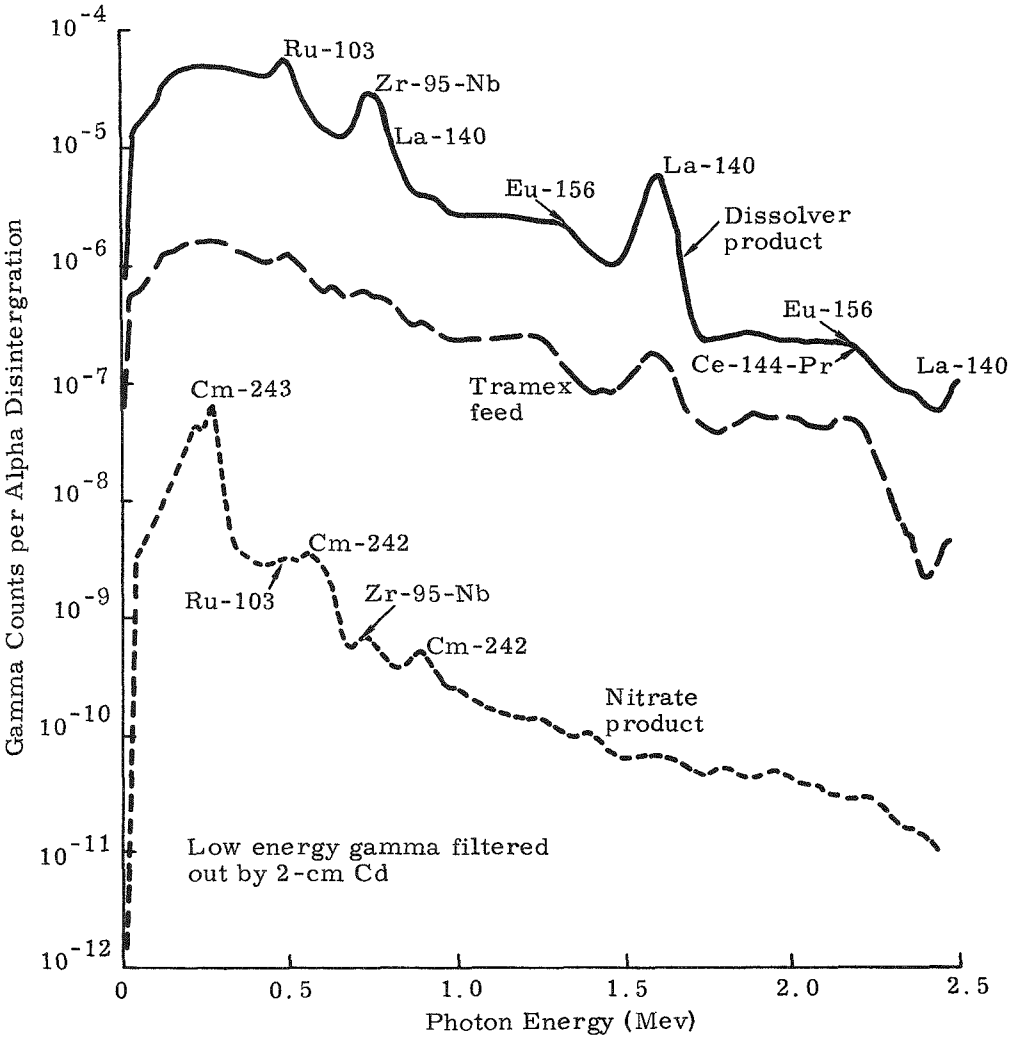

Fig. V-13. Gamma Scans of Principal Streams Handled in Cm-242 Program for 1966

(1) Fuel loading 925 watts (t) $^{+0}_{-25}$

(2) Maximum allowable fuel block outer surface contamination = 20,000 alpha dpm

(3) Fuel containment must be demonstrated.

In addition, the design of the fuel block (see Fig. V-2) dictated that certain assembly procedures be used. Finally, the type of material used for the components of the fuel block required that consideration be given to avoid detrimental material contamination.

The fuel loading of 925 watts (t) $^{+0}_{-25}$ was established on the basis of 813 watts(t) required for the demonstration test plus an excess amount of fuel for a shelf test. This shelf test was included as part of the fueling sequence and was intended to be approximately a 20-day hold period. During this time, the TZM capsule was to be maintained at anticipated operating temperature and periodically helium leak tested to determine whether satisfactory fuel containment was being maintained. Helium gas release from the decaying isotope would serve as the signal gas during this shelf test.

To further assure that safe fuel containment was achieved, satisfactory welds on the TZM fuel capsule, platinum housing and Haynes-25 housing had to be demonstrated. To accomplish this, a weld development program was established and included as part of the prefueling effort. This is discussed later in this section. In addition, TZM weld qualification capsules were introduced in the fueling sequence. The qualification capsule welding was scheduled just prior to and just after welding of the fueled capsule. Thus, by sectioning the qualification capsules, further assurance of a satisfactory closure weld would be obtained.

In addition to fuel containment, gas fill containment within the Haynes-25 housing had to be established. This was considered vital since loss of the gas fill under a vacuum condition would result in an escalation of internal component temperatures. As was previously discussed in Section A, containment of the fuel was determined to be marginal at the temperatures resulting from a loss of the gas fill. To assure gas fill containment, a helium leak test of the Haynes-25 seal welds was added to the fueling procedure. The signal gas for this test would be provided from the helium in the helium-argon gas fill mixture.

Consideration was also given to the handling and assembly of the block in the hot cell. Since the fuel block is made up of a number of components, maximum advantage of out-of-cell subassemblies was taken. As was pointed out in Section A, it was desirable to keep temperature cycling of the fuel block and its subassemblies to a minimum

because of the detrimental effects of differential thermal expansion. Therefore, temperature monitoring and limitations on temperature cycles were introduced into the fueling procedure. In addition, preheating of cold subassemblies was also introduced in the procedure to compensate for differential expansion.

Finally, material temperature limitations and material compatibility were considered. To avoid exceeding the temperature limits of the fuel and fuel block components (especially the TZM fuel capsule), chill blocks were used. In addition, monitoring of the temperatures during critical fuel encapsulation steps was included in the fueling sequence. Material compatibility was also considered and was found to be critical in the case of the TZM capsule. TZM, which is basically molybdenum, oxidizes very rapidly at elevated temperatures, and the liquid oxide of molybdenum is rather corrosive to the base metal. Further, absorption of small quantities of oxygen into the base metal causes large increases in the ductile-brittle transition temperature. Since the surface temperature of the capsule was expected to exceed 1800° F after fuel encapsulation, a hot cell purity of less than 50 ppm of oxygen was specified.

As mentioned earlier, the fuel was chemically processed in Cell 1 of the Source Fabrication Facility. Because of a space limitation, final preparation of the fuel before encapsulation was planned to take place in Cell 2 (pressing of the pellets) and in Cell 3 (conversion to sesquioxide form). Encapsulation of the fuel into the TZM capsule and assembly of the capsule into the preassembled platinum-graphite subassembly was planned for Cell 3. As was mentioned earlier, a high purity atmosphere (argon) was required for Cell 3. Final assembly of the fuel block was planned for Cell 4. This was done to minimize outer fuel block contamination during the final assembly step.

Once these requirements and considerations were established, detailed procedures were prepared for the fueling operation. In its simplest form, the operation consisted of the following steps:

(1) Conduct a TZM qualification weld just prior to the fuel encapsulation operation.

(2) Install the TZM capsule for fueling in the welder.

(3) Insert the curium-242 fuel pellets in the capsule.

(4) Weld the cover on the TZM fuel capsule.

(5) Insert the fueled TZM capsule into the platinum-graphite assembly.

(6) Install the platinum cap but do not weld.

(7) Transfer the TZM-platinum-graphite assembly to the shelf test chamber and raise the temperature of this assembly to that predicted during operation.

(8) Conduct a TZM post-fueling qualification weld.

(9) Conduct a shelf test of at least seven days, and conduct periodic helium leak checks of the TZM capsule.

(10) After the shelf test transfer the TZM-platinum-graphite assembly from the shelf test chamber to the welder, and weld the platinum cap in place.

(11) Remove the subassembly from the welder and install the threaded graphite cap.

(12) Transfer the TZM-platinum-graphite subassembly from Cell 3 to Cell 4.

(13) Establish a cell atmosphere of 65% argon-35% helium.

(14) Install the TZM-platinum-graphite subassembly into the preheated Haynes-25 beryllium subassembly.

(15) Install the threaded beryllium cap.

(16) Install the Haynes-25 primary cap, weld the cap and perform a helium leak check.

(17) Install the Haynes-25 secondary cap, weld the cap and perform a helium leak check.

(18) Smear test the outer surface of the fuel block for contamination level and decontaminate, if necessary.

(19) Transfer the fuel block to the thermal vacuum test facility for installation in the SNAP 11 generator.

(20) Install the fuel block in the preheated SNAP 11 generator.

(21) Initiate thermal vacuum testing of the fueled SNAP 11 generator under simulated lunar environment.

3. Weld Development and Procedure Checkout

In preparation for the fueling operation, a weld development program and a fueling and facilities checkout procedure were established. As mentioned earlier, the weld development program was included to demonstrate that reliable welds could be obtained. The purpose of the fueling procedure and facilities checkout was to determine whether all vital fueling requirements could be met.

For the weld development program the following procedure was established:

(1) The ORNL was to weld 15 TZM weld development samples on the bench outside of the hot cell. These samples duplicated the weld joint area of the capsule and were approximately one-third the length of the actual capsule. The configuration of the samples is shown in Fig. V-14. These samples were to be used to refine the weld joint design and to determine proper welding conditions.

(2) ORNL was to weld three Haynes-25 weld development samples on the bench outside of the hot cell. These samples were to duplicate the top one-third of the Haynes-25 container and were to be used for establishing weld settings. These samples are shown in Fig. V-15.

(3) A dry run assembly was to take place outside of the cell on one fuel block assembly, and was to include full-scale welds on the TZM, platinum and Haynes-25 assemblies. Appropriate preheating to simulate the fuel was to be included; and welding was to take place in the actual welding equipment planned for in-cell welding.

(4) The full-scale out-of-cell welded fuel block was to be diagnostically sectioned and, if there were no significant changes, as a result of this prototype, a similar full-scale in-cell assembly was specified to demonstrate both the remote assembly operations and the welding of the full-scale components under remote hot cell conditions.

Welding effort on the TZM weld development samples revealed that a modification was required to the weld joint design. This change was required to assure full penetration without cracks in the tungsten inert gas (TIG) weld and to prevent excessive weld overhang at the outside diameter of the capsule. After redesign of the joint, the welding was successful. Figure V-14 shows a view of the final joint design.

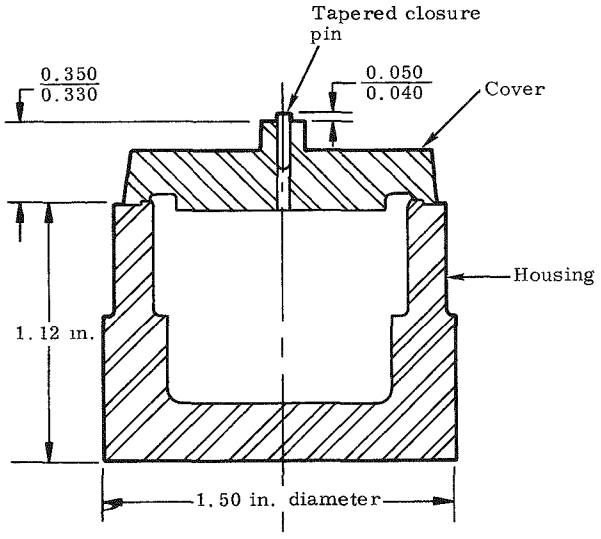

Fig. V-14. TZM Weld Development Sample

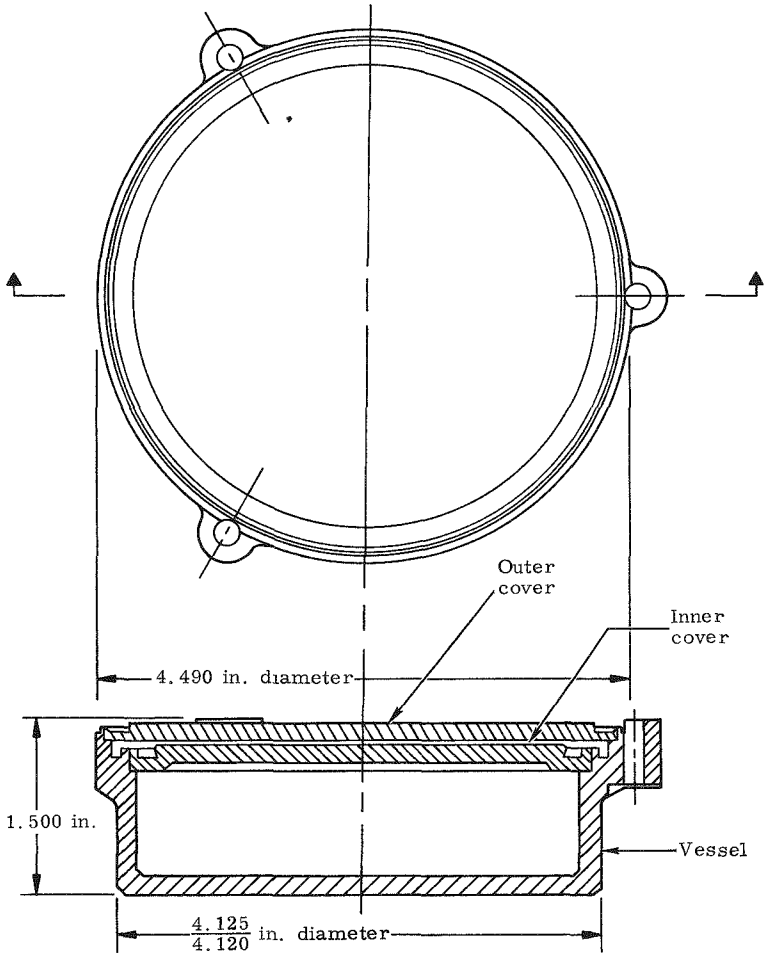

Fig. V-15. Haynes-25 Weld Development Sample

Following successful welding of the TZM weld development samples, problems were encountered by ORNL in welding the full-scale TZM capsules in that occasional small cracks occurred at the root of the weld. These root cracks were attributed to the rapid cooldown of the capsule body following welding. The chill block used with the full-scale TZM capsules was a split tapered chill block made of copper, and it was believed that this chill block was considerably more efficient than the one used with the TZM weld development samples. It was concluded during the actual fueling operation that the ~900 watts of isotope heat would prevent the TZM capsule from cooling rapidly and re-entering the brittle zone, thereby preventing cracking in the weld.

Preliminary investigations of the Haynes-25 development samples welded by ORNL indicated that very good results had been obtained. The welds appeared satisfactory under external examination, and helium leak checks indicated a leak-tight weld. Sectioning and photomicrographs, however, exhibited evidence of occasional small cracks in the heat affected zone (toward the inside the capsule) along grain boundaries. Further, it was noted that grain sizes in the parent material were larger than those normally present in Haynes-25. The cracks were at first believed to be caused by technique, but were later attributed to a bad heat of Haynes-25 material.

As a result of the problems encountered during the weld development program, the following conclusions were established:

(1) Even though some problems were being experienced in weld cracks in the TZM and Haynes-25 components, the fueling operation should proceed in accordance with the established detailed procedure. As discussed earlier, it was believed that the isotope heat source would prevent the TZM capsule from cooling down too fast and would thereby prevent occurrence of the small cracks.

(2) The decay of the isotope inventory did not allow time to procure and manufacture new Haynes-25 containers which might have eliminated the cracking problems. Since the occasional cracks were small and were located at the root of the weld in the parent material, it was considered unlikely that the cracks would propagate to the surface and release the fuel block inert fill gas during the demonstration tests.

(3) To meet the oxygen purity requirement, ORNL installed a purification train in Cell 3. The ORNL hot cells are not designed to be gas-tight and even with the purification train, the atmosphere purity proved to be very difficult to control. After considerable effort was spent in sealing the cells and in developing techniques, the requirement for <50 ppm O_2

was achieved for cases where the manipulators were not being used. Use of the manipulators, however, produced a pumping action, and this caused the oxygen contaminant in the inert gas to increase slowly. Therefore, it was concluded that if the hot cell gas purity was allowed to reach <50 ppm O_2 before the start of any particular series of manipulator movements, the O_2 impurity would not exceed 300 ppm during the movements. A continuous plot of actual O_2 concentration would be maintained during the encapsulation operation and subsequent transfer operations.

4. Generator and Test Facility Checkout

Two SNAP 11 generators, Q/N-2 and Q/N-1M, were shipped from Martin Marietta to ORNL. The Q/N-2 generator, together with a field test kit, was shipped at an earlier date to allow initial checkout of the test instrumentation and vacuum facility. Data were obtained from the Q/N-2 generator for both lunar day and lunar night conditions. A review of the data showed satisfactory results and, after final changes in instrumentation, it was concluded that the test facility was satisfactory for the fueled generator demonstration test. In addition, this initial test run made with the Q/N-2 generator allowed ORNL operators to become familiar with the hardware to be tested.

Following the initial checkout of the test facility, the Q/N-1M generator was shipped. Upon arrival at ORNL, a Martin Marietta representative was present to monitor unpacking, initial inspection and to assure proper storage of the Q/N-1M unit. The Q/N-1M (cold demonstration) and the Q/N-2 (hot demonstration) generators were then used in simulating the fueling operation. In the cold fueling demonstration, the electrical heater block was removed from the Q/N-1M prior to initial generator heatup, and the ORNL weld development fuel block was used in a simulated fueling operation. After development fuel block and holddown assemblies were properly fitted in the Q/N-1M unit, a hot fueling demonstration was performed on the Q/N-2 generator by the ORNL technicians who would perform the actual fueling.

Initial heatup of the Q/N-1M unit was performed on June 24 and air performance data obtained. The initial air test data as well as data taken prior to fueling are compared in Table V-11 to data previously obtained at Martin Marietta. Direct comparison of the data is difficult since the generator was on a different type stand at ORNL and was positioned at the door of a vacuum chamber whose cryowall was heated to prevent condensation. However, examination of generator internal resistance, R_i, open circuit voltage, E_{oc}, and contact resistivity, C_T, values indicates generator performance was virtually the same as when tested at Martin Marietta.

TABLE V-11

Q/N-1M Generator Air Performance Data for Electrically Heated Unit

	MM Data (6-6-66)	ORNL Data (6-24-66)	ORNL Data (6-27-66)	Prefueling (7-12-66)
P_{in} (watts)	808	820	810	800
P_{out} (watts)	25.65	25.4	24.95	25.2
$\overline{HJ}$ temperature (°F)	974	1008	987	986
$\overline{CJ}$ temperature (°F)	343	371	359	360
R_L (ohms)	0.284	0.299	0.295	0.341
R_i (ohms)	0.288	0.309	0.301	0.293
E_{oc} (volts)	5.439	5.599	5.479	5.450
E_L (volts)	2.700	2.757	2.711	2.929
I_L (amp)	9.5	9.2	9.2	8.6
C_T ($\mu\Omega$-cm^2)	~750	~750	~750	~750
Operating time (hr)	300	325	400	755

The electrically heated Q/N-1M generator was also checked out in the ORNL vacuum facility under both simulated lunar night and lunar day conditions. A comparison of the ORNL and the Martin Marietta vacuum test data is given in Table V-12. Figure V-16 compares the data graphically. As can be seen, data agreement with the previous testing at Martin Marietta was satisfactory. The slightly lower temperatures noted at ORNL for the end-of-life, lunar night condition can be attributed to the less thermally efficient door fitting. When the electrically heated block was reinstalled after the cold fueling demonstration, the heater block thermocouple wires caused the shutter door to be open slightly more than before heater removal, resulting in a lower hot junction temperature for a given electrical input. After completion of the vacuum checkout, the generator was removed from the chamber and operated in air until it was fueled.

Q/N-1M lunar performance comparison

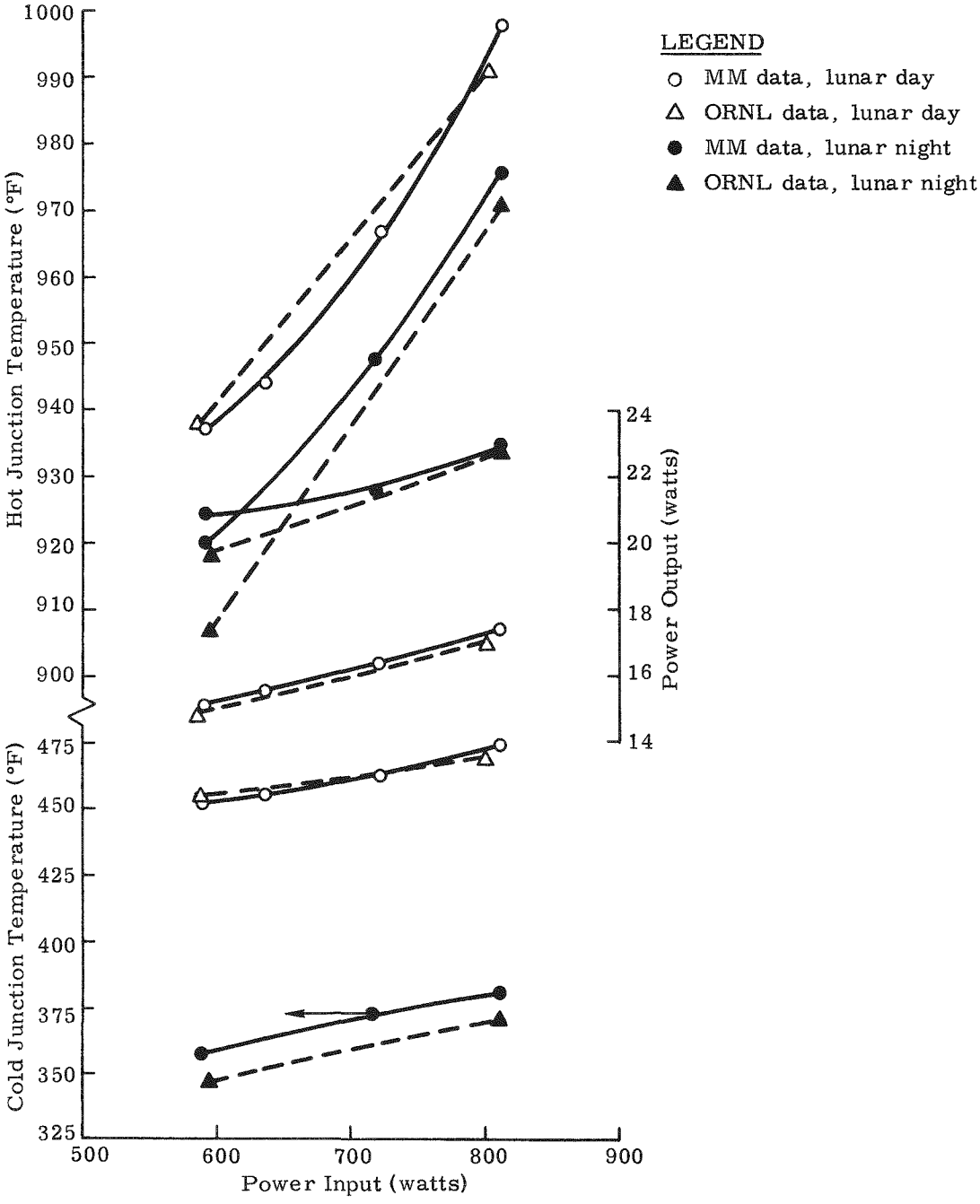

Fig. V-16. Q/N-1M Generator Vacuum Test Data Comparison Curves

TABLE V-12

Comparison of ORNL and Martin Marietta
Q/N-1M Vacuum Data

	Beginning-of-Life Lunar Day		Beginning-of-Life Lunar Night	
	MM Data	ORNL Data	MM Data	ORNL Data
Date	6/2/66	6/28/66	6/1/66	6/28/66
P_{in} (watts)	810	800	810	810
P_{out} (watts)	17.46	17.07	22.94	22.75
$\overline{HJ}$ (°F)	998	991	976	971
$\overline{CJ}$ (°F)	475	469	379	371
R_L (ohm)	0.383	0.380	0.377	0.374
R_i (ohm)	0.331	0.333	0.300	0.295
E_{oc} (volts)	4.819	4.779	5.279	5.218
E_L (volts)	2.587	2.545	2.941	2.915
I_L (amp)	6.75	6.7	7.80	7.8
	End-of-Life Lunar Day		End-of-Life Lunar Day	
Date	6/2/66	6/30/66	6/3/66	6/29/66
P_{in} (watts)	590	585	591	595
P_{out} (watts)	15.17	14.80	20.86	19.70
$\overline{HJ}$ (°F)	937	938	920	907
$\overline{CJ}$ (°F)	452	454	357	347
R_L (ohm)	0.362	0.384	0.362	0.361
R_i (ohm)	0.312	0.319	0.278	0.277
E_{oc} (volts)	4.369	4.360	4.859	4.720
E_L (volts)	2.346	2.384	2.752	2.664
I_L (amp)	6.47	6.2	7.58	7.4

C. FUELING EFFORT*

In preparation for the fueling operation, five pellets weighing from 1.1 to 1.75 grams each were pressed from the oxide product obtained from chemical processing. Conversion to the sesquioxide form (Cm_2O_3) was accomplished by heating the pellets for 10 hours at 1250° C in an argon atmosphere containing <1000 ppm of oxygen. The fuel was then encapsulated and placed on the shelf test. Subsequently, assembly of the fuel block was completed and transferred to the Q/N-1M generator for the demonstration test.

1. Fuel Encapsulation

The first attempt to encapsulate the isotope heat source was made in mid-June 1966. The operation had to be terminated, however, when the welder turntable seized during prefueling qualification welding of the TZM capsule. The fueling operation was then postponed until the end of June so that corrections could be made to the equipment.

The fuel was successfully encapsulated on July 1, 1966. The heat output of the five pellets and a small quantity of oxide powder was measured by calorimetry. The values obtained are listed in Table V-13. The fuel inventory was corrected to 896.5 watts to allow for the measured quantity of fuel remaining in the calorimeter cup after

TABLE V-13

Heat Output of Cm_2O_3 Pellets on 6/30/66

Pellet No.	Watts
1	202
2	173
3	207
4	155
5	129
Powder	33
Subtotal	899
Heel (bottoms)	-2.5
Total	896.5

* A portion of the information used in preparing this section was provided by E. Lamb, ORNL.

the transfer. This inventory was less than the 925 watts $^{+0}_{-25}$ required. However, since the 925 watts was based on a 20-day shelf test, it was decided that the 896-watt fuel loading would be sufficient if the length of the shelf test were reduced. This was found to be more desirable than adding more fuel; hence, the shelf test was reduced to 10 days.

The loading of the Cm_2O_3 into the TZM capsule and subsequent handling operations were accomplished in an atmosphere of argon maintained at <300 ppm of oxygen. The TZM capsule was seal welded by the tungsten-inert gas method in a welding assembly containing argon with <10 ppm oxygen. Welded quality control samples were prepared by the same technique immediately before and after the fueled capsule welding operation. Examination of the sectioned sample capsules revealed the welds to be within specifications. The TZM capsule was then inserted in the platinum-graphite subassembly in preparation for the shelf test.

Generally, the fueling operation proceeded as planned. Following is a list of observations and conclusions concerning the fueling operation:

(1) The problem of maintaining a pure inert gas in the hot cells proved to be difficult since the available hot cells were not designed for this type of operation. However, this did not result in any noticeable adverse effects on the TZM capsule.

(2) Prior to insertion of the fuel, the temperature of the pellets was measured at 1200° to 1250° C (a dull white-hot color) while the pellets were sitting on a water-cooled pan. After insertion of the fifth pellet, the fuel mass was a very bright white hot and is estimated to have melted or approached melting (1600° to 1650° C), even though the capsule body was maintained below visible color by the chill block.

(3) Transfer of the fueled TZM capsule to the platinum-graphite subassembly was considered to be the most critical step in the fueling operation because of the potential oxidation problems and/or overtemperature of the capsule. Therefore, this step was observed closely. The TZM capsule temperature was measured at approximately 500° F just prior to removal from the water-cooled chill block. Transfer time was approximately 30 seconds. During this period of time the TZM temperature climbed to a bright cherry red and the oxygen concentration in the cell reached ~140 ppm. When the TZM capsule was released and allowed to drop into the platinum-graphite subassembly, the TZM capsule immediately dropped below the visible heat range. At this point it was observed that the TZM cap showed no discoloration. It was therefore concluded that the allowable TZM material temperature had not been exceeded and that negligible oxidation had resulted from the transfer operation.

2. Shelf Test

After insertion of the TZM capsule into the platinum-graphite subassembly, the unsealed assembly was placed on shelf test for 10 days. During this period of time, the assembly was maintained at 1100° F under an argon atmosphere. Helium leak tests of the argon atmosphere surrounding the capsule were made at intervals with no indication of a detectable leak at a sensitivity of 4.6×10^{-8} cm^3/sec helium.

3. Final Assembly of the Fuel Block

The final assembly of the fuel block took place on July 11 and 12. When the cover of the shelf test chamber was opened, the graphite was glowing a dull red. The TZM/platinum-graphite assembly was removed from the shelf test chamber and transferred to the welding chamber for welding of the platinum cap. After insertion of an appropriate size TZM shim, the platinum cap was positioned and welded. Following inspection of the weld, the assembly was removed from the welder, and the threaded graphite cover was installed.

The assembly was then transferred to Cell 4 and immediately installed in the preheated (~1300° F) beryllium-Haynes-25 subassembly. After the assembly had stabilized thermally, the graphite cover was tightened (to ~20 in. -lb torque), and the end thrust disc was placed in position. The beryllium cover was then threaded into place and tightened to ~20 in. -lb torque. Finally, the cell atmosphere was converted from 100% argon to 65% argon-35% helium, and the Haynes-25 covers were positioned and welded. A leak check indicated no leakage to a sensitivity of 2×10^{-7} cm^3/sec helium.

During transfer of the assembled fuel block to the leak check chamber, smears were taken on each end of the block and on each of the four quadrants on the cylindrical portion. The highest smear contained 12,500 dpm alpha, one contained 3000 dpm, and the others were ~300 dpm. Fuel block decontamination was therefore not required, since these levels were considerably lower than the limitations previously established. The two high levels were well within the maximum desired level of 20,000 dpm. Following a final leak check, radiation measurements were obtained at 18 inches from the fuel block. The results were:

400 mrem/hr neutrons from spontaneous fission

400 mrem/hr beta-gamma.

Preparations were then made to transfer the fuel block to the space chamber building.

4. Transfer of Fuel Block to Q/N-1M Generator

Upon completion of the testing in the vacuum chamber, the Q/N-1M generator had been placed on a stand in front of the vacuum chamber. The heater block was operating with 810 watts of electrical heat, and the heater block holddown assembly had been removed in preparation for fuel block installation. Also, all thermocouples to the heater block had been cut.

The fuel block was transferred from the fuel block assembly cells to the vacuum test facility in a sealed and insulated transfer cask. When the cask was in position, power to the electrical heater block was terminated, and the heater power leads were cut. The heater block was then removed, and the fuel block was lifted from the transfer cask and inserted into the generator. The fuel block was retained in the generator by installation of the Haynes-25 holddown shield and locking nuts.

The generator was without a heat source for an estimated 60 to 90 seconds. The following is a history of the average hot junction temperatures:

Elapsed Time (min)	Operation
0	Generator operating in air with electrical heater block. T_{HJ} = 940° F
1	Electrical heater block removed and fuel block inserted
6	T_{HJ} = 752° F
14	T_{HJ} = 718° F, lowest hot junction
31	Generator installed in space chamber and vacuum pumps started. T_{HJ} = 794° F
196	T_{HJ} = 962° F
201	Cooldown of cryowall started for lunar night condition.

Following this history pattern, the generator reached lunar night test conditions at 2100 hours on July 12 for the initiation of the 90-day demonstration test.

D. DEMONSTRATION TEST

Figure V-17 shows the ORNL instrumentation and lunar simulation chamber used in the 90-day test of the fueled Q/N-1M generator. Shroud temperatures were automatically controlled during lunar night simulation (-235° F) with LN_2, while lunar day simulation (+235° F) was maintained with GN_2. Chamber pressure was reduced to less than 10^{-6} torr under both lunar night and day environments. Generator load voltage, open circuit voltage and current were determined with a digital voltmeter. Direct temperature readout was obtained from a push-button console and a continuous recorder which incorporated a high temperature alarm to warn of any generator overtemperature during operation. To detect any leakage of the 65% argon-35% helium cover gas from the fuel block (which would result in excessive fuel block internal temperatures), a helium leak detector was employed in the evacuation line to actuate an alarm upon detecting helium. The SNAP 11 field test kit (see Chapter VIII) functioned as backup instrumentation for determining generator voltage and current and contained the load resistance for the generator output. A short-circuit switch for the generator output was provided at the chamber feedthroughs to allow shorting of the output leads to take advantage of Peltier cooling in the thermoelectrics in the event of a generator overtemperature.

During testing the generator was supported in a horizontal position within the chamber by small diameter wires to simulate a zero g environment for the thermal control system and minimize heat conduction through the generator support structure (Fig. V-18). Parameters monitored during testing were as follows:

(1) Chamber pressure and shroud temperature

(2) Forty-eight generator thermocouples

(3) Generator internal pressure (pressure transducer)

(4) Generator load voltage, open circuit voltage and load current.

Figure V-19 outlines the planned sequence for the demonstration test; Fig. V-20 shows the normalized fuel inventory present at any time during the 90-day test period. Initially a five-day period at lunar night would be imposed and an E-I curve generated just prior to changing to lunar day conditions for 80 days. At the conclusion of the 80-day period, lunar night conditions would again be established and an E-I curve generated prior to removal of the generator from the chamber for defueling.

The initial five-day, simulated lunar night test was performed during the period of July 12 to 17; lunar day testing was initiated on July 17. During the period of July 15 to 17 a steady-state E-I curve, shown in Fig. V-21, was generated at lunar night conditions by varying the external load resistance and noting the change in generator load voltage

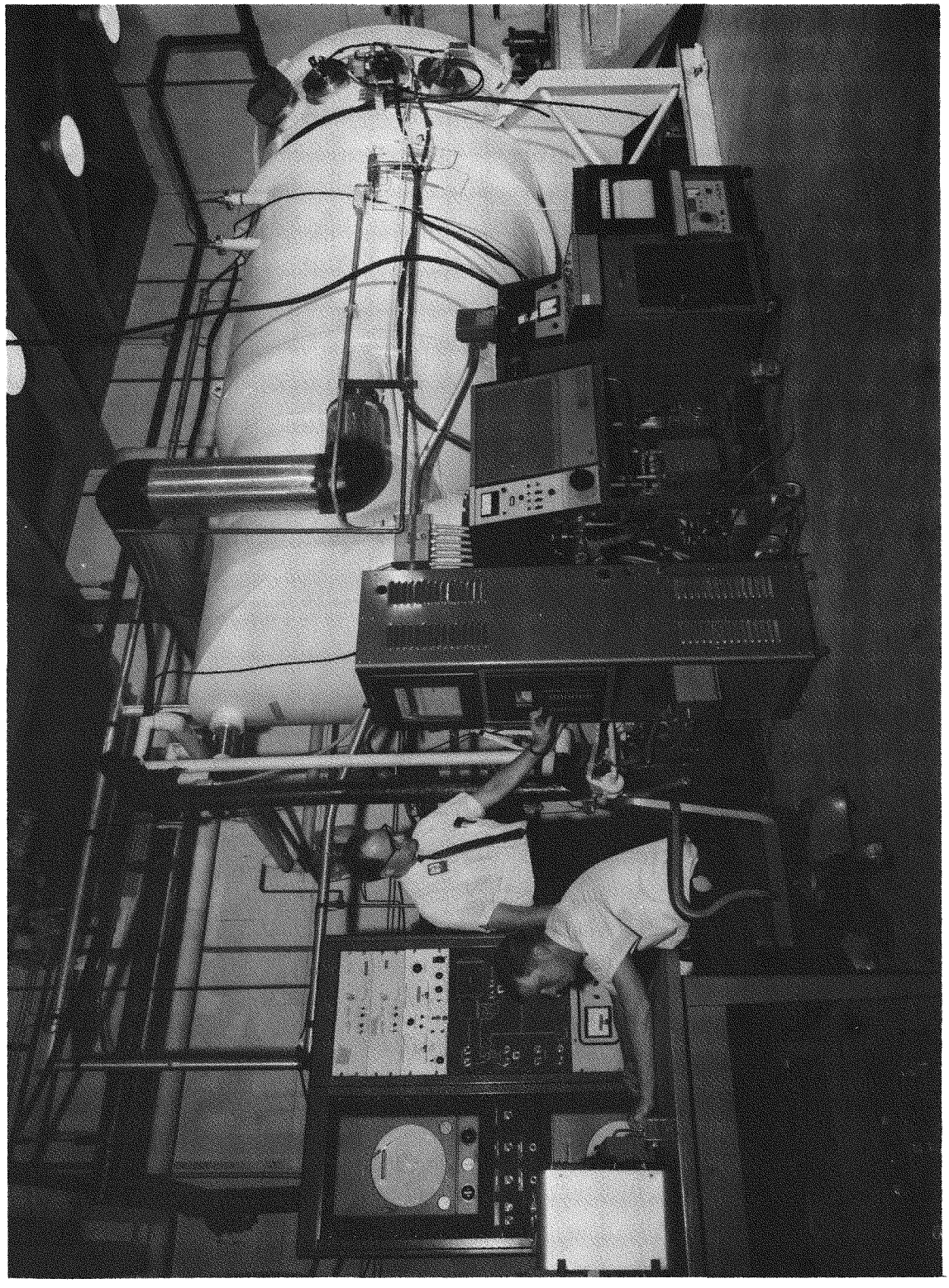

Fig. V-17. Instrumentation and Lunar Simulation Chamber

Fig. V-18. SNAP 11 Generator in Lunar Simulation Chamber

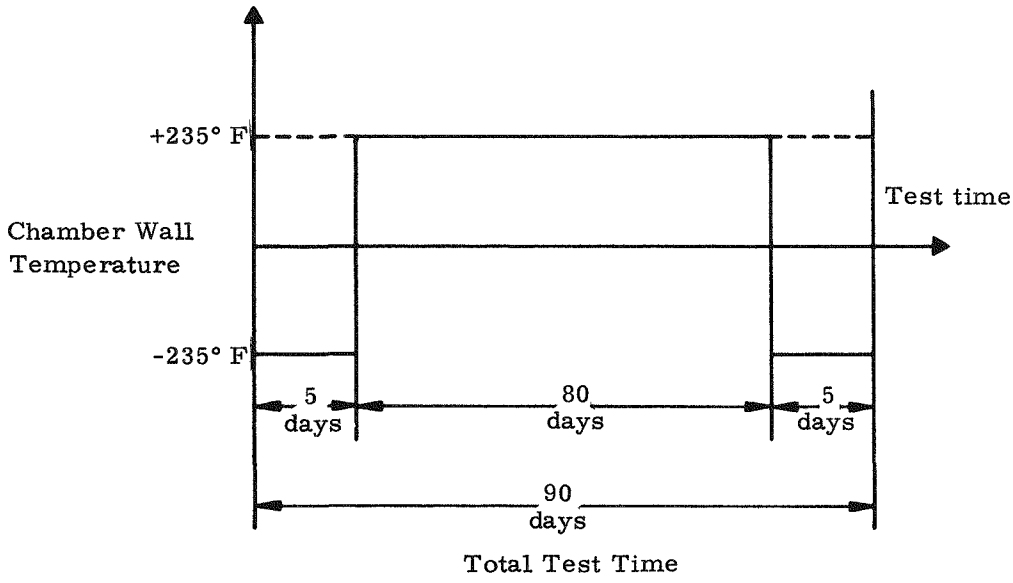

Fig. V-19. Planned Test Sequence for the Q/N-1M Generator Demonstration Test

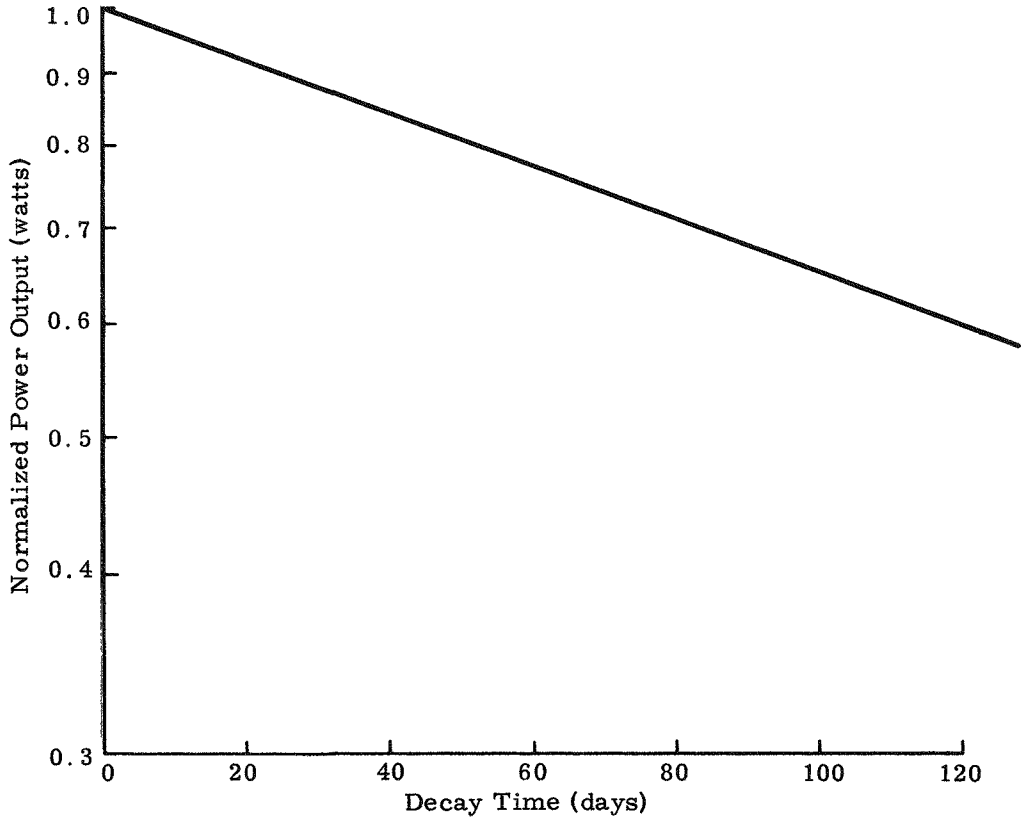

Fig. V-20. Plot of Normalized Power Output of Cm-242 Isotopic Fuel as Function of Decay Time

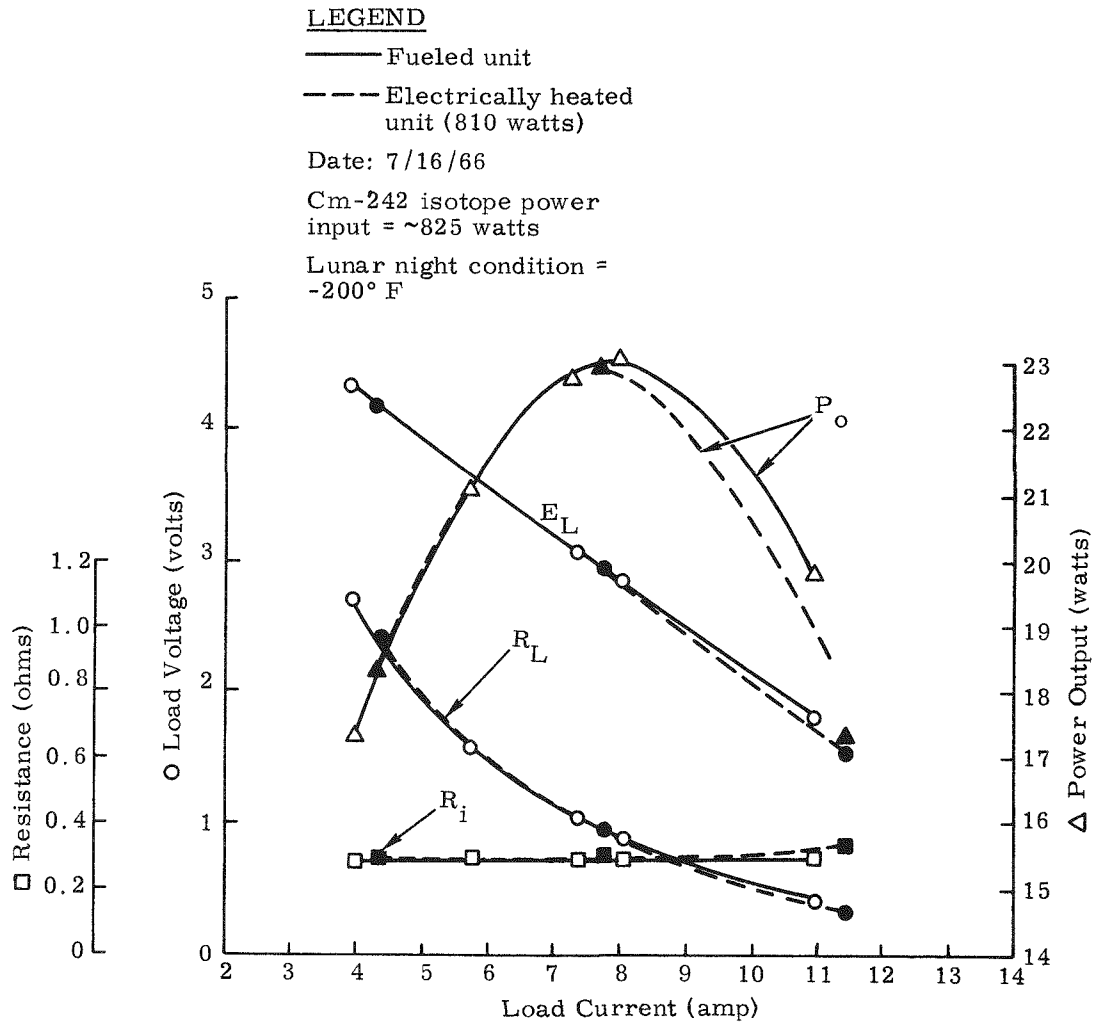

Fig. V-21. SNAP 11 Q/N-1 Modified Generator, Electrical and Fueled Parametric Performance

and current. The decrease in power input (theoretically determined)* while generating the curve was from 831 to 824 watts due to the Cm-242 fuel decay. From the E-I curve, the maximum power output of 23.1 watts occurred at a load resistance of 0.370 ohm. For the demonstration test, Martin Marietta specified a load resistance range of 0.350 to 0.390 ohm for both lunar day and night operations. (This allowable load range was determined by previous testing at MM to yield the highest generator efficiency at the EOL generator design point.) The generator internal resistance (~0.29 ohm) remained essentially constant for the range of load voltages investigated.

Also included in Fig. V-21 is the E-I curve generated at Martin Marietta on the electrically heated unit with an 810-watt input at lunar night conditions. Maximum power output was 22.9 watts and the internal resistance was ~0.30 ohm, showing close agreement with the fueled unit parameters.

Figure V-19 shows the originally planned test sequence for generator operation in the simulated lunar environment. Testing was performed as shown except for a 24-hour period (with ~640 watts isotope power input) during which time additional data were obtained at lunar night conditions. (The reason for this additional point will be discussed in more detail later in this section.)

Generator power output during testing is shown in Fig. V-22. Generator power output remained within ~1% of predicted values throughout the 90-day test period. On October 5, at the conclusion of the lunar day phase of testing, the generator power output was 14.9 watts at an isotope power input of 583 watts. The predicted power output for this isotope power input was 15 watts as shown by the electrically heated (predicted value) curves included in Fig. V-22 for reference. The excellent agreement between predicted and measured values at both lunar day and night conditions is apparent. The sharp power drop to below 590 watts power input at lunar night conditions is due to the precalibrated door closure for this EOL input value (see Chapter III). For a given decrease in power input after the door closes, a greater decrease in input to the thermoelectrics results than for the same given decrease when heat is being dumped through the shutter door.

Data taken during both the lunar night and day phases of testing revealed that, for a given power input, measured hot and cold junction temperatures were in all instances less than those recorded during initial electrical checkout at Martin Marietta. However, as shown in Fig. V-22, generator efficiency remained virtually unchanged. To

* All isotope input powers discussed are based on calorimetry measurement performed on fuel block after completion of 90-day test.

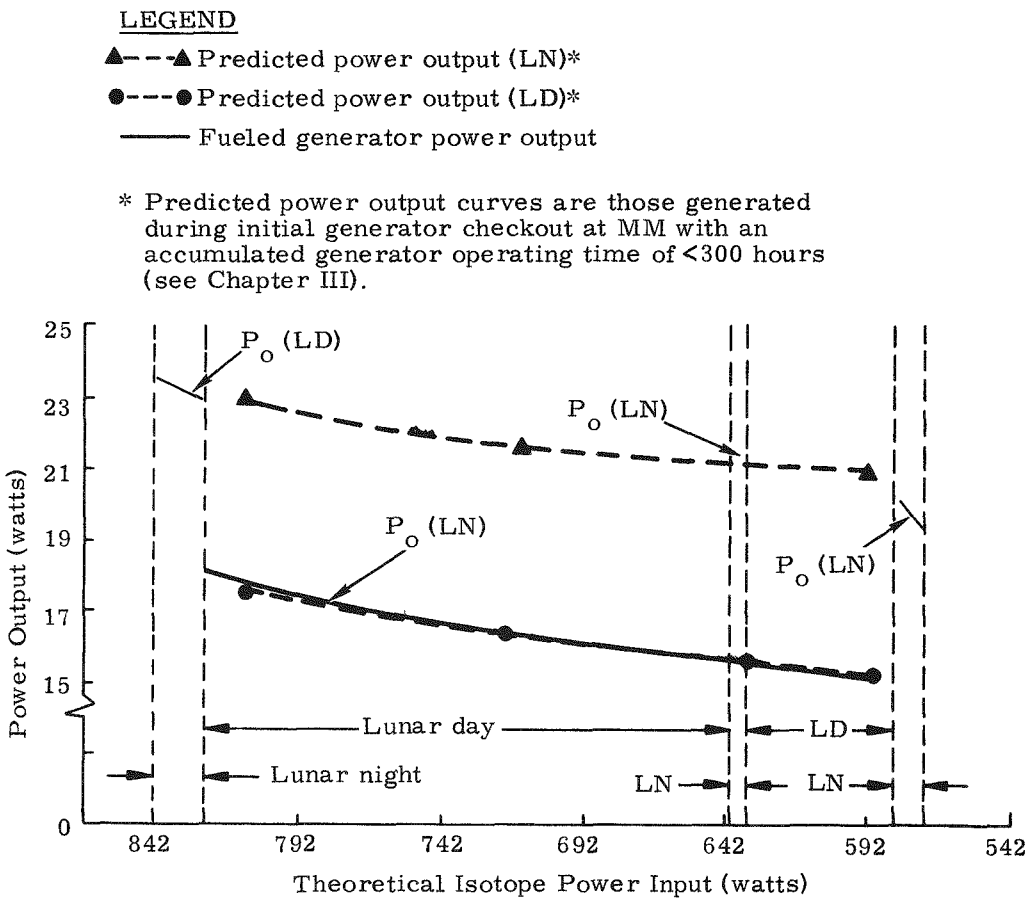

Fig. V-22. Fueled Generator Power Output

obtain additional data that might clarify the temperature discrepancies noted at lunar night conditions, a lunar night performance check was made at an isotope power input of ~640 watts. This check was performed on September 14; results are shown as a single point in Fig. V-22. Measured power output was 21.4 watts, agreeing closely with the predicted power output of 21 watts for this power input (as determined from MM testing of the electrically heated unit). However, as had been noted during lunar day testing, measured hot and cold junction temperatures were lower than predicted.

Examination of both the lunar day and night test data revealed the hot and cold junction temperature discrepancies to be the result of an asymmetric temperature profile on the generator inner periphery. On the electrically heated unit, the generator inner can thermocouples indicated that no significant circumferential hot junction temperature gradient existed. Therefore, the thermoelectric junction thermocouples, all located on one module, could be considered as representative of the average generator junction temperatures. On the fueled generator, however, the hot junction circumferential gradient was significant (~50° F) with the instrumented module being located at the coolest location on the inner can, thus explaining the lower junction temperatures noted.

The asymmetrical temperature distribution in the fueled generator is believed to be a result of the fuel block orientation during testing. The instrumented module in the Q/N-1M generator is located on the top side of the generator with respect to the generator orientation in the vacuum chamber. (The generator is installed in the vacuum chamber with the longitudinal axis in the horizontal plane to minimize the effects of gravity on the thermal shutter operation. This is shown in Fig. V-18.) With this orientation, the fuel block internals, i.e., the beryllium, graphite, platinum and TZM components, would settle toward the lower side of the fuel block. Thus, the clearances between these components from manufacturing tolerances and thermal expansion would accumulate at the top side of the fuel block, inhibiting heat rejection from the fuel capsule to the portion of the inner can at the top of the generator. Thermal analysis performed during the fuel block design indicated that accumulated diametrical clearances between the fuel block internal components would range from 37 to 60 mils during generator operation.

On October 5, the generator operating environment was changed to lunar night. Subsequently, an E-I curve, shown in Fig. V-23, was generated with an isotope power input of 578 watts. Maximum power output was 20 watts at corrected hot and cold junction temperatures of 901° and 348° F, respectively. (Junction temperatures were corrected by using inner can temperatures to determine the hot and cold junction circumferential temperature gradients.) Also included in Fig. V-23 is the E-I curve generated for the Q/N-1M generator at Martin Marietta

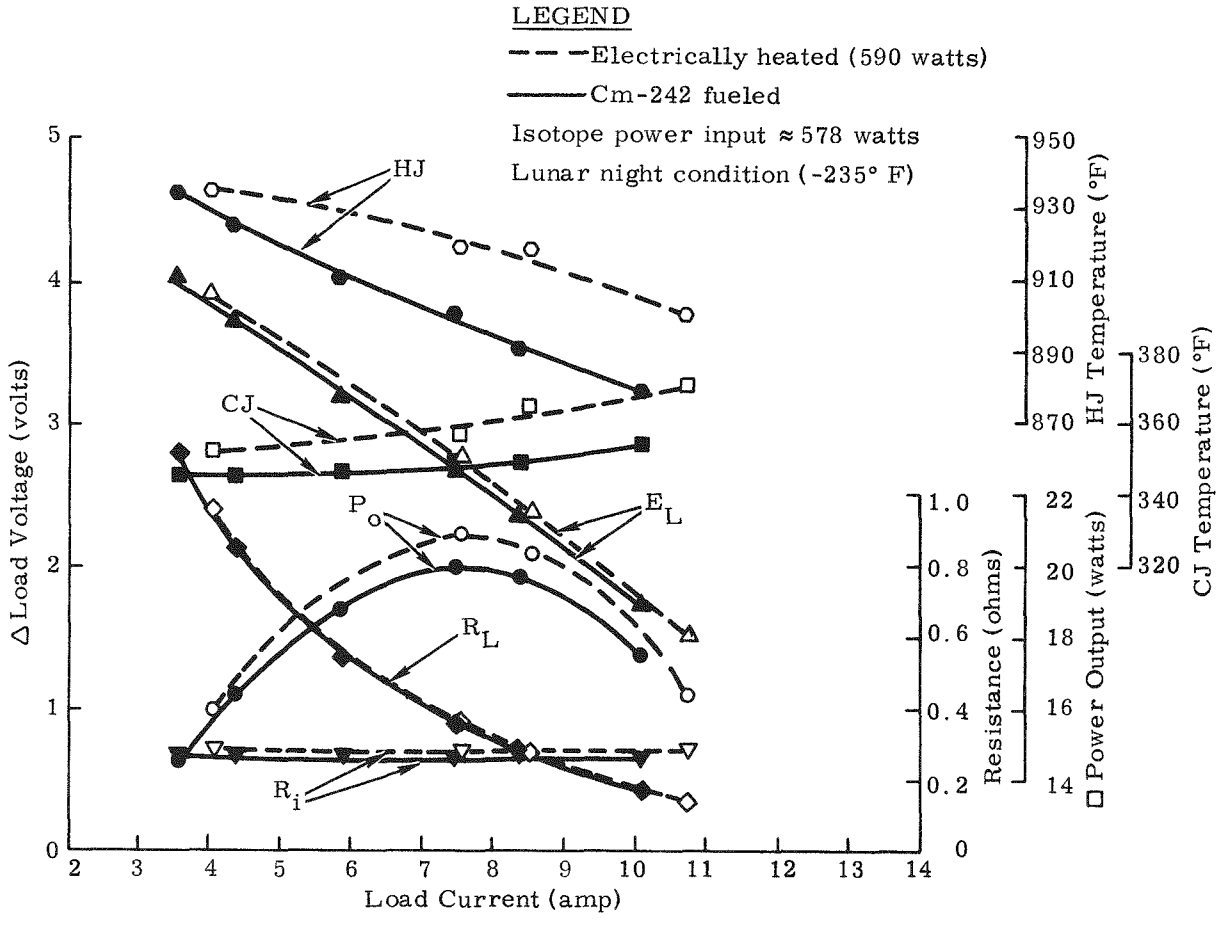

Fig. V-23. Q/N-1M Generator End-of-Life Parametric Performance Curves

during electrical checkout before fueling. With a 590-watt(e) heater input, maximum power output was 20.9 watts at hot and cold junction temperatures of 920° and 357° F, respectively. The lower power input of the fueled unit is evident in the lower junction temperatures and lower internal resistance as well as in the lower power output.

Table V-14 summarizes data points taken during the demonstration test that were near corresponding input power points taken during testing of the generator while it was being electrically heated. As previously observed, the fueled generator efficiency was virtually identical to that of the electrically heated unit with no significant change in internal resistance or open circuit voltage evident.

To compare the electrically heated and fueled generator performance at EOL lunar night conditions, the predicted generator power output as a function of power input at lunar night conditions can be obtained from Fig. V-24. (The curves shown are parametric in cold junction temperature since this temperature is least affected by the junction temperature corrections required. Hot junction values are shown to allow comparison with corrected values.) The curves in Fig. V-24 were generated assuming the values for generator contact resistivity and heat losses determined at Martin Marietta during generator checkout prior to fueling, i.e., no thermoelectric degradation or change in generator thermal efficiency. For an isotope power input of 578 watts and a cold junction temperature of 348° F, the predicted generator power output and hot junction temperatures are 20 watts and 899° F, respectively. These predicted values agree closely with the 20-watt power output and 901° F hot junction temperature determined for the fueled unit and indicate no significant generator thermoelectric or insulating material degradation occurred during testing. Considering the ±5-watt uncertainty (as determined by ORNL) in the calorimetry measurement performed on the fuel block (Fig. V-24), the predicted power output for a 578-watt nominal power input ranges from 19.7 to 20.3 watts.

Power output at conclusion of the test on October 10 was 19.3 watts at hot and cold junction temperatures of 891° and 346° F, respectively. This output agrees within ~1% of the 19.5-watt predicted value for the 572-watt isotope power input available (Fig. V-24).

Figure V-25 is a plot of the generator internal pressure (absolute) as a function of power input during the lunar day phase of testing (from 824 to 583 watts input). During this period, the generator internal pressure decreased from 16.1 to 6.9 psia. (Approximately 0.6 psia of this decrease can be attributed to the decrease in generator operating temperatures resulting from the fuel decay.) This pressure decrease corresponds to a calculated leak rate of $\sim 2 \times 10^{-4}$ cm^3/sec argon, and is considered to be primarily due to the 14 Viton O-ring sealed outer

TABLE V-14

Comparison of Q/N-1M Operation Parameters

	Lunar Night (-235° F)		Lunar Day (+235° F)		Lunar Day (+235° F)	
	Electrically Heated	Fueled	Electrically Heated	Fueled	Electrically Heated	Fueled
Power (watts)						
Input	810	824*	810	810*	720	722*
Output	22.94	22.6	17.46	17.8	16.38	16.3
Junction temperatures (°F)						
Hot	976	971**	998	982**	967	967**
Cold	379	380**	475	465**	463	458**
Resistance (ohms)						
Internal	0.300	0.294	0.331	0.322	0.323	0.317
Load	0.377	0.354	0.383	0.370	0.363	0.386
Voltage (volts)						
Open circuit	5.28	5.18	4.82	4.80	4.61	4.57
Load	2.94	2.83	2.59	2.58	2.44	2.51
Load current (amp)	7.80	8.0	6.75	6.9	6.72	6.5
Accumulated operating time to data point (hr)	<300	877	<300	1872	<300	1941

	Lunar Day (+235° F)		Lunar Day (+235° F)		Lunar Night (-235° F)	
	Electrically Heated	Fueled	Electrically Heated	Fueled	Electrically Heated	Fueled
Power (watts)						
Input	635	633*	590	583*	591	578*
Output	15.54	15.5	15.17	14.9	20.86	20.0
Junction temperatures (°F)						
Hot	944	953**	937	926**	920	901**
Cold	456	453**	452	447**	357	348**
Resistance (ohms)						
Internal	0.315	0.312	0.312	0.311	0.278	0.261
Load	0.362	0.379	0.362	0.388	0.362	0.355
Voltage (volts)						
Open circuit	4.44	4.42	4.37	4.33	4.86	4.63
Load	2.37	2.43	2.35	2.40	2.75	2.67
Load current (amp)	6.55	6.4	6.47	6.2	7.58	7.5
Accumulated operating time to data point (hr)	<300	2461	<300	2795	<300	2845

* Corrected theoretical power input on basis of calorimetric test performed on fuel block after defueling.

** Corrected average junction values based on inner can circumferential temperature distribution as determined from inner can T/C readings.

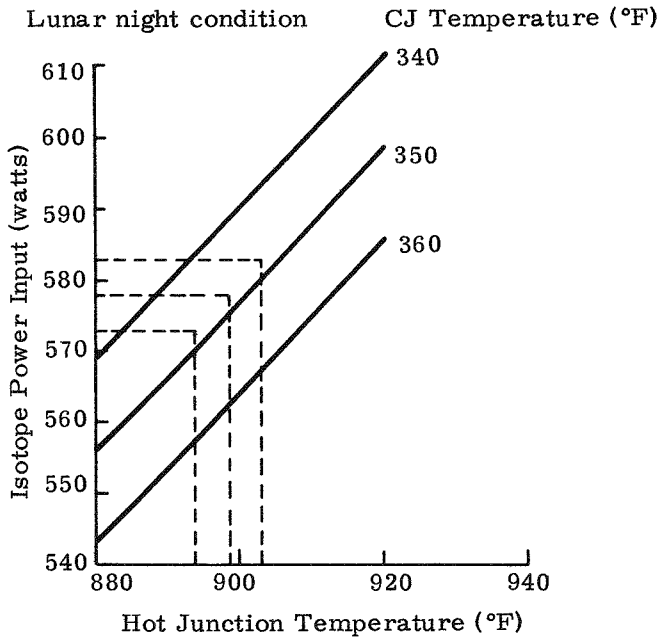

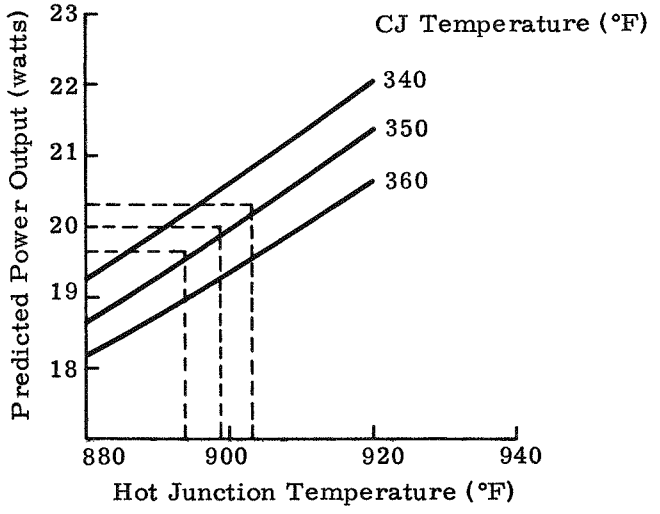

Fig. V-24. Predicted Q/N-1M Generator Performance

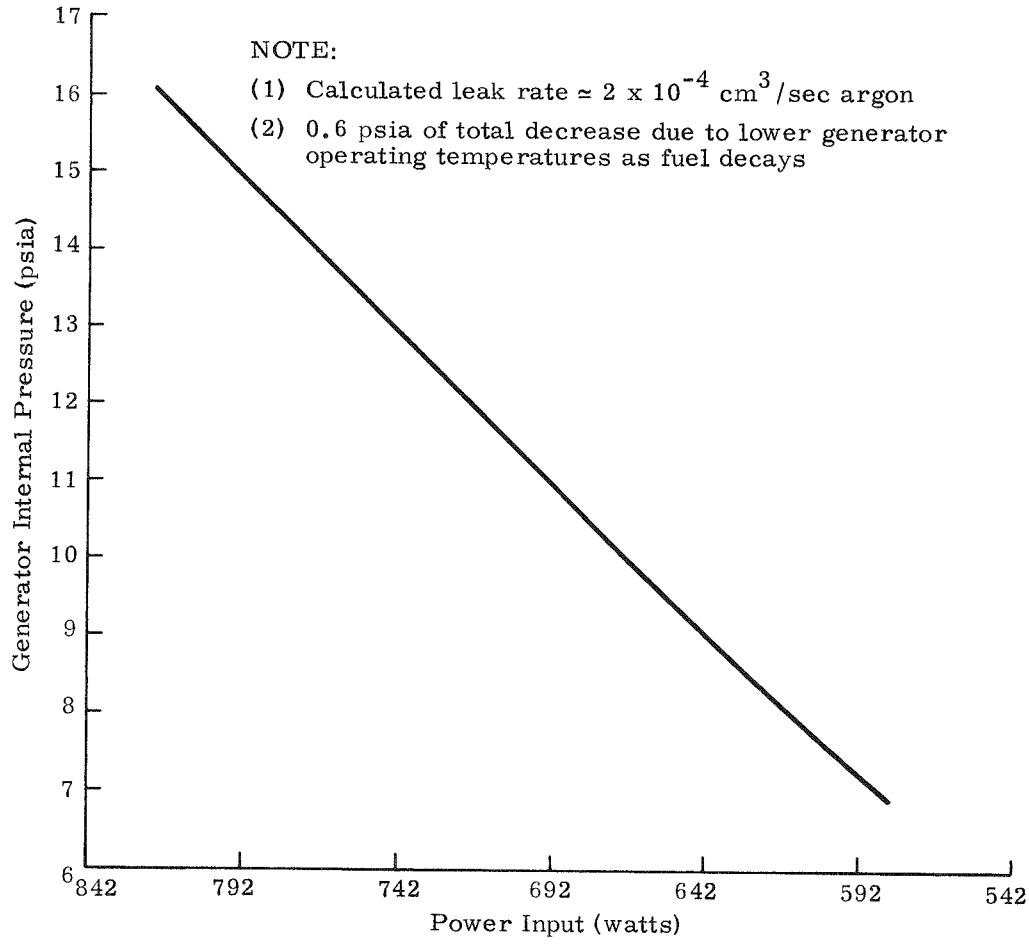

Fig. V-25. Q/N-1M Fueled Generator Internal Pressure During Lunar Day Phase

shell penetrations. Though the pressure decreased by over a factor of two, as anticipated, no noticeable change in the generator thermal operating characteristics was evident.

Total accumulated operating time on the Q/N-1M generator at completion of the 90-day test was 2915 hours, including electrical heating prior to fueling. The total accumulated operating time at defueling was 2965 hours.

The following general observations were made when the generator was removed from the vacuum chamber:

(1) All generator gold-coated surfaces were in excellent condition.

(2) The generator outer housing emissivity coating appeared in excellent condition with the exception of several small areas where the coating was loose prior to generator fueling.

(3) The shutter door remained open ~1/8 inch due to the thermocouple leads which pass through the shutter door opening. This door opening was identical to that for the electrically heated unit. Thus, EOL fueled generator performance should be directly comparable with electrically heated EOL data.

(4) The Haynes-25 outer surface of the fuel block retained its black oxide coating during vacuum operation.

Defueling of the generator was enacted with no incidences, and a calorimetric check was performed on the complete fuel block assembly. Fuel inventory on October 12 was determined to be 567 watts ± 5, nominally eight watts lower than the 575-watt predicted value, based on calorimetry measurements performed on the fuel pellets before fuel block assembly.

Smear tests on the generator proved negative, with no readings encountered above normal background levels. All generator accessible areas were found to be free of surface contamination. The generator has subsequently been shipped to Sandia Corporation for further air evaluation with an electrical heat source.

VI. THERMOELECTRIC DEVELOPMENT PROGRAM

The SNAP 11 generator thermoelectric conversion system contains 72 couples arranged in 12 modules of six couples each. The couples are connected in parallel pairs with the resultant 36 couple pairs connected in series. The thermoelectric elements used are fabricated by Minnesota Mining and Manufacturing Company (3M). Both the N and P elements are 0.346 inch in diameter and 0.500 inch in length.

An important parameter used to describe the performance of thermoelectric generators is contact resistivity. This term is used to account for thermocouple performance being different from the performance predicted by the nominal property data of the known materials in the thermoelectric circuit. Contact resistivity can be calculated by either of the two methods listed:

(1) The first method of calculating contact resistivity consists of subtracting the cold strap, hot shoe, wiring and integrated average N and P thermoelectric element resistances (based on published property data) from the total electrical circuit internal resistance. The remaining unaccounted for resistance per couple, R_C, is then considered as contact resistance and can be expressed as contact resistivity, C_T, for a fixed T/E element area, A, i.e., $C_T = AR_C$. Note that this determination of contact resistivity depends principally on the published element resistivity property data and that no direct comparison of T/E materials based on contact resistivities calculated from different sets of property data should be made. Thus, the term contact resistivity is in a sense a misnomer since the resistance does not necessarily occur at element junctions.

(2) The second method of determining contact resistivity uses the power performance prediction of the Martin T/E code which uses published property data for Seebeck coefficient, thermal conductivity and electrical resistivity. Thus, this method of determining contact resistivity depends on all three types of published property data. Curves to be presented later in this section show that as the contact resistivity increases, the electrical performance decreases for a given temperature distribution.

Thermoelectric generators fabricated with TEGS-2P and TEGS-2N thermoelectric elements and performance evaluated on the SNAP 11 program have shown that power output at operating hot junction temperatures (900° to 1000° F) degrades with time. Degradation rates vary from generator to generator, but as a general rule the output decreases by 15 to 20% during test times of 2000 to 3000 hours. Most of the power degradation can be attributed to an increase in the thermoelectric circuit resistance. Tests on the Q/N-1 and Q/N-2 generators exhibited degradation rates even higher than previous units such as the

S/N-4 modified. Calculated contact resistivity based on experimental results showed that the Q/N-1 initial value of 2800 $\mu\Omega$-cm^2 increased to approximately 5000 $\mu\Omega$-cm^2 in less than 1000 hours due possibly to an overtemperature of the cold junction during testing. That of the Q/N-2 increased from 2700 to 4500 $\mu\Omega$-cm^2 in 2000 hours. On the other hand, the S/N-4 modified generator contact resistivity was 4600 $\mu\Omega$-cm^2 after life testing for 3300 hours.

Test data from overhead programs and the SNAP 21A program indicate that degradation in the 2N-2P thermoelectric couple is a function of temperature and occurs primarily in the 2P leg of the couple. TEGS-3P thermoelements appeared to degrade less than the TEGS-2P type based on available data. To obtain additional data on factors affecting performance, T/E couples of 2N-2P and 2N-3P materials were evaluated both analytically and by long-term testing at hot junction temperatures of 900° and 1000° F. Results from these evaluations were used in specifying design changes for SNAP 11 generators fabricated subsequent to the Q/N-2 generator. In addition, both pressure and bonded contacts at the 3P hot junction were evaluated at a hot junction operating temperature of 1100° F. These tests are continuing under the SNAP 19 Program and additional life data can be obtained through the SNAP 19 Program progress reports.

A. ANALYTICAL COMPARISON OF 2N-2P AND 2N-3P COUPLES

The SNAP 11 program utilized 3M Company TEGS-2N and TEGS-2P thermoelements up through the Q/N-2 generator. Power degradation of these generators was considered to be unacceptable, and an analytical investigation was performed to compare the theoretical performance of an alternate P-leg material, TEGS-3P, with that of 2P. The N-leg material, TEGS-2N, was retained due to its virtually stable performance characteristics.

The analytical study of TEGS-2P and TEGS-3P elements, in couples with TEGS-2N elements, compared the gross power output and thermoelectric efficiency of the two types of couples. Curves for thermoelectric efficiency versus hot junction temperature, parametric in cold junction temperature, T_{CJ}, and contact resistivity, C_T, are shown in Figs. VI-1 and VI-2 for 2N-2P and 2N-3P, respectively. To obtain the same thermoelectric efficiency at a fixed cold junction temperature (i.e., at the same heat flow through the thermoelectric modules and the same heat rejection capability), 2N-3P couples must operate at a higher hot junction temperature and/or a lower contact resistivity (based on published element property data). Table VI-1 and Figs. VI-1 and VI-2 illustrate the condition for a selected operating point, the original SNAP 11 end-of-life lunar night operational temperatures and the anticipated end-of-life contact resistivity value.

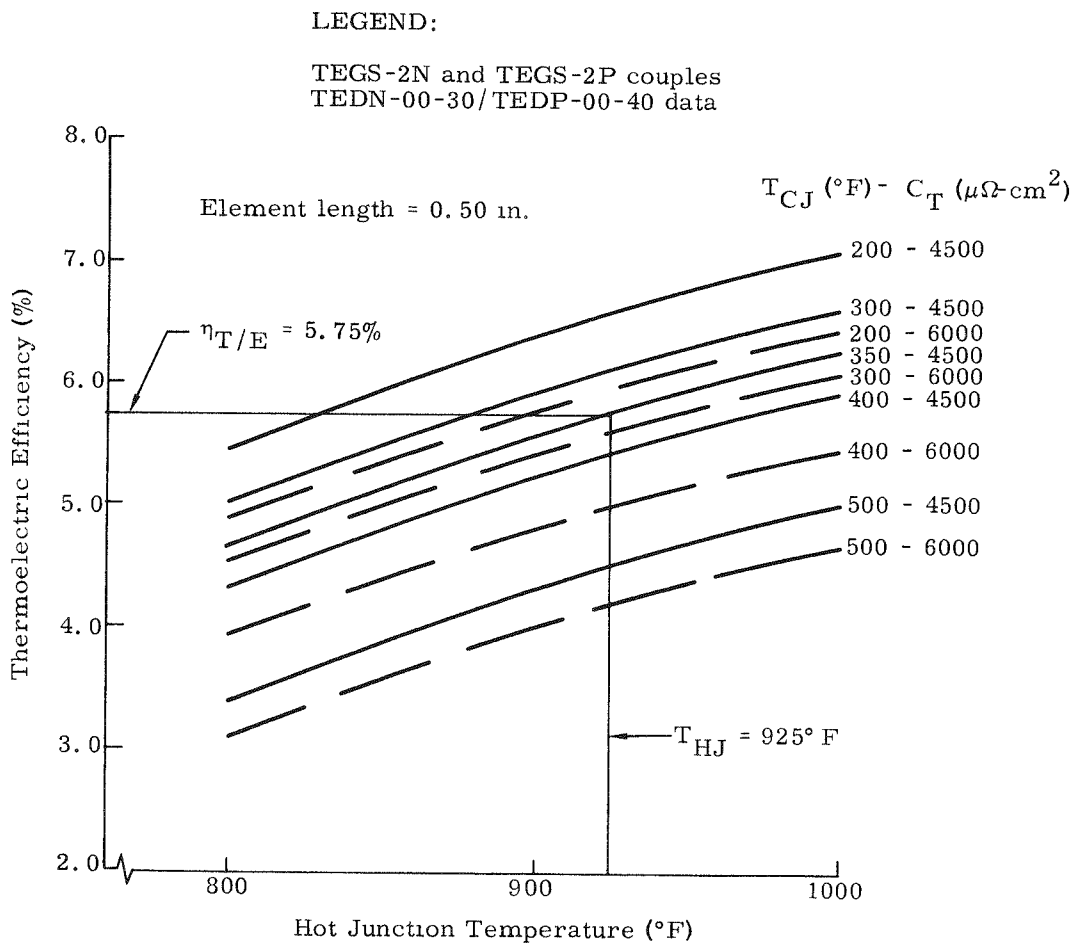

Fig. VI-1. Theoretical Thermoelectric Efficiency

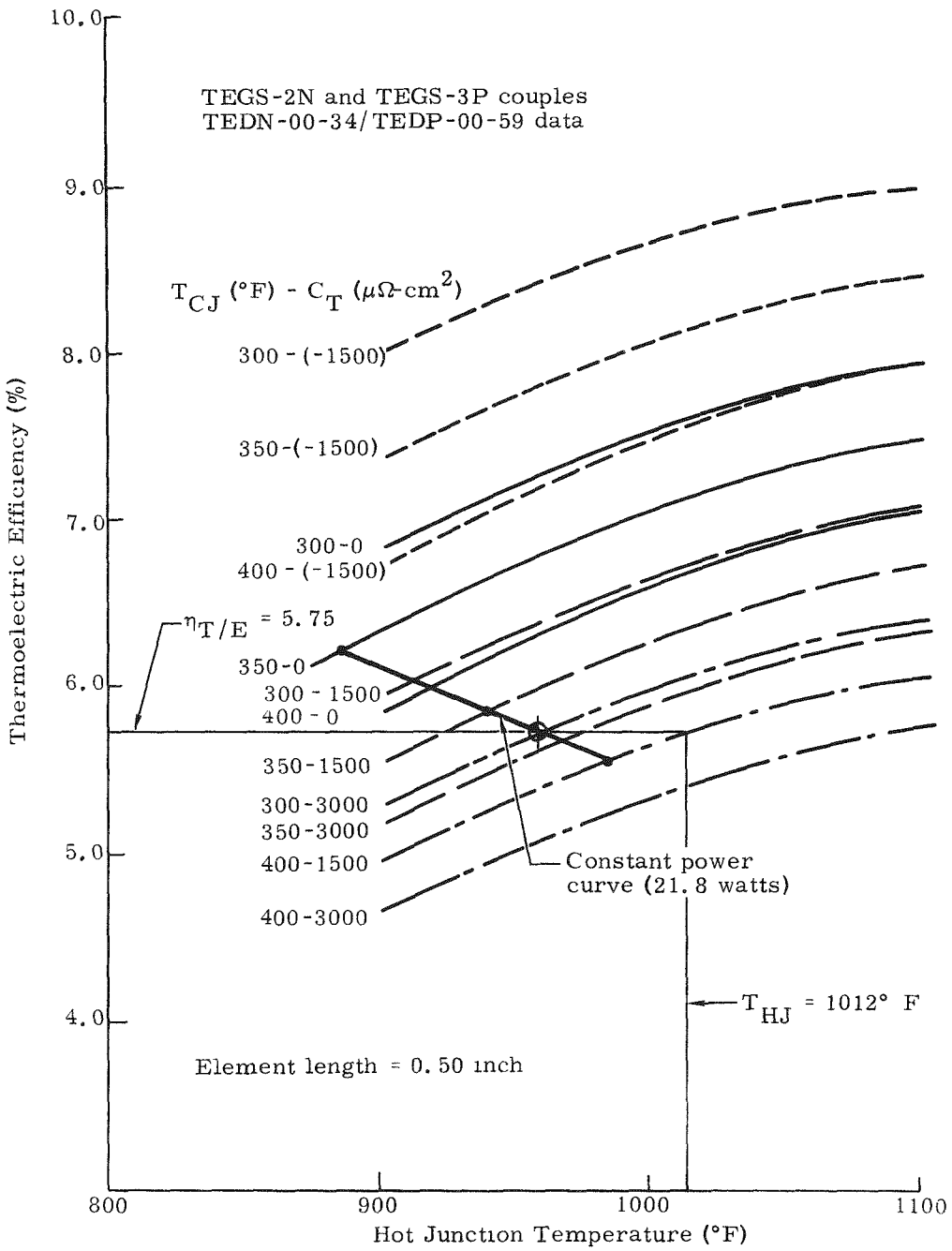

Fig. VI-2. Thermoelectric Efficiency

TABLE VI-1

2N-2P and 2N-3P Comparison at Same T/E Efficiency and Junction Temperatures (element length = 0.50 in.)

Couple	$n_{T/E}$ (%)	T_H (°F)	T_C (°F)	C_T ($\mu\Omega$-cm^2)
2N-2P	5.75	925	350	4500
2N-3P	5.75	925	350	1500

Thus, for the selected operating point, a reduction of 3000 $\mu\Omega$-cm^2 in contact resistivity is required when using 2N-3P couples.

Curves for gross power output (generator net power output plus generator internal terminal strap I^2R losses) versus hot junction temperature, parametric in cold junction temperature and contact resistivity for the present SNAP 11 element size (0.346 in. diameter by 0.500 in. long), are shown in Figs. VI-3 and VI-4 for 2N-2P and 2N-3P, respectively. The interchanging of 2P with 3P results in a loss of gross power unless a higher hot junction temperature and/or a lower contact resistivity can be attained. Table VI-2 illustrates these conditions for the original SNAP 11 end-of-life lunar night operation temperatures.

TABLE VI-2

2N-2P and 2N-3P Comparison at Same Gross Power Output and Junction Temperatures (number of couples = 72)

Couple	T_{HJ} (°F)	T_{CJ} (°F)	C_T ($\mu\Omega$-cm^2)	P_{gross} (watts)
2N-2P	925	350	4500	21.8
2N-3P	925	350	1250	21.8

Thus, for the selected operating point, a reduction of 3250 $\mu\Omega$-cm^2 in contact resistivity is required to obtain the same gross power for the 2N-3P couples.

For 2N-3P operation at the design cold junction temperature of 350° F, and present gross output power (with 2N-2P couples) of 21.8 watts, the required operating hot junction temperatures for contact resistivities of 0, 1500 and 3000 $\mu\Omega$-cm^2 are determined from Fig. VI-4; values obtained are 885°, 940° and 985° F, respectively. The corresponding thermoelectric efficiency values for these hot junctions are

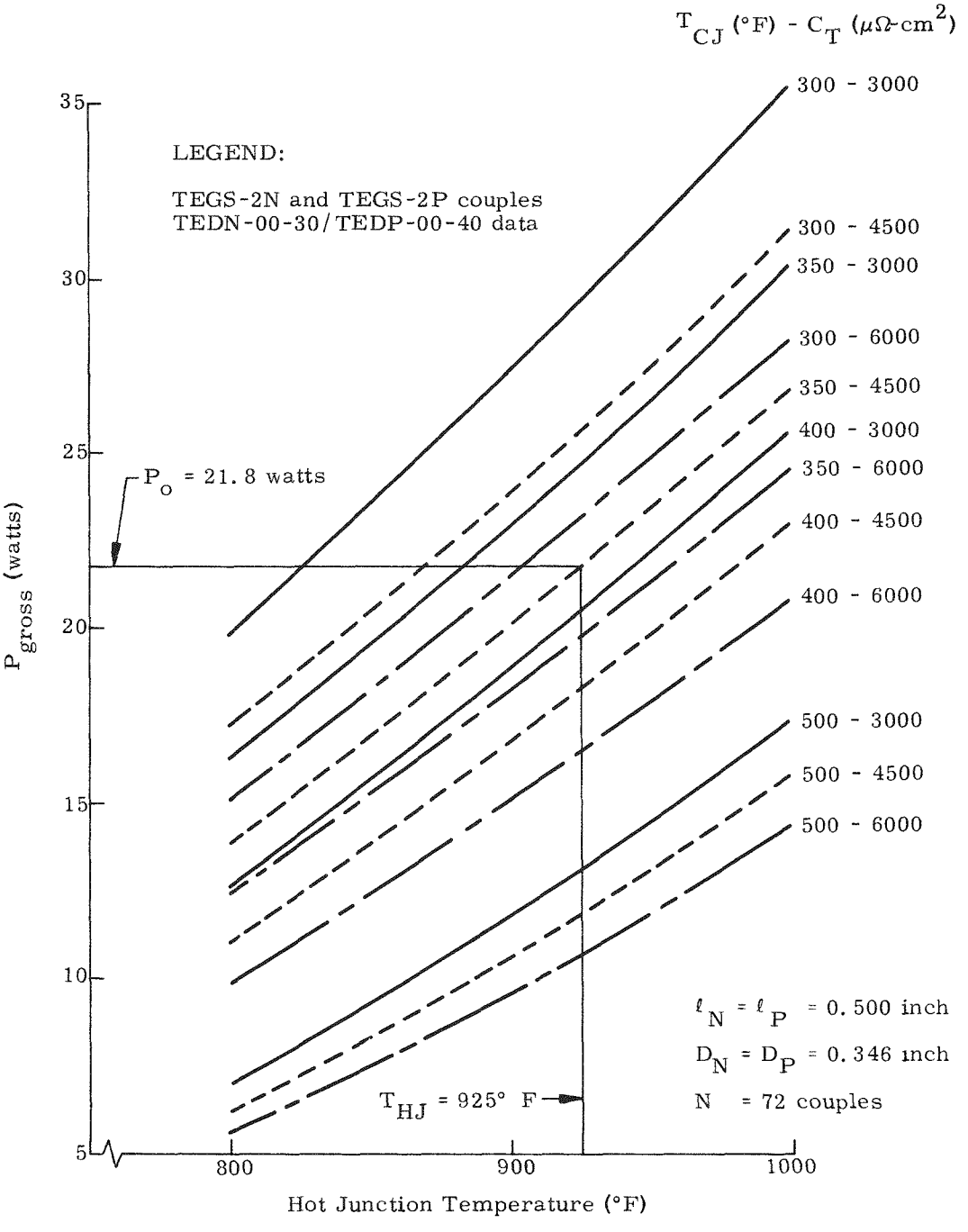

Fig. VI-3. Theoretical Gross Output Power

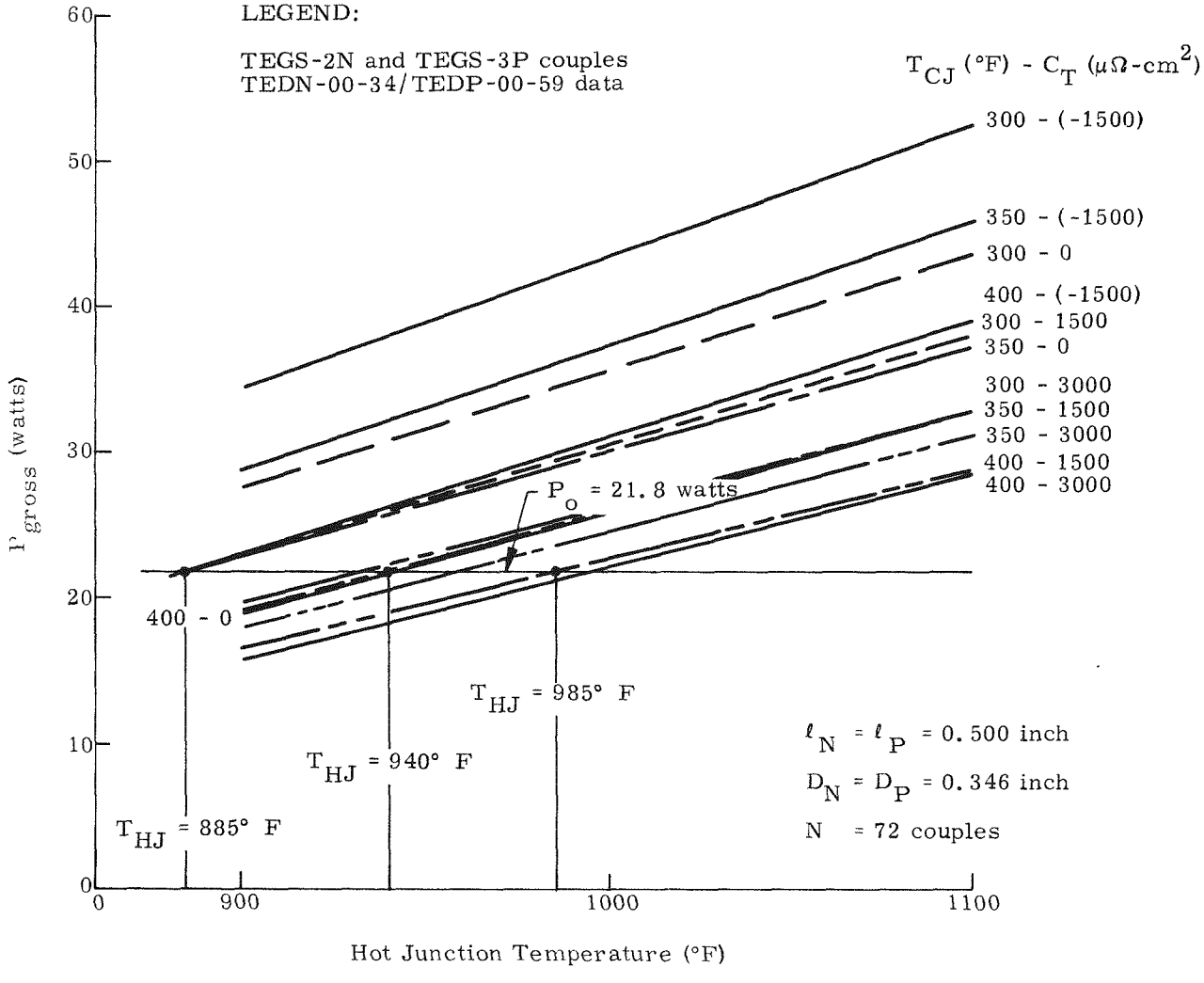

Fig. VI-4. Theoretical Gross Power Output

determined from Fig. VI-2 and are 6.24, 5.86 and 5.56%. Thus, if the fuel inventory is not to be increased, the contact resistivity must be maintained below 2100 $\mu\Omega$-cm^2, above which the thermoelectric efficiency is less than 5.75%. At this point, the resulting hot junction temperature will be ~960° F. If the original end-of-life design junction temperatures are maintained (925° F HJ-350° F CJ), the maximum allowable contact resistivity is ~1250 $\mu\Omega$-cm^2, as in Table VI-2, with an increase in efficiency to 5.96%. Since going to a higher hot junction temperature is not considered feasible on the SNAP 11 generator due to the ~75° F greater hot junction temperature at the beginning-of-life lunar day as opposed to the end-of-life lunar night conditions, the 2N-3P couples must exhibit a contact resistivity of ~1250 $\mu\Omega$-cm^2 or less if the present element dimensions are retained.

Increasing the N and P element diameters to 0.375 inch for either a 2N-2P or 2N-3P couple results in an increase in gross power directly proportional to the element area increase (for identical operating parameters). Thus, from the data presented in Table VI-2, the gross power output would increase to 25.5 watts(e). However, this increase in gross power output is accompanied by the same proportional increase in the heat flow to the larger thermoelectric elements. This heat flow increase of 17% must ultimately be rejected by the generator fins. Increasing the fin heat rejection capability by increasing the fin width and/or fin root thickness is possible, but this adds prohibitively to generator weight and fin vibrational problems if the same generator configuration is maintained.

To gain a better understanding of the performance, degradation rates and structural properties associated with 2P and 3P materials at various temperatures, a couple development and evaluation effort was initiated.

B. THERMOELECTRIC COUPLE EVALUATION PROGRAM

The thermoelectric couple evaluation program was initiated with the following objectives:

(1) Perform a short term creep comparison of 2P and 3P elements at operating temperature.

(2) Determine the effect of compressive loads (spring pressure) on the couple performance (~70, 140 and 210 psi element contact pressures).

(3) Compare the performance stability of TEGS 2N-2P couples with TEGS 2N-3P couples at hot junction temperatures of 900° and 1000° F.

(4) Compare the performance of fully bonded 2N-3P couples with 2N-3P couples that utilize a nonbonded pressure contact on the 3P leg hot junction at an 1100° F hot junction temperature.

(5) Compare the performance of 3P thermoelectric legs in Item 4 which have a pressure contact on a plain surface hot shoe with 3P legs which are pressure contacted to a knurled surface hot shoe.

The program scope was limited in that no extensive investigations were performed on the N leg (2N material with nickel bonds) or hot shoe configuration. (The existing SNAP 11 FerroVacE iron hot shoe with a shallow counterbore was retained.)

1. Test Program Description

a. T/E element creep test

In this test, 2P and 3P elements were placed under various contact pressures in a nonoxidizing dry box atmosphere. A hot end temperature of 1000° F was maintained by a hot plate. Elements were isothermal as nearly as possible. A summary of test conditions follows:

Number of elements	Six 2P and six 3P
Diameter (in.)	0.377
Element contact pressure (psi)	200 to 300
Test time, approximate (hr)	50 to 100
Environment	Argon atmosphere
Hot end temperature (°F)	1000 (hot plate)
Cold end temperature	Not controlled
Objective	Compare short term creep of 2P and 3P elements at 1000° F

b. T/E couple spring pressure test

In this evaluation, a module test fixture containing two six-couple modules--one 2N-2P couple module and one 2N-3P couple module--was tested at 1000° F hot junction and 350° F cold junction temperatures. Element contact pressures evaluated were approximately

210, 140 and 70 psi. A summary of test conditions for the spring pressure test follows:

Number of test fixtures	One
Number of modules	One 2N-2P, one 2N-3P
Number of couples	Six 2N-2P, six 2N-3P
Environment	Argon atmosphere
Junction temperatures (°F)	1000 hot, 350 cold
Element contact pressure (psi)	Two each 2N-2P and 2N-3P at 70 Two each 2N-2P and 2N-3P at 140 Two each 2N-2P and 2N-3P at 210
Electrical connection	2N-2P couples in series 2N-3P couples in series
Element size (in.)	0.377 diameter, 0.500 long
Objective	Determine effect of spring pressure on element performance

c. Thermoelectric stability test

These module tests allowed comparison of 2N-2P and 2N-3P couple stability at hot junction temperatures of 900° and 1000° F. Tests were conducted in two, two-module test fixtures, each containing 2N-2P and 2N-3P modules as in (b). One module box was operated at a 900° F hot junction temperature and the other at 1000° F to determine the effect of temperature on stability. A summary of test conditions follows:

Number of test fixtures	Two
Modules per fixture	One 2N-2P, one 2N-3P module
Total couples per test fixture	Six 2N-2P, six 2N-3P
Environment	Argon atmosphere
Junction temperatures (° F)	One fixture at 900 hot; 350 cold One fixture at 1000 hot; 350 cold
Element contact pressure (psi)	140
Element size (in.)	0.377 diameter; 0.500 long
Objective	Compare performance of 2N-2P and 2N-3P couples

In addition to these two test fixtures, a fixture containing two 2N-3P modules was tested. One module contained 2N-3P couples with all element junctions bonded, while in the other module only the N element junctions and the P element cold junctions were bonded. In the latter module, three couples were fabricated with a smooth hot shoe for the P leg pressure contact, and the remaining three shoe surfaces were knurled at the P leg contact. This module box was tested at a hot junction temperature of 1100° F. Test objectives were:

(1) To compare the performance of 2N-3P couples having all contacts bonded with that of couples with a pressure contact at the P leg hot junction.

(2) To determine the effect of hot shoe surface condition on the performance of the couples with pressure contacts.

2. Development Tests

a. Element creep tests

In this test, three specimens each of TEGS-2P and 3P thermoelements were placed under compressive loads of 200 and 300 psi for approximately 90 hours at a hot junction temperature near 1000° F. Results are shown in Table VI-3 which presents the 2P and 3P element creep data for 200- and 300-psi compressive loadings, respectively. The ability of 3P material to carry a higher compressive load is clearly demonstrated by the results. Note that the 2P material shortened an average of 9.8% under 300-psi loading while the 3P material shortened an average of only 0.7%. Under 200-psi compressive loading, these values reduce to 2.3 and 0.04%, respectively. Thus, no creep problems are anticipated with the 3P material at the nominal SNAP 11 operating pressure of 140 psi.

b. Couple fabrication

Some development effort was required in establishing the processes for fabrication of the 2P and 3P T/E couples with SnTe bonds for use in the module testing. Initially, the P and N legs were hot press-bonded simultaneously. A comparison was made of the N legs obtained in this manner with those obtained by furnace bonding methods, as used on previous SNAP 11 couples, to demonstrate that essentially no electrical difference existed between the two processes. Evaluation of the N legs produced by the two processes showed that the room temperature resistances of the N legs were essentially identical. However, hot pressing of the P and N legs simultaneously resulted in excessive cracking in the P legs of both the 2P and 3P couples. The P leg cracking was due to the expansion mismatch between the graphite hot pressing

TABLE VI-3

T/E Creep Test

Element No.	Diameters (in.) Before Test	Diameters (in.) After Test	Change in Diameter (%)	Lengths (in.) Before Test	Lengths (in.) After Test	Change in Length (%)	Hot End Temperature (°F)
			Test 1--200 psi for 92.5 hours				
2P-200-1	0.3785	0.3788	0.08	0.4959	0.4831	2.6	1037
(2P-42)	0.3783	0.3870	0.34				
	0.3791	0.3909	3.0				
2P-200-2	0.3784	0.3795	0.29	0.4962	0.4859	2.1	1037
(2P-43)	0.3787	0.3860	0.71				
	0.3787	0.3881	2.5				
2P-200-3	0.3777	0.3796	0.69	0.4905	0.4786	2.4	1020
(2P-44)	0.3781	0.3892	2.95				
	0.3786	0.3880	2.5				
3P-200-1	0.3764	0.3763	0	0.4946	0.4946	0	970
(3P-11)	0.3764	0.3766	0.05				
	0.3766	0.3771	0.13				
3P-200-2	0.3766	0.3765	0	0.4992	0.4989	0.06	995
(3P-29)	0.3766	0.3766	0				
	0.3769	0.3771	0.05				
3P-200-3	0.3762	0.3762	0	0.4903	0.4900	0.06	950
(3P-31)	0.3766	0.3765	0				
	0.3765	0.3766	0.03				
			Test 2--300 psi for 71.8 hours				
3P-300-1	0.3765	0.3763	0				
(3P-34)	0.3765	0.3766	0	0.4940	0.4940	0	980
	0.3765	0.3779	0.3				
3P-300-2	0.3765	0.3765	0				
(3P-27)	0.3766	0.3768	0.053	0.4924	0.4917	0.141	995
	0.3767	0.3769	0.053				
3P-300-3	0.3766	0.3765	0				
(3P-47)	0.3771	0.3770	0	0.4927	0.4924	0.061	960
	0.3766	0.3786	0.5				
2P-300-1	0.3784	0.3815	0.55				
(2P-45)	0.3796	0.4000	5.4	0.4970	0.4710	5.3	1040
	0.3800	0.408	7.4				
2P-300-2	0.3783	0.3840	1.5				
(2P-46)	0.3786			0.4991	0.4305	13.7	1035
	0.3784	0.475	25.5				
2P-300-3	0.3785	0.385	1.72				
(2P-47)	0.3793			0.4905	0.4497	10.3	1022
	0.3796	0.438	14.2				

die and the FerroVacE iron hot shoe. The P legs subsequently hot pressed alone (no N leg) revealed cracking was reduced to a level considered acceptable as determined by metallographical sectioning and room temperature resistance measurements. On the basis of this success, the N leg hole in the graphite hot pressing die was enlarged 1/16 inch in diameter to allow uninhibited thermal expansion and contraction of the hot shoe with the N leg in place. Final hot pressing of the P leg with a prefurnace bonded N leg (with provisions for the enlarged N leg hole) showed that couples with minimal cracking in the P leg could be obtained.

In addition to these hot pressed couples, additional couples were fabricated using a furnace bonding technique similar to that used for previous SNAP 11 generators. These were included in modules as indicated in Table VI-4 for comparison with the hot pressed couples discussed.

c. Six-couple module testing

For evaluation of module performance, eight modules containing six couples each were fabricated and placed on test. Table VI-4 summarizes the important characteristics of each module along with its operating conditions. To assure that a meaningful performance comparison could be made, two modules containing couples to be compared are contained in the same module box, but are electrically separated to allow individual monitoring of module performance. Instrumentation allows monitoring of the hot and cold junction temperatures of each module and the voltage across the individual couple legs. Figure VI-5 shows a module box prior to installation of the top cover plate, and Fig. VI-6 includes a cross sectional view of the module box and instrumentation. Assembly of the module boxes was performed in a dry box under an argon atmosphere in the same manner as the SNAP 11 generators to minimize contamination from external sources.

3. Test Results

Performance results for data points taken through November 30, 1966 are summarized in Table VI-5. The power output of each module is presented at intervals of approximately 1000 hours, and power decay rates for each interval are included to illustrate the trend for each module. Total accumulated test times of 8673, 7916, 1830 and 7577 hours were attained on Test Fixtures 1--Modules 1 and 2, 2--Modules 3 and 4, 3--Modules 5 and 6 and 4--Modules 7 and 8, respectively.

The raw data points for the four test fixtures are shown in Figs. VI-7 through VI-10. Included are hot and cold junction temperatures, power outputs and average module N and P leg resistances. A problem

TABLE VI-4

Summary of SNAP 11 Test Modules
$D_N = D_P = 0.375$ in.; L = 0.500 in.

Module Box No.	Module No.	Material	T_{HJ} (°F)	T_{CJ} (°F)	Hot Bond and Process P Leg	Hot Bond and Process N Leg	Spring Pressure (psi)	Comments
1	1	2N-2P	1000	350	SnTe-HP(1)	Ni-FB(2)	70, 140, 210	2 couples at 70 psi 2 at 140 psi, 2 at 210 psi
1	2	2N-3P	1000	350	SnTe-HP	Ni-FB	70, 140, 210	2 couples at 70 psi 2 at 140 psi, 2 at 210 psi
2	3	2N-2P	900	350	SnTe-HP	Ni-FB	140	
2	4	2N-3P	900	350	SnTe-HP	Ni-FB	140	
3	5	2N-2P	1000	350	SnTe-HP(3)	Ni-FB	140	
3	6	2N-3P	1000	350	SnTe-HP(3)	Ni-FB	140	
4	7	2N-3P	1100	400	SnTe-HP(3)	Ni-FB	140	
4	8	2N-3P	1100	400	No bond(4)	Ni-FB	140	

NOTES:

(1) HP = hot pressed
(2) FB = furnace bonded
(3) Two couples (2 and 4) furnace bonded, four couples hot pressed
(4) Pressure contacts, three knurled, three plain

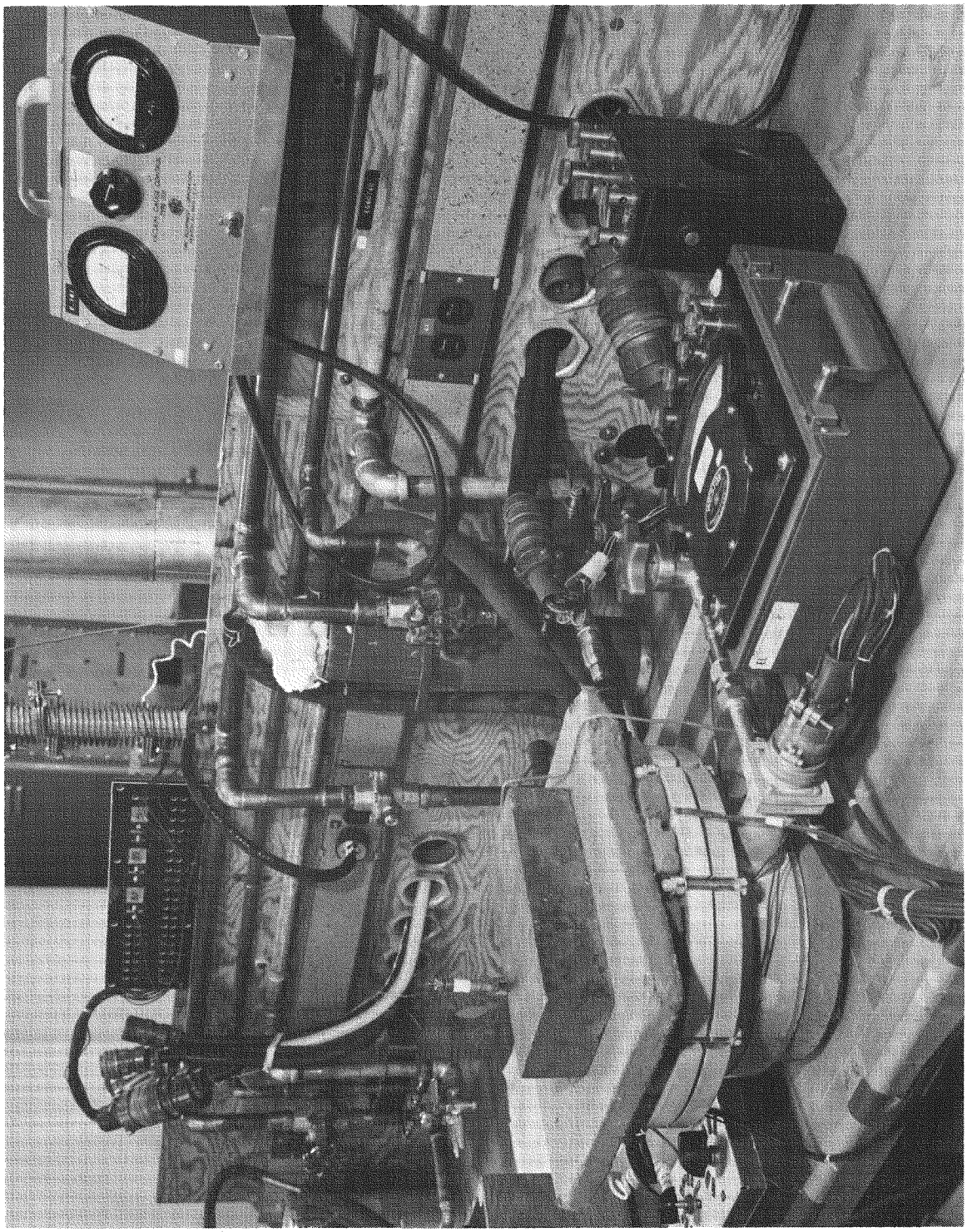

Fig. VI-5. Module Test Fixture Installation

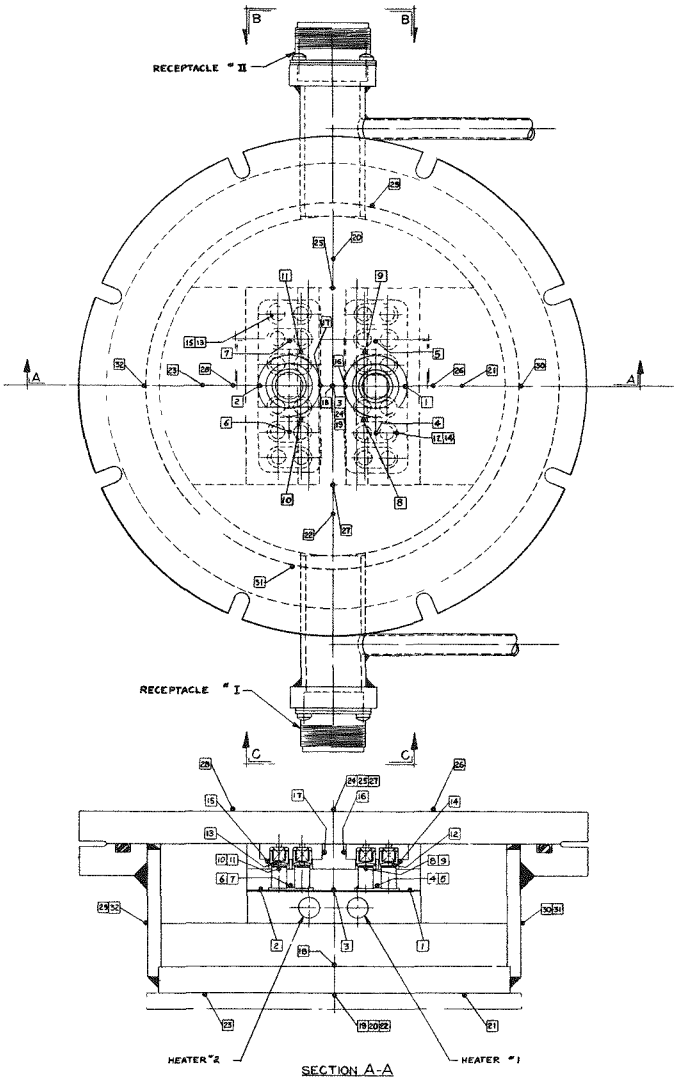

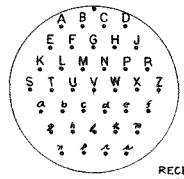

INSTRUMENTATION (THERMOCOUPLE) & WIRING TABULATION

SYMBOL	LOCATION (REF)	PINS POS	PINS NEG	RECEPTACLE	COMMENTS
1	HEATER BLOCK UPPER SURFACE	n	g	"II	
2		p	h	"II	
3	HEATER BLOCK UPPER SURFACE	L	E	"I	
4	HOT SHOE UPPER SURFACE	M	F	"I	
5		N	G	"I	
6		P	H	"I	
7	HOT SHOE, UPPER SURFACE	r	f	"II	
8	COLD STRAP	R	J	"I	
9		T	K	"I	
10		a	S	"I	
11	COLD STRAP	b	U	"I	
12	BUTTON "N"	c	V	"I	
13	BUTTON "P"	d	W	"I	
14	PISTON "N"	L	X	"I	
15	PISTON "P"	k	Z	"I	
16	MODULE BAR	s	A	"I	INSTALLATION ON EITHER SIDE OF BAR PERMISSABLE
17	MODULE BAR	r	f	"I	
18	FLOOR PLATE, INNER SURFACE	x	t	"I	
19	FLOOR PLATE, OUTER SURFACE				
20					
21					
22					
23	FLOOR PLATE, OUTER SURFACE				
24	COVER PLATE, OUTER SURFACE				
25					
26					
27					
28	COVER PLATE, OUTER SURFACE				
29	SIDE WALL, OUTER				
30					
31					
32	SIDE WALL, OUTER				
+	SEE WIRING DIAGRAM	S, T		"II	
−			U, V	"II	
+		Z, f		"II	
−	SEE WIRING DIAGRAM		W, X	"II	
HEATER"1	SEE WIRING DIAGRAM	A, B		"I	
HEATER"2	SEE WIRING DIAGRAM	C, D		"I	

VOLTAGE TAP NO.	1	2	3	4	5	6	7	8	9	10	11	12	13	14	15	16	17	18	19	20	21	22	23	24	25	26
RECEPTACLE NO.	I	I	I	II	II	II	II	II	II	II	II	II	II	II	II	II	II	II	II	II	II	II	II	II	II	II
PIN LETTER	f	m	d	A	B	C	D	E	F	G	H	J	K	L	M	N	P	R	a	b	c	d	e	h	m	s

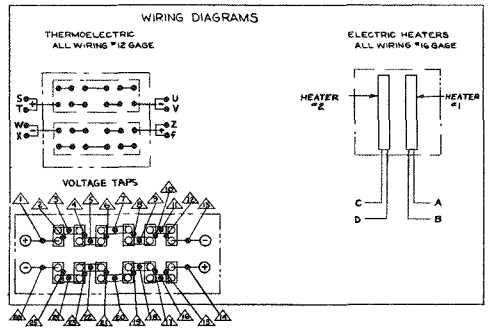

NOTES:

1. THERMOCOUPLE & VOLTAGE TAP LOCATIONS ARE APPROXIMATE.
2. METHOD OF SECURING THERMOCOUPLES & VOLTAGE TAPS:
   T/C & VOLTAGE TAPS TO IRON & SST - SPOTWELD
   T/C & VOLTAGE TAPS TO CU - SOLDER (ALLOY "55)
   T/C & VOLTAGE TAPS TO AL - DRILL HOLE & PEEN

Fig. VI-6. Thermoelectric Module--Test Fixture

TABLE VI-5

Six-Couple Module Test Results

Test Fixture	1		2		3		4	
Module No.	1	2	3	4	5	6	7	8
T/E Material	2N-2P	2N-3P	2N-2P	2N-3P	2N-2P	2N-3P	2N-3P	2N-3P
Operating Temperature (°F)								
Hot junction	1000	1000	900	900	1000	1000	1100	1100
Cold junction	350	350	350	350	350	350	400	400
Accumulated Testing Time (hr)	8673	8673	7916	7916	1830[2]	1830[2]	7577	7577
	Normalized Power Output (watts)[1]							
Approximate Operating Time (hr)								
0	3.22	3.00	2.72	2.22	3.08	3.14	3.61	2.94
1000	2.84	2.88	2.48	2.12	2.88	2.89	3.35	2.80
2000	2.62	2.80	2.37	2.12	2.75	2.85	3.29	2.89
3000	2.44	2.70	2.28	2.12	--	--	3.24	2.96
4000	2.41	2.63	2.22	2.11	--	--	3.22	2.96
5000	2.40	2.64	2.17	2.10	--	--	3.07	2.98
6000	2.47	2.60	2.17	2.07	--	--	3.38[3]	2.97
7000	2.45	2.61	2.15	2.09	--	--	3.47	3.03
8000	2.45	2.62	2.12	2.08	--	--	3.45	2.98
9000	2.44	2.60	--	--	--	--	--	--
	Decay Rate (%/1000 hr)							
Test Period (hr)								
0 to 1000	11.8	4.0	11.3	4.5	6.5	8.0	7.2	4.7
1000 to 2000	7.7	3.8	4.5	0.0	5.4	1.8	1.8	-3.0
2000 to 3000	6.8	3.6	5.0	0.0	--	--	2.1	-2.5
3000 to 4000	1.6	2.6	2.6	0.5	--	--	0.7	0.0
4000 to 5000	0.4	-0.4	2.3	0.5	--	--	4.6	-0.6
5000 to 6000	-2.9	1.5	0.0	1.4	--	--	-10.1[3]	0.3
6000 to 7000	0.8	-0.4	0.9	-1.0	--	--	-2.7	-2.0
7000 to 8000	0	-0.4	1.4	0.5	--	--	0.6	1.7
8000 to 9000	0.4	0.8	--	--	--	--	--	--

[1] All power values are normalized power at time indicated for temperature only.
[2] Test stopped at 1830 hours because of repeated heater failure.
[3] Hot junction thermocouples lost during this period.

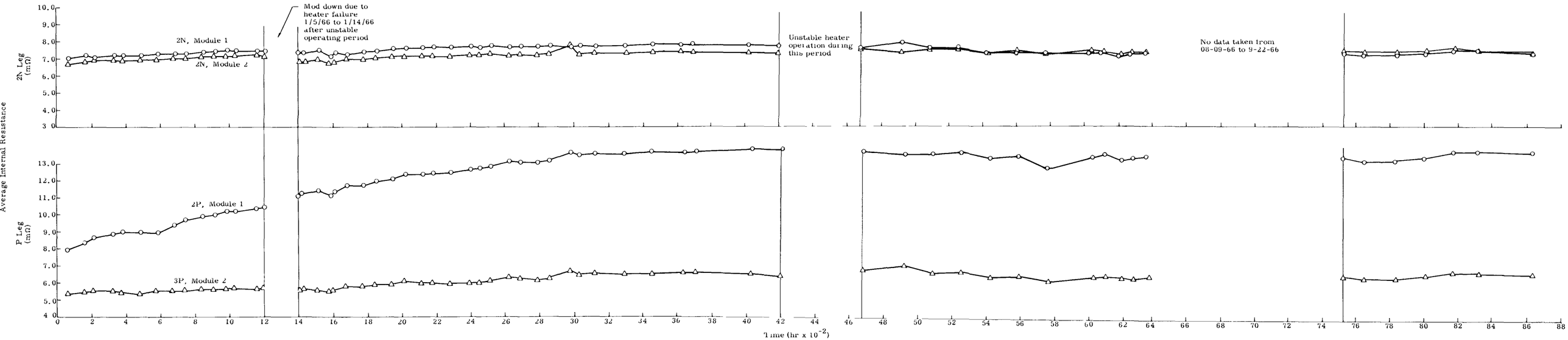

Fig. VI-7. Raw Data Points

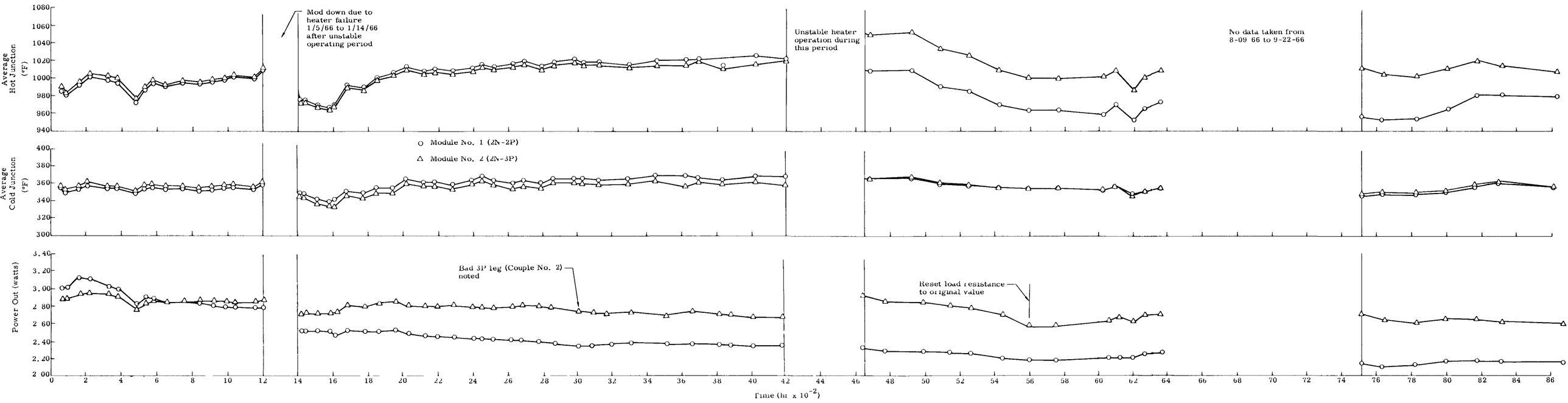

Fig VI-7. (continued)

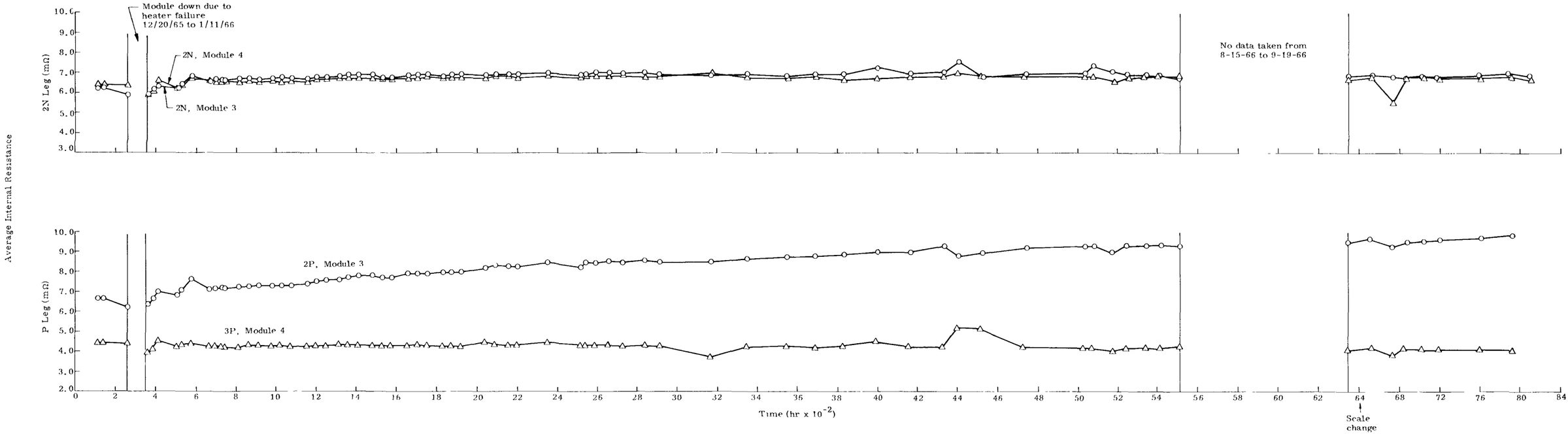

Fig. VI-8. Raw Data Points

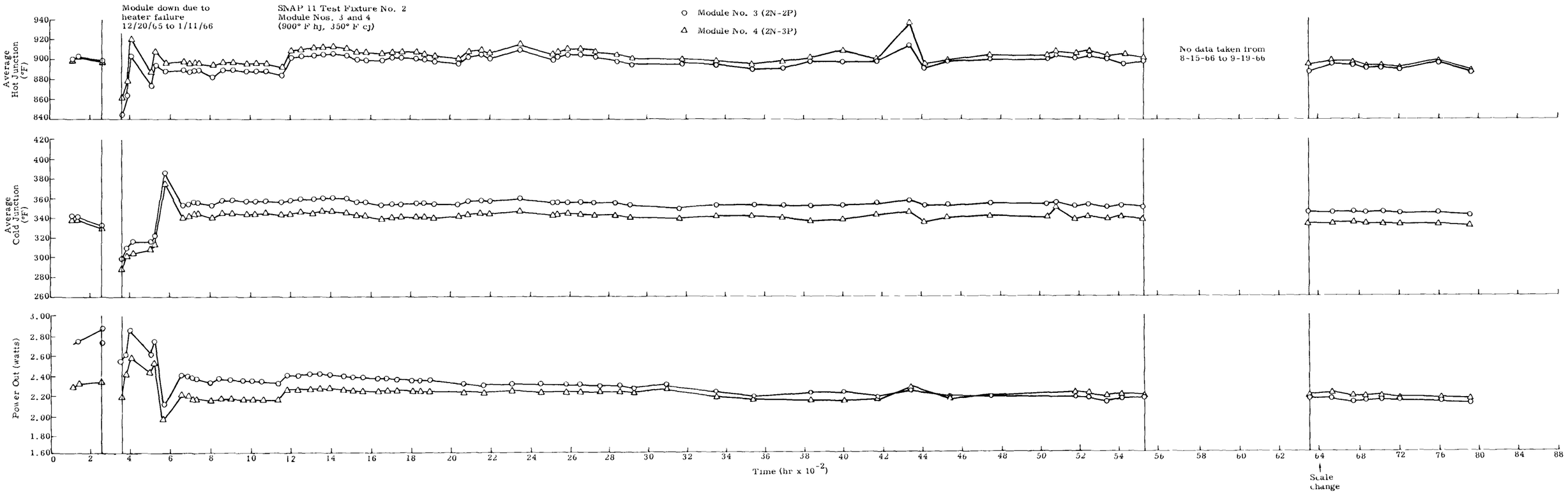

Fig. VI-8. (continued)

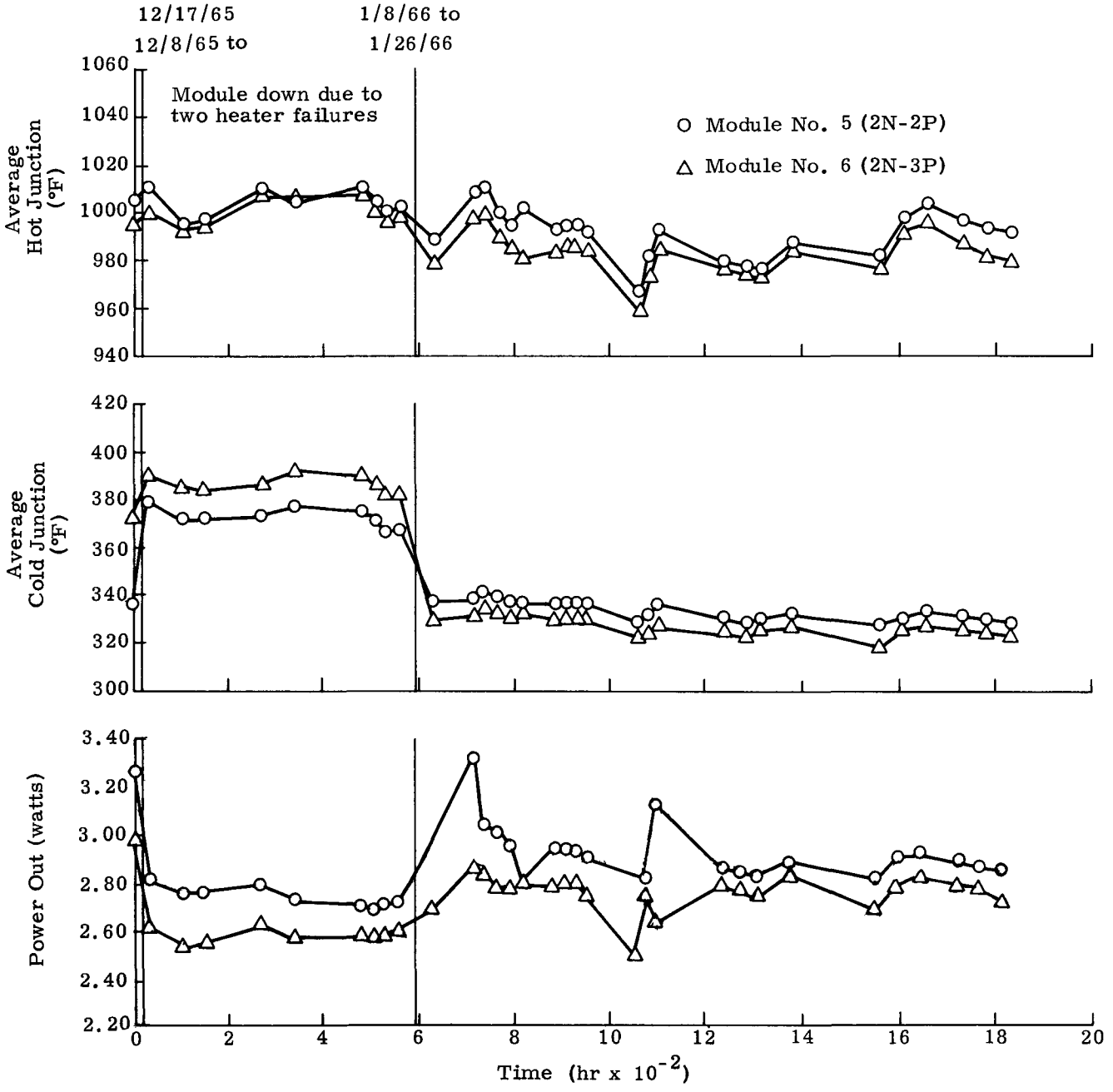

Fig. VI-9. Raw Data Points

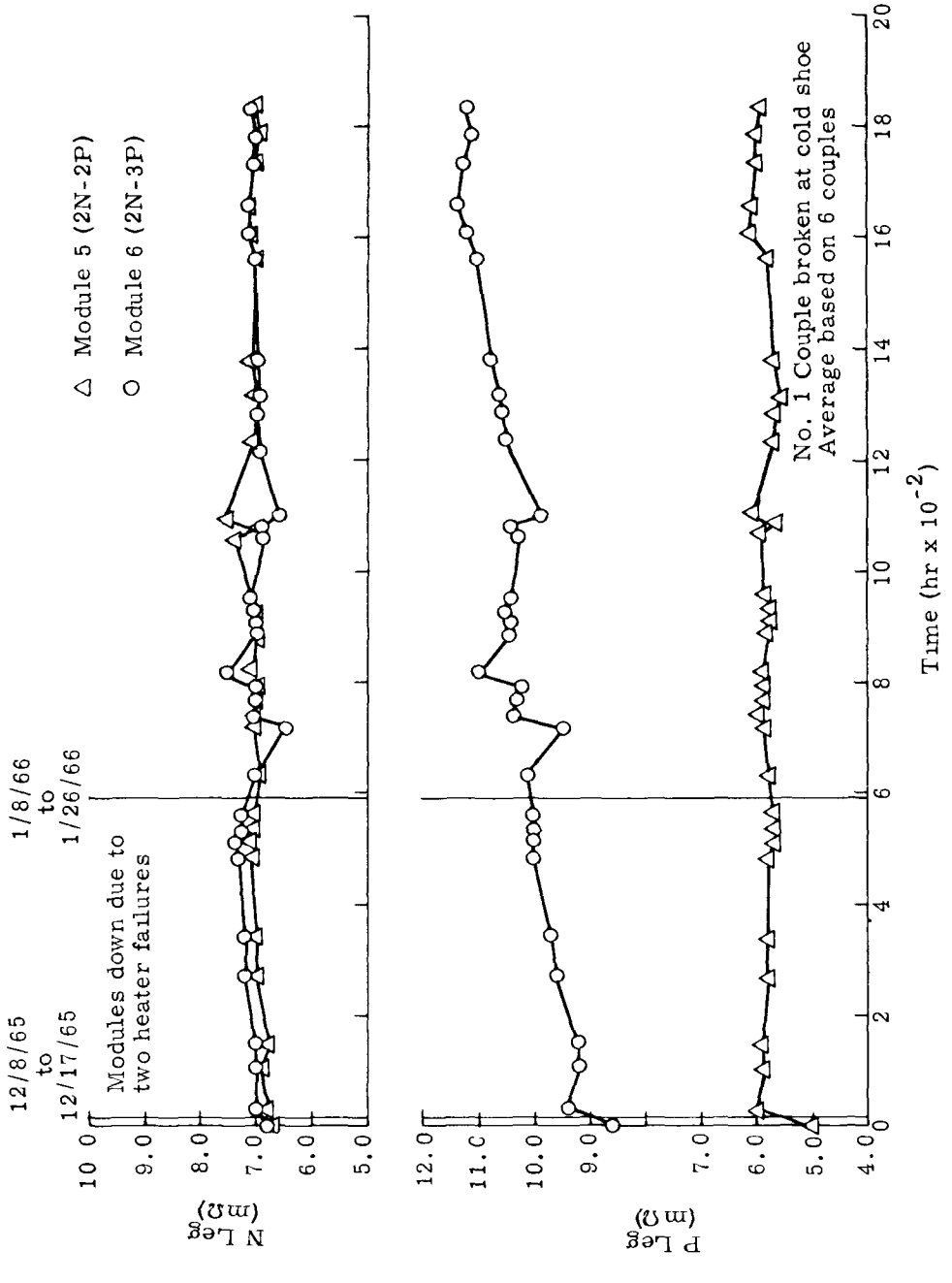

Fig. VI-9. (continued)

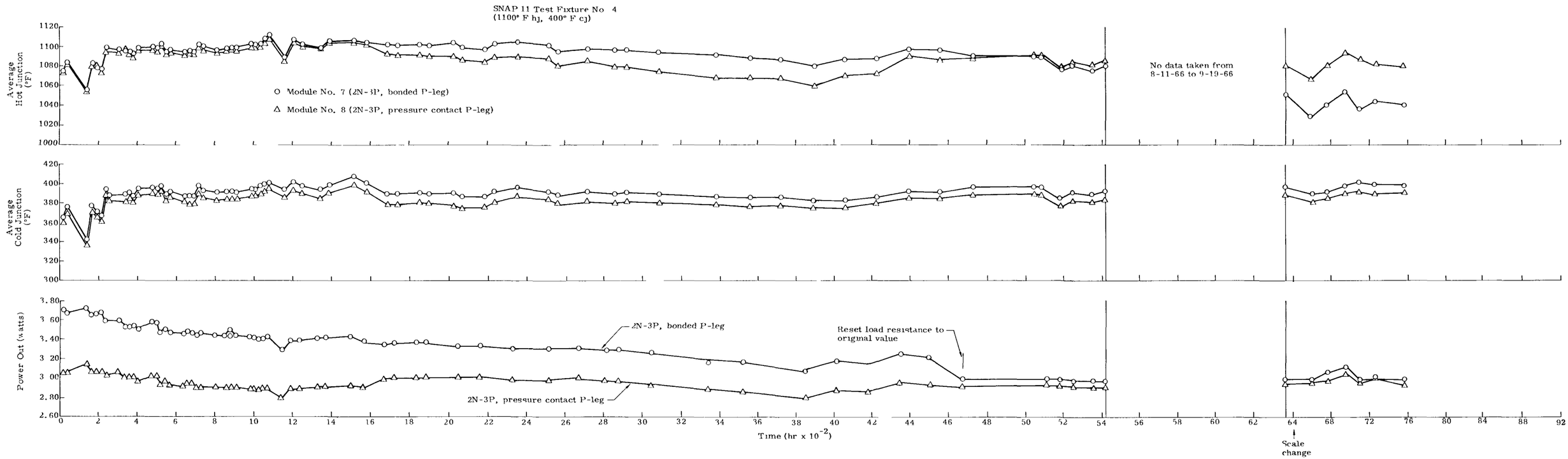

Fig. VI-10. Raw Data Points

Internal Resistance, 2N-3P Material

Average Internal Resistance 3P Leg (3 couples) Knurled Contact (mΩ)

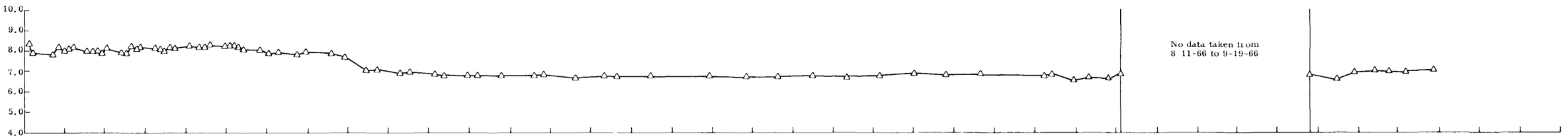

Module 8 Average

Average Internal Resistance 3P Leg (3 couples) Plain Pressure Contact (mΩ)

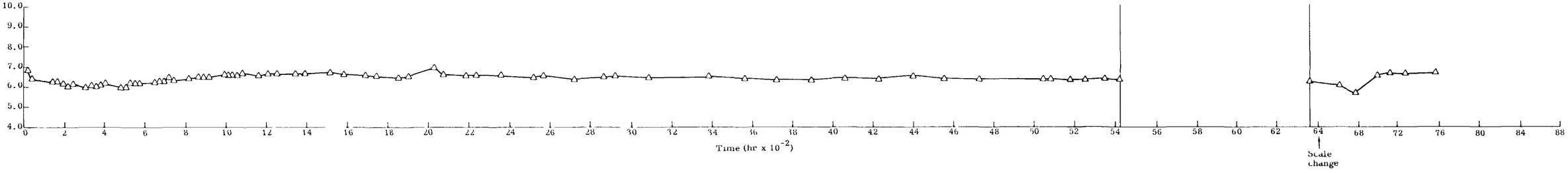

Fig. VI-10. (continued)

Module Nos. 7 and 8, Average Internal Resistance

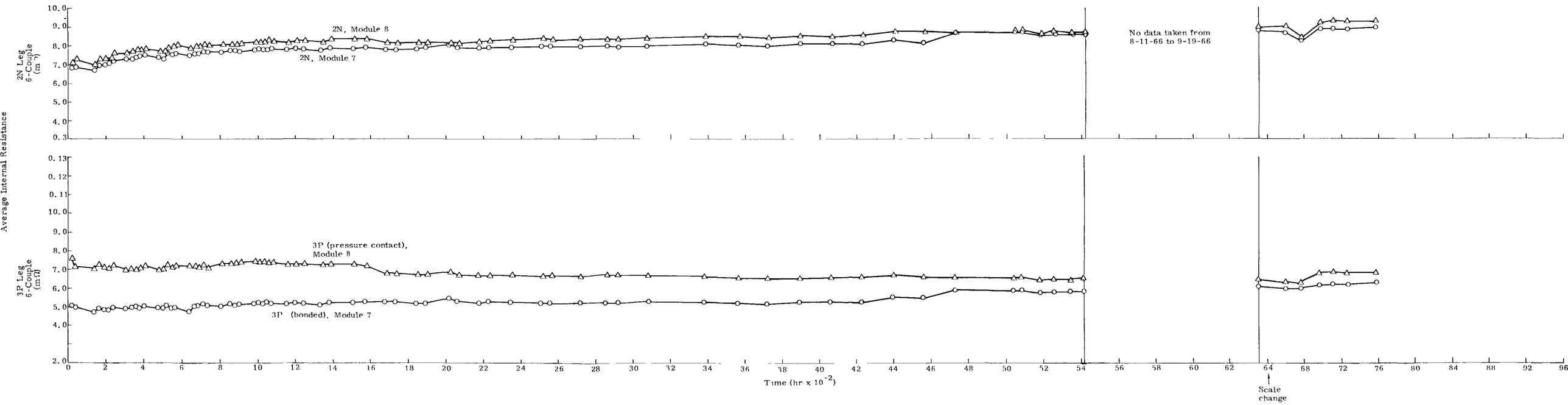

Fig. VI-10. (continued)

throughout the test was erratic heater operation. Periods during which testing was discontinued for heater repair are so indicated on the raw data sheets. Testing of Modules 5 and 6 was discontinued after 1830 hours because of continued heater failures.

Table VI-6 compares the leg resistances of each module at the beginning of the test with values determined at the last data point taken. The resistance values are not normalized to a set of given temperature conditions, but do illustrate in which legs large resistance changes were observed. Readily apparent is the large resistance increase of the 2P legs in Modules 1, 3 and 5 and the relatively stable resistance of the 3P and 2N material. In Test Fixture 4--Modules 7 and 8, the resistance of the 3P leg with plain pressure contacts was relatively stable, while an increase in the bonded 3P leg resistance and a decrease in the knurled pressure contact resistance were noted. Also, the N leg resistance was not as stable at the 1100° F hot junction as at the 900° and 1000° F values but is still considered acceptable.

TABLE VI-6

Summary of Module Leg Resistances

Module	N Leg Resistance at t = 0 (mΩ)	N Leg Resistance at Last Point (mΩ)	P Leg Resistance at t = 0 (mΩ)	P Leg Resistance at Last Point (mΩ)
1	7.05	7.30	7.95	14.10
2	6.65	7.50	5.30	6.70
3	6.20	6.90	6.65	9.95
4	6.40	6.70	4.45	4.10
5	6.80	7.10	8.60	11.20
6	6.70	7.00	5.00	5.90
7	6.90	9.10	5.10	6.40
8	7.10	9.55	N/A	N/A
8(1)	N/A	N/A	6.85	6.75
8(2)	N/A	N/A	8.40	7.00

(1)Plain pressure contact

(2)Knurled pressure contact

A comparison of the individual leg resistances in Module 1 was made to determine the effect of spring pressure on the change in leg resistance. Results are summarized in Table VI-7. Examination of the resistance changes determined led to the conclusion that no apparent advantage exists for the higher spring pressures in stabilizing leg resistance.

To effectively compare the performance of the thermoelectric modules in a test fixture, the raw power curves for each module presented previously in this chapter were normalized to the same hot and cold junction operating temperatures. Normalizing in this manner allows comparison at similar junction operating conditions. Power points were normalized by first determining the module contact resistivity from the data point parameters taken, and then determining the power output at this contact resistivity from performance curves at the hot and cold junction temperatures used for normalization. (Figures VI-3 and VI-4 are similar performance maps for a complete generator.)

Figures VI-11 through VI-13 are plots of normalized power output as a function of time for Test Fixtures 1, 2 and 3. In Test Fixture 1, the 2N-3P module produced 6.9% less power than the 2N-2P module at the beginning of the test, but since ~700 hours of operation has out performed the latter. After 8673 hours, the 2N-3P module is producing 6.5% more power than the 2N-2P module. Total power decrease since the beginning of the test is 13.4 and 24.2% for the 2N-3P and 2N-2P modules, respectively.

In Test Fixture 2, the 2N-3P module produced 18.4% less power than the 2N-2P module, and after 7916 hours is still producing 1.9% less power. Total power decay from the beginning of the test is 6.3 and 22.1% for the 2N-3P and 2N-2P modules, respectively.

In Test Fixture 3, the 2N-3P produced 1.9% more power than the 2N-2P module at the test beginning, and after 1830 hours, at which time testing on this fixture was discontinued due to repeated heater failures, the 2N-3P module was producing 3.6% more power than the 2N-2P module. Total power decay from the beginning of the test was 9.2 and 11% for the 2N-3P and 2N-2P modules, respectively. (Due to the repeated heater failures in this fixture, test results are considered suspect, and results for the 1000° F hot junction test conditions are considered to be representative of Test Fixture 1 conditions.)

TABLE VI-7

T/E Couple Leg Resistances for Modules 1 and 2

Module 1

Module	Couple Leg	T/E Material	Spring Pressure (psi)	R_i (mΩ) T_{HJ} = 980° F T_{CJ} = 349° F (t = 0 hr)	R_i (mΩ) T_{HJ} = 1011° F T_{CJ} = 362° F (t = 2189 hr)	R_i (mΩ) T_{HJ} = 1024° F T_{CJ} = 368° F (t = 3692 hr)	R_i (mΩ) T_{HJ} = 982° F T_{CJ} = 358° F (t = 8673 hr)	ΔR_i (mΩ) (from t = 0)
1	1	2P	140	9.0[1]	--	--	--	--
1	2	2P	70	7.8	12.4	13.9	13.8	6.0
1	3	2P	210	7.5	11.8	13.0	13.8	6.3
1	4	2P	210	7.6	11.0	12.2	12.6	5.0
1	5	2P	70	7.8	11.2	13.0	13.4	5.6
1	6	2P	140	8.3	11.4	12.4	12.6	4.3
1	1	2N	140	7.0	8.0	8.0	7.9	0.9
1	2	2N	70	7.5	7.8	8.0	7.5	0
1	3	2N	210	7.1	8.0	7.7	6.3	-0.8
1	4	2N	210	7.0	7.8	7.8	7.5	0.5
1	5	2N	70	7.0	7.6	7.6	7.7	0.7
1	6	2N	140	6.8	7 2	7.4	7.3	0.5

Module 2

Module	Couple Leg	T/E Material	Spring Pressure (psi)	R_i (mΩ) T_{HJ} = 983° F T_{CJ} = 353° F (t = 0 hr)	R_i (mΩ) T_{HJ} = 1007° F T_{CJ} = 358° F (t = 2189 hr)	R_i (mΩ) T_{HJ} = 1021° F T_{CJ} = 363° F (t = 3692 hr)	R_i (mΩ) T_{HJ} = 1010° F T_{CJ} = 359° F (t = 8673 hr)	ΔR_i (mΩ) (from t = 0)
2	1	3P	140	5.2	6.3	6.8	7.6	2.4
2	2	3P	70	5.7	6.7	8.5	9.1	3.4
2	3	3P	210	5.5	5.8	6.1	5.9	0.4
2	4	3P	210	5.0	5.4	5.6	5.6	0.6
2	5	3P	70	5.3	6.0	6.5	6.2	0.9
2	6	3P	140	5.2	5.7	6.0	5.9	0.7
2	1	2N	140	6.9	6.7	7.0	7.9	1.0
2	2	2N	70	6.8	7.3	7.5	8.2	1.4
2	3	2N	210	6.6	6.7	6.8	7.4	0.8
2	4	2N	210	6.5	7.1	7.3	6.9	0.4
2	5	2N	70	6.8	7.5	7.6	7.7	1.1
2	6	2N	140	6.5	7.5	7.8	7.1	0.6

[1] 2P leg broken during heater repair.

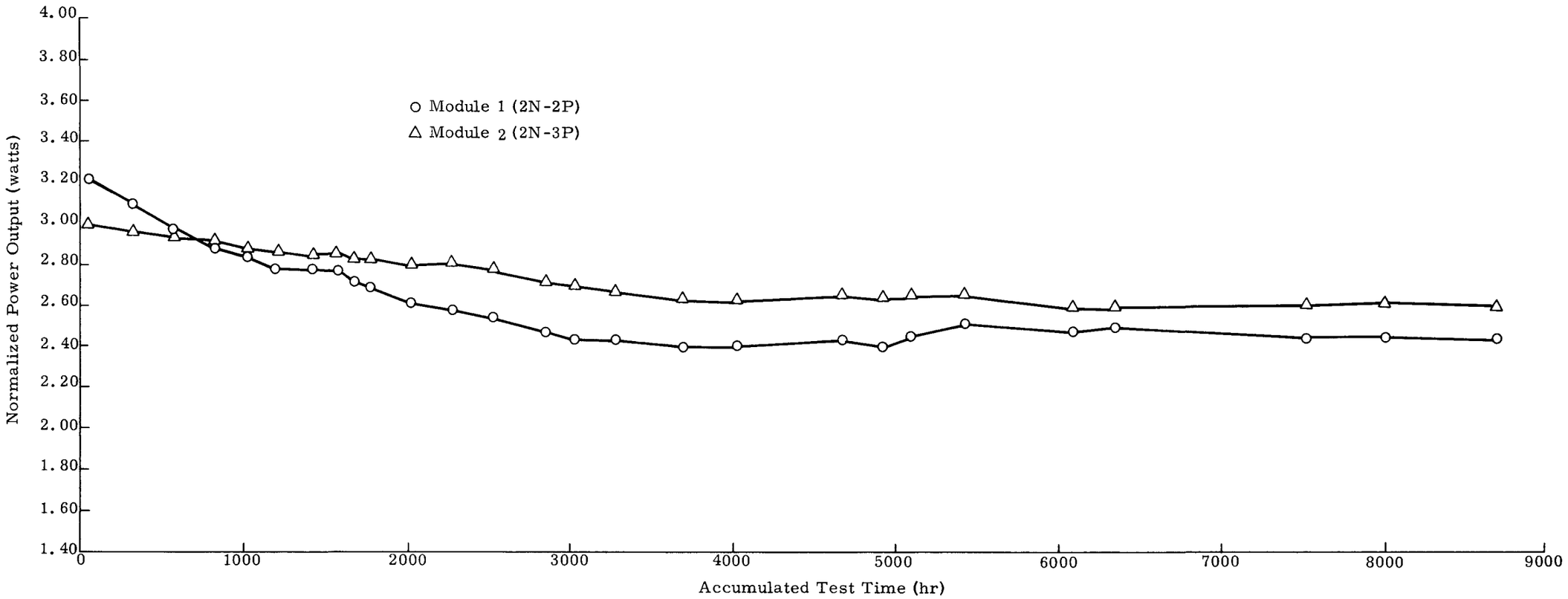

Fig. VI-11. Normalized Power Curves for Test Fixture 1 (data normalized to 1000° F HJ; 350° F CJ)

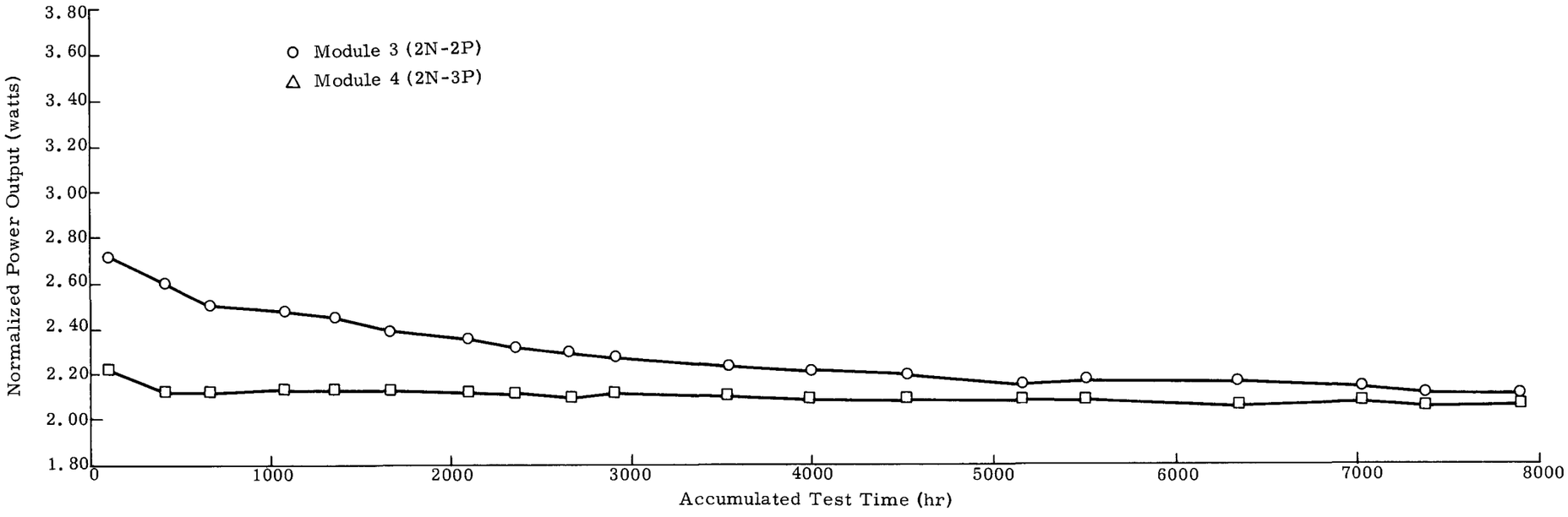

Fig. VI-12. Normalized Power Curves for Test Fixture 2 (data normalized to 900° F HJ; 350° F CJ)

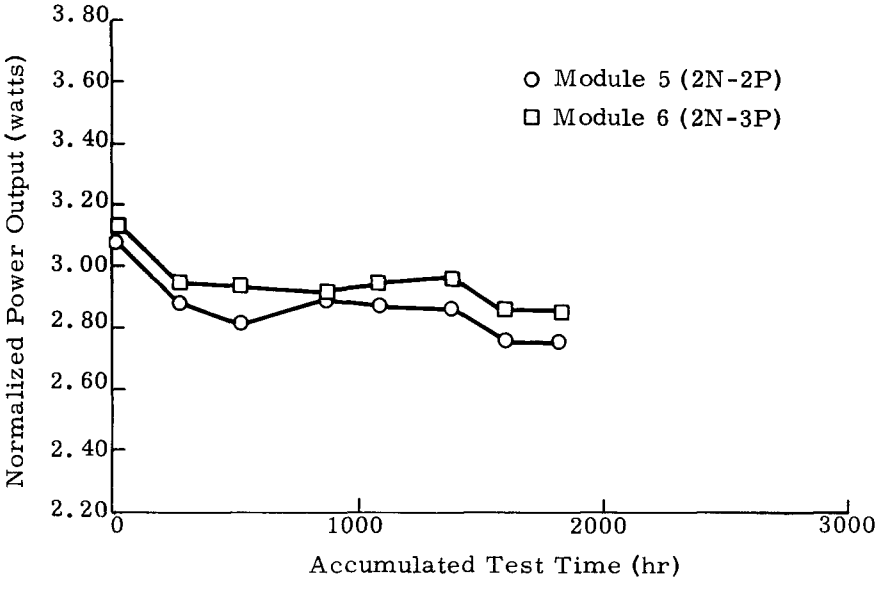

Fig. VI-13. Normalized Power Curves for Test Fixture 3 (data normalized to 1000° F HJ; 350° F CJ)

Figures VI-14 and VI-15 show the contact resistivity and E_{oc}/predicted E_{oc} for Modules 1 through 6. As anticipated, the modules operating at a 1000° F hot junction temperature exhibited the highest contact resistivities during testing, with Module 1 approaching 5900 $\mu\Omega$-cm^2 and Module 2 approaching 1000 $\mu\Omega$-cm^2 at the last data point (8673 hours). Measured open circuit values were within 5% of reduced values in all cases during testing with a notable increase noted in all 2N-2P modules with time.

Figure VI-16 shows the normalized power curves for Test Fixture 4. At the initiation of the test, the bonded 2N-3P module was producing 22.4% more power than the module with unbonded 3P hot junction contacts. At the test conclusion, considered to be at ~5500 hours, the performance margin was reduced to 5%. At ~5500 hours thermocouples on both modules were lost, thus precluding any normalized power calculations.

Figure VI-17 shows plots of contact resistivity and E_{oc}/predicted E_{oc} for Modules 7 and 8. From Fig. VI-17, it can be seen that the bonded module exhibited the largest increase in contact resistivity, but the end value was still below that of the more stable unbonded module. Also evident from Fig. VI-17 is the E_{oc}/predicted E_{oc} value increase after ~5500 hours due to the loss of hot junction thermocouples on both modules.

Figure VI-18 shows the contact resistivity of the three types of 3P legs in Test Fixture 4, i.e., bonded, knurled pressure and plain pressure contacts. The bonded contact 3P leg showed an increase in contact resistivity, the value for the plain contact leg remained virtually constant, and the knurled contact decreased due to seating of the elements.

4. Conclusions

In summary. the following conclusions can be drawn from the testing:

(1) The 3P material is more stable than the 2P material at all hot junction operating temperatures.

(2) The superior performance of 3P over 2P is evident at hot junction temperatures of 1000° F and higher.

(3) The selection of 3P over 2P at a 900° F hot junction temperature is not quite as evident as at the higher hot junction temperatures.

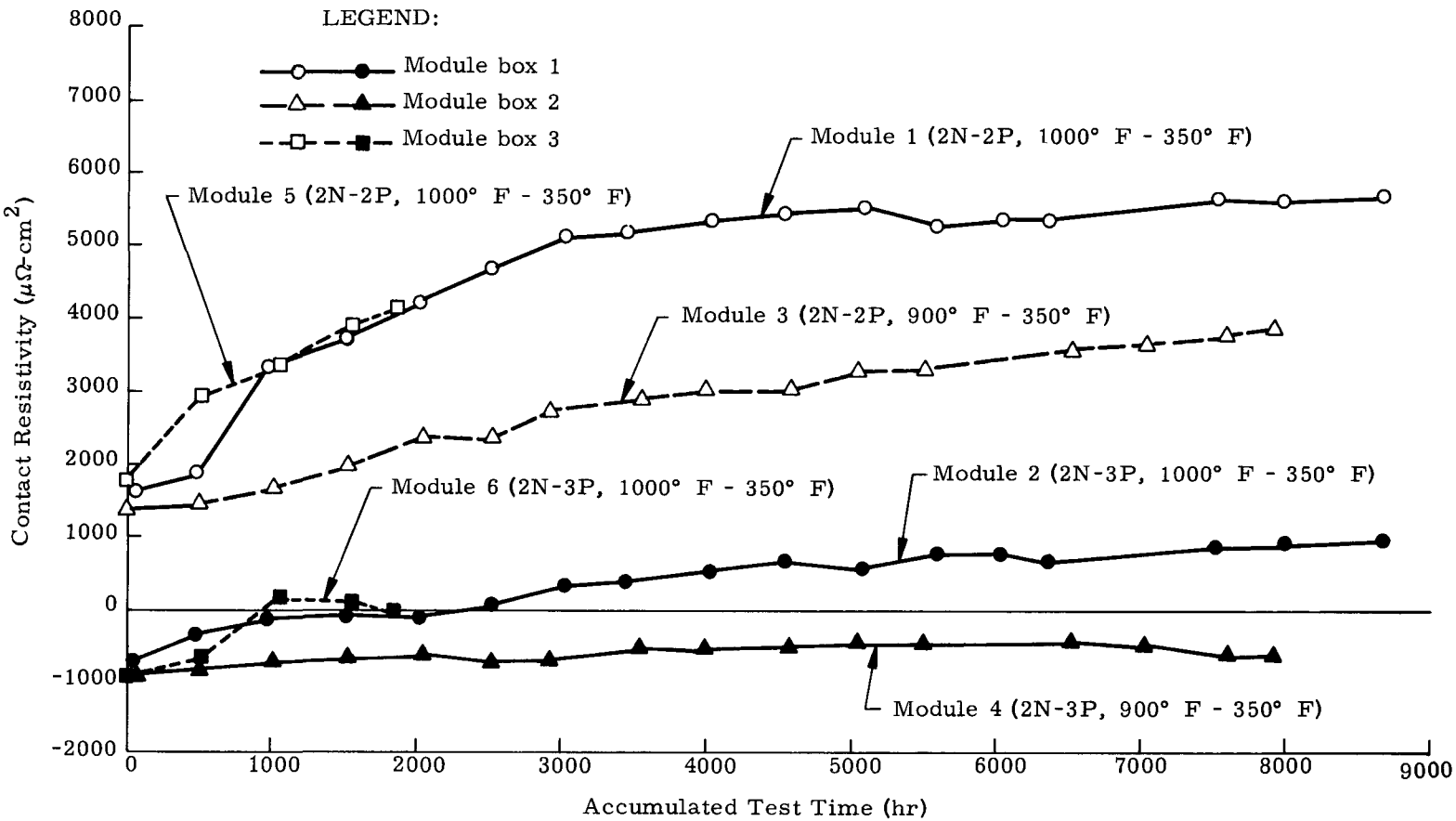

Fig. VI-14. Contact Resistivity Versus Test Time

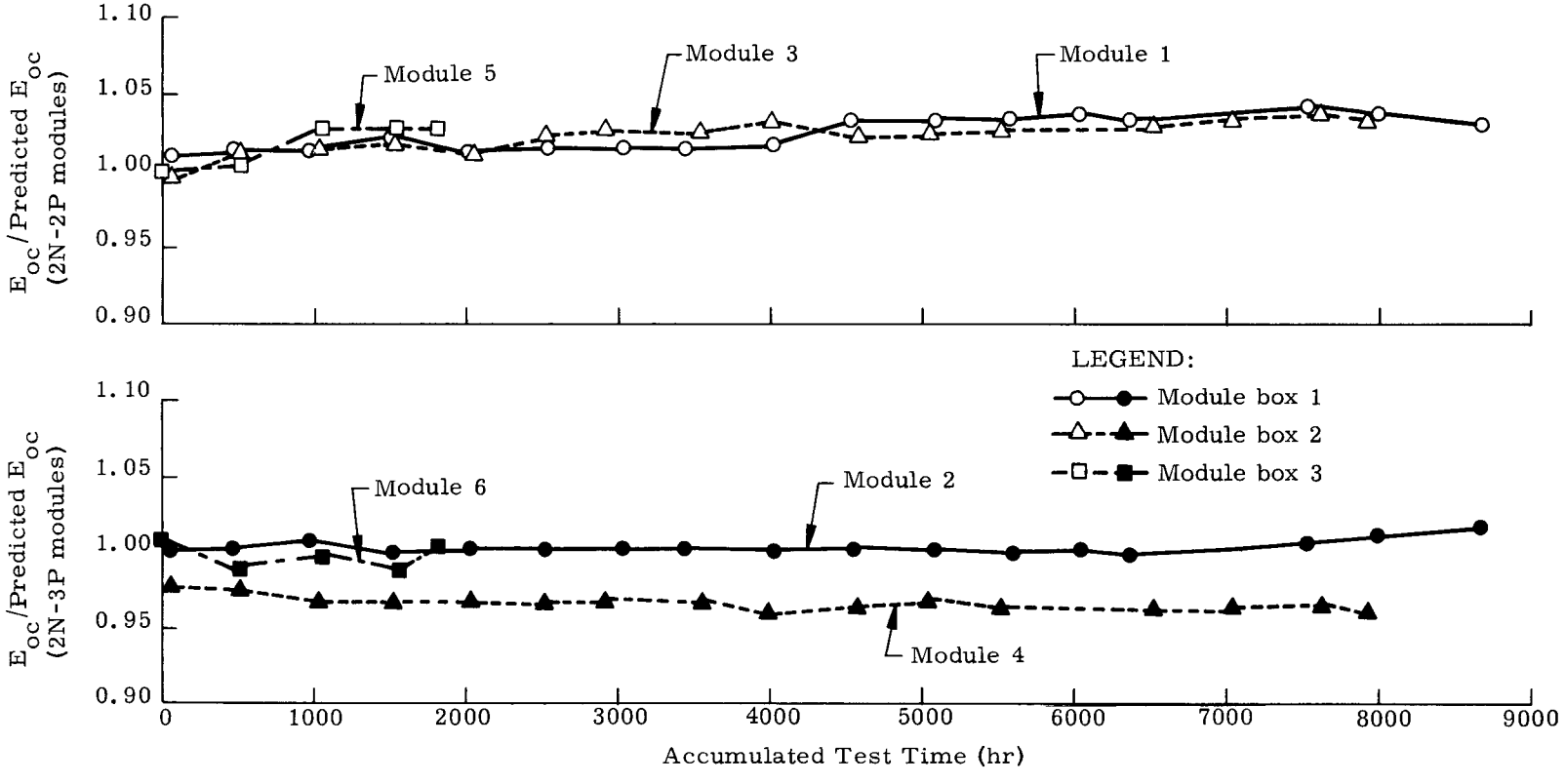

Fig. VI-15. E_{oc}/Predicted E_{oc} Versus Test Time

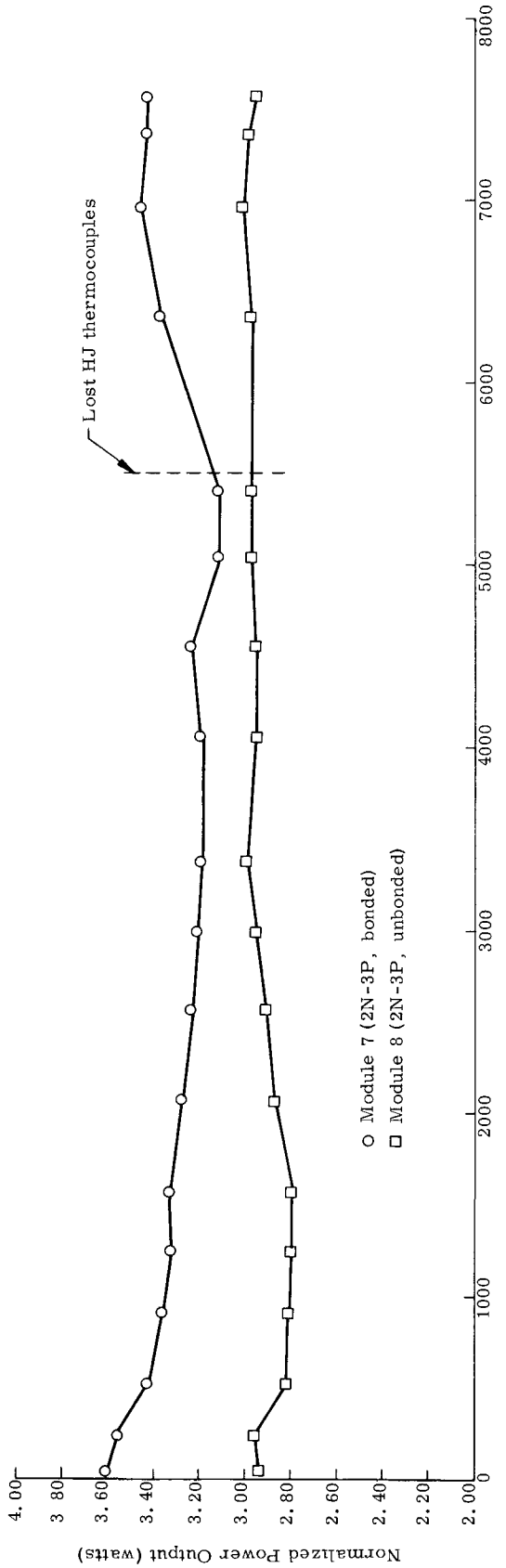

Fig. VI-16. Test Fixture 4, Normalized Power Output

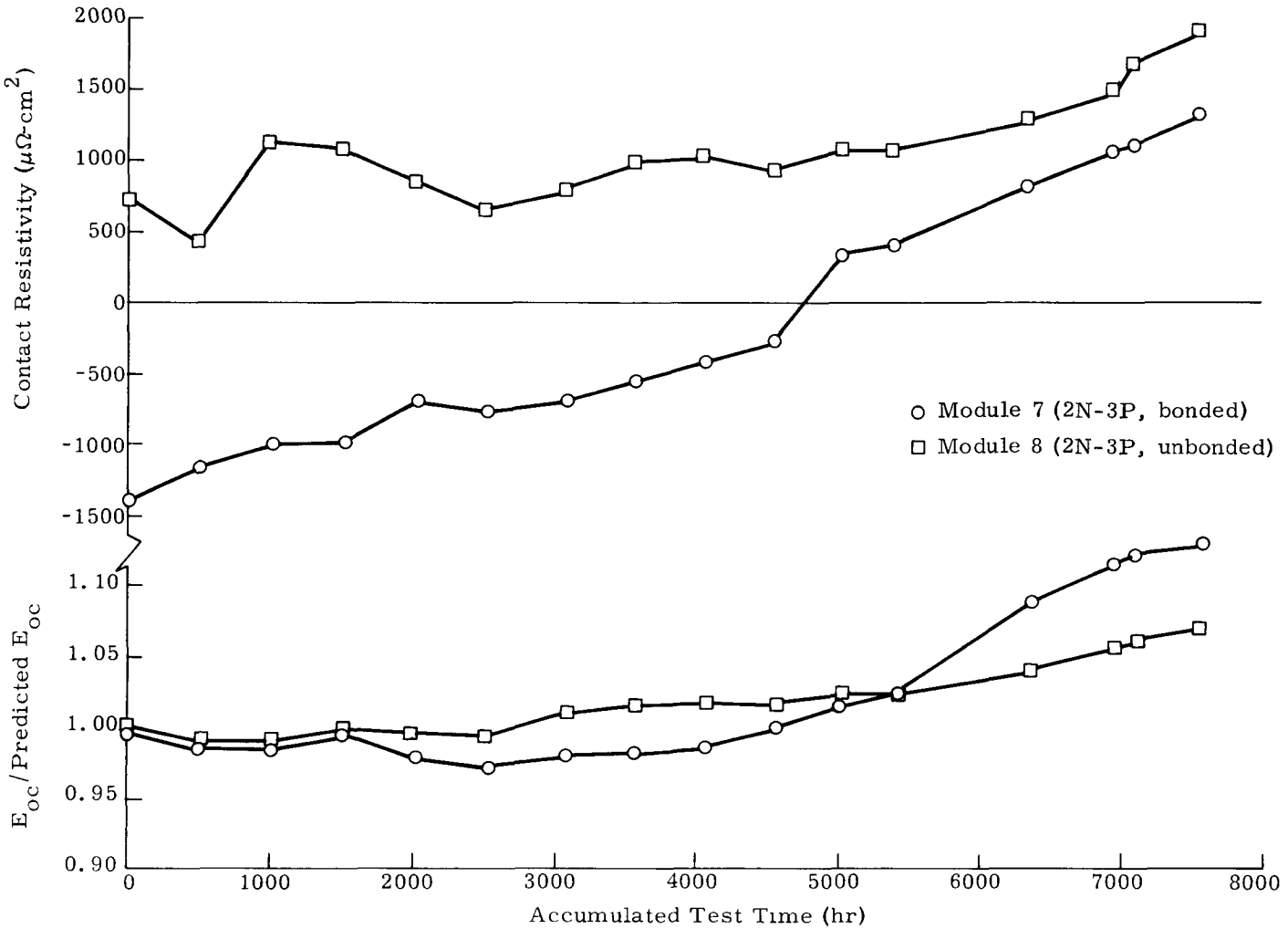

Fig. VI-17. Test Fixture 4, Open Circuit Voltage and Contact Resistivity

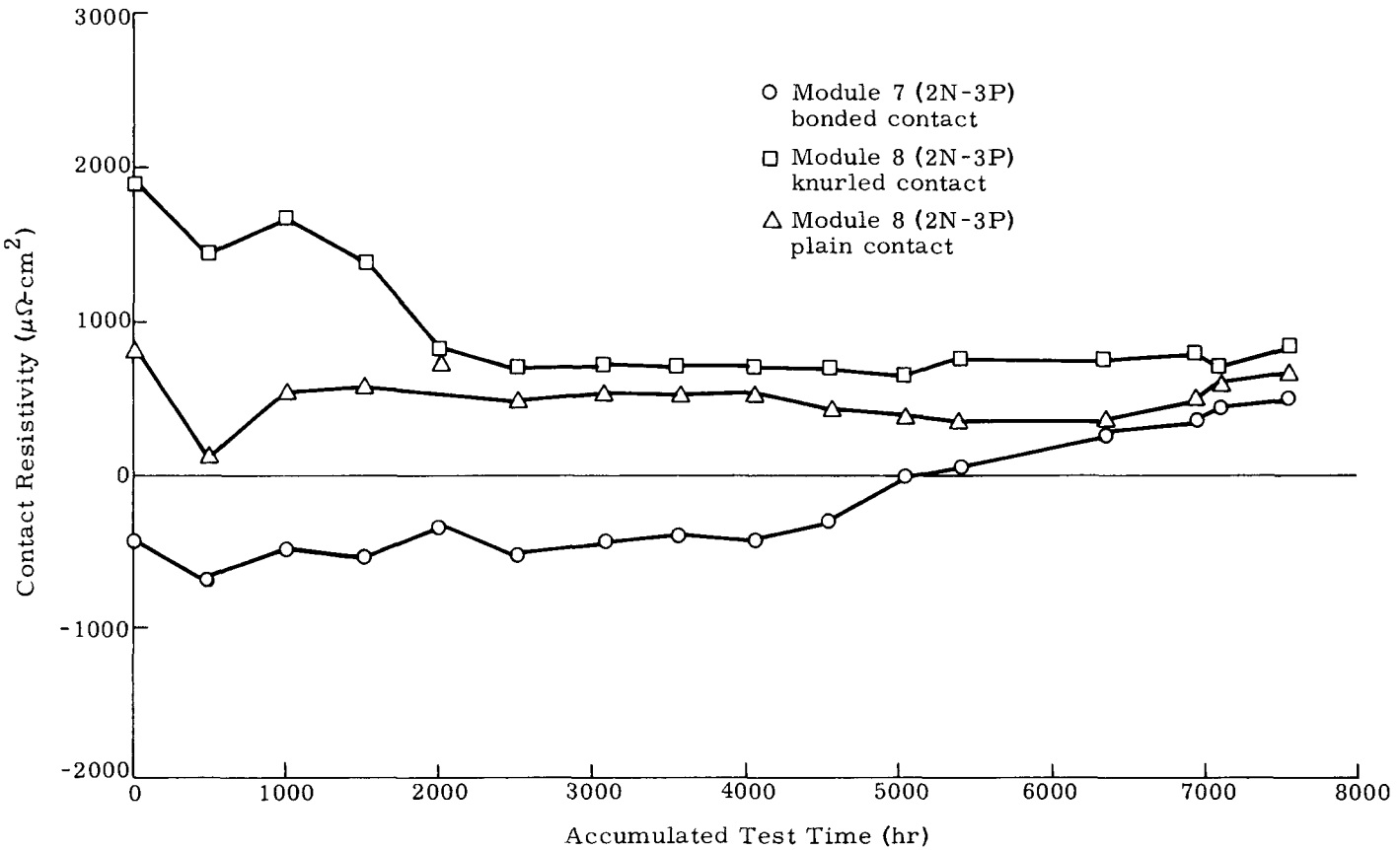

Fig. VI-18. Test Fixture 4, Comparison of Types of Contact

CONFIDENTIAL

(4) Plain pressure contacts appear to be more stable than either knurled or bonded contacts, although still possessing a resistance higher than that of bonded legs.

(5) Operation of 2N-3P material at hot junction temperatures as high as 1100° F appears feasible.

(6) In the spring pressure evaluation, i.e., 70, 140 and 210 psi, no apparent advantage existed as to reduction in element resistance increase with time.

BLANK

VII. DC-TO-DC CONVERTER

A. DESIGN

The dc-to-dc converter is designed to convert the three-volt d-c output of the generator to 29 volts dc for use in the spacecraft power system. Conversion efficiency is 85% or greater. Maximum peak-to-peak ripple is 1% of the output voltage. The converter, in conjunction with the generator, operates as an unregulated power source; and the output power is supplied directly to the regulated bus in the spacecraft power system.

The converter is designed to operate in a vacuum and to withstand the Atlas-Centaur dynamics of shock, vibration and acceleration. It is installed in the spacecraft in a temperature-controlled compartment and is designed to operate between 0° and 125° F.

Figures VII-1 and VII-2 show the converter configuration, and Fig. VII-3 shows the converter components and electrical schematic. The electrical components are packaged and housed in a magnesium alloy casting with integral cooling fins. Protection is provided by a conformal coating of MMSL-611. The cover is fabricated of 0.031-inch magnesium sheet. Power connections are made to press-fitted teflon feedthrough terminals. The weight of the unit is approximately 2.5 pounds with a volume of 55 $in.^3$.

The dc-to-dc converter provides a usable level of d-c voltage from the generator to the load. Since the output voltage of the generator is only three volts dc and since direct current voltages cannot be transformed or stepped up, it is necessary to change the d-c voltage to alternating current voltage, and then, by means of a transformer, step up the voltage to the desired 29 volts. The stepped up a-c voltage is then rectified and filtered to provide the 29 volts dc to the load.

The converter consists of an oscillator-driver, an amplifier, a power transformer and a rectifier filter. The oscillator driver is an overdriven push-pull transistor blocking oscillator which is transformer-coupled to the bases of the amplifier transistors. (The amplifier transistors are very low-loss germanium power units.) The outputs from the collectors of the amplifier transistors are connected to the power transformer. (The power transformer has a toroidal core of extremely high permeability nickel-iron material.) The a-c output from the power transformer is fed into a rectifier circuit containing two germanium power units, with only the collector-base junction used to perform the rectifying function. The filter section is a dry electrolytic capacitor of sufficient capacity to reduce the ripple voltage on the output to less than 1% of the nominal output voltage.

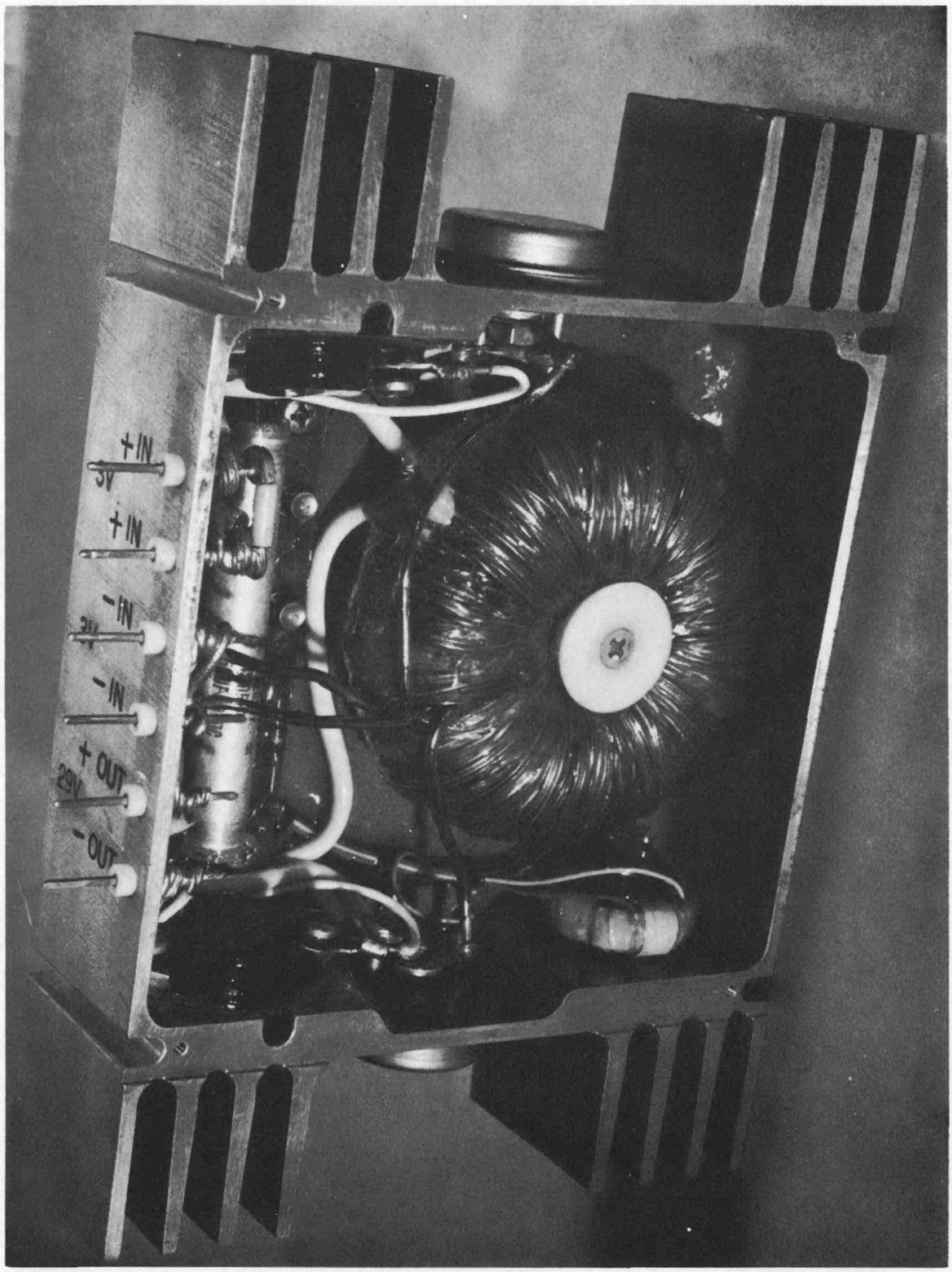

Fig. VII-1. DC-to-DC Converter Packaged in a Magnesium Housing

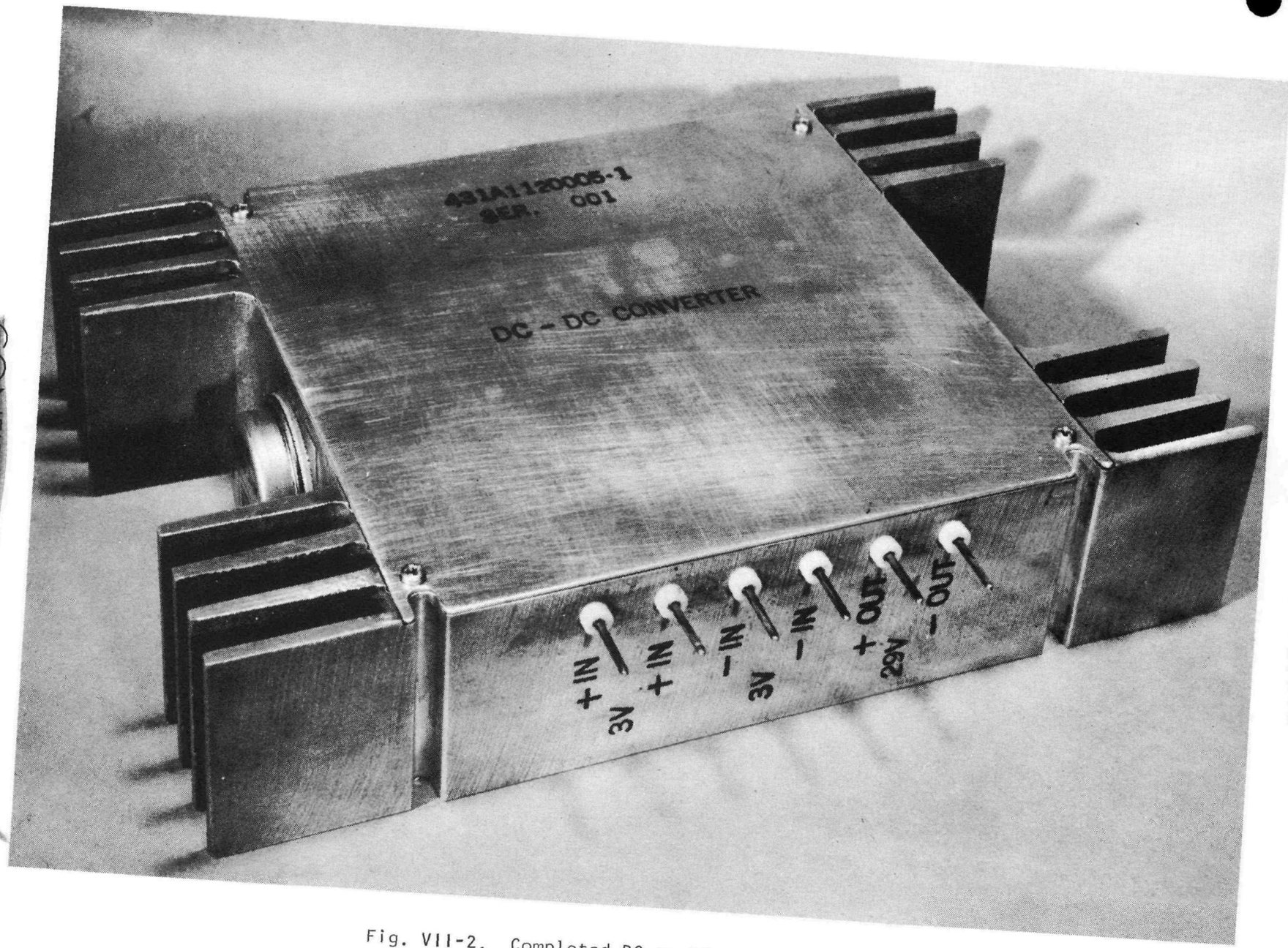

Fig. VII-2. Completed DC-to-DC Converter

CONFIDENTIAL

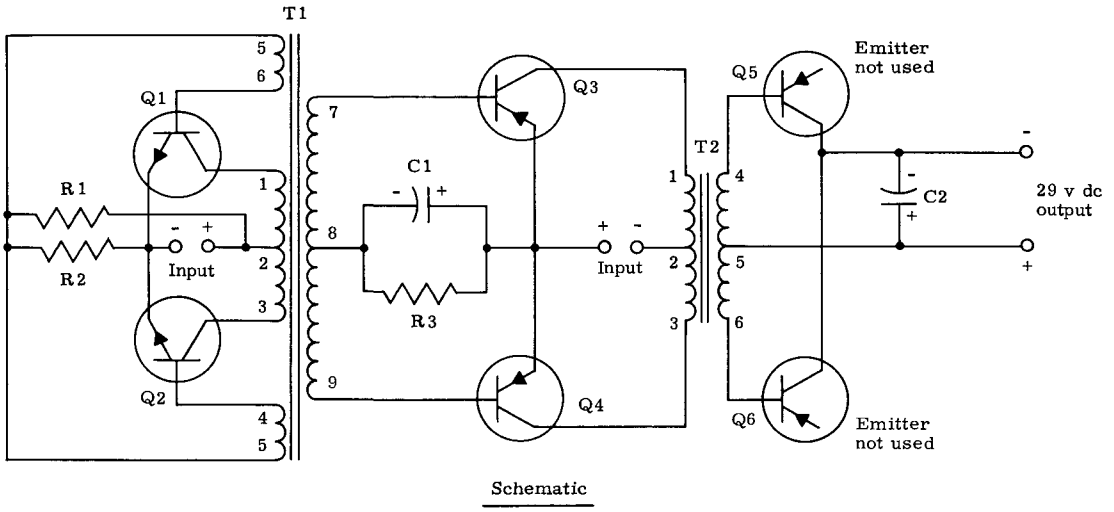

Schematic

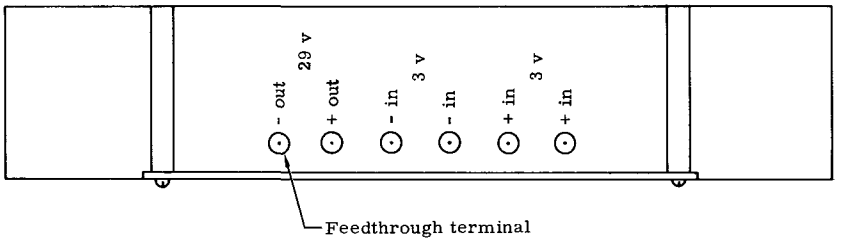

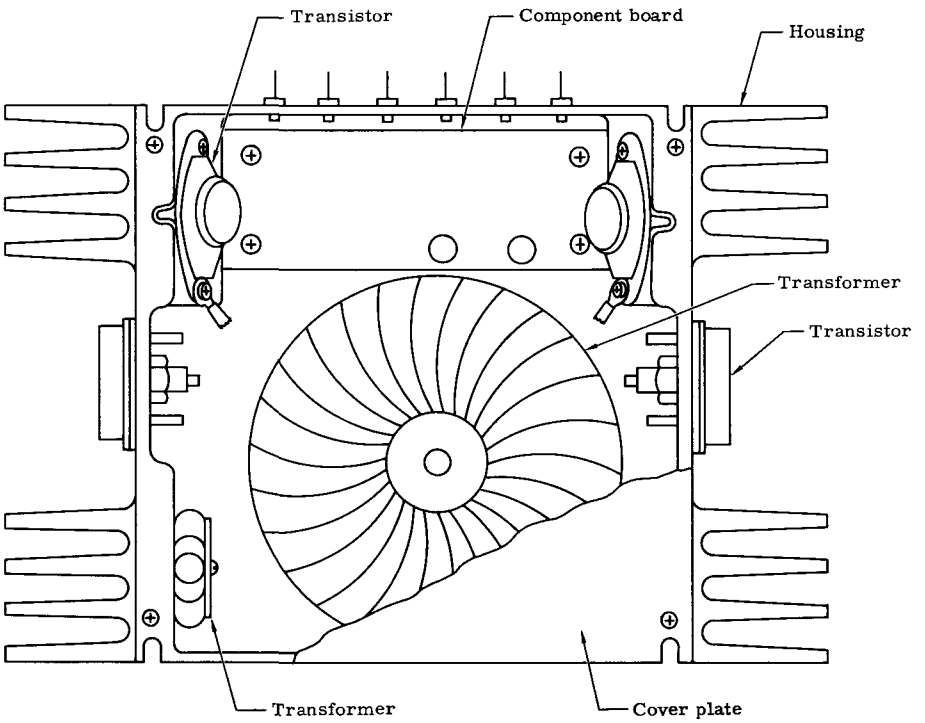

Fig. VII-3. Converter Details and Schematic

Initial development problems were centered about selection of a power transistor which could withstand sterilization temperatures of 125° C without damage. Initial breadboard tests of a dc-dc converter indicated that the germanium power transistors selected had insufficient current carrying capacity. They were replaced with Motorola transistors (P/N 2N1166). Subsequently, the performance of a high efficiency germanium power transistor (Minneapolis-Honeywell type MHT 2305) was evaluated in a breadboard converter assembly. Efficiency was measured as a function of switching frequency. The following results were obtained:

Switching Frequency (cps)	Converter Efficiency (%)
2500	81.5
1000	82.0
400	88

The 400 cps switching frequency converter was selected for packaging.

Four converters were fabricated and functionally tested. Test results are summarized in Table VII-1.

B. DYNAMIC AND ENVIRONMENTAL TESTS

Converter S/N-1 incurred a failure during setup. While making the output load adjustment, a loss of contact in a slide wire rheostat (later replaced by a decade resistance box) apparently created an open circuit to the converter secondary. The open circuit caused the output voltage to increase, and a high voltage was impressed across the collector base junction of the rectifier diode, causing it to fail. In the circuitry used for application of power to the converter during environmental testing, the input impedance was higher than that of the SNAP 11 generator. Under this condition, the effect of an open circuit on the converter secondary was more severe than normal.

Prototype Converter S/N-2 was subjected to vibration, shock and acceleration tests to determine its mechanical and electrical stability under these dynamic environments.

The converter was operated at a stabilized input during all tests from a d-c input source simulating the output of a thermoelectric generator. Operational parameters were monitored throughout all tests, with data continuously recorded during the acceleration, shock and vibration exposures.

TABLE VII-1

Functional Test Results

Unit Serial No.	Input Voltage (volts, dc)	Input Current (amp)	Output Voltage (volts, dc)	Output Current I_{out} (MA) (mamp)	Ripple Voltage (P-P)	Efficiency (%)	Conditions
001	2.99	8.33	29.210	770	0.18	90.5	Nominal load
001	4.32	3.69	46.560	300			Reduced load
001	3.00	0.81	35.240	0			Open circuit
001	2.21	9.62	0	--			After 1 min, R_L shorted
002	3.00	8.33	29.249	778	0.155	91.2	Nominal load
002	4.00	4.74	45.000	300			Reduced load
002	3.00	0.75	35.230	0			Open circuit
002	2.13	10.56	0	--			After 1 min, R_L shorted
003	3.00	8.33	29.258	768	0.170	90.0	Nominal load
003	4.04	4.62	45.423	300			Reduced load
003	3.00	0.87	35.572	0			Open circuit
003	2.380	10.50	0	--			After 1 min, R_L shorted
004	3.00	8.33	29.11	779	0.140	90.7	Nominal load
004	4.35	3.57	46.86	300			Reduced load
004	3.00	0.15	34.42	0			Open circuit
004	2.36	10.50	0	--			After 1 min, R_L shorted

1. Test Specimen and Apparatus

The test specimen converter was of the configuration designed for use in the Surveyor vehicle in conjunction with the SNAP 11 thermoelectric generator; it conformed to Drawing 431A1120005-001. Figure VII-1 shows an internal view of the unit. The test axes of the unit are defined in Fig. VII-4.

The circuitry used for operation and instrumentation of the converter during the tests is shown schematically in Fig. VII-5. Power for simulation of the SNAP 11 generator output was provided by an NJE Model QR-36-10 d-c power supply. The converter output load consisted of a power resistor decade box.

The input and output power leads were soldered to the converter terminals to prevent any opening of the circuits during application of the environments. Input and output voltage and current were measured and recorded before and after each environmental test and during the performance tests. Converter efficiency was calculated from these data. In addition, the input and output data were continuously recorded during the acceleration, shock and vibration tests by means of the oscillograph.

2. Test Conditions

The test specimen was subjected to environmental and functional tests in accordance with the following:

a. Acceleration test (thrust axis)

An acceleration of 10 g was applied, stabilized and maintained for four minutes. The acceleration was then reduced to 5 g, stabilized and maintained for seven minutes.

b. Shock tests

Thrust axis. A total of four shock pulses were applied, each consisting of a half-sine wave of 25 g peak and 5^{+2}_{-0} msec duration.

Lateral Axis I. Two shock pulses were applied for each of the two directions of this axis, each shock consisting of a half-sine wave of 15 g peak and 5^{+2}_{-0} msec duration.

Lateral Axis II. Two shock pulses were applied in each of the two directions of this axis, each shock consisting of a half-sine wave of 15 g peak and 5^{+2}_{-0} msec duration.

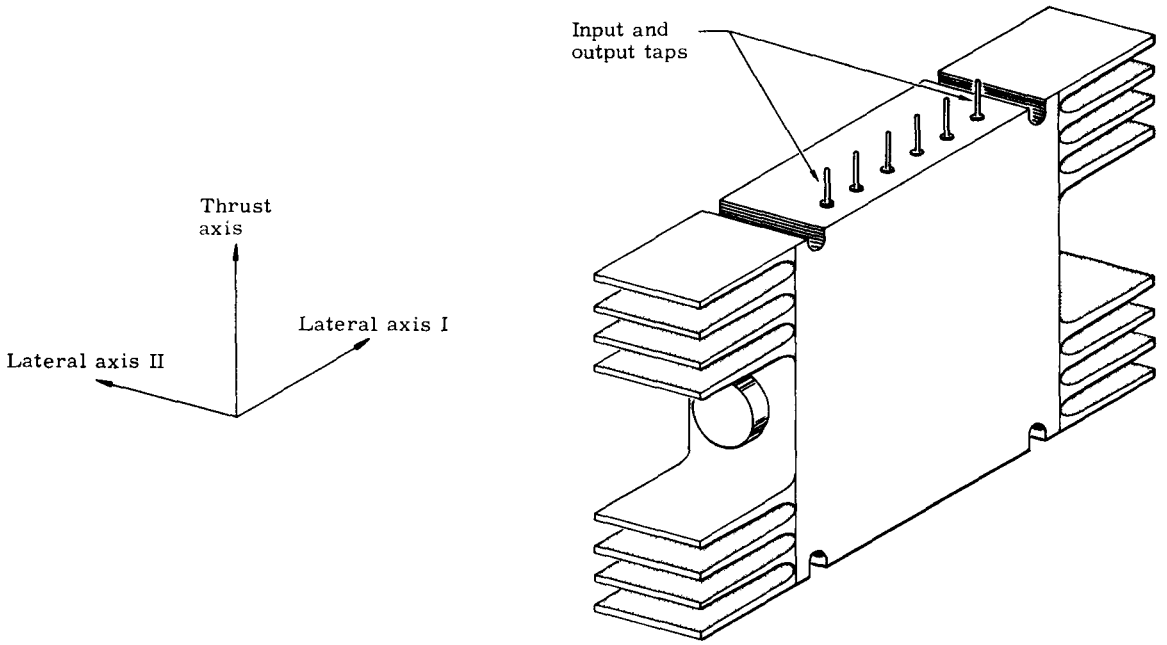

Fig. VII-4. Definition of Test Axes

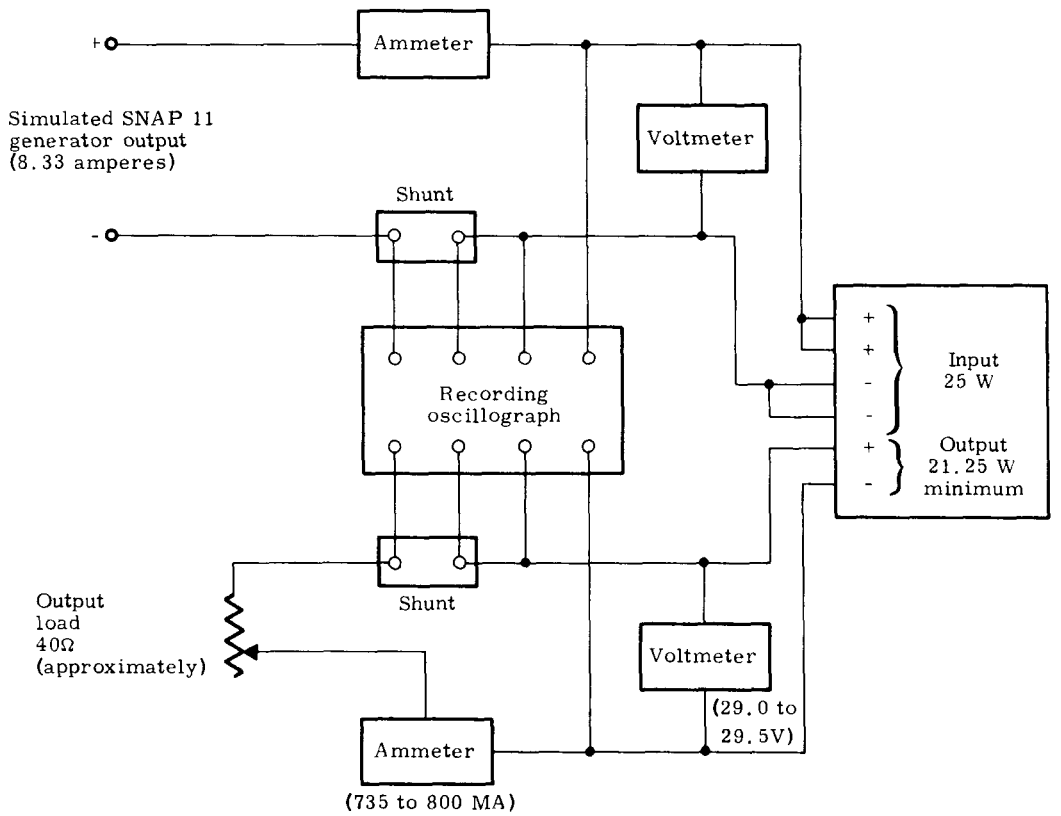

Fig. VII-5. Operation and Instrumentation Circuitry for SNAP II DC-to-DC Converter

c. Vibration tests (combined sine and random)

Thrust axis. A sinusoidal logarithmic frequency sweep was conducted from 5 to 30 cps at 0.4-inch double amplitude and 30 to 1500 cps at ±18 g in a total of two minutes. Combined with this signal was a 4.5 g rms random input, with a flat spectrum band limited from 100 to 1500 cps.

This vibration run was repeated five more times with the random spectrum reduced to 2 g rms.

Lateral Axis I. Six vibration runs were made, conforming to the specifications used in the thrust axis.

Lateral Axis II. Six vibration runs were made, conforming to the specifications used in the thrust axis.

3. Method of Test

The SNAP 11 converter and its associated circuitry was connected according to Fig. VII-5. As the input power to the converter was applied by means of the d-c power supply, the output load resistor was adjusted to obtain the necessary input voltage-to-current relationship. The input power was adjusted to a nominal 25 watts at 3 volts, thus simulating the electrical output of the SNAP 11 thermoelectric generator. This setting was used throughout the series of tests.

Specific input and output data measured during the test program are given in Table VII-2. Input and output current and voltage were used to calculate power in and out and, in turn, the percent efficiency of the converter. The environmental test was performed to determine any degradation; therefore, measured voltages, currents and efficiencies are not indicative of optimum matched load operation.

a. Acceleration test

The converter was mounted to the bucket of the Genesco G accelerator, oriented for acceleration along the thrust axis.

As shown in Table VII-2, no failures or changes in operational characteristics were experienced due to acceleration. The oscillograph recording made during acceleration showed no measurable fluctuation in input and output voltage and current.

b. Shock test

After calibration of the machine for the proper pulse shape and duration, the test specimen was mounted to the HYGE shock machine, using dummy weights. Four shock pulses were applied along the thrust axis, and two in each direction along each of the two lateral axes.

TABLE VII-2

SNAP 11 DC-to-DC Converter Operational Data

		Converter Input			Converter Output				
Date	Time	Volts	Current (amp)	Power (watts)	Volts	Current (ma)	Power (watts)	Efficiency (%)	Remarks
3-9-64	9:45	3.03	8.30	25.15	29.2	758	22.13	88.0	Preacceleration
3-9-64	10:45	3.03	8.30	25.15	29.2	758	22.13	88.0	Postacceleration
3-10-64	3:20	3.03	8.30	25.15	29.2	759	22.16	88.1	Preshock (Lateral Axis I)
3-10-64	4:00	3.03	8.30	25.15	29.2	759	22.16	88.1	Post Lateral Axis I, prethrust axis
3-10-64	4:05	3.02	8.30	25.15	29.2	759	22.16	88.1	Postshock (thrust axis)
3-11-64	10:30	3.03	8.30	25.15	29.2	758	22.13	88.0	Preshock (Lateral Axis II)
3-11-64	11:10	3.03	8.30	25.15	29.2	758	22.13	88.0	Postshock (Lateral Axis II)
3-11-64	1:30	3.02	8.30	25.07	29.0	756	21.92	87.4	Previbration (thrust axis)
3-11-64	1:50	3.02	8.30	25.07	29.0	754	21.87	87.2	After 4.5-g rms run in thrust axis
3-11-64	2:15	3.01	8.30	24.98	29.0	754	21.87	87.6	Postvibration (thrust axis)
3-11-64	2:50	3.01	8.30	24.98	28.9	752	21.73	87.0	After 4.5-g rms run in Lateral Axis I
3-11-64	3:15	3.01	8.30	24.98	28.9	752	21.73	87.0	Postvibration (Lateral Axis I)
3-11-64	4:05	3.06	8.15	24.94	28.7	750	21.53	86.3	After 4.5-g rms run in Lateral Axis II
3-11-64	4:30	3.01	8.30	24.98	28.9	752	21.73	87.0	Postvibration (Lateral Axis II)
3-12-64	9:30	3.01	8.30	24.98	29.0	755	21.90	87.7	Pretemperature test
3-12-64	11:10	3.03	8.30	25.15	29.1	760	22.12	88.0	At 40° F
3-12-64	1:15	3.00	8.30	24.90	28.8	750	21.60	86.7	At 100° F
3-12-64	3:00	3.01	8.30	24.98	29.0	755	21.90	87.7	Posttemperature test (room temperature)
3-12-64	3:15	3.75	7.40	27.75	38.0	650	24.70	89.0	125% of nominal voltage
3-12-64	3:15	3.75	4.65	17.44	39.5	385	15.21	87.2	One-half rated load
3-12-64	3:25	3.01	8.30	24.98	29.0	758	21.98	88.0	After short circuit test

No mechanical or electrical failures occurred during the shock tests, and the oscillograph recordings showed no change in the operating values during the actual impacts.

c. Vibration test

The converter test specimen was subjected to six combined vibration runs of two minutes each in each of three test axes. Vibration in the thrust axis and Lateral Axis I was accomplished by mounting the specimen to an upright fixture attached to the head of the C25HB shaker. The converter was mounted to the shaker head by means of a flat plate for vibration in Lateral Axis II.

Data recorded before and after each axis of vibration indicated no degradation of converter performance, and no mechanical failures occurred. Oscillograph recordings made during each vibration run demonstrated that no intermittencies or fluctuations in electrical characteristics occurred during the tests.

The converter output was subjected to a magnetic influence upon application or removal of the shaker field current before and after vibration testing, but the condition was normal and did not exist when the steady field was maintained. During collapse of the magnetic field, the output power was lowered by approximately one-half watt, but returned to its previous value when the field was stabilized.

Significant resonances were noted in the converter cover plate at approximately 350 and 1100 cps, during vibration in Lateral Axis II, but were not of a destructive nature and did not affect the internal components of the specimen.

4. Test Results

The test program carried out on Converter S/N-2 proved its ability to withstand critical environments of acceleration, shock and vibration. No failures, intermittencies or changes in performance were noted either during or as a result of the tests.

C. TEMPERATURE, PARTIAL LOAD AND SHORT CIRCUIT PROTECTION TESTS

Immediately following the dynamic environmental tests, the S/N-2 prototype converter was subjected to functional tests.

1. Temperature Test

The converter test specimen was placed in the Tenny temperature chamber. Thermocouples were positioned so as to indicate chamber air and converter case temperatures, and their readings were used to establish temperature stabilization.

The temperature of the specimen was reduced to 40° F and stabilized. Power was then applied to the converter, and its electrical performance was measured and recorded. The temperature was raised to 100° F and stabilized; then the electrical performance was again measured and recorded. After returning the temperature to room ambient conditions, the performance functions were once again recorded.

Performance data, as recorded in Table VII-2, show no adverse effects due to the temperature environment.

2. Partial Load Protection Test

Power was applied to the test specimen, and the input voltage was increased to 125% of its nominal value. After recording operational data, the input voltage was held at 125% while the output load on the converter was reduced to 50% of its rated value. These conditions were maintained for one minute, at which time the performance data were again recorded. The external load and input voltage were then returned to their normal values.

Data recorded during the test are presented in Table VII-2 and illustrate acceptable converter efficiency during the abnormal input and output conditions.

3. Short Circuit Protection Test

Normal power was applied to the converter, and a short circuit was created across the output terminals. This condition was maintained for a one-minute period, at the end of which the short circuit was removed and the electrical performance recorded.

The performance data, as shown in Table VII-2, indicate no adverse effects on the converter as a result of short-circuited operation.

D. VACUUM TEST

Prototype Converter S/N-3 was performance evaluated in a vacuum environment over a continuous period of eight days. Pressure ranged from 1×10^{-4} to 7.5×10^{-5} torr. Ambient temperature was maintained between 94° and 108° F. The input power, supplied by a d-c regulated power supply, was held constant at 3 volts and 8.33 amperes. Converter output voltage remained constant at 29.2 volts with a current of 0.734 to 0.736 milliampere, thus giving an overall efficiency of approximately 85.7%. Load resistance on the converter output was held at 39.7 ohms.

Prototype Converter S/N-4 was subjected to electrical performance tests while operating in a vacuum environment maintained at room temperature. Tests were conducted using an NJE regulated d-c power supply and also the S/N-4 thermoelectric generator as the power input source.

The vacuum system was maintained at a constant pressure of 8×10^{-5} mm Hg throughout the 320-hour test period. Using the d-c power supply as the source and the load resistance at the nominal 39-ohm value, the input to the converter was adjusted to 3 volts dc at 8.33 amperes to simulate the generator output of 25 watts at lunar night, end-of-life conditions. The converter output was 28.91 volts at 0.739 ampere for an efficiency of 85.46% Data were then taken at variable load resistance ranging from 29 to 80 ohms to obtain the efficiency and impedance for the nonregulated system. Efficiency at the nominal load resistance, in all cases, was in excess of 85%. Equilibrium temperature on the converter, measured at several points on the external housing, ranged from 95° to 97° F in a 77° F ambient environment. Typical test data are shown in Table VII-3.

TABLE VII-3

S/N-4 Converter Vacuum Test

Input (volts)	Input (amp)	Output (volts)	Output (amp)	Load Resistance (ohms)	Converter Efficiency (%)
3.000	8.33	28.91	0.739	39.12	85.46
3.078	5.95	30.94	0.514	60.19	86.86
3.120	4.66	32.01	0.401	79.90	88.28
2.500	6.90	23.88	0.606	39.41	83.89
2.564	4.90	25.63	0.431	59.47	87.95
2.500	3.84	26.54	0.334	79.46	88.82
3.500	9.88	33.89	0.861	39.36	84.35
3.594	7.01	36.25	0.614	59.04	88.36
3.643	5.53	37.51	0.467	80.32	86.93
1.97*	6.78	12.51	0.612	20.4	57.25
2.37*	6.07	22.66	0.554	40.9	87.30
2.85*	5.10	28.66	0.468	61.2	92.25

*Prototype Generator S/N-4, operating at ~14 watts, was used as input power source.

E. GENERATOR S/N-2 AND CONVERTER S/N-3 MARRIAGE TEST

Prior to shipment of the S/N-2 generator and S/N-3 converter to JPL, an integrated systems test was performed to assure proper operation. The test conditions were unstable due to the preparation-for-shipment activities; therefore, the data obtained for generator output, converter output and overall efficiencies provide an indication only.

The generator was under lunar day conditions with a hot junction temperature of 990° F. The converter was contained in a separate vacuum chamber at essentially room temperature. The results of this test are summarized in Table VII-4.

TABLE VII-4

Generator-Converter Marriage Test

Generator Output (watts)	Converter Output (watts)	Converter Load (ohms)	Efficiency (%)
24.37	17.98	21.8	73.8
26.00	22.20	40.3	85.5
25.90	22.22	60.8	85.9

F. CONCLUSIONS

The SNAP 11 dc-to-dc converter is structurally and electrically adequate to withstand the critical environmental and functional conditions to which it was subjected.

Open-circuit protection was not included in the converter design, since this was not a normal operating condition. Experience gained during testing indicated that this feature would be desirable in future designs. A preliminary investigation revealed that the incorporation of a Zener diode across the converter output is a feasible method of open-circuit protection.

The present dc-to-dc converter is designed for a 2N-2P generator. With the incorporation of 2N-3P material in the generators, the converter operating point must be changed to optimize system output power.

VIII. GENERATOR FIELD TEST KIT

The generator field test kit is a portable instrumentation package for use in monitoring the significant performance characteristics of the SNAP 11 power supply at test locations where other suitable instrumentation is not available. The kit configuration and electrical schematic are as shown in Figs. VIII-1 and VIII-2.

The test kit contains provisions for monitoring 25 thermocouples located on the generator. Thermocouple selection is by means of a 24-position thermocouple switch and an auxiliary input. These inputs are fed into a pyrometer indicator, where the thermocouple output is measured in millivolts. The same pyrometer indicator is also used in monitoring the generator internal pressure as sensed by the pressure transducer located on the generator. A switch in the pyrometer input leads allows selection of the input from either the pressure transducer or thermocouple switch.

Contained within the test kit is a bank of load resistors, across which the generator output is connected. These load resistors are arranged in parallel and are individually switched so that the desired load resistance can be obtained by switching in the appropriate parallel resistors. However, to prevent an inadvertent open circuiting of the generator, one switch (R_1 in Fig. VIII-4) is a momentary switch which remains in the closed position, except when held in the open position.

A Zener diode-controlled circuit is connected to the converter output and mocks up a 29-volt dc regulated spacecraft bus. A switch directs the generator output to either the bank of load resistors or the converter input. With the circuit so designed, the performance of the generator and converter can be individually monitored.

Monitoring of generator performance is conducted as follows:

(1) Temperature--The temperature-measuring thermocouples are connected to a pyrometer indicator by a 24-position thermocouple switch. The pyrometer measures the millivolt output of the thermocouple. The millivolt reading is converted to degrees Fahrenheit by a standard thermocouple conversion table.

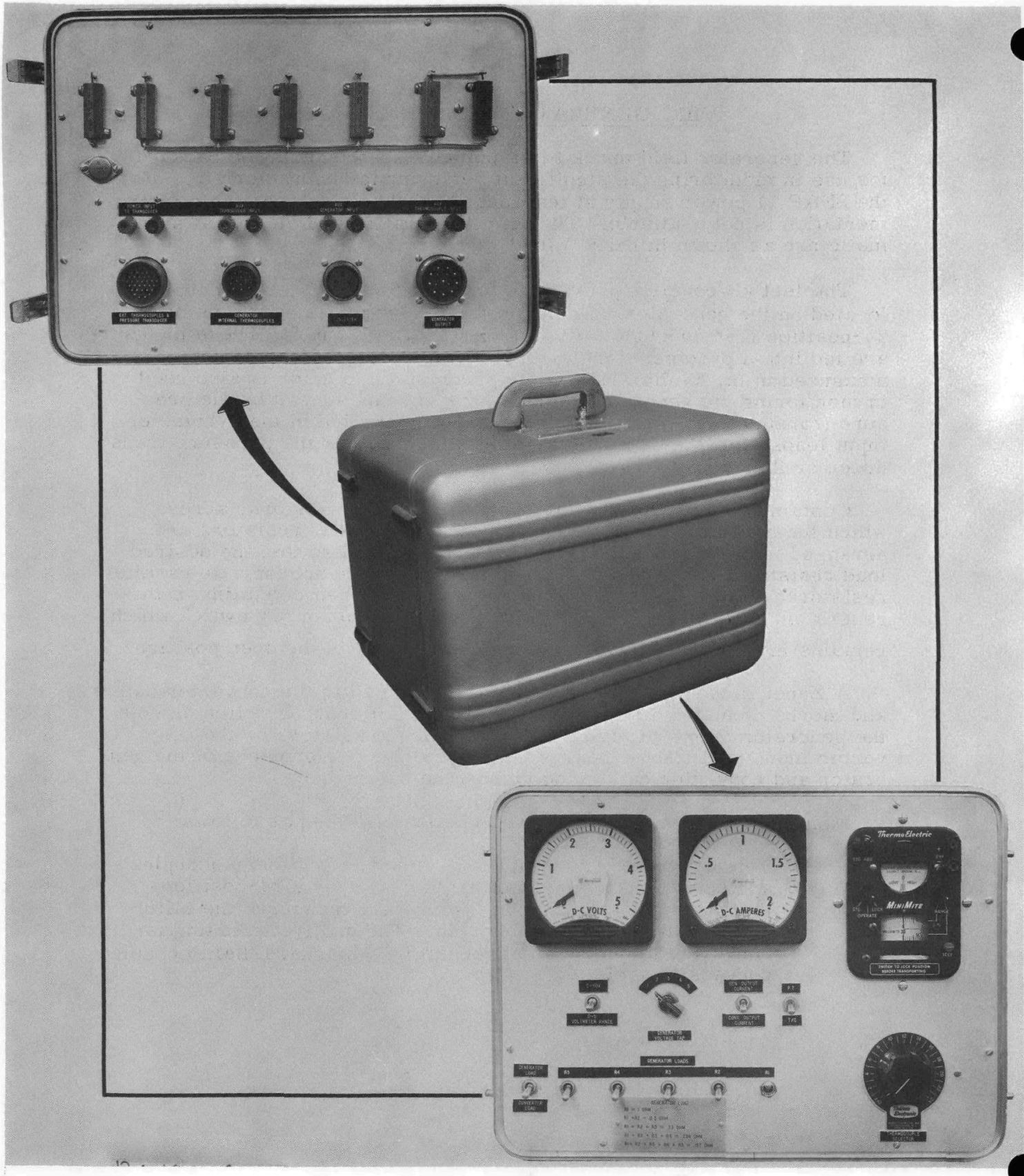

Fig. VIII-1. SNAP 11 Field Test Kit

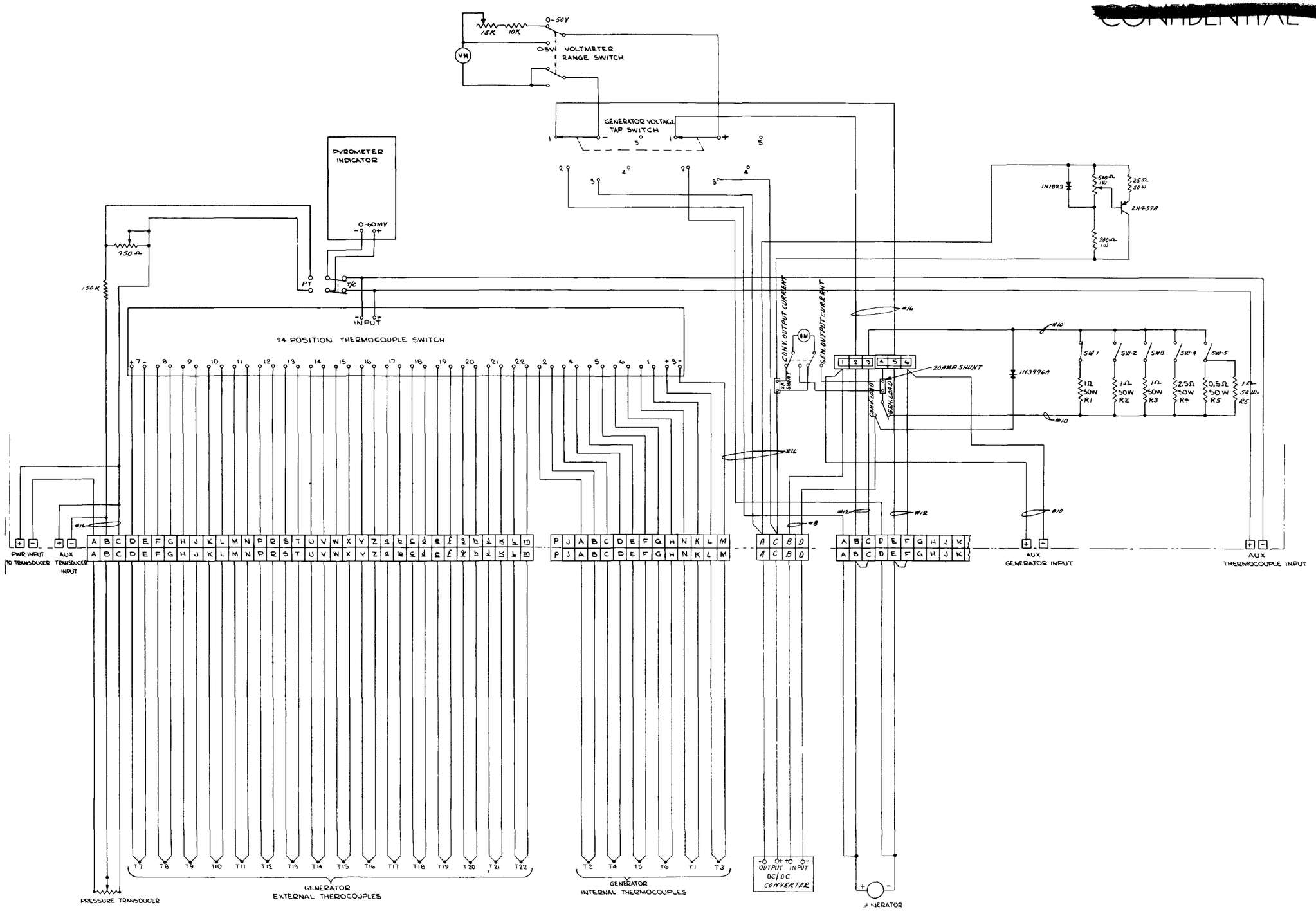

Fig. VIII-2. SNAP 11 Field Test Kit--Electrical Schematic

(2) Generator internal pressure--The power input-to-transducer terminals are connected in parallel with the power output leads of the dc-to-dc converter (noting the polarity) to obtain a 29-volt dc regulated voltage across the pressure transducer resistor. Do not open circuit converter. The internal pressure of the generator is measured with the pyrometer by placing the toggle switch in the pressure transducer position. The pressure is obtained by taking the ratio of the millivolt reading to 50 millivolts and multiplying by 30 psia; that is,

$$P = \frac{\text{millivolt reading}}{50 \text{ millivolts}} \times 30 \text{ psia.}$$

(3) Generator output current--The generator output current is found by placing the current toggle switch in the generator position and reading the ammeter. Full-scale reading of the ammeter is 20 amperes.

(4) Generator output voltage--The generator output voltage is obtained by placing the voltage tap switch on Position 2, with the voltmeter switch on the 5-volt position. Full-scale reading is 5 volts.

(5) Converter output voltage--The output voltage of the converter is obtained by placing the voltmeter switch in the 50-volt position and the voltage tap switch in Position 3. Full-scale reading is 50 volts.

(6) Converter output current--The converter output current is obtained by placing the current switch in the converter position and reading the ammeter. Full-scale reading is 2 amperes.

IX. NUCLEAR SAFETY

In designing the SNAP 11 generator, as in any other generator, it was necessary to establish a safety philosophy as a guide. This philosophy is governed by the handling requirements and the ultimate use of the generator; it results in the definition of design criteria. The design criteria for SNAP 11 were intended to provide a heat source design which could maintain capsule integrity during the helium pressure buildup, prevent release of the fuel through corrosive forces for approximately 10 half-lives, preclude melting of the fuel capsule during fire or re-entry conditions and contain and/or restrain fuel dispersion upon high velocity earth or lunar impact. These criteria were established and testing performed with the intent of utilizing the SNAP 11 generator for the Surveyor spacecraft mission.

During the course of the SNAP 11 program, however, the application of this generator in the Surveyor mission was deleted. The philosophy and design criteria were, therefore, relaxed to satisfy the requirements for terrestrial accidents and test environments since the generator was to be fueled at the Oak Ridge National Laboratory for demonstration purposes only. The present fuel block design is oriented toward laboratory use only and is not satisfactory as intact re-entry flight hardware. The discussions which follow in Sections A, B, C and D refer to the original fuel block design while Section E refers to the new design.

A. SAFETY PHILOSOPHY AND DESIGN CRITERIA

1. Safety Philosophy

The basic safety philosophy for the SNAP 11 radioisotope-fueled power supply intended for the Surveyor spacecraft mission was that no undue radiation hazard should exist for the general populace during any phase of generator handling or mission performance. The phases included fueling, transportation, storage, prelaunch activities and launch trajectory or lunar trajectory impact. Credible accidents during each of these phases were considered in the safety evaluation of the system.

Impact philosophy included absolute fuel containment for earth impact, launch pad abort and lunar impact at any velocity less than the velocity necessary to penetrate the lunar surface (about 700 fps). For lunar impact velocities greater than the penetration velocity, containment of the fuel should be kept within the near vicinity of the crater that is formed. Absolute fuel containment is defined as containment within the primary and secondary containers. The lunar specifications comply with the Space Science Board of the National Academy of Science request that all reasonable precautions should be taken to limit the extent and vicinity of any contamination of the lunar surface which might result from accidental fuel release.

Absolute containment is required for all earth accidents because of the hazard associated with the high specific activity of curium-242. Therefore, the system was designed to survive aerodynamic re-entry heating and subsequent land impact.

Criteria were specified to satisfy the basic philosophy for each of the mission phases. The phases and credible accidents include:

(1) Prelaunch phase--transportation incidents including collision between ground or air vehicles, fire, water submergence and soil burial.

(2) Launch pad phase--overpressures from propellant explosions, fire temperatures and duration for propellant fires, and radiation levels for the system both exposed to accidents and in the ready-to-launch condition.

(3) Launch abort phase--explosion during launch, impact after abort and radiation levels for aborted, impacted systems.

(4) Orbit phase--powered or nonpowered re-entries and the effects on aerodynamic heating and impact considerations for re-entered systems.

(5) Lunar orbit and impact phase--containment of fuel at various impact velocities.

2. Design Criteria

Four major design criteria were established for:

(1) Maintaining capsule integrity during helium pressure buildup for the life of the design mission

(2) Preventing deterioration of encapsulation materials through corrosive forces for approximately 10 half-lives of the fuel

(3) Protecting the fuel capsule from melting during fire or re-entry heating conditions

(4) Containing and/or restraining fuel dispersion subsequent to high velocity impacts either on the earth or on the moon.

a. Pressure buildup

The design mission lifetime for the fuel capsule is 120 days. After this time the capsule pressure buildup would be approximately 3500 psi at operating temperature. Pressure tests showed that creep at these pressures was negligible. As a result of both analysis and testing, it was concluded that the selected capsule could contain the pressures generated during and following mission life, and that the maximum pressure buildup (3860 psi) would occur 230 days after encapsulation.

b. Corrosion

In the event of an earth-deposited capsule, the probability of widespread contamination will be significantly reduced if the capsule can retain the fuel for about 10 half-lives of the fuel--less than five years for curium-242. The super metals such as Haynes-25, TZM and Hastelloy are all sufficiently inactive with seawater and the fuel forms to guarantee integrity for at least five years. Choice of the encapsulation material is more dependent on the re-entry heating and impact considerations.

c. Re-entry heating and fires

Maximum heat and temperature environments are encountered during a possible abort re-entry of the system from high altitude. A maximum heating of 135,000 Btu/ft^2 will be imposed on the fuel block during a high speed, low angle earth re-entry (see Section C-4). This condition requires the fuel source to be protected by heat shield and ablator materials to ensure heat block integrity during re-entry. Complete protection of the fuel block is required to meet the impact criteria.

d. Impact

The terminal velocity of the fuel block at sea level is 185 fps based on a ballistic coefficient of 40 lb/ft^2. Lunar impact velocities can conceivably be as high as 9000 fps. The design criterion for impact integrity was established initially using the 9000 fps lunar impact speeds, but this proved too difficult to meet. As a result, the criterion for lunar impact was reduced from total containment to limited fuel dispersion, i.e., within the boundary of the impact crater. Since the heat block design has been shown to maintain integrity up to 3300 fps impact speeds, the earth impact at terminal velocities does not jeopardize capsule integrity upon impact.

B. SAFETY ASPECTS OF GENERATOR DESIGN

The fuel block assembly, shown in Fig. IX-1, is comprised of the encapsulated fuel contained within a radiation shield, an ablative material and an outer shroud. The fuel block is designed to provide the proper thermoelectric thermal input and temperature profile while maintaining the necessary ablative and impact features required by the safety criteria.

The fuel is encapsulated in a molybdenum base alloy (TZM) capsule which serves to contain the helium resulting from alpha decay, to contain the fuel during high velocity impact and to resist internal or external corrosion. The TZM capsule fits inside a platinum sphere which provides the required radiation shielding and serves as an impact energy absorber. Graphite and beryllium surround the platinum sphere to provide the thermal protection necessary for a nonburnup re-entry. The

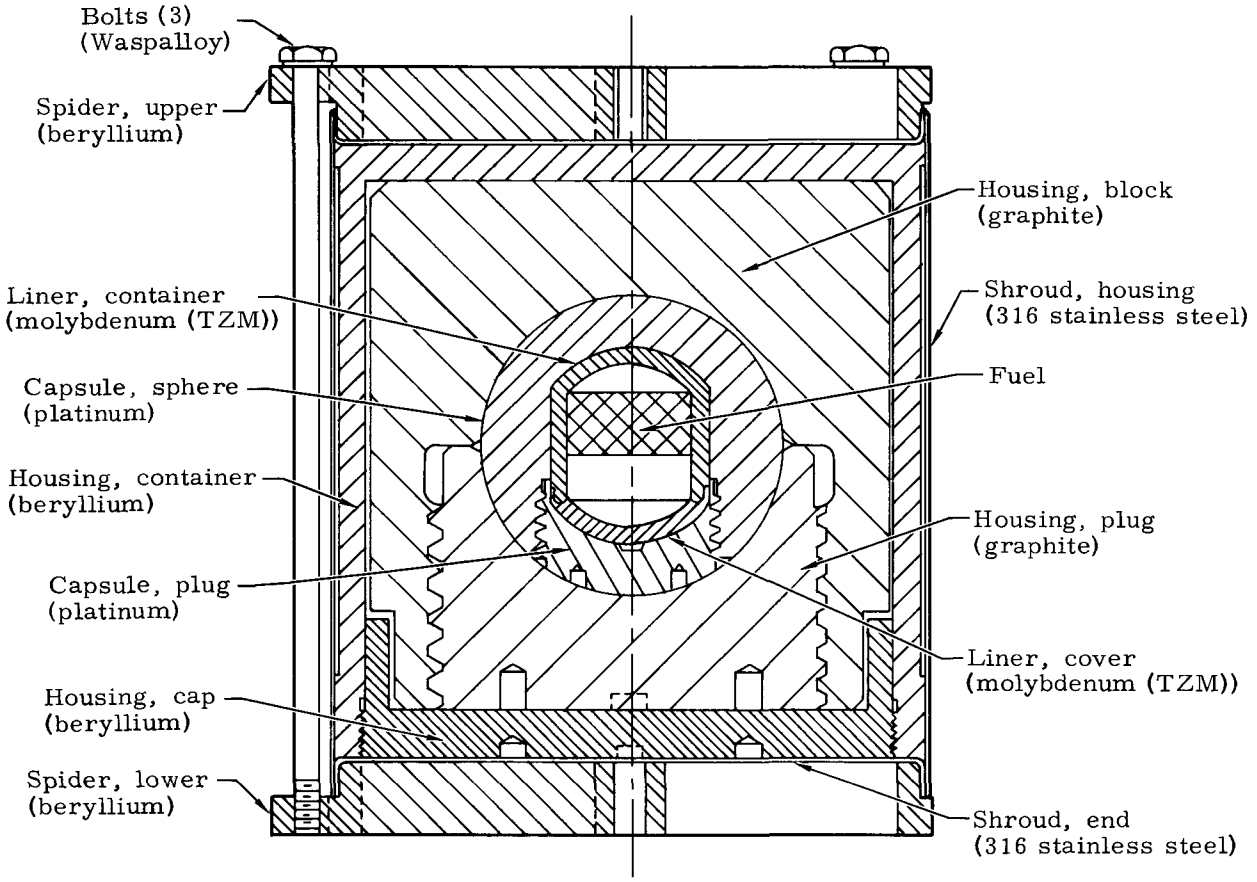

Fig. IX-1. Original Fuel Block Assembly

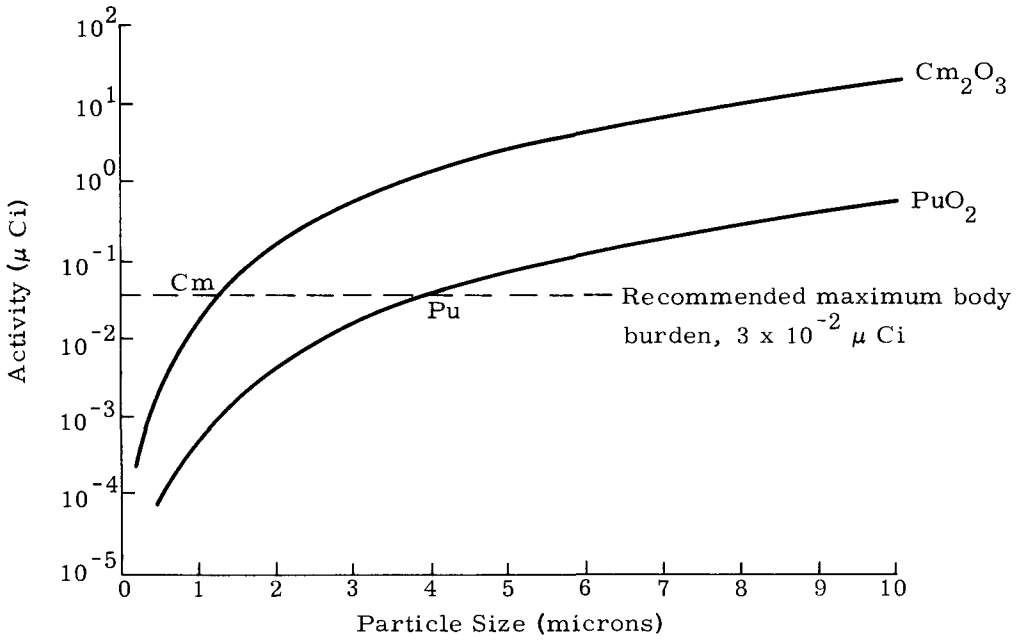

Fig. IX-2. Fuel Activity as Function of Particle Size

graphite can survive aerodynamic heating due to its high sublimation temperature. However, during the most severe abort conditions, heat can be transmitted through the graphite in sufficient quantities to melt the platinum sphere. Therefore, a beryllium shield was provided to absorb and dissipate sufficient heat by the ablation mechanism to eliminate the possibility of melting the platinum during the worst abort situations. A stainless steel shroud encases the beryllium and graphite to protect the materials during terrestrial handling and retains the helium gas atmosphere within the fuel block to assure adequate heat transfer at the various component interfaces.

A review of the safety considerations to be discussed includes:

(1) Fuel form compatibility--Test results, utilizing gadolinium oxide to simulate the curium fuel form and a molybdenum capsule, revealed that no attack occurred up to 2000° F.

(2) Radiation dose rates--The calculated dose rates indicate a person can work in the vicinity of the generator for reasonable periods of time.

(3) Helium pressure buildup--Analyses and tests show that the fuel capsule will maintain its integrity when exposed to maximum expected pressure buildup.

(4) Creep due to pressure buildup--Measurements of the fuel capsule at maximum pressure buildup showed that the capsule material did not creep.

(5) Fuel capsule meltdown--An analysis showed that under the most severe credible conditions, meltdown of the fuel in an iridium matrix would not occur.

(6) Explosion overpressures--Calculations have shown that a Centaur explosion would produce a maximum pressure of 375 psi; fuel block stainless steel shroud will withstand a pressure of 1400 psi.

(7) Dropping the fuel block--Analysis has shown that the generator will contain the fuel when dropped from a height of 125 feet. A half-scale impact test program revealed that containment was also maintained for impact against a granite block for velocities up to 3356 fps.

(8) Fire--The generator outer housing will not fail when exposed to the temperatures resulting from Centaur fire balls or continuing fires.

C. ANALYSIS SUMMARY

1. Fuel Study

a. Fuel activity analysis

Curium-242 is created by neutron irradiation of americium-241 in a nuclear reactor. Once created, the curium-242 decays by alpha emission to plutonium-238 with a half life of 162.5 days. The plutonium-238 decays to uranium-234 by alpha emission with a half life of 87.5 years. The specific activity of curium-242 is 3.3×10^3 Ci/gm and that of plutonium-238 is 17 Ci/gm. Obviously, the plutonium does not materially contribute to the system power requirements. However, it does remain a hazard just as curium does with respect to biological considerations.

For the compound Cm_2O_3, the specific activity is 346 Ci/gm. If one assumes the plutonium daughter product forms PuO_2, the specific activity of this oxide would be 12.1 Ci/gm. The density of Cm_2O_3 is 11.75 gm/cm^3, and that of PuO_2 is 11.46 gm/cm^3. Based on these data, a curve of curies per particle size can be generated as shown in Fig. IX-2. The maximum recommended body burden for each fuel is also shown in the figure, emphasizing the undesirability of fuel form release under any condition. As shown in the figure, inhalation of a Cm_2O_3 particle larger than 1.5 microns or a PuO_2 particle larger than 4.5 microns immediately yields a body burden in excess of that recommended by the International Committee on Radiation Protection (ICRP). Obviously, any accident, including re-entry burnup, which yields micron size particulates is a serious personnel hazard and should be avoided through adequate containment design.

b. Fuel compatibility

Two significant compatibility tests were conducted at Martin Marietta. Screening or selection tests were first conducted at 2000° F in argon with both gadolinium oxide (Gd_2O_3) and gadolinium carbide (GdC_2). Except for tests which included iron and nickel, studies were conducted in which pellets of the compound were placed in direct contact with the various metals under investigation. Iron and nickel were tested in cermet form. Compatibility was determined metallographically. Table IX-1 lists the results. The SNAP 11 liner is TZM which is greater than 99% molybdenum, and results for molybdenum should be applicable.

TABLE IX-1

Compatibility of Gd_2O_3 and GdC_2 with Metals During 150-Hour Tests (2000° F in argon atmosphere)

Material	Compatibility	
	Gd_2O_3	GdC_2
Haynes-25	No attack	No attack
Hastelloy C	No attack	No attack
Inconel X	No attack	No attack
Type 316 stainless steel	No attack	No attack
Nickel	No attack	No attack
Iron	Discoloration of oxide	Discoloration of carbide
Columbium	No attack	
Tantalum	No attack	
Molybdenum	No attack	
Tungsten	No attack	

Another series of compatibility tests was conducted at 2952° F. The number of materials suitable at higher temperatures is very limited. Only the refractory metals and platinum group metals were tested. In these experiments, pellets of gadolinium oxide and carbide were placed in contact with the metals being investigated. This method was not successful in all cases because a reaction took place between certain metal specimens and impurities in the furnace atmosphere. To eliminate side reactions, the pellets of the gadolinium compound were placed in tubes of the metals (tantalum, columbium and platinum) to be tested; the tubes were evacuated, crimped shut and seal welded before exposure to elevated temperatures. The results of these experiments are given in Table IX-2.

c. Radiobiological considerations

Alpha particles from Cm-242 are completely absorbed in an inch or two of air and cannot penetrate ordinary clothing or skin. The situation is quite different if the nuclide enters the body through the lungs, digestive system or breaks in the skin. The nuclide would tend to concentrate in various parts of the body where prolonged action of the alphas could cause serious damage.

TABLE IX-2

Compatibility of Gd_2O_3 and GdC_2 with Various Metals in a Vacuum Environment at 2952° F

Material	Time (hr)	Compatibility	
		Gd_2O_3	GdC_2
Molybdenum (arc cast)	64	No attack	No attack
Tungsten (arc cast)	64	No attack	Questionable
Tantalum	64	No attack	Attack
Columbium	112	No attack	Attack
Platinum	112	Pt melted*	Pt melted
Zirconium	64	Badly attacked	Badly attacked

* Experiments with Gd_2O_3 in a platinum cermet at 2950° F revealed a dentritic growth of the oxide in the platinum. No serious deterioration of the pellets occurred.

Table IX-3 gives the maximum permissible concentration (MPC) levels for curium-242. The low concentrations allowed are a direct result of the long biological half life of curium (2.4×10^4 days). All MPC values are given for a 40-hour week as well as for continuous exposure or a 168-hour week. The values of body burden, q, are based on that amount of radionuclide which, when deposited in the body, produces the maximum permissible biological dose to the body organ listed. The values are also based on continuous occupational exposure for a period of 50 years.

In most cases, significantly different values of body burden result when effects on different organs are considered. The critical organ is considered to be that organ of the body where damage by radiation results in the greatest damage to the body. The critical organs are underlined in the table.

The low maximum permissible concentrations in both air and water emphasize the reasons for the care taken in the design of the fuel encapsulation to prevent escape under all credible accident environments.

TABLE IX-3

Maximum Permissible Concentrations for Curium-242

Organ	Maximum Body Burden (g)	MPC 40-Hour Week $\mu Ci/cm^3$ W*	MPC 40-Hour Week $\mu Ci/cm^3$ A*	MPC 168-Hour Week $\mu Ci/cm^3$ W*	MPC 168-Hour Week $\mu Ci/cm^3$ A*
Soluble Fuel					
Gastrointestinal tract	--	7×10^{-4}	2×10^{-7}	2×10^{-4}	5×10^{-8}
Liver	0.05	3×10^{-3}	1×10^{-10}	9×10^{-4}	4×10^{-11}
Bone	0.09	5×10^{-3}	2×10^{-10}	2×10^{-3}	8×10^{-11}
Kidney	0.2	9×10^{-13}	4×10^{-10}	3×10^{-3}	1×10^{-10}
Body	0.2	1×10^{-2}	6×10^{-10}	5×10^{-3}	2×10^{-10}
Insoluble Fuel					
Lung	--	--	2×10^{-10}	--	6×10^{-11}
Gastrointestinal tract	--	7×10^{-4}	1×10^{-7}	2×10^{-4}	4×10^{-8}

* W = Water, A = Air

d. Alternate fuel analysis

An alternate fuel study was performed to determine if polonium-210 or promethium-147 could be used as fuels. Safety provisions and shielding requirements for the two fuels were evaluated. From these analyses, it was concluded that the polonium requires only a minor fuel block revision, whereas promethium requires a major generator redesign to satisfy intact re-entry criteria.

The polonium fuel, gadolinium-polonide, requires a small increase (about 10% in diameter) in capsule size to be comparable with a Cm_2O_3 system. Since no other component design modifications are required, the weight of the polonium-210 fueled generator is essentially the same as the curium generator. The initial thermal power of the polonium system will be higher than the curium system due to its shorter half life. On this basis, it is concluded that Po-210 is an acceptable alternate fuel for the SNAP 11 generator.

The use of promethium fuel (Pm_2O_3) results in a significantly larger fuel block which will not fit within a generator sized for curium or polonium fuel. This is primarily due to the much lower power density (1.8 watts/cm^3), increased shielding requirements and subsequent structural requirements for meeting an intact criterion. Since promethium-147 is a beta emitter, compared with curium and polonium which are alpha emitters, a new hazard analysis would have to be performed to evaluate the relative safety of the promethium system. Based upon redesign considerations necessitated by safety criteria, low efficiency and increased weight, it is concluded that Pm-147 is an unacceptable alternate fuel for a SNAP 11 generator.

Fuel characteristics for a typical 25-watt generator design are compared in Table IX-4 for each of the three fuels, curium, polonium and promethium.

TABLE IX-4

Fuel Form Comparisons

Parameter	Cm-242	Po-210	Pm-147
Fuel form	Dilute Cm_2O_3	GdPo	Pm_2O_3
Power (watts(e))	25	25	25
Generator weight (lb)	35	35	111
Fuel block weight (lb)	8.5	8.5	75
Fuel volume (cm^3)	6.2	6.75	403
Fuel weight (gm)	72.8	40.5	2241
Activity (k curies)	25.2	31.9	1680
Melting point (°F)	4081	2911	4171

A comparison of the shielding required for the alternate fuels was made by determining the amount of uranium shielding which would reduce the gamma flux at one meter to the value prevailing for a curium-fueled generator or about 10^4 gamma/cm^2-sec. The volumes of required fuel were assumed to be cylindrical with an L/D of 1 and encapsulated with Haynes-25. Fluxes were calculated by equations given in "Reactor Shielding Design Manual" by T. Rockwell, T1D7004.

Figure IX-3 shows the calculated fluxes at one meter from the heat source as a function of uranium shielding thickness. Figure IX-4 presents the same data in terms of dose rate.

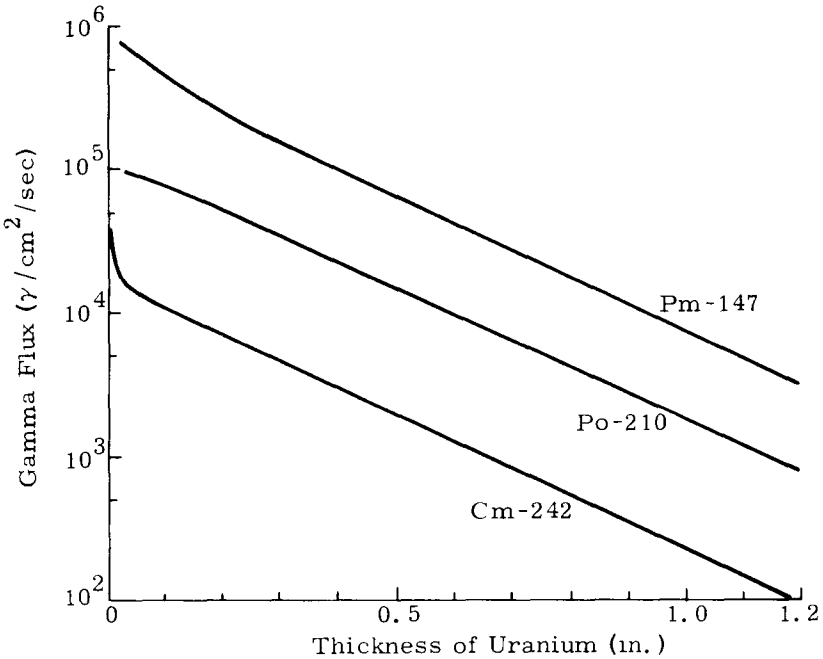

Fig. IX-3. Gamma Flux at One Meter from Axis of Generator

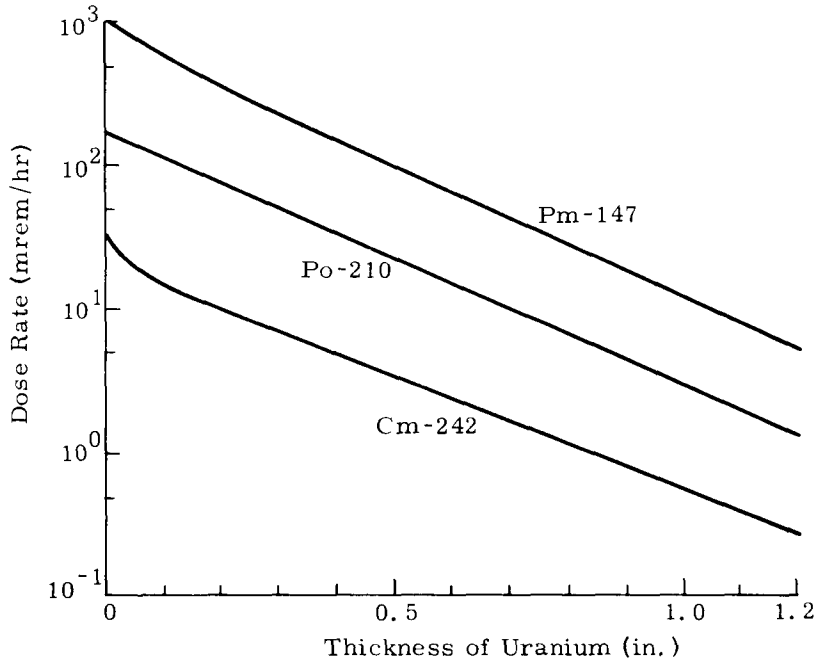

Fig. IX-4. Gamma Dose Rate at One Meter from Axis of Generator

The alpha-emitting isotopes also emit neutrons that originate from spontaneous fissioning and from alpha-neutron reactions with light elements such as the oxygen in the oxide fuel form. Polonium does not fission spontaneously, but trace amounts of oxygen which remain in the purified fuel produce neutrons when bombarded with alphas. Neutron dose rates from an unshielded generator fueled with the alpha-emitters are listed in Table IX-5.

TABLE IX-5

Neutron Dose Rates from Alpha-Emitting Fuels
(mrem/hr 1 meter from axis of generator)

	Cm-242	Po-210
Spontaneous fissioning	149	--
Alpha-neutron reactions	7	7
Total neutron dose rate (mrem/hr)	156	7

If beryllium is to be used as an ablative material during re-entry of the fuel block, the generation of neutrons by photo-neutron reactions must be considered in a shielding analysis. This phenomenon was not considered in this analysis.

Maximum permissible concentrations for polonium-210 and promethium-147 are given in Table IX-6.

A calculation was performed to determine the concentration of each fuel form over the area between 70 and 20 degrees north latitude assuming an area of 5.4×10^{14} square meters for dispersion in a high altitude release. These calculations show that the concentration of polonium-210 and promethium-147 will be 5.9×10^{-11} and 3.1×10^{-9} counts/m^2, respectively. Permissible surface concentrations are given in Table IX-7. Comparison of the data and the table reveals that the concentrations for each of the fuels are at least two orders of magnitude less than that allowed.

For each of the alpha-emitting fuels, Po-210 and Cm-242, the Tp_{max} was determined. The Tp_{max} for Po-210 occurred in 200 days, creating a maximum pressure of 3700 psi; Tp_{max} for Cm-242 occurred in 230 days, creating a maximum pressure of 3860 psi. The capsules were tested at 3850 psi at 1470° F. The capsules showed minimum creep over a 30-day test period (average dimensional change was 5×10^{-4} inch).

TABLE IX-6

Maximum Permissible Concentrations for Promethium and Polonium

Fuel Form	Organ	Maximum Body Burden (q)	MPC 40-Hour Week $\mu Ci/cm^3$ W*	MPC 40-Hour Week $\mu Ci/cm^3$ A*	MPC 168-Hour Week $\mu Ci/cm^3$ W*	MPC 168-Hour Week $\mu Ci/cm^3$ A*
Pm-147	Body	300	--	--	--	--
Soluble	Gastro-intestinal tract	--	6×10^{-3}	--	2×10^{-3}	--
	Bone	60	--	6×10^{-8}	--	2×10^{-8}
Insoluble	Lung	--	--	1×10^{-7}	--	3×10^{-8}
	Gastro-intestinal tract	--	6×10^{-3}	--	2×10^{-3}	--
Po-210	Body	0.4	--	--	--	--
Soluble	Spleen	0.03	2×10^{-5}	5×10^{-10}	7×10^{-6}	2×10^{-10}
	Kidney	0.04	2×10^{-5}	5×10^{-10}	--	--
Insoluble	Lung	--	--	2×10^{-10}	--	--
	Gastro-intestinal tract	--	--	--	--	--

* W = Water, A = Air

TABLE IX-7

Surface Concentration Limits for Promethium and Polonium

Fuel	168-Hour MPC ($\mu Ci/cm^3$)	Half Life (yr)	Surface Concentration Limit (counts/m^2)
Pm-147	2×10^{-8}	2.6	$< 2 \times 10^{-4}$
Po-210	7×10^{-11}	0.38	$< 7 \times 10^{-7}$

2. Thermal Studies

a. Shipping cask analysis

In addition to standard AEC shipping regulations, design specifications require that the fuel block surface temperature be maintained between 950° and 1200° F to prevent damage from thermal expansion since the fuel block is press fitted into the balsa and lead ribs of the shipping cask to ensure minimum movement during shipping. Thermal analyses were conducted to demonstrate cask design feasibility.

Analyses were made at 120° F ambient temperature and maximum solar heat input to the cask surface, and at the more normal conditions of 70° F ambient temperature and no solar heating. The analysis assumed all outside surfaces of the cask to be coated with white lacquer which has a low absorptivity (0.39) and a high emissivity (0.95) to minimize solar heat input and facilitate heat transfer from the surfaces.

The heat balance equation used was:

$$q_T = h_c A_e (T_1 - \phi) + \sigma \epsilon A_e (T_1^4 - \phi^4)$$

where

q_T = 5086 Btu/hr (fuel plus solar heating)

h_c = $0.3(T_1 - \phi)^{0.25}$, heat transfer coefficient for free convection (large cylinders)

σ = 0.1714×10^{-8} Btu/hr-ft^2-°K^4, Stefan-Boltzmann constant

ϵ = 0.95, emissivity of lacquered surface

ϕ = 120° F, ambient temperature

T_1 = °F, cask surface temperature.

Solving the equation for T_1 yields a cask surface temperature of 160° F. The calculated surface temperature of the stainless steel fuel block shroud surrounding the graphite was 226° F. Final calculation of the fuel block surface temperature yielded 1038° F which is within the range specified by design requirements.

Table IX-8 summarizes the results of the two analyses for the normal and maximum expected environments during shipping. A system utilizing a diphenyl shield was also evaluated and yielded fuel block

surface temperatures about 30° F higher than the graphite system for both temperature environments.

TABLE IX-8

Fuel Block Temperatures During Shipping

Position	ϕ = 70° F	ϕ = 120° F
Cask surface (°F)	102	160
Surface of steel (°F)	169	226
Surface of fuel block (°F)	1031	1038

b. Launch pad fire analysis

The object of this analysis was to verify encapsulation integrity within the environments created during a launch pad accident. A simulated Atlas explosion and fire were experimentally generated for previous safety work involving the SNAP 3 and 9A generators. The time-temperature profile of this simulation is given in Table IX-9. The temperature and time durations agreed with the predicted most severe values within 3%. Theoretical values were lower than the measured values by the 3% margin. The total time of the fire was approximately 30 minutes.

TABLE IX-9

Fire Temperature as a Function of Time

Temperature (°F)	Duration (sec)	Elapsed Time (sec)
6200	Microseconds	--
5100	4	4
2800	5	9
1900	410	419
1600	720	1139
1200	720	1859

The generator thermal model which was analyzed consisted of fuel block and capsules, platinum impact absorber, graphite radiator and ablation shield, a beryllium ablator, and a stainless steel shroud. An additional outer housing consisted of a steel shroud, Min-K insulation and a magnesium alloy outer casing. The fuel block and the fuel block plus outer generator fixtures were analyzed for meltdown.

Table IX-10 presents the results of the fireball analysis. The magnesium alloy outer housing is expected to melt and the Min-K insulation to fall away, exposing the inner steel shroud which does not melt. Analysis of the fuel block alone (assuming it had been exposed during an explosion) showed the outer steel jacket did not melt and, therefore, the inner beryllium was not exposed.

TABLE IX-10

Fireball Heating Effects

	Melting (°R)	Temperatures Initial (°R)	After 4 Seconds (°R)	After 9 Seconds (°R)
Generator				
Mg	1580	530	1580 (melted)	--
Steel	2770	1390	1589	1739
Fuel block				
Steel	2985	1860	2527	2590

c. Beryllium dispersion

It has been shown that fireball heating is not sufficient to expose the beryllium to the atmosphere. However, explosions yielding high velocity impact and generator disassociation followed by high residual fireball temperatures could release beryllium to the atmosphere.

A hypothetical situation in which the fuel block was exposed to the explosion and fire was examined and yielded the following results:

(1) The stainless steel shroud covering the beryllium will rupture if impacted on the launch pad concrete.

(2) If the shroud fails, the beryllium will be exposed and approximately 5% of the beryllium will be converted to beryllium oxide.

In order to determine the ground level concentration and extent of contamination as a function of the amount of beryllium released as shown in Fig. IX-5, the following equation was used:

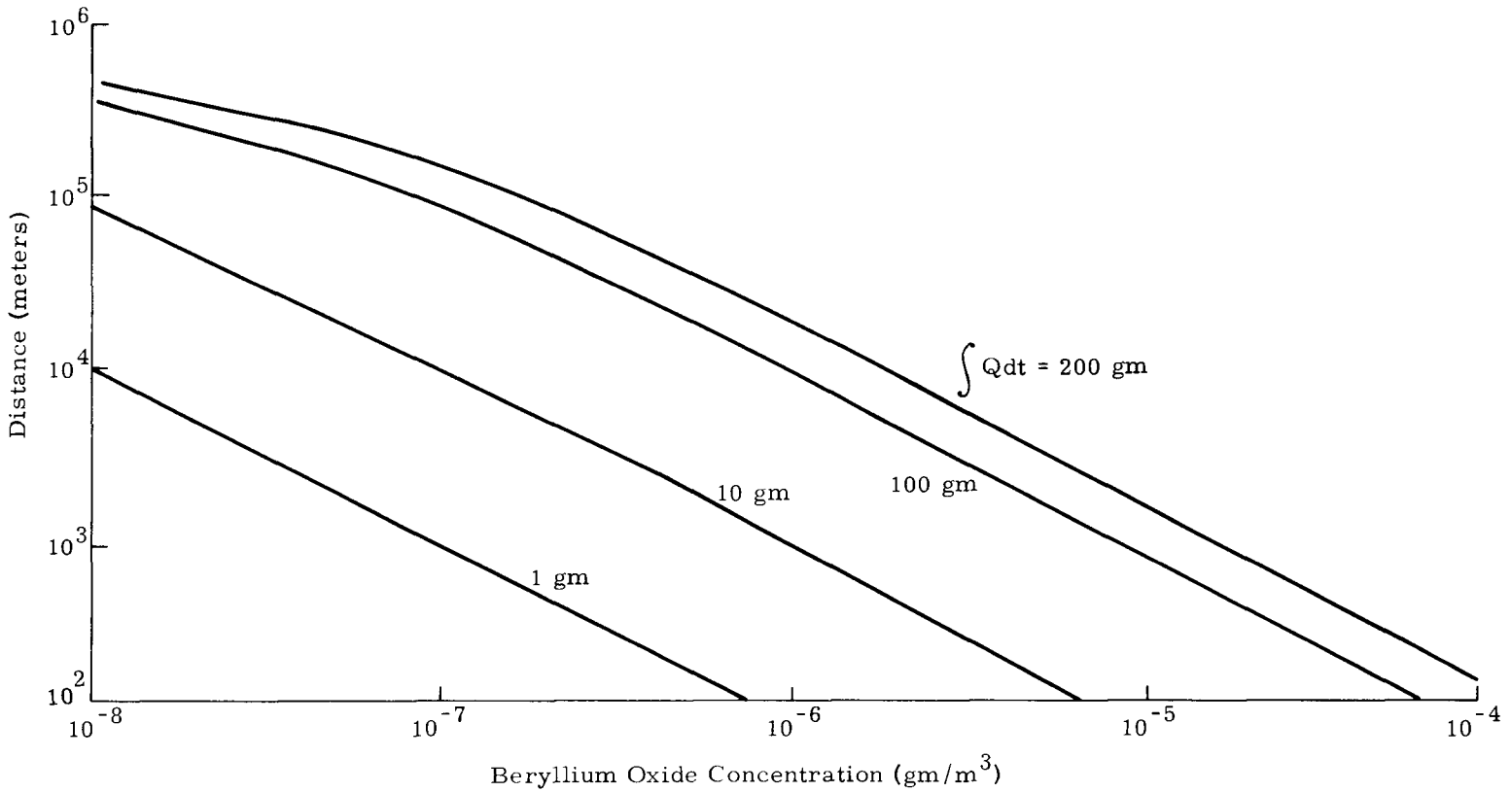

Fig. IX-5. Beryllium Oxide Ground Concentrations

$$X = (Q/\pi\mu\sigma_y\sigma_z)\, e^{-z^2/2\sigma_z^2} \; *$$

where

X = concentration (gm/m^3)

Q = addition rates (gm/sec)

μ = wind velocity (m/sec)

z = height of source above ground (meters)

σ_y = horizontal meteorological factor

σ_z = vertical meteorological factor.

Figure IX-5 is based on the worst atmospheric conditions, i.e., those which yield maximum concentration at any given distance from the source.

Experimental evidence has indicated that the lower amounts released are most realistic, since the formation of beryllium oxide on beryllium metals retards further formation due to the tightly clinging characteristics of beryllium oxide at temperatures less than 2345° F.

3. Structural Analysis

a. Fuel capsule impact craters

A study was made to determine the threshold penetrating velocities of the projectile and target crater volumes which might be expected during impact test programs. Crater volume data are required to assess the safety criterion implication of restricting release of contamination to within the impact crater. Six different specimens were evaluated by the following equations:

(1) Threshold penetrating velocity

$$V_{\sigma_t} = \sqrt{\frac{2\sigma_t}{\rho_p}} \left[\frac{(\lambda\rho_p)^{1/2} + \rho_t^{1/2}}{(\rho_p\rho_t)^{1/4}\,\lambda^{3/4}} \right] \; **$$

* Gilford, F. A., Jr., "Atmospheric Dispersion Calculations Using the Generalized Gaussian Plume Model," Nuclear Safety, Vol. 2, p 56, 1960.

** Corde, T. M., "An Investigation of Spalling and Crater Formation by Hypervelocity Projectiles," AB-62.

where

V_{σ_t} = velocity at which projectile will penetrate target (cm/sec)

σ_t = compressive strength of target (1.98×10^{-9} dynes/cm^2)

ρ_p = density of projectile (gm/cm^3)

ρ_t = density of target (gm/cm^3)

λ = jet factor, 2.0.

(2) Crater volume

$$\frac{V_t}{V_p} = 27\left(\frac{\rho_p}{\rho_t}\right)^{3/2}\left(\frac{V}{C}\right)^2$$

where

V_t = volume of crater in target (cm^3)

V_p = volume of projectile (cm^3)

V = impact velocity (cm/sec)

C = sonic velocity in target (6×10^5 cm/sec).

Input data and results of the calculations are shown in Table IX-11.

TABLE IX-11

Crater Volume

Specimen	Shape	Diameter (cm)	Length (cm)	Mass (gm)	Volume (cm^3)	Bulk Density (gm/cm^3)	Threshold Penetrating Velocity (cm/sec)	Crater Volume* (cm^3)
1	Spherical	1 046		9 507	0 596	15 935	26,700	30 15
2	Cylindrical	1 494	1 494	13 207	2 596	5 086	41,700	25 56
3	Cylindrical	1 494	1 494	9 134	2 596	3 518	48,900	13 55
4	Cylindrical	1 494	1 494	7 325	2 596	2 821	54,000	9 74
5	Cylindrical	1 494	2 24	15 625	3 904	4 003	46,100	24 76
6	Cylindrical	1 494	1 494	4.783	2 596	1 842	65,900	5 14

* Impact velocity = 213,000 cm/sec = 700 fps

b. Pressure analysis

During normal operation the fuel capsule will be subjected to internal pressure buildup due to helium formation from alpha particle decay of curium-242. The maximum pressure was determined from the equation:

$$PV = N/A(1 - e^{-\lambda t})RT$$

where

P = pressure (atm)

V = volume (liters)

N = number of curium atoms

A = Avogadro's number

λ = curium decay constant (4.28×10^{-3} days^{-1})

t = time since encapsulation (days)

R = universal gas constant

$$T = (T_o - T_a)e^{-\lambda t_i} + T_a$$

T_o = initial operating temperature (°K)

T_a = ambient temperature (°K)

t_i = time after mission completion.

The time after mission completion is determined by the equation $t_i = t - 130$ since the temperature is assumed to be constant through the mission lifetime of 120 days plus 10 for fueling and storage.

The temperature equation was substituted into the PV equation and the time derivative (dP/dt) was taken and equated to zero. The resulting equation was solved for t, the time at which the pressure would become maximum. This time was calculated to be approximately 230 days after encapsulation. Maximum pressure in the capsule was determined to be 3860 psi which is below the pressure required to cause rupture or extensive creep. Figure IX-6 gives the temperature and pressure time history of a typical capsule design.

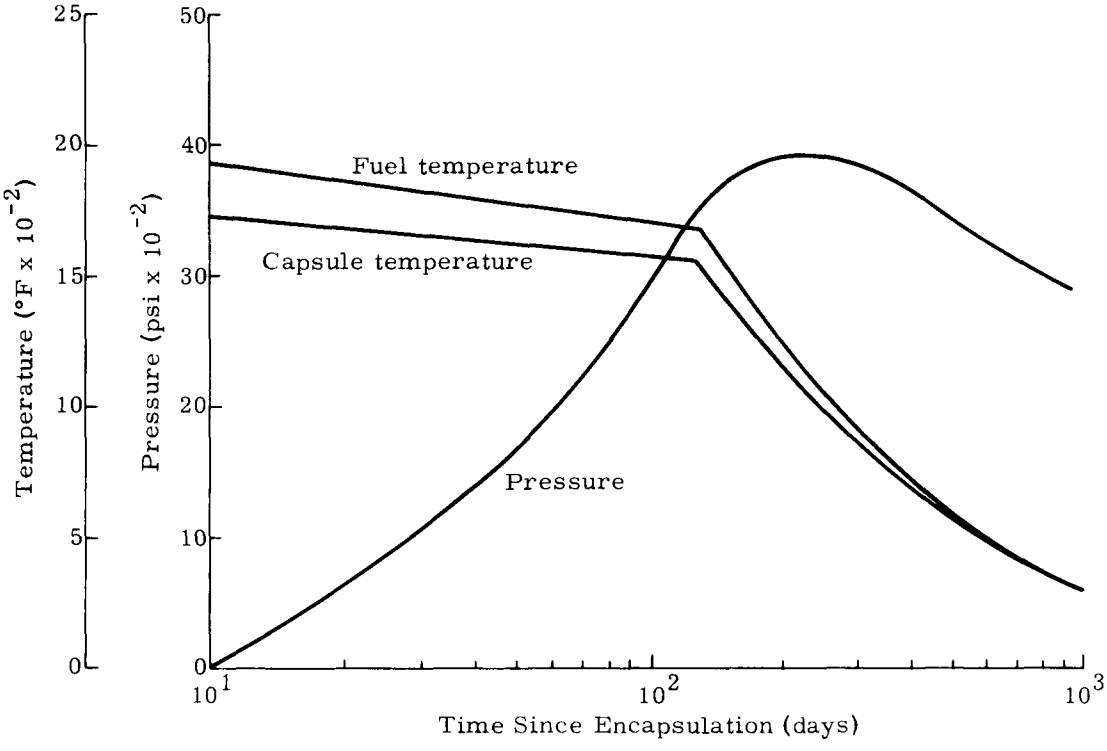

Fig. IX-6. Capsule Pressure Buildup Curve

c. Shipping cask analysis

The shipping container consists of three major items: an inner container to hold the generator and shield material; a crushable structure for impact; and an outer containment to encase the crushable structure. In this analysis, balsa wood and Type 5052 aluminum honeycomb were evaluated for impact energy absorption characteristics.

Energy absorption was defined by

$$E = \frac{1}{2} \frac{W}{g} V_f^2$$

where

W = weight of assembly (lb)

V_f = velocity of impact (fps)

g = gravitation acceleration (fps^2).

The deceleration rate was given by

$$G = V_f^2 / 2g\, s_c$$

where s_c is the stopping distance in feet. For the preliminary design, a limiting deceleration of 200 g was used.

Several materials with desirable characteristics (balsa wood, aluminum honeycomb, styrofoam and rubber) were available for use as an impact cushion. For the SNAP 11 design, styrofoam was eliminated from consideration because of its low crushing strength, and rubber was eliminated because of its temperature limitations. A comparison of balsa wood and aluminum honeycomb resulted in a choice of balsa for the impact material. The reasons for this choice are as follows:

(1) Test results indicated the energy absorbing capability of balsa wood was greater than Type 5052 aluminum honeycomb.

	Density (lb/ft^3)	Energy Absorbed ($ft\text{-}lb/ft^3$)
Balsa	6-12	144,000 to 288,000
Aluminum honeycomb	8.0	88,000

(2) Maximum service temperatures are comparable. Aluminum is not recommended for use above 400° F and the decomposition temperature of balsa wood is about 500° F. Temperature should not be a problem during normal operation. The calculated maximum temperature of balsa at the inner container interface, based on a graphite shield material, is 209° F.

(3) A minimum radial gap is desired between the crushable material and the inner and outer containers to minimize motion of the inner container due to shipping loads. Balsa wood should provide a good fit.

The following balsa wood geometry was determined based on an inner container assembly weight of 3260 pounds which included the graphite shield.

Side balsa. Balsa blocks having a thickness of 3-1/2 inches are to be placed around the outer surface of the inner container. The balsa grain must be perpendicular to the inner container. The calculated deceleration resulting from a side drop from a height of 30 feet was 130 g.

End balsa. The end balsa was designed as solid cylinders of 5.2 inches diameter and 3-1/2 inches thick. Again, the balsa grain should be perpendicular to the container surface. The calculated deceleration for an end drop of 30 feet is 130 g.

Outer container. The outer container of 1.4-inch steel plate has the shape of a cylinder. The container acts as protection for the balsa wood, a mounting structure for lifting and a fire shield.

d. Bureau of Explosives Permit

Thermal, radiation and structural analyses of the shipping cask for the fuel block were completed and accepted by the Bureau of Explosives (BOE) for compliance with Interstate Commerce Commission regulations. Compliance with all specifications was established with the exception of the requirement that the radiation at one meter perpendicular to the long axis of the source be less than 10 mrem/hr. The calculated radiation at this point for the proposed cask was 25 mrem/hr.

A request was made to the BOE for a special permit with a waiver for this requirement. The request was granted and BOE Permit No. 1775 was issued to the Martin Marietta Corporation.

4. Aerothermodynamics

a. Re-entry heating equations

Aerodynamic heat transfer analyses were required to determine the maximum heat flux and total heat as a function of time for an atmospheric re-entry. The analyses were performed utilizing the following equation developed for a hemispherical re-entry configuration.

$$q_s = \frac{17,600}{\sqrt{R}} \sqrt{\frac{\rho}{\rho_o}} \left(\frac{V}{V_c}\right)^{3.15} \left[\frac{h_{si} - h_{ws}}{h_{si} - h_{ws_{300}}}\right]$$

where

q_s = heat flux (Btu/ft^2-sec)

R = body nose radius (ft)

ρ = ambient density (lb/ft^3)

ρ_o = sea level density (lb/ft^3)

V = flight velocity (fps)

V_c = satellite velocity (26,000 fps)

h_{ws} = wall enthalpy (Btu/lb)

$h_{ws_{300}}$ = wall enthalpy at 300° K (Btu/lb)

h_{si} = stagnation enthalpy (Btu/lb).

This equation was modified to agree with the SNAP 11 flight model re-entry mode. The re-entry mode is a tumbling cylinder with a ballistic coefficient (W/C_DA) of 39.8 lb/ft^2.

The heating equations for hemispherical noses were further modified to agree with the SNAP 11 fuel block assembly by utilizing the following correction factors to convert stagnation heating rates to total capsule heating.

(1) Cylinder normal to air flow, 0.707

(2) Cylinder tumbling, 0.584

(3) Surface averaging factor, 0.321.

To determine the amount of ablator required to allow intact re-entry, the trajectory heating data were determined by a Martin UB003 two-dimensional trajectory code which calculates the heat flux and total heating for a sphere of unit radius. These data were used in conjunction with the following equation to determine the amount of beryllium required to protect the capsule.

$$q_{AV_T} A_n (K) Z^{1/2} = M C_p \Delta T + M_{Be} h_{f_{Be}} + \sigma \epsilon A_s (T_1^4 - T_2^4) t$$

where

q_{AV_T} = total heat available from trajectory (Btu/ft^2)

A_n = cross-section area of fuel block (ft^2)

K = Appropriate surface averaging techniques

$$Z = \frac{W_n / C_{D_n} A_n}{W_o / C_{D_o} A_o} \times \frac{R_o}{R_n}$$

W_n = weight of fuel block (lb)

C_{D_n} = C_{D_o} = coefficient of drag (lb/ft^2)

R_o = radius of reference re-entry sphere (ft)

W_o = weight of reference re-entry sphere (lb)

A_o = cross-section area of reference re-entry sphere (ft^2)

R_n = radius of fuel block (ft)

M = weight of fuel block components (lb)

C_p = specific heat of fuel block components (Btu/lb-°R)

ΔT = change in temperature of fuel block components

M_{Be} = mass of beryllium ablator (lb)

$h_{f_{Be}}$ = heat of fusion for beryllium (470 Btu/lb)

σ = Stefan-Boltzmann constant

ϵ = emissivity of material

T_1 = final temperature of radiating material (°R)

T_2 = initial temperature of radiating component (°R)

t = time interval (sec)

A_s = external radiating surface (ft^2).

Each component was assumed to heat up from its operating temperature to a temperature approaching the melting point of beryllium. The beryllium was assumed to be at its melting temperature ($T_{M_{Be}}$), the graphite was assumed to be at ($T_{M_{Be}}$ - 100° R), the platinum at ($T_{M_{Be}}$ - 200° R), and the fuel and capsule at ($T_{M_{Be}}$ - 250° R). The radiating component was assumed to be the beryllium ablator at its melting temperature for 300 seconds of trajectory time.

The present generator design was assessed to be adequate for intact re-entry, but a detailed analysis of the system is required to establish confidence factors.

b. Re-entry heating analysis

Aerothermodynamic studies have shown minimum heating conditions occur following a control malfunction yielding a subsequent atmospheric re-entry from both the parking orbit and the lunar interception phases of operation. For this condition, the capsule would be exposed to a maximum stagnation heating rate of 1600 Btu/ft^2-sec and a total integrated heat input of 14,500 Btu/ft^2 over an effective 16-second heating interval.

Maximum heating occurs at certain critical times during the final firing of the Centaur vehicle, during thrust-misaligned failures, or during earth re-entry from a lunar orbit at very high speeds and low re-entry angles. These conditions result in a maximum stagnation heating rate of 1053 Btu/ft^2-sec and a total integrated heat input of 135,000 Btu/ft^2 over an effective 280-second heating interval.

The SNAP 11 system was analyzed as part of the Surveyor spacecraft on an Atlas-Centaur booster. The ascent phase of flight consists of booster and sustainer firing of the Atlas engines, followed by two burn

periods of the Centaur vehicle. The first Centaur firing will eject the payload in a 100-nautical mile parking orbit. The second firing places the payload in the lunar transfer trajectory Failure to ignite the Centaur' s second maneuver will yield an orbital decay re-entry with heating as shown in Fig. IX-7. Thrust and guidance failures during the second firing can yield the maximum or minimum heating environment, depending on the time and magnitude of malfunction. Maximum heating is shown in Fig. IX-8 as a function of time; minimum heating is shown in Fig. IX-9.

c. Powered re-entry analysis

As shown in Fig. IX-7, the maximum heat flux and total heat generated by the capsule during a natural orbital decay were about 330 Btu/ft^2-sec and 92,000 Btu/ft^2, respectively. It was also desirable to establish a heating environment for a typical retrorocket powered re-entry from an established parking orbit. The maximum heat flux and total heat generated by the capsule during the powered re-entry were about 700 Btu/ft^2-sec and 95,000 Btu/ft^2 as shown in Fig. IX-10. Time intervals were about 1500 seconds for natural decay compared to 350 seconds for the powered re-entry.

d. Heat shield analysis

The fuel capsule and heat shield (ablator) configuration which has been developed during the design studies is shown in Fig. IX-11. The spherical platinum fuel capsule is surrounded by graphite and beryllium cylinders.

The graphite alone would survive the aerodynamic heating, but heat could be transmitted through it in sufficient quantity to melt the platinum fuel capsule. The beryllium cylinder was added as a thermal delay feature. Heat will be dissipated by ablation of the beryllium shield; therefore, less energy will be available to affect the platinum capsule. Because the system cannot be sealed at the beryllium shield, the ablator assembly will be encapsulated in a stainless steel container.

A plasma test program was conducted to evaluate experimentally the reaction of a SNAP 11 fuel block to earth re-entry heating. The object of the program was to determine if the platinum impact absorber surrounding the fuel capsule would melt under the most stringent conditions imposed by a stable mode re-entry. The experimental program was performed at the Plasmadyne Corporation on test models provided by the Martin Company. The fuel block did not indicate platinum temperatures above 2200° F, nearly 1000° F below its melting point. Temperature distributions in the beryllium were in agreement with those determined analytically. Platinum temperatures were lower in the analytical results than the experimental model.

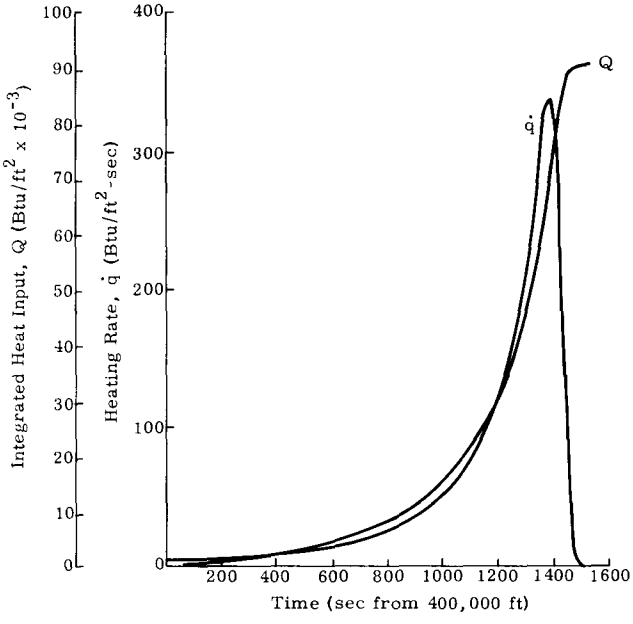

Fig. IX-7. Orbital Decay Heating

Fig. IX-8. Maximum Re-entry Heating

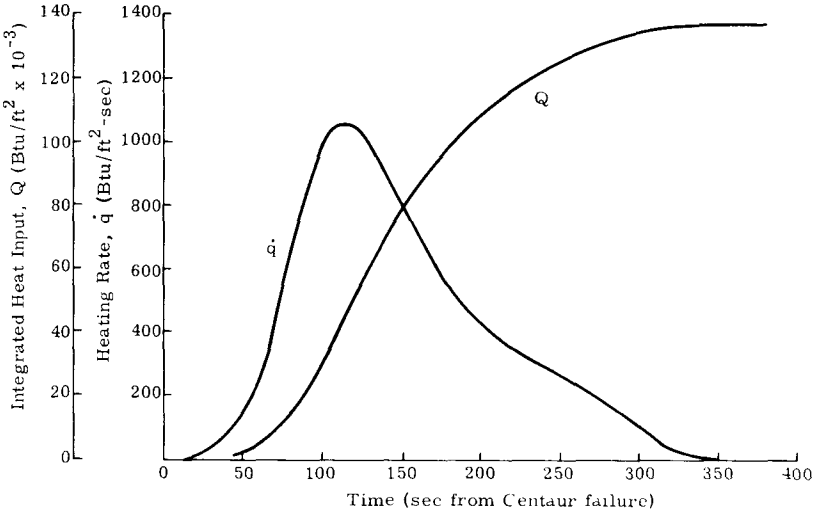

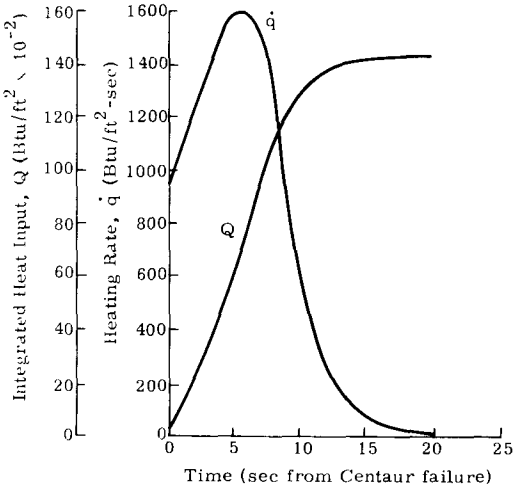

Fig. IX-9. Minimum Re-entry Heating

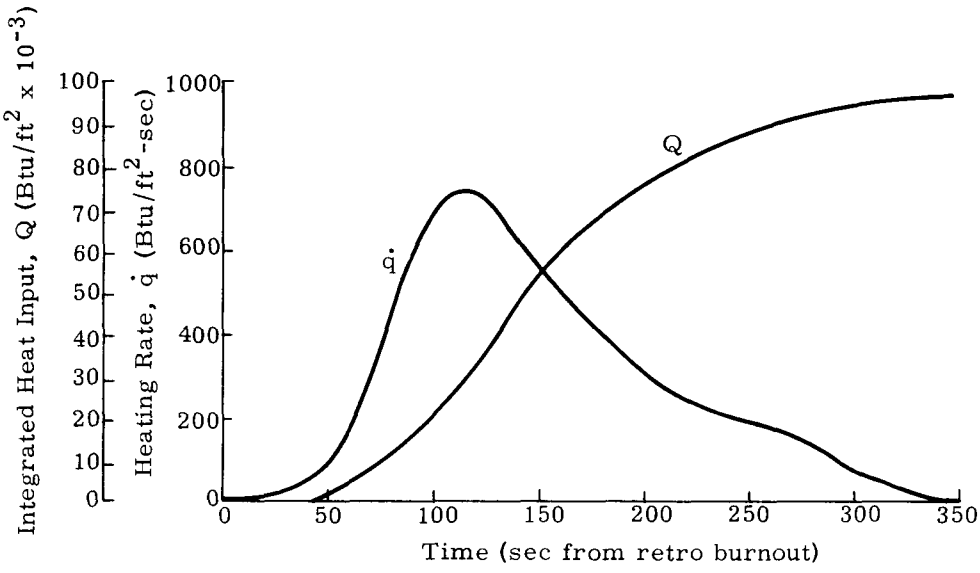

Fig. IX-10. Powered Re-entry Heating from Parking Orbit

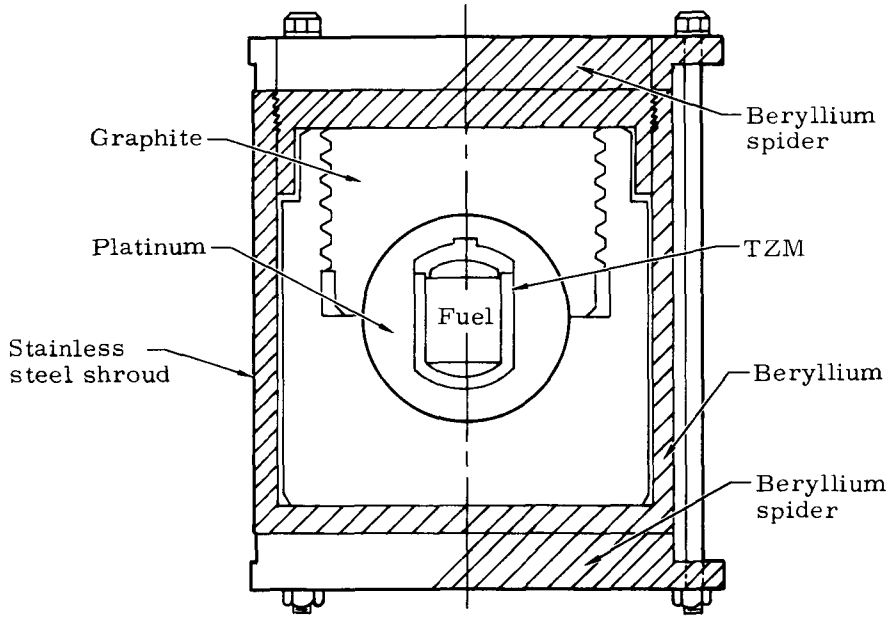

Fig. IX-11. Fuel Capsule and Heat Shields

Although the conditions within the plasma stream did not simulate re-entry exactly, the results indicate than the Martin Heat Transfer Program FB-090, gave applicable, valid results for comparison of analytical and experimental temperature distributions for comparable heating rates. Further, the results illustrate the system can survive re-entry and will impact, satisfying design conditions.

5. Impact

a. Impact analysis

The initial impact analyses were conducted in conjunction with testing performed by Aberdeen Proving Ground to establish the feasibility of:

(1) Determining projectile and target parameters on the penetrating threshold velocity of the model

(2) Determining cratering characteristics as a function of projectile parameters

(3) Correlation of projectile parameters with fuel containment

(4) Determining the degree which empirical equations derived from other high velocity impact tests describe the mechanisms of the composite SNAP 11 fuel capsule model.

The impact program was divided into three phases

In the first phase of testing, 50 specimens were fired into granite blocks from a smooth-base powder gun. During these tests, impact velocity, crater radius, penetration depth, rebound velocity and projectile physical dimensions were measured. Results of the initial testing showed that crater volume varied in proportion to the fourth power of impact velocity. No attempt was made to explain this relation although other experimenters have indicated crater volume varies as the square of the velocity. (Test data are reported under Impact Tests.) In this series of tests, the specimens were approximately 1/2-inch diameter balls encased in magnesium cylinders about 5/8 inch in length. Maximum impact velocities were 6300 fps.

The second phase consisted of impacting half-scale fuel block specimens (Fig. IX-12) with tantalum substituting for the platinum spherical capsules. However, since a new launch mechanism was required for the larger half-scale models, the fuel block tests were preceded by solid cylinder impact tests. The preliminary shots were designed to explore test parameters, equipment adequacy, recovery techniques and test operational procedures. Once the testing techniques were established, three aluminum, three steel and five tantalum models were

tested at impact velocities of 1000 to 8000 fps. Post-test examinations consisted of photographic reproduction of impact specimens and radiographs of the impacted tantalum spheres. These analyses indicated only slight metal flow (tantalum) at impact velocities of about 1200 fps. However, as the impact velocity increased, the induced metal flow rapidly increased, especially above 4000 fps. Loss of weight from the sphere was insignificant up to 4000 fps impact velocities. Even at the lower impact velocities of 1000 fps, the outer structures of the fuel assembly simulating the ablative heat shield (magnesium) and heat shield (graphite) were pulverized at impact. The tantalum impact models did exhibit absolute containment of the fuel when impacted with the fuel block assembly. Tests which impacted bare tantalum spheres indicated only partial fuel containment.

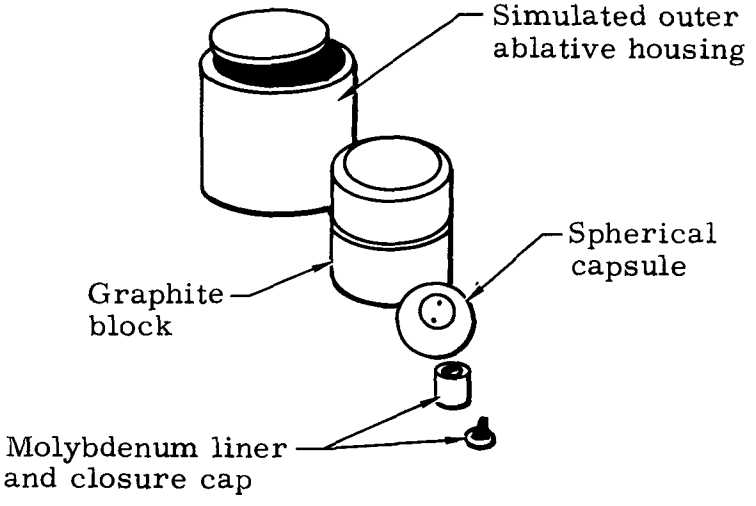

Fig. IX-12. Half-Scale Impact Test Specimens

The third and final phase of testing evaluated half-scale fuel blocks with platinum spheres as shown in Fig. IX-12. Post-test examinations consisted of metallographic, helium leak check and hardness testing. The objectives of the examinations were to determine the internal condition of the assemblies, the post-impact location of the fuel cavity, the condition of the liner and the degree of containment. The impacted fuel assemblies contained all components of the flight model, including a simulated fuel form.

The following is a discussion of impact energy distribution and impact characteristics.

The fuel block imparted kinetic energy to the granite target in a few microseconds. A certain amount of the energy was dissipated in the fuel block and the remaining portion dissipated in the granite.

The total energy remaining in the fuel block caused the material to be highly compressed, resulting in fracturing and flowing of the material from the assembly, thereby dissipating its energy.

The total energy imparted to the target caused the material to be fractured. The structural properties of the target material (granite) did not permit the energy to be dissipated by a flow mechanism as would have occurred in a more ductile material. The fractured material was ejected from the free surface, thus causing the energy in the material to be reduced.

The contact pressure between the fuel block and the target remained high as penetration occurred. However, the pressure dropped off very rapidly in the granite and in the fuel block due to side ejecta and free edge flow of the metal.

The effects of increasing impact velocity on the primary containment structure of the fuel block assemblies were:

(1) The low velocity impacts resulted in metal flow which continued until the internal energy in the metal dropped below the quantity necessary to exceed the yield strength of the material.

(2) The high velocity impacts resulted in metal flow, first according to hydrodynamic considerations, and secondly according to crystallographic and strength properties. Metal flow continued until the internal energy dropped below the cutoff yield strength value. The flow of metal from the free edges was insignificant up to approximately 1200 fps, and weight losses were negligible up to approximately 4000 fps. However, as the impact velocity increased, induced metal flow and weight losses increased accordingly.

The impacting fuel assembly did not remain in the crater because of the strength properties of the particular impacted material (granite). Mechanical attachment due to flow of the platinum component during the impact event locked the assembly to the target material in the fractured zone of the crater. Since the threshold energy required to break this material from the target is extremely low, the fuel block was therefore ejected from the crater.

The outer structural components of the fuel block assembly that are required from an aerothermodynamic standpoint were separated from the primary impact containment structure for the entire impact velocity spectrum of 641 to 8409 fps. Therefore, containment of the isotope can only be afforded by the platinum and the inner fuel liner. The outer structure, which consists of the ablative and heat shield, did act as an initial energy absorber upon impact. This structure reduced the total energy which had to be absorbed by the primary containment structure.

b. Impact conclusions

The impact phenomena of the SNAP 11 fuel assembly for both the earth and lunar impact were evaluated by the half-scale impact test program. Prior to this program, fuel assembly impact phenomena were unknown. The program was conducted to investigate design requirements, impact reactions and fuel containment characteristics of the fuel assembly.

The conclusions of the test program were:

(1) Containment afforded the fuel at impact velocities of less than 4000 fps would be primarily by the platinum component since significant fracturing of the molybdenum liner occurred at the lower impact velocities.

(2) Containment afforded the fuel at impact velocities greater than 4000 fps would be primarily by the molybdenum fuel liners, since the platinum is forced from around the liners at these impact velocities in order to dissipate the impact energy.

(3) Complete containment of the simulated fuel pellet was exhibited up to 3356 fps and partial containment was exhibited up to 6815 fps.

(4) Platinum seal welds retained their integrity regardless of impact orientation.

(5) Platinum exhibited good impact characteristics by permitting large energy dissipation from the free edges of the model without fracture and release of the fuel liner and simulated fuel.

(6) The molybdenum fuel liner did not retain its integrity for low impact velocities (<4000 fps).

(7) Flow and/or shear of material from the primary containment structure (platinum) is negligible up to approximately 3000 fps.

(8) The fuel assembly will initiate surface penetration (<1/8 inch) when impacted on granite at approximately 700 fps.

(9) The fuel containment assembly will not be contained within the crater caused by the impact.

These conclusions cannot be directly applied to a flight model RTG fuel assembly, but can be utilized in establishing a feasible design and evaluating impact reactions and fuel containment characteristics. The reasons that these conclusions cannot be extended to the flight model are:

(1) The inaccuracy of scaling laws to predict the effects on the flight model.

(2) The limited number of fuel assemblies tested.

(3) Impacted fuel assemblies were not preheated to approximate operating temperatures prior to impact.

Therefore, the impact considerations necessary to determine the conformance of the RTG fuel assembly to the safety criteria are incomplete.

6. Radiation

a. Analysis

A radiation analysis was made of the curium-fueled SNAP 11 generator and its subassemblies. Dose rate calculations were performed for:

(1) Fuel, TZM liner and platinum shield

(2) These plus the graphite block, beryllium ablator and stainless steel shroud

(3) Assembled generator.

A schematic sketch of the assemblies is shown in Fig. IX-13.

The spectrum for gammas includes those from decay, prompt fission and fission products. Neutron dose rates were based upon a production of 1.7×10^5 neutrons/sec/watt which include both spontaneous fission and alpha-neutron reaction products. The generalized shielding code developed at Martin Marietta was used to calculate the dose rates.

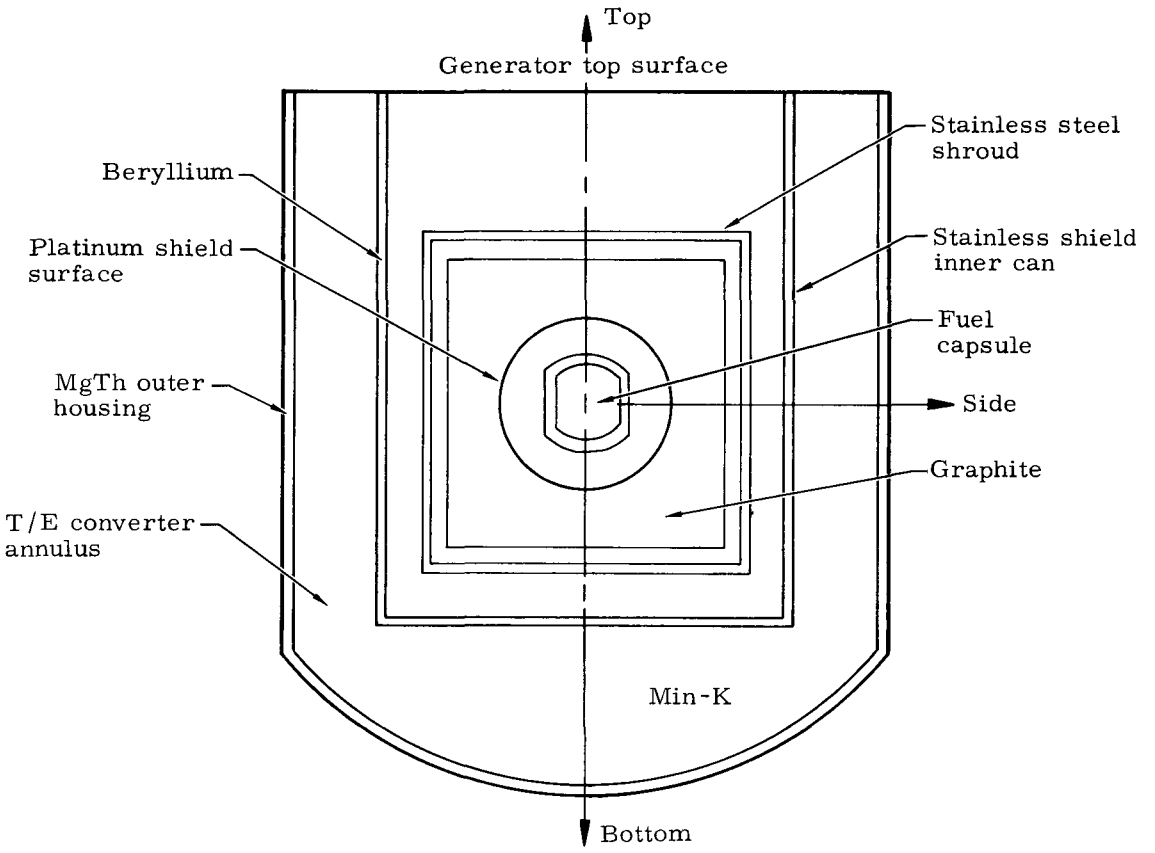

Fig. IX-13. Generator Assembly Schematic

The maximum and minimum dose rates occur, respectively, in the directions designated top and side in Fig. IX-13. Dose rates at the surface and at several distances from the center of the fuel are given in Table IX-12 for the three configurations. For comparison, dose rates for a rhodium and an iridium matrix are given for the top of the platinum shield. An iridium matrix was assumed for all other assemblies. Examination of the data shows the neutron dose rate is essentially the same for both matrix materials, while the gamma dose rates are 40 to 50% higher for the rhodium matrix.

TABLE IX-12

Dose Rates from SNAP 11 Generator

		Dose Rates (mrem/hr)					
	Distance from Fuel	Side		Top		Bottom	
Assembly	Center	Gamma	Neutron	Gamma	Neutron	Gamma	Neutron
Platinum shield	Surface	1 69 (+3)	1 20 (+5)	3 28 (+3)	1 05 (+5)		
	3 in	2 18 (+2)	1 61 (+4)	5 13 (+2)	1 73 (+4)	Same as top	
	6 in	53 3	4 01 (+3)	1 32 (+2)	4 53 (+3)		
	12 in	13 2	1 00 (+3)	33 6	1 16 (+3)		
	1 meter	1 22	92 7	3 2	1 10 (+2)		
Rhodium matrix*	Surface			4 68 (+3)	1 11 (+5)		
	3 in			7 50 (+2)	1 83 (+4)		
	6 in			1 95 (+2)	4 83 (+3)		
	12 in			49 6	1 24 (+3)		
	1 meter			4 7	1 17 (+2)		
Fuel block	Surface	3 65 (+2)	2 21 (+4)	7 17 (+2)	1 83 (+4)		
	6 in	47 5	2 95 (+3)	1 20 (+2)	3 15 (+3)	Same as top	
	12 in	11 8	7 36 (+2)	30 5	8 07 (+2)		
	1 meter	1 08	68 3	2 9	76 2		
Generator	Surface	78 8	5 36 (+3)	2 23 (+2)	5.83 (+3)	1 55 (+2)	4 37 (+3)
	6 in	38 5	2 64 (+3)	1 20 (+2)	3 15 (+3)	1 17 (+2)	3 32 (+3)
	12 in	9 5	6 57 (+2)	30 5	8 07 (+2)	28 3	8 05 (+2)
	1 meter	0 88	61 0	2 9	76 2	2 6	73 2

* All other values listed are for iridium matrix

(x) means 10^x

Particle fluxes at one meter from the center of the fuel are given in Table IX-13. Fluxes at a distance greater than a meter can be estimated by using the inverse square relationship between dose rate and distance.

TABLE IX-13

Particle Flux at One Meter from Fuel Center

Direction from Generator	Particles/cm^2/sec	
	Gammas	Neutrons
Side	500	430
Top	1500	530
Bottom	1400	510

b. Environmental radiation considerations

The amount of time a person can work around a generator can be determined from the dose rates given in Table IX-14. Maximum dosages allowed by Federal regulations per calendar quarter are 1.25 rem for the whole body or the eyes, and 18.75 rem for the hands and forearms, or feet and ankles. Based upon examination of human body dimensions and working patterns, it seems reasonable to assume the maximum dose received by the hands and forearms will be at a distance of six inches from the center of the fuel, the dose to the eyes at 12 inches and the dose for the whole body at one meter.

Based on these criteria, the time to accumulate the maximum quarterly dose can be calculated. The data are presented in Table IX-14 and represent the time limitations for a worker intimately engaged in generator or subassembly handling.

TABLE IX-14

Worker Time Limitations for Direct Handling

	Allowable Time Per Calendar Quarter (hr)		
	Hands (18.75 rem)	Eyes (1.25 rem)	Body (1.25 rem)
Platinum shield	4.0	1.0	11
Fuel block	5.7	1.5	16
Generator	5.7	1.5	16

c. Shielding analysis

A comparison of the relative gamma and neutron dose rates from generators fueled with curium-242 shows that only the neutron component requires shielding to meet shipping regulations. The code used in this analysis was the DTK code developed at Los Alamos. This code is an improved version of the earlier DSN code based on Carlson's SN method of discrete ordinates for numerically integrating the Boltzmann transport equations. The neutron cross sections were used for a 16-group neutron flux as listed in Table IX-15.

Graphite, iron, nickel, uranium, tantalum and paraffin were evaluated as surface shields. Their effectiveness is illustrated in Table IX-16. Pure iron and aluminum were investigated, but the resultant dose rates were higher than those from pure graphite. Many salts including powdered borax were considered, but were rejected because of thermal considerations.

TABLE IX-15

Energy Grouping of 16-Group Cross Sections

Group	Energy Range	Group	Energy Range
1	3 Mev	9	100 to 550 ev
2	1.4 to 3.0 Mev	10	30 to 100 ev
3	0.9 to 1.4 Mev	11	10 to 30 ev
4	0.4 to 0.9 Mev	12	3 to 10 ev
5	0.1 to 0.4 Mev	13	1 to 3 ev
6	17 to 100 Kev	14	0.4 to 1 ev
7	3 to 17 Kev	15	0.1 to 0.4 ev
8	0.55 to 3 Kev	16	0.025 ev (thermal)

TABLE IX-16

Dose Rates at Shield Surface for Various Materials--SNAP 11 Fuel Block, 922 Watts, Cm-242

Shield	Dose Rate (mrem/hr)	Shield Weight (lb)
Graphite (in.)		
8	1145	506
10	803	835
12	380	1280
16	146	2587
20	63	4568
3-in. Fe + 7-in. graphite	660	1115
3-in. Ni + 7-in. graphite	592	1160
4-in. Ni + 6-in. graphite	567	1340
5-in. Ni + 5-in. graphite	559	1570
2-in. U-238 + 8-in. graphite	393	1256
2-in. Ta + 8-in. graphite	331	1210
3-in. Ni + 9-in. graphite	331	1600
3-in. Ni + 11-in. graphite	199	2180
Paraffin 8 in.	253	286

The results of the shielding analysis are shown in Fig. IX-14. The figure shows the variation in dose rate as a function of distance from the selected 16-inch graphite and 8-inch paraffin shields. Either of the shields is suitable as a shipping cask for the SNAP 11 fuel block.

D. SUMMARY OF SAFETY TESTS

1. Helium Leak Test

Helium leak tests were performed to evaluate the degree of containment that would be afforded the fuel after impact. By this test it was possible to determine the integrity of the structure at locations other than at the sectioned plane for metallographic analysis.

The containment structures were leak tested on a mass spectrometer leak detector. The sensitivity of the instrument was 10^{-10} cm^3/sec of helium.

Test models were prepared by sectioning the containment structure into approximately equal sections and testing as illustrated in Fig. IX-15. The leak tests were performed on models which had been impacted up to 3356 fps.

The results of the tests indicated that all containment structures exhibited some small leakage. The leakage occurred through the platinum at the edges of the molybdenum liner, where the erosion of platinum from the impact event was most severe. Due to the irregularities in the profile of the model, no calibrated leak rate for the models could be established. However, a quantitative calibration was achieved by comparing the maximum evacuation achieved on the models to known hole sizes and vacuums This comparison yielded a maximum hole size of approximately 10^{-3} inch in diameter. It is believed that this size hole would represent an insignificant release point for the fuel and any possible release that would occur would be of a low order.

2. Capsule Pressure Test

The fuel capsule for the SNAP 11 generator will be subjected to an internal pressure buildup due to helium formation from alpha particle emission of the curium-242 fuel. If the capsule creeps while under pressure, increased surface contact between the capsule and the platinum sphere will result. Such an event will increase conduction of heat between the components. While such an increase would aid transfer of heat to the generator during the mission, the increased conductive heat transfer into the system during re-entry could affect the potential for melting. Thus, examination of the capsules for creep was required.

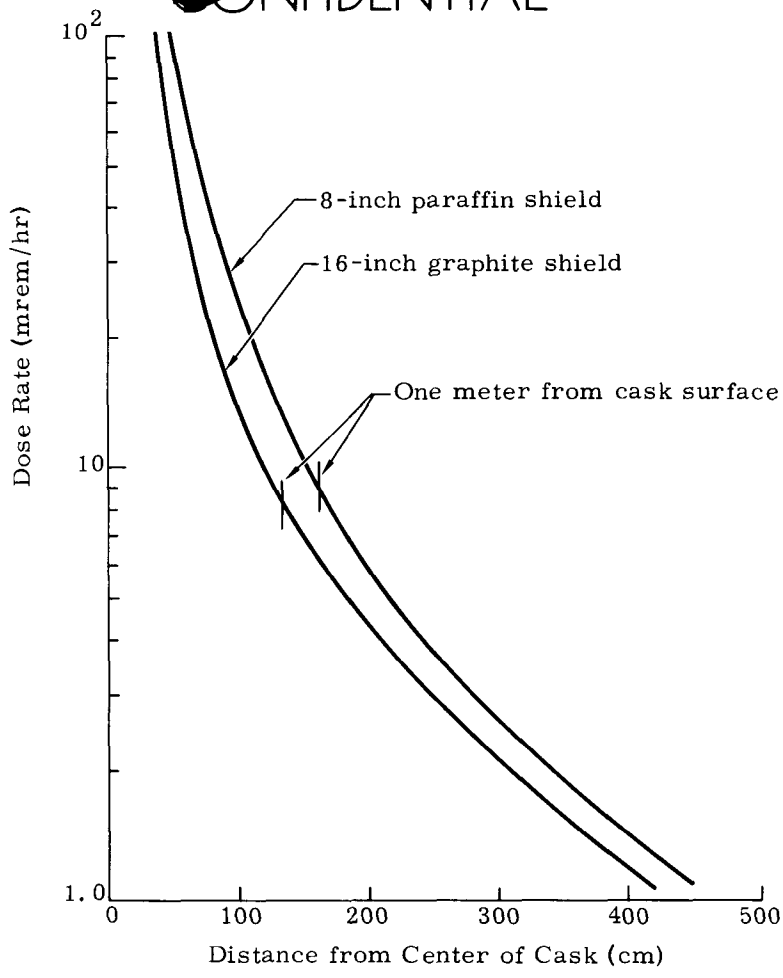

Fig. IX-14. Neutron Dose Through Shipping Cask

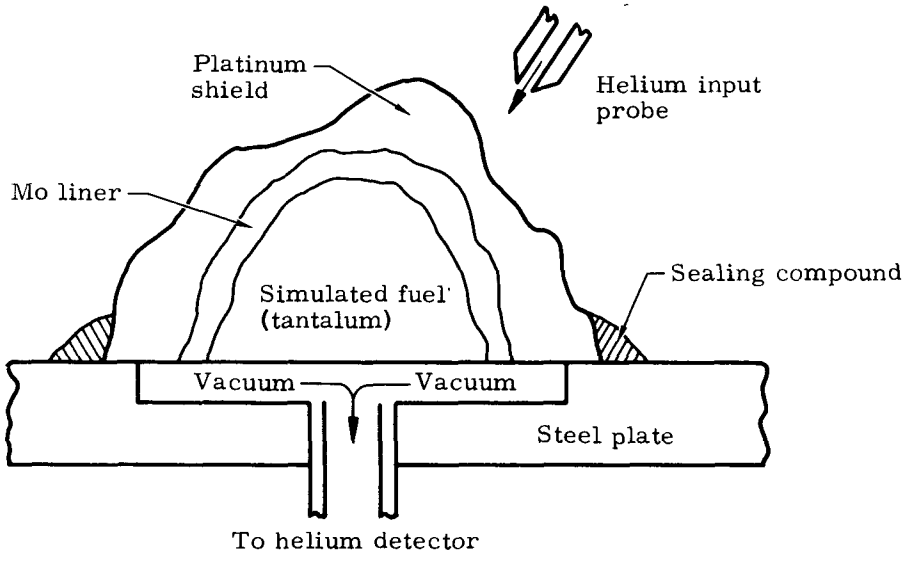

Fig. IX-15. Helium Leak Test Setup

Although rupture of the capsules was considered to be unlikely at these conditions, the test would also yield information on rupture. Six fuel capsules were manufactured according to SNAP 11 design drawings since the flight model is constructed so that the fuel capsules are completely enclosed within the platinum. Platinum impact absorbers were also manufactured.

The fuel capsules were composed of TZM material (0.5% titanium, 0.07% zirconium, balance molybdenum). This material is extremely brittle at room temperature, but exhibits excellent high temperature properties. The cylindrical capsules, 1.180 inches in diameter with hemispherically rounded ends, were subjected to the calculated maximum pressure of 3860 psi, which occurs at approximately 230 days. Since the temperature decays exponentially after mission completion, the temperature at approximately 200 days (approximately 1470° F) was taken as the test temperature to devise a conservative test.

After completing approximately 850 hours at test conditions, in an atmosphere of argon, the pressure was decreased to zero, the furnace was disconnected and the specimens were allowed to cool. The specimens had oxidized slightly on the outer surface, but no leaks or rupture failures had occurred. Results of before-test and after-test measurements of the three test specimens are presented in Table IX–17.

As determined from Table IX-17, the change in diameter dimensions ranged from a minimum of 0.0000 to a maximum of 0.0008 inch. The length change varied from 0.0000 to 0.0014 inch. The maximum deflection occurred on the third capsule as measured from the bottom of the capsule through the 1.0-inch section of tubing and the diameter of the manifold. This dimension is somewhat misleading since the tubing section and the manifold also deflected under pressure. However, a dimensional change of this magnitude would still meet specifications.

The average diameter deflection was 0.0004 inch, while the average length deflection was 0.0003 inch. These values are at the reliability limit of the measuring device. Although these values were obtained, the technical deflection was actually zero. For this reason, testing was terminated after the first test period.

It is therefore concluded that the fuel capsules will withstand the helium pressure buildup resulting from the decaying curium fuel; the capsules will not creep, much less rupture within the mission lifetime.

TABLE IX-17

Dimensions of Test Specimens

Measured Point*		Dimension (in.) Capsule 1	Capsule 2	Capsule 3
1. Diameter	Before	1.178	1.1790	1.1785
	After	1.1788	1.1795	1.1802
2. Diameter (90° to 1)	Before	1.1784	1.1790	1.1790
	After	1.1788	1.1792	1.1795
3. Diameter	Before	1.1788	1.1798	1.1788
	After	1.1790	1.1798	1.1792
4. Diameter	Before	1.1795	1.180	1.1798
	After	1.1798	1.1803	1.1805
5. Diameter (90° from 4)	Before	1.1797	1.7999	1.180
	After	1.180	1.1804	1.1804
6. Diameter	Before	1.1797	1.180	1.1798
	After	1.180	1.1802	1.1804
7. Length	Before	1.4938	1.4884	1.4936
	After	1.4970	1.4888	1.4937
8. Length (90° to 7)	Before	1.4960	1.4887	1.4933
	After	1.4960	1.4890	1.4940
9. Length plus TZM section	Before	--	2.6055	1.4668
	After	--	--	1.4682

*

1, 2, 3, 4, 5, 6 = diameters
7, 8, 9 = length measurements

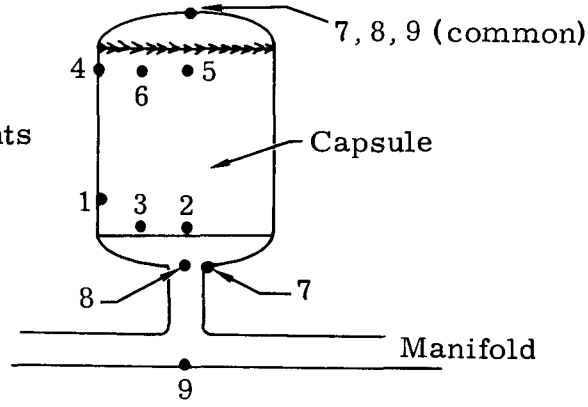

3. Plasma Arc Tests

Full-scale generator fuel block assemblies were subjected to simulated atmospheric re-entry conditions to evaluate design conformance to the established intact re-entry safety criterion. The tests were performed in a high energy plasma arc tunnel at Plasmadyne Corporation, Santa Ana, California. Four full-scale models were tested under both steady-state and transient (re-entry trajectory) conditions to determine their behavior during various modes of re-entry. In the stable mode, the models were subjected to the total integrated heat. For the transient mode, the leading edge of the models was subjected to the surface averaged heat flux.

The test facility was capable of producing stagnation enthalpies of up to 25,000 Btu/lb and can operate with up to one megawatt of input power. The plasma arc was operated at maximum heat flux conditions during the steady-state tests to subject one face of the model to the total thermal energy of a stable re-entry. The heat flux was varied during the transient mode to obtain surface averaged heat fluxes, i.e., the heat flux defined by the total heat input divided by the total model surface area.

Plasmadyne test equipment and a Martin calorimeter were used to calibrate the plasma arc for both steady-state and transient conditions; the data are presented in Table IX-18. To ensure repeatability, the plasma arc was recalibrated with the Plasmadyne equipment before each steady-state run. The trajectory or transient test parameters, however, were calibrated during a preliminary run prior to the actual model test.

Each test model was instrumented with 15 thermocouples identified as follows:

(1) Beryllium ablative shield (9 ea)

(2) Graphite heat transfer shield (2 ea)

(3) Platinum containment capsule (4 ea).

A preliminary copper test model was used to determine plasma arc characteristics, model response and optimum test procedures prior to the full-scale model tests. Three full-scale re-entry models were tested; one model contained a beryllium ablative shield, while copper-bronze was substituted for the beryllium in the other two models because of toxicity considerations. Table IX-19 shows the results of the tests. It is most significant that the beryllium model did not yield fuel containment temperatures greater than 2200° F.

TABLE IX-18

Plasma Arc Tests--Calibration Data

Model	Stagnation Enthalpy (Btu/lb)	Stagnation Heat (Btu/ft^2-sec)	Stagnation Pressure (atm)	Mass Flow (lb/sec)	Input Power (kw)
Preliminary	11,980	316.8	0.0855	0.0180	22.75
Copper-Bronze	Variable simulating re-entry heating curve (Ref. Section C.4)				
Copper-Bronze	12,120	316.0	0.0854	0.0180	23.02
Beryllium	12,050	316.4	0.0855	0.0180	22.88

TABLE IX-19

Plasma Arc Test Results

Model	Exposure Time (sec)	Test Condition	Maximum Platinum Temperature (°F)
Preliminary Copper	346	Steady state	3000
Copper-Bronze		Trajectory	1575
Copper-Bronze	320	Steady state	2800
Beryllium	346	Steady state	2200

Previous aerothermodynamic analyses indicated that burnup of the re-entering fuel block of the SNAP 11 generator did not occur, although the platinum did melt during re-entry only to solidify prior to impact. The plasma tests, however, indicated that the platinum was several hundred degrees below its melting point.

Examination of both analysis and experiment indicated that:

(1) The heat flux seen by the entire calibration probe and model was not as great as that seen by a re-entering body, since the plasma stream was not large enough to engulf the probe or model.

(2) The tested probe had spaces or gaps between the beryllium, graphite and platinum components.

The analysis had assumed close, complete contact between components Conduction was the main factor determining temperature in the analysis, whereas internal radiation was the determining factor in the experimental work.

To complete the evaluation of the data, a second probe was manufactured to recalibrate the facility. Agreement between theoretical radial distributions and experimental distribution was found to be within 10% for that portion of the probe within the plasma stream.

Upon completion of the data reduction for the recalibration work, an analytical examination was conducted on the beryllium clad specimen. This analysis revealed that the internal radiation was indeed the primary factor determining temperature within the specimen.

As a result, it was concluded that the platinum sphere does not melt during plasma tests or re-entry heating conditions. The system will impact as designed under the specified conditions.

4. Impact Tests

One-eighth scale impact tests were conducted to study material and target characteristics and equipment parameters. One-half scale tests were also conducted to determine fuel liner containment, post-impact material properties, component compatibility and post-impact oxidation effects for two different capsule materials, TZM and Haynes-25. Additional observations were made of post-impact structural characteristics, impact characteristics and degree of fuel containment with all components in place, crater and ejection material properties, and the degree of containment afforded by the craters.

Fifty specimens of various materials including steel, aluminum and platinum were impacted at various velocities against a granite block in the 1/8-scale tests.

Equipment characteristics were determined; velocity was chosen as the most important criterion; target characteristics were recorded; and steel, aluminum and platinum were selected for the 1/2-scale tests. These tests involved impacting 19 specimens at various speeds against a granite block target. Containment characteristics were investigated at several different impact speeds.

Containment for the 1/2-scale tests was exhibited for speeds up to approximately 3350 fps. Primary containment at these impact speeds is effected by the platinum spheres.

a. One-eighth scale tests

Six different specimen types were tested during this phase of the impact program. Fifty individual specimens were fired against granite blocks from a smooth bore powder gun. Tantalum balls with 0.275, 0.330 and 0.412 inch diameters, some encased in magnesium cylinders 0.588 and 0.882 inch in length, were used to generate the required impact data. Table IX-20 lists the six types of specimens used for the tests.

TABLE IX-20

One-Eighth Scale Impact Specimens

Type	Ball Diameter (in.)	Magnesium Length (in.)
1	0.412	None
2	0.412	0.588
3	0.330	0.588
4	0.275	0.588
5	0.412	0.882
6	None	0.588

A correlation of crater volume as a function of impact velocity for all specimens is shown in Fig. IX-16. Note that the type six specimen data are displaced from the other types, indicating that a higher velocity is required for lighter projectiles to create equivalent crater displacement volumes.

b. One-half scale tests

The test consisted of impacting 19 specimens against a granite target. The test program was divided into three phases:

(1) Phase I was designed to explore test parameters, equipment capabilities, recovery techniques and operational procedures. Three solid aluminum and three solid steel specimens were fired in this phase.

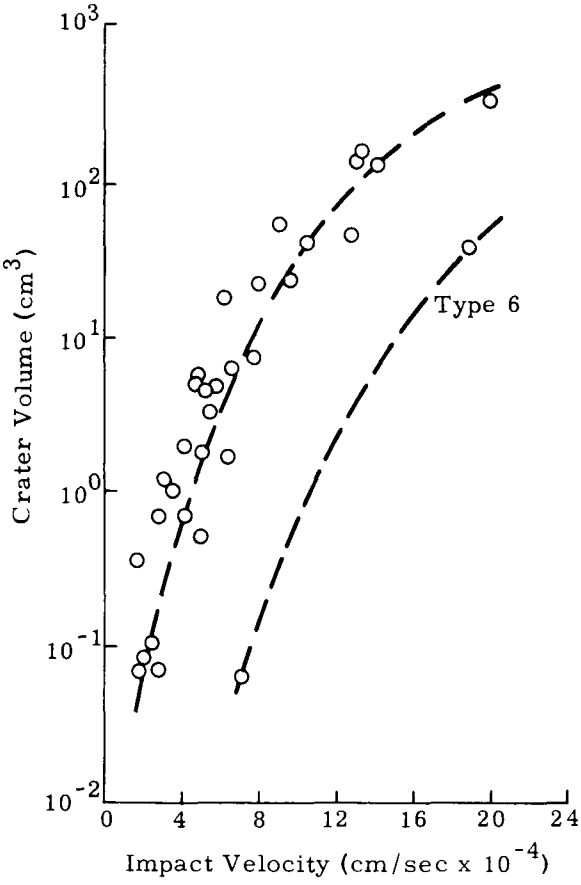

Fig. IX-16. Crater Volume as Function of Impact Velocity

(2) Phase II was designed to establish and refine the testing techniques used in Phase I prior to launching the platinum models. Five tantalum models were fired in this phase.

(3) Phase III consisted of firing eight platinum fuel block assemblies.

The test facility consisted of a launcher, target material, recovery system and data acquisition equipment. The launcher was a 105-mm Howitzer mounted on a self-propelled carriage. Models were fired by a separable sabot mechanism. This allowed unrestricted impact at the granite target.

A high speed (40,000 frames/sec) Dynafax Continuous Writing Camera was used for obtaining flight data and impact speeds. Results of the tests are given in Table IX-21.

Conclusions have been presented under the section entitled, "Impact Conclusions."

TABLE IX-21

One-Half Scale Impact Specimen Results

No.	Test Material	Impact Velocity (fps)	Crater Data: Surface Area ($in.^2$)	Crater Data: Depth (in.)
1	Aluminum	1123	9	0.25
2	Aluminum	6574	210	2.0
3	Steel	7460	851	5.5
4	Steel	1227	23	1.0
5	Aluminum	4770	138	1.5
6	Steel	7709	464	5.7
7	Tantalum	1188	4	0.5
8	Tantalum	3975	210	3.2
9	Tantalum	8409	365	5.5
10	Tantalum	7247	265	5.0
11	Tantalum	7817	164	7.2
12	Platinum	1207	4	0.5
13	Platinum	3356	165	2.8
14	Platinum	4993	206	3.7
15	Platinum	5932	307	4.5
16	Platinum	938	2	0.25
17	Platinum	641	1	0.12
18	Platinum	6815	318	5.7
19	Platinum	5816	24	4.7

E. SAFETY APPLICATION TO NEW DESIGN

Based on the requirement for a new fuel block design for the ORNL Fueling Demonstration Test Plan, the AEC relaxed the original aerosafety requirements for the SNAP 11 system. The revised goal for the program was to fuel a generator scheduled for operation in a controlled laboratory with facilities for simulating lunar day and lunar night environments. As a result, re-entry impact, aeroheating survival and launch pad accident criteria were deleted. However, during terrestrial accidents and test environments, fuel containment would be maintained.

The new fuel block design was reviewed from a safety standpoint, and the following comments represent a general evaluation of the design:

(1) Lack of compatibility data on Cm-242 (oxide) with TZM is perhaps the weakest point in the SNAP 11 fuel block design. Although some data on Cm-244 (oxide) were available before fueling, the fueled SNAP 11 generator itself will provide the first meaningful study of the compatibility of the fuel with a TZM primary capsule.

(2) The present fuel block design is oriented toward laboratory use only and is not satisfactory for an intact re-entry flight article. Numerous configuration changes would be necessary for this system to be launched successfully and for intact re-entry; materials could remain unchanged if diagnostic disassembly of the ORNL fuel block indicates no compatibility problems and if a subsequent safety effort shows the materials will satisfy safety requirements.

(3) The initial fuel block design basically reflects the state of the art in re-entry that existed near the design commencement of the SNAP 11 program (~1962) and as such is somewhat antiquated. If the block were redesigned for actual flight purposes, a different design approach would be required.

(4) The thermal analysis performed on the fuel block in the event of total weld failures, i.e., the vacuum condition, is conservative to the extent that it would be desirable to test a fuel block with an electrical heater under this condition.

(5) The TZM primary capsule has been shown to be structurally adequate for a 120-day life if the capsule temperature does not exceed 2000° F and full penetration is achieved at the cover-to-body weld joint.

(6) Times to rupture the TZM fuel capsule have been approximated for a condition which assumes loss of the Haynes-25 shroud (loss of gas fill). This evaluation accounts for loss of the shroud at various times after fuel block assembly and for several assumed TZM temperatures.

Although in most instances a reasonable theoretical period of time is shown to be available before TZM failure after loss of the shroud, it is recommended that from a safety standpoint, loss of the TZM capsule should be assumed to occur at the time of shroud failure. It is felt that this approach must be taken because of the following undefined areas which are not accounted for in the theoretical analysis.

(a) TZM temperature after shroud failure cannot be accurately predicted though believed to be conservative.

(b) The Larson-Miller stress-rupture parameter for TZM is questionable because of the limited number of test data points used to develop it.

(c) The cover-to-cylinder weld characteristics (efficiency, penetration, ductility, etc.) are not presently defined and, hence, cannot be accounted for. Those weld characteristics have, however, been specified and will be determined in the weld development effort.

(d) TZM compatibility with fuel at the anticipated elevated temperatures upon shroud failure is presently unknown.

F. FUTURE SAFETY ANALYSIS

Within the past year, nuclear aerospace safety has witnessed the development of a numerical analytical technique to evaluate the ultimate safety of an isotopic system. The technique evaluates the probabilities for numbers of people receiving given doses from any credible accident associated with a given system. The PDN analysis (probability, dose, number of people) is used to define the risk level of a given system. Even more recent has been the publication of criteria which define the maximum acceptable risk. For example, given an intact system, the risk criterion might state, "the system shall be designed such that no person shall be subjected to a dose of 100 Rem with a probability greater than 1 in 10^{-6}." Another way of stating the criterion might be that the PDN product shall not exceed 10^{-4} for any conceivable system accident. Although a single, acceptable criterion has not yet been established, the PDN analysis has been proven as a valuable method in determining the risk level associated with a given system.

The safety analysis and testing reported in this document have shown the design is capable of meeting various fuel containment constraints. However, it is known that there are accidents which can result in fuel release. The consequence of these releases or, for that matter, their probability of occurrence is not known. For this reason it is suggested that all future safety analysis of the SNAP 11 be conducted on a PDN basis which will define the hazard and probability thereof.

BLANK

APPENDIX A

FUEL BLOCK THERMAL ANALYSIS

The details of the thermal analysis are presented in this appendix.

A. MINIMUM GAP ANALYSIS (NORMAL OPERATION)

1. Haynes-Beryllium

Between these surfaces, heat is transferred by radiation and conduction:

$$q = \bar{\epsilon}\sigma A\left(T_B^4 - T_H^4\right) + \frac{kA}{\ell}\left(T_B - T_H\right)$$

$$\bar{\epsilon} = \frac{1}{\frac{1}{\epsilon_1} + \frac{1}{\epsilon_2} - 1} = 0.56$$

where

q = heat transferred laterally = 510 watts

σ = Stefan-Boltzmann constant = 1713×10^{-12} Btu/ft^2-hr-°R^4

ϵ_1 = Haynes-25 emissivity (material oxidized at 2250° F) = 0.9

ϵ_2 = beryllium emissivity = 0.6

k = argon conductivity = 0.028 Btu/ft-hr-°F

A = lateral surface area = 0.42 ft^2

T_H = Haynes-25 temperature = 1400° F

ℓ = minimum hot gap = 0.001 inch

T_B = outer beryllium temperature, minimum.

Solution is

$$T_B = 1412° \text{ F} = 1872° \text{ R}$$

This temperature is the minimum beryllium surface temperature. To calculate the average beryllium temperature, the conservative ap-

proach is to superimpose the axial delta temperature due to excess heat flow out of the shutter. For this calculation

$$\Delta T_{axial} = \frac{q}{\sum_{i}^{3} \frac{k_i A_i}{\ell_i/2}} = 68° F$$

where

k = thermal conductivity

A = cross-sectional area

$\ell_i/2$ = half path length (since heat is first transferred out of the capsule lateral surface uniformly)

= 2 inches

i = subscript indicating the materials platinum, graphite or beryllium

q = excess heat = 303 watts.

The half axial drop is 34° F and represents the difference between minimum part temperature and average part temperature. Thus, the average outer beryllium temperature is 34° F higher or

T_B = 1446° F = 1906° R.

2. Through Beryllium

The temperature increase radially through the beryllium is given by

$$\Delta T = \frac{q \ln \frac{D_2}{D_1}}{2 \pi k \ell} = 5° F$$

where

q = total inventory = 813 watts

D_2 = outer beryllium diameter = 3.9 inches

D_1 = inner beryllium diameter = 3.3 inches

k = beryllium conductivity = 44 Btu/ft-hr-°F

ℓ = beryllium length = 4.16 inches.

Thus, the average beryllium liner temperature is 1451° F = 1911° R.

3. Beryllium-Graphite

For this gap, using the same equation:

q = 813 watts

ϵ_β = beryllium emissivity = 0.60

ϵ_g = graphite emissivity = 0.70

A = total outer graphite area = 0.42 ft^2

σ = Stefan-Boltzmann constant = 1713 x 10^{-12} Btu/ft^2-hr-°R^4

k = argon conductivity = 0.028 Btu/ft-hr-°F

ℓ = minimum hot gap = 0.016 inch

T = average beryllium temperature = 1451° F

T_G = average outer graphite temperature.

The solution is

T_G = 1594° F = 2054° R.

4. Through Graphite

The temperature increase radially through the graphite (ATJ grade) is given by

$$\Delta T = \frac{q \ln \frac{D_2}{D_1}}{2 \pi k \ell} = 22° F$$

where

q = 813 watts

D_2 = outer diameter = 3.3 inches

D_1 = inner diameter = 3.0 inches

k = conductivity (with grain) = 29 Btu/ft-hr-°F

ℓ = length = 4.16 inches.

Thus, the average inner graphite temperature is 1616° F = 2076° R.

5. Graphite-Platinum

For this gap,

$$q = \sigma \bar{\epsilon} A (T_p^4 - T_G^4) + \frac{kA(T_p - T_G)}{\ell}$$

$$\bar{\epsilon} = \frac{1}{\frac{1}{\epsilon_1} + \frac{1}{\epsilon_2} - 1} = 0.12$$

where

q = 813 watts

ϵ_1 = platinum emissivity = 0.13

ϵ_2 = graphite emissivity = 0.70

A = lateral area = 0.114 ft^2

σ = Stefan-Boltzmann constant = 1713 x 10^{-12} Btu/ft^2-hr-°R^4

ℓ = minimum hot gap = 0.0005 inch

T_G = average inner graphite temperature = 1616° F

T_p = average outer platinum temperature.

The solution is

T_p = 1648° F = 2108° R.

6. Through Platinum

The temperature increase radially through the platinum is given by

$$\Delta T = \frac{q\left(\ln \frac{D_2}{D_1}\right)}{2\pi k \ell} = 33^\circ F$$

where

q = 813 watts

D_2 = outer diameter = 2 inches

D_1 = average inner diameter = 1.25 inches

k = conductivity = 38 Btu/ft-hr-°F

ℓ = effective length = 2 inches.

Thus, the average inner platinum temperature is 1681° F = 2141° R.

7. Platinum-TZM

For this gap, radiation can be neglected since the effective emissivity is only 0.06 (less than 2% of the heat will be transferred by radiation). Then

$$\Delta T = \frac{q\ell}{kA} = 132^\circ F$$

where

q = 813 watts

ℓ = gap = 0.01 inch

k = argon conductivity = 0.032 Btu/ft-hr-°F

A = lateral area = 0.055 ft^2.

Thus, the outer average TZM temperature is 1813° F = 2273° R.

8. Through TZM

The temperature increase radially through the TZM wall is given by

$$\Delta T = \frac{q\left(\ln \frac{D_2}{D_1}\right)}{2\pi k \ell} = 13^\circ F$$

where

q = 813 watts

D_2 = average outer diameter = 1.25 inches

D_1 = average inner diameter = 0.95 inch

k = TZM conductivity = 50 Btu/ft-hr-°F

ℓ = capsule length = 2 inches.

Thus, the average inner wall temperature on the TZM is 1826° F = 2286° R.

9. Maximum Gap Analysis (Normal Operation)

The same calculations and values were repeated for the maximum gaps.

B. COMPONENT TEMPERATURES DURING ASSEMBLY

During the fuel block assembly, it is necessary to know the surface temperature of several of the components as they reach equilibrium in the argon environment of the hot cells. These temperatures are computed for the Haynes-25 shroud, the graphite enclosure and the platinum* capsule. The capsule equilibrium temperature was previously computed by ORNL and found to be an average of 2800° F for an emissivity of 0.16.

All component temperatures have been computed under the assumption that the components are suspended in the argon and are not exposed to additional cooling by contact with a water-cooled hot cell floor or other solid objects.

In the following section, where the Haynes-25 surface temperature is computed, temperatures of the other components inside the Haynes-25 are also computed for both maximum and minimum gap cases.

---

* Surface of the platinum is normally not directly exposed for free convection but is housed inside the graphite. This calculation is of interest in the event the graphite shatters if dropped and exposes the platinum.

1. Haynes-25 Shroud

The temperature of the shroud is determined by radiation and free convection for which

$$q = \sigma \epsilon A(T^4 - \theta^4) + hA(T - \theta)$$

where

q = fuel inventory = 813 watts(t) = 2770 Btu/hr

ϵ = emissivity (oxidized) = 0.90

A = surface area = 0.59 ft^2

θ = ambient temperature = 560° R

h = natural convection heat transfer coefficient for argon = 1.7 Btu/ft^2-hr-°F (for this geometry and the temperatures involved)

T = Haynes-25 surface temperature.

The solution is

T = 1245° R = 785° F.

Temperatures on the other components internal to the Haynes-25 shroud were computed in a fashion identical to the previous calculations for the normal operation of the block as shown in Section A. For assembly conditions, the following predicted gaps were used:

	Radial Gap (mils)	
Interface	Minimum	Maximum
Haynes-25-beryllium	2	6
Beryllium-graphite	6	10
Graphite-platinum	1.7	5.7
Platinum-TZM	1	1

The results are presented in Section V-A. A fuel loading of 813 watts was used and argon was the gas fill.

2. Graphite Housing

The temperature of the graphite assembly when suspended in argon is similarly determined by

$$q = \sigma \epsilon A (T^4 - \theta^4) + hA(T - \theta)$$

where

q = 925 watts = 3150 Btu/hr

ϵ = 0.65

A = 0.42 ft^2

θ = 560° R

h = 1.9 Btu/ft^2-hr-°F.

The solution is

T = 1510° R = 1050° F.

When the inventory decays to 813 watts, the temperature will be

T = 1460° R = 1000° F.

3. Platinum Secondary Capsule

The temperature is given by

$$q = \sigma \epsilon A (T^4 - \theta^4) + hA(T - \theta)$$

where

q = 925 watts = 3150 Btu/hr

ϵ = 0.16

A = 0.18 ft^2

θ = 560° R

h = 2.05 Btu/ft^2-hr-°F.

The solution is

T = 2630° R = 2170° F.

C. FAILURE ANALYSIS

1. Internal Vacuum Condition

The basis of this calculation is that total weld failure in the fuel block is credible, for which case it is necessary to determine the resultant temperature distribution. The calculation is conservative since no allowance was made for contact conduction between components within the fuel block--that is, only radiation transfer was assumed. It is further assumed that the shutter will not simultaneously fail closed.

The method of calculation follows the pattern presented in the case of normal operation (except that gaseous conduction is not present). Based on the temperatures involved, the following emissivities were used:

Haynes-25 (stably oxidized)	0.90
Beryllium	0.60
Graphite	0.70
Platinum	0.16 to 0.20
TZM	0.18

These calculations were performed both at the beginning-of-life condition (813 watts(t)) and at the end of life (555 watts(t)).

2. Generator Open Circuit Condition

In general, an open circuit in a thermoelectric device is to be avoided since it terminates Peltier cooling in the thermoelements and causes a consequent rise in hot junction and fuel block temperatures. In the SNAP 11 generator, the most critical time for such a failure is at beginning of life, lunar day, when the elements are near 1000° F hot junction temperature. For the fueled demonstration test, the corresponding total thermal inventory is 813 watts(t). At this time, about 400 watts are normally transferred through the elements only. Since the shutter on SNAP 11 provides the capability of handling a maximum fuel inventory of ~925 watts during normal operation, at the time of failure, the shutter can open fully and dump part of the heat that normally is carried through the elements by Peltier cooling. The shutter excess capability is 925 watts less 813 watts or 112 watts. Thus, the elements need only conduct 288 watts (instead of 400) for the open circuit condition.

The new hot junction temperature at lunar day is given by

$$T_{hot} = T_{cold} + \frac{q\ell}{kA} = 1065° F$$

where

T_{cold} = cold junction temperature = 450° F

q = heat through elements = 288 watts(t) = 982 Btu/hr

A = total element cross-sectional area = 0.094 ft^2

k = average (2N and 3P) element thermal conductivity

= 0.71 Btu/ft-hr-°F

ℓ = element length = 0.5 inch.

The resultant lunar day fuel block surface temperature (open circuit condition) is computed from the following relationship

$q \alpha (T_{FB}^4 - T_{IC}^4)$ normal, beginning of life

$q \alpha (T_{FB}^4 - T_{IC}^4)$ open circuit, beginning of life

where

T_{FB}, normal = normal operation fuel block surface temperature ≈ 1400° F = 1860° R

T_{FB}, open circuit = open circuit operation fuel block surface temperature

T_{IC}, normal = normal inner can temperature, lunar day ≈ hot junction temperature + 50° F = 1050° F = 1510° R

T_{IC}, open circuit = inner can temperature during open circuit, lunar day ≈ hot junction temperature + 50° F ≈ 1115° F = 1575° R

The solution is

T_{FB}, open circuit = 1900° R = 1440° F.

APPENDIX B

FUEL BLOCK STRESS ANALYSIS

The details of the stress analysis are presented in this appendix.

A. FUEL CAPSULE PRESSURE-TEMPERATURE STUDY (NORMAL OPERATION)

A pressure-temperature study was performed to determine the variation of these thermodynamic properties with time for normal operation. The fuel investigated was curium-242. The ideal gas relation was used as the equation of state. With the assumption that all heat loss from the capsule is by radiation, the pressure versus time curves were generated from the equation

$$P = \frac{mR}{VM}(1 - \epsilon^{-\lambda t}) \left[(T_o^4 - T_{ambient}^4)\, \epsilon^{-\lambda t} + T_{ambient}^4\right]^{1/4} \qquad \text{(B-1)}$$

where

P = helium pressure caused by decay of fuel (lb/ft^2)

V = volume of helium gas (ft^3)

R = universal gas constant = 1545.33 ft-lb/lb-mole-°R

T = helium gas temperature at time, t (°R)

m = weight of pure isotope (lb)

M = molecular weight of isotope (lb/lb-mole)

t = time (days)

λ = fuel decay constant ($days^{-1}$).

For this study, the initial temperature of the helium gas was taken to be 2000° F. The fuel inventory was 972 watts(t). The parametric void volumes used were 20, 30, 50 and 100 cm^3. The temperature versus time curve was generated by setting

$$T = \left[(T_o^4 - T_{ambient}^4)\, \epsilon^{-\lambda t} + T_{ambient}^4\right]^{1/4} \qquad \text{(B-2)}$$

The results of this study are presented in Fig. V-8.

B. FUEL CAPSULE STRESS ANALYSIS (NORMAL OPERATION)

The fuel capsule is made in the form of a tapered circular cylinder having constant wall thickness. The end closures are flat circular plates. At the small diameter end, the cover is an integral part of the bar material used to make the cylindrical section. At the large diameter end the cover is a separate part which is fusion welded to the cylindrical section. For purposes of analysis only the large diameter cover and attached cylinder were considered since maximum stresses occur in these sections.

Due to the change of section from cylinder to end cover, redundant forces, which result in secondary stresses, are developed. To define these forces, an analysis which utilizes compatibility of deflection and slope at a common point of the cover-to-cylinder attachment was performed. Since the finished weld geometry at this junction did not lend itself to easy analysis, a simplified geometry was assumed. A sketch of the anticipated weld joint and the assumed joint are shown as Fig. B-1.

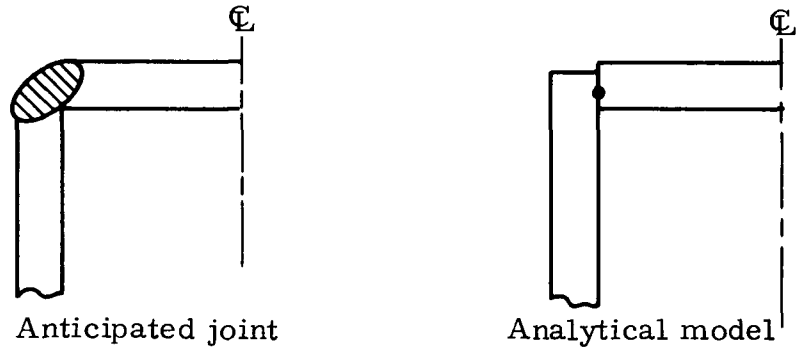

Fig. B-1. TZM Cover-to-Cylinder Attachment

1. Nomenclature

a. Symbols and meanings

M = redundant moment (in. -lb/in.)

R = redundant shear (lb/in.)

V = shear (lb/in.)

P = pressure (psi)

δ = displacement (in.)

θ = rotation (rad)

E = Young's modulus (psi)

ν = Poisson's ratio (in./in.)

t = thickness (in.)

r = radius (in.)

m = $1/\nu$

σ = stress (psi).

b. Subscripts

1--refers to Body 1 (cylinder)

2--refers to Body 2 (cover)

P, R, M, M_Y--deflection and/or rotation due to indicated force or moment.

For this analysis the capsule was considered as a hollow cylinder with flat cover plates. An equivalent cylinder having a geometry equal to that of the capsule's large diameter end was assumed. In addition, a material compatibility allowance was included by mathematically decreasing the inside and outside of the cylinder and cover by 0.020 inch each (i.e., decreasing the thickness by 0.040 inch).

Due to the change in meridional slope of cylinder and cover (i.e., discontinuity), redundant bending and shear forces develop at the junction. To solve for these redundant forces a compatibility analysis was performed. This requires equating slopes and deflections at the junction of the cylinder and cover plate and solving the resulting equations simultaneously for the redundant forces.

A free body force diagram of the capsule structural model is shown as Fig. B-2.

Sign convention:

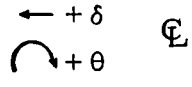

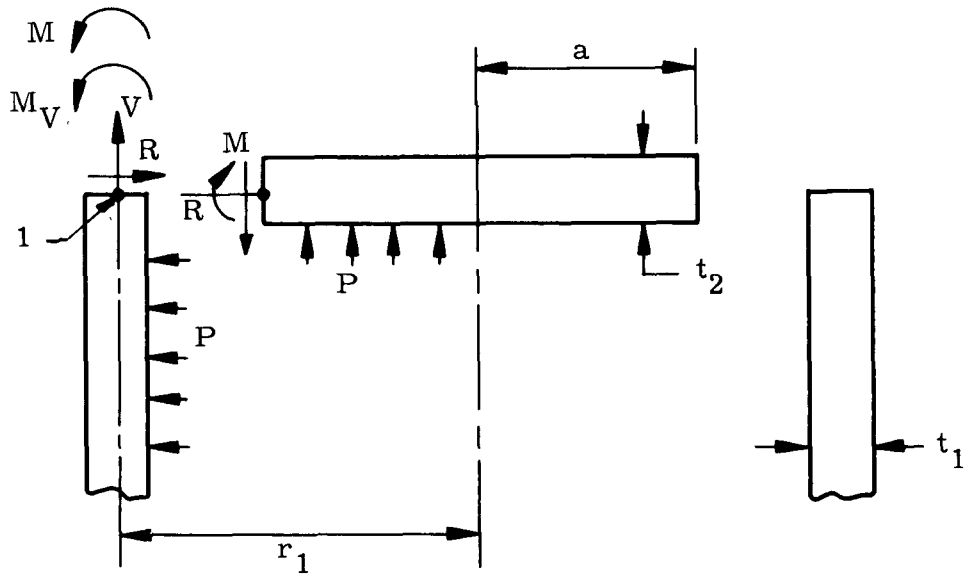

Fig. B-2. Free Body Force Diagram of Capsule Structural Model

Values for geometry and constants are as follows:

t_1 = 0.11 inch

t_2 = 0.21 inch

r_1 = 0.625 inch

a = 0.57 inch

E = 30×10^6 psi (Ref. B-1)

ν = 0.3

m = $1/\nu$ = 3.333

$$T_1 = \sqrt[4]{\frac{3(1-\nu^2)}{r_1^2 t_1^2}} = 4.90$$

$$D_1 = \frac{E t_1^3}{12(1-\nu^2)} = 3.657(10)^3$$

For compatibility, the radial deflections and rotation of the cylinder and cover plate at their junction are equated.

$$\delta_{1_P} + \delta_{1_R} + \delta_{1_M} + \delta_{1_{M_V}} = \delta_{2_P} + \delta_{2_R} + \delta_{2_M} \tag{B-3}$$

$$\theta_{1_P} + \theta_{1_P} + \theta_{1_M} + \theta_{1_{M_V}} = \theta_{2_P} + \theta_{2_R} + \theta_{2_M} \tag{B-4}$$

Due to relative stiffness and geometry δ_{1_P}, δ_{2_R}, δ_{2_M}, θ_{1_P} and θ_{2_R} are assumed to be negligible; hence, Eqs (B-3) and (B-4) reduce to

$$\delta_{1_P} + \delta_{1_R} + \delta_{1_M} + \delta_{1_{M_V}} = 0 \tag{B-5}$$

$$\theta_{1_R} + \theta_{1_M} + \theta_{1_{M_V}} = \theta_{2_P} + \theta_{2_M} \tag{B-6}$$

The terms in Eqs (B-5) and (B-6) are now found

δ_{1_R} (Ref. B-4, page 268, Case 1)

$$\delta_{1_R} = \frac{Pr_1^2}{Et_1} = 0.1184(10)^{-6} P \tag{B-7}$$

δ_{1_R} (Ref. B-4, page 271, Case 10)

$$\delta_{1_R} = -\frac{R}{2D_1 \tau_1^3} = -1.162(10)^{-6} R \tag{B-8}$$

δ_{1_M} (Ref. B-4, page 271, Case 11)

$$\delta_{1_M} = \frac{M}{2D_1 \tau_1^2} = 5.6951(10)^{-6} M \tag{B-9}$$

$\delta_{1_{M_V}}$ (Ref. B-4, page 271, Case 11)

$$\delta_{1_{M_V}} = \frac{M_V}{2D_1 \tau_1^2} \tag{B-10}$$

where

$$M_V = \frac{Vt_1}{2}$$

$$V = \frac{r_1 P}{2}$$

Thus

$$\delta_{1_{M_V}} = 0.0979(10)^{-6} P \qquad \text{(B-11)}$$

θ_{1_R} (Ref. B-4, page 271, Case 10)

$$\theta_{1_R} = \frac{R}{2D_1 \tau_1^2} = 0.5695(10)^{-5} R \qquad \text{(B-12)}$$

θ_{1_M} (Ref. B-4, page 271, Case 11)

$$\theta_{1_M} = \frac{-M}{\tau_1 D_1} = -5.5812(10)^{-5} M \qquad \text{(B-13)}$$

$\theta_{1_{M_V}}$ (Ref. B-4, page 271, Case 11)

$$\theta_{1_{M_V}} = \frac{-M_V}{\tau_1 D_1} = \frac{-r_1 t_1}{4\tau_1 D_1} P$$

$$\theta_{1_{M_V}} = -0.0960(10)^{-5} P \qquad \text{(B-14)}$$

θ_{2_P} (Ref. B-4, page 194, Case 1)

$$\theta_{2_P} = \frac{3Pa^3(m-1)}{2Emt_2^3} = -0.070(10)^{-5} P \qquad \text{(B-15)}$$

θ_{2_M} (Ref. B-4, page 197, Case 12)

$$\theta_{2_M} = \frac{12(m-1)Ma}{Emt_2^3} = 1.7233(10)^{-5} M \qquad \text{(B-16)}$$

Substituting Eqs (B-7) through (B-16) into Eqs (B-5) and (B-6) and solving for M and R produces,

$$M = 0.01773\ P \text{ (in.-lb/in.)}$$

$$R = 0.2730\ P \text{ (lb/in.)}$$

2. Determine Stress for Cover Plate

A free body force diagram for the cover plate is shown in Fig. B-3.

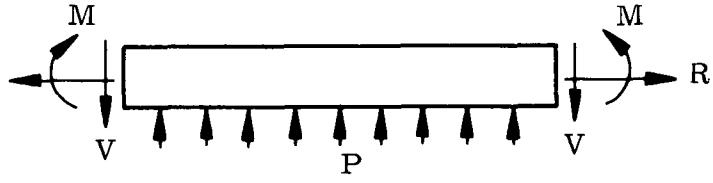

Fig. B-3. Free Body Force Diagram for Cover Plate

Bending stress at the plate center due to pressure is

$$\sigma_P = \frac{3a^2}{8m t_2^2}(3m + 1)\ P \text{ (Ref. B-4, page 194, Case 1)} \qquad \text{(B-17)}$$

$$\sigma_P = 0.117\ P \text{ (tension on outside surface).}$$

Bending stress at the plate center due to redundant moment is

$$\sigma_M = -\frac{6M}{t_2^2} \text{ (Ref. B-4, page 197, Case 12)} \qquad \text{(B-18)}$$

$$\sigma_M = -2.412\ P \text{ (compression on outside surface)}$$

Thus, the total stress at the plate center is

$$\sigma_{tot} = \sigma_P + \sigma_M = 6.705\ P \qquad \text{(B-19)}$$

The stress in the cylinder is determined in the following manner.

A free body force diagram for the cylinder is as shown in Fig. B-4.

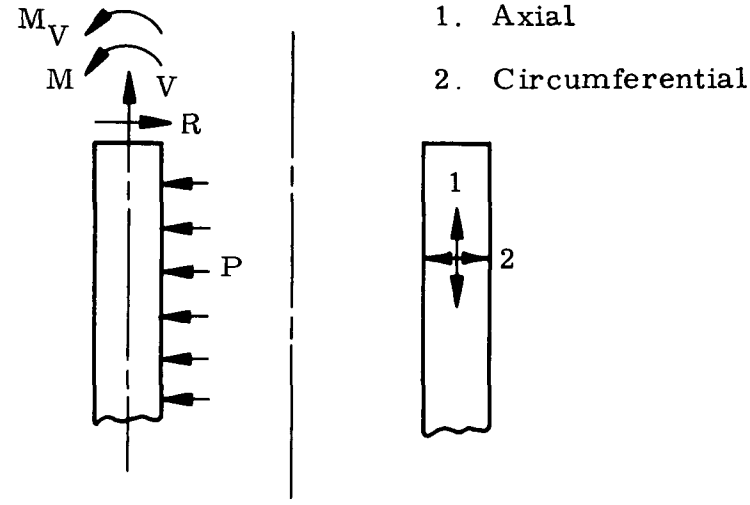

Fig. B-4. Free Body Force Diagram for Cylinder

Stress sign convention

$\sigma = \pm$ → the upper sign relates to the cylinder outer surface and the lower sign to the inner surface. A positive (+) sign indicates tension and a negative (-) sign, compression.

Stress due to pressure (σ_P)

$$\sigma_{P_2} = \frac{r_1}{t_1} P = \overset{+}{+} 5.68\ P$$

$$\sigma_{P_1} = \frac{\sigma_{P_2}}{2} = \overset{+}{+} 2.84\ P \qquad \text{(B-20)}$$

Stress due to redundant force R (σ_R)

$$\sigma_{R_2} = \frac{2R}{t_1} \tau_1 r = \overset{-}{-} 15.20\ P$$

$$\sigma_{R_1} = \frac{1.932\ R}{\tau_1 \tau_1^2} = \overset{+}{-} 8.896\ P \qquad \text{(B-21)}$$

Stress due to moments M and M_V (σ_{M^*})

$$M^* = M + M_V \qquad \text{(B-22)}$$

where:

$$M_V = \frac{t_1}{2} V = \frac{t_1 r_1}{4} P = 0.0172\ P$$

Thus,

$$M^* = (0.0177 + 0.0172)\ P = 0.0349\ P$$

Hence,

$$\sigma_{M_2^*} = \frac{2M^* \tau_1^2 r}{t_1} = \pm 0.522\ P$$

$$\sigma_{M_1^*} = \frac{6M^*}{t_1^2} = \mp 17.31\ P$$

The combined stresses are as follows:

Circumferential stress

$\sigma_2 = (5.68 - 15.2 + 9.522)\ P = \pm 0.002\ P$ at junction

$\sigma_2 = \pm 5.68\ P$ at the location below the junction.

Axial stress

$\sigma_1 = (\pm 2.84 \pm 8.896 \mp 17.31)\ P.$

Thus,

$\sigma_1 = -5.57\ P$ at outer surface

$\sigma_1 = +11.25\ P$ at inner surface.

The maximum stresses are now summarized:

Cylinder

σ_{h_1} = circumferential stress due to pressure (membrane stress) = 5.68 P

σ_{a_1} = combined axial stress at cylinder end due to direct pressure and redundant forces (membrane + secondary stress) = 11.25 P

Cover

σ_{b_2} = bending stress at cover center due to direct pressure and redundant forces (membrane + secondary stress) = 6.705 P

C. HAYNES-25 SHROUD FAILURE ANALYSIS

In this analysis, the effect of a TZM capsule failure on the Haynes-25 shroud is investigated. Specifically, the effect of gross deformation on cover plate stress levels is evaluated. A deformation of the cover at its center of 1/4 inch as shown in the following sketch (Fig. B-5) was assumed.

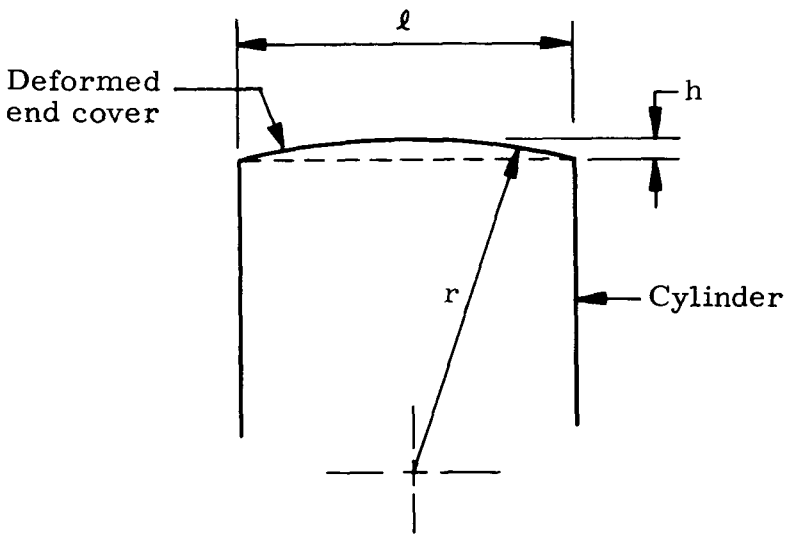

r = equivalent radius of dished head

h = deflection = 0.25 inch

ℓ = 4 inches.

Fig. B-5. Deformation of the Cover

The radius (assuming a spherical sector) is

$$r = \frac{4h^2 + \ell^2}{8h} = 8.125 \text{ inches.}$$

The volume, V, of this sector is

$$V = \frac{2\pi r^2 h}{3} - \pi\left(\frac{\ell}{2}\right)^2 \frac{(r - h)}{3} = 1.58 \text{ in.}^3 = 25.875 \text{ cm}^3$$

assuming identical deformation of both end covers produces a total increase in void volume of

$$V_{tot} = 2V = 51.75 \text{ cm}^3.$$

This results in a total void volume (including radial gaps and capsule) of $20 + 22.2 + 51.75 = 93.95 \text{ cm}^3$. In terms of the capsule internal pressure, the Haynes-25 (L-605) contained internal pressure becomes

$$p_{L\text{-}605} = \left(\frac{20}{93.95}\right) p_c = 0.213\, p_c$$

Again, based on TZM failure at 90 days after encapsulation, the Haynes-25 pressure is

$$p_{L\text{-}605} \leq 17.9 + 0.213\,(840) \cong 197 \text{ psi}.$$

Assuming the cover as a dished head with radius r = 8.125 inches, the following membrane stress was found.

$$\sigma_m = \frac{pr}{t} = \frac{197(8.125)}{0.150} = 10,700 \text{ psi}.$$

This is considerably lower than the 98,250-psi flexure stress found for the flat plate that was not deformed.

A check was then made to see if the above deformation is available. The flat plate has a radius of 2 inches. The deformed plate has a half arc length of

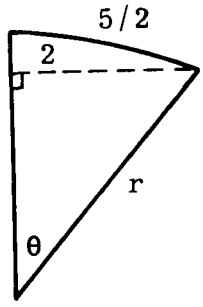

$$\sin\theta = \frac{2}{r} = \frac{2}{8.125} = 0.246$$

$$\theta = 14.25° = 0.249 \text{ radian}$$

$$s/2 = r\theta = 8.125(0.249) = 2.0231 \text{ inches}.$$

The elongation of the plate is 2.0231 - 2 = 0.0231 inch in 2 inches, hence, the percent elongation, e, is

$$e = \frac{0.0231}{2} \times 100 = 1.155\%$$

To achieve the assumed cover deformation, the lower cover-to-housing weld must survive a rotation of at least $\theta = \tan^{-1}\left(\frac{0.25}{2}\right)$ or $\theta =$ 7.1 degrees. The most practical way to show that this magnitude of rotation is available in the weld, without inducing weld failure, is by structural test. Since yielding of the material is required, calculated stress values are meaningless because the available equations are based on linear theory.

D. HAYNES-25 SHROUD FAILURE TEMPERATURE

For the failure analysis of the Haynes-25 shroud, an approximate upper limit failure temperature for the Haynes-25 was found to be 2000° F. This temperature was based on rupture of the side wall in a 150-day period assuming (at assembly) one atmosphere internal pressure at 1300° F; it was determined as follows;

The side wall circumferential stress (σ) is given by

$$\sigma = \frac{pr}{t}$$

where

r = radius $\cong$ 2.06 inches

t = wall thickness = 0.100 inch

p = internal pressure.

Assuming one atmosphere initial pressure at 1300° F and a constant volume process, pressure as a function of temperature is found as follows

$$p_2 = p_1 \frac{T_2}{T_1} = 15\left(\frac{T_2}{1760}\right) = \text{psi}$$

A listing of assumed temperatures, T_2, and corresponding pressure, p_2, and shroud side wall stress, σ, is given in the following tabulation.

In Ref. B-5, by extrapolation, the stress to rupture Haynes-25 bar in 4000 hours at 2100° F is 460 psi. Hence, 2000° F at 433-psi stress for 150 days (3600 hours) should provide a conservative estimate of failure temperature. It is noted that failure of the Haynes-25 end covers could occur before the side wall, particularly in the welded end cover

T_2 (°F)	T_2 (1) + 460 (°R)	p_2 $\frac{15}{1760}$ x (2) (psi)	σ $\frac{2.06}{0.10}$ x (3) (psi)
1400	1860	15.85	326
1500	1960	16.7	344
1600	2060	17.55	362
1700	2160	18.4	379
1800	2260	19.3	398
1900	2360	20.1	414
2000	2460	21	433
2100	2560	21.8	450

joint. Since no accurate analytical means is available for predicting failure due to bending stress in the creep temperature range of a material, it is suggested that only by test will a reasonable failure temperature and pressure be found for the Haynes-25 shroud assembly.

REFERENCES

B-1. "The Engineering Properties of Molybdenum and Molybdenum-Based Alloys " (DMIC-190), September 20, 1963.

B-2. "Larson-Miller Parameter for the Molybdenum Alloy TZM " (MNERS-RKG-6511), Martin Company, March 17, 1966.

B-3. "Developmental Data Climelt TZM," Climax Molybdenum Company of Michigan, January 1962.

B-4. "Formulas for Stress and Strain," R. J. Roark, Third Edition, McGraw-Hill Book Company, New York, New York, 1954.

B-5. "Haynes Alloy No. 25," Haynes Stellite Co., March 1959.

BLANK

APPENDIX C

LIST OF DRAWINGS FOR MODEL 431D: Q/N-1M, Q/N-3 AND Q/N-4

I. Generator Assembly

431D1110000	Sh 1	(CDI)	Generator Assembly (Electrically Heated)
	Sh 2	(CDI)	Generator Assembly (Fueled)
431D1110001		(CDI)	Inner Can and Module Strip Assembly
431B1110002	Sh 1		Outer Shell Assembly
	Sh 2		Outer Shell Assembly
	Sh 3		Outer Shell Assembly
431Bppp0003		(CDI)	Instrumentation
431Bppp0004			Bottom Assembly, Inner Shell
431D1110006		(CDI)	Module Assembly
431Dppp0007		(CDI)	Couple Assembly
431D1110008		(CDI)	Thermocouple Elements
431A1110008			Details, Bottom Assembly
431D1110009		(CDI)	Button, Piston
431D1110010		(CDI)	Element Disc
431D1110012		(CDI)	Shoe, Hot Junction
431B1110013			Inner Can Assembly
431B1110014			Outer Dome
431A1110015			Outer Housing
431A1110016			Outer Housing Details
431A1110017			Seal Plug
431A1110019			Insulation Details
431A1110020			Miscellaneous Details
431B1110023			Reinforcing Ring
431B1110024			Hold-down Plate, Reservoir
431A1110025			Flange, Upper
431B1110025			Support Bracket, Pressure Transducer
431B1110026			Flange and Diaphragm Bracket Assembly
431B1110027			Insulations
431B1110028			Insulation, Diaphragm Bracket
431-1110029			Inner Shell Details
431B1110029			Cover Plate, Auxiliary
431B1110030			Heat Shield Assembly
431B1110031			Inner Heat Shield
431B1110032			Cover Plate
431B1110033			Heat Baffle; Inner Shield
431-1110034		(CDI)	Insulation, Module Strip
431A1110034			Lock Washer
431B1110034			Diaphragm Support Bracket
431B1110035			Fitting, Tee
431D1110037			Evacuation Assembly
431-1110038		(CDI)	Module Bar
431B1110038			Sleeve, Module Strip Connector

431-1110040			Lug, Terminal
431B1110040			Fueling Tool
431B1110041			Insulation Foil and Straps
431D1110041			Strap, Heat Shield
431-1110042			Seal Plug and Ring Details
431D1110042			Strap, Inner Can Assembly
431B1110043			Insulation Ring, NaK Tube
431-1110044			Mica Sheet
431B1110044			Nut, Transducer Attachment
431-1110045			Terminal Lug Assembly
431D1110045		(CDI)	Transfer Procedure (Sealing of Generator)
431D1110046		(CDI)	RTG Argon Hot Leak Test Procedure
431D1110047		(CDI)	Thermal Vacuum Test Procedure
431D1110048			Environmental Test Procedure
431D1110049		(CDI)	Outgassing and Sealing Procedure
431D1110050		(CDI)	Fuel Block Assembly
431D1110051			Nut
431D1110053		(CDI)	TZM Primary Capsule
431D1110054		(CDI)	Capsule, Platinum, Secondary
431D1110055		(CDI)	Housing, Graphite
431D1110056		(CDI)	Housing, Beryllium
431D1110057		(CDI)	Outer Housing, Haynes-25
431D1110061		(CDI)	Graphite Housing and Compensator Assembly
431D1110062			Skin
431D1110063		(CDI)	Fueled Capsule Assembly
431D1110065			Heater Block Assembly
431D1110066			Heater Block
431D1110067			Lower Flange Assembly
431D1110068			Upper Flange Assembly
431D1110069			Housing
431D1110070			Heater Assembly
431D1110071			Hold-down and Shield Assembly
431D1110072			Upper, Lower Ring, Shield Assembly
431D1110073			Insulation Disc, Heater Block Assembly
431D1110074			Hold-down and Shield Assembly

II. Thermal Control Assembly

431B1310000	Sh 1	(CDI)	Thermal Control Assembly
	Sh 2		Thermal Control Assembly
431-1310001			Reservoir Assembly
431-1310002			Reservoir Details
431-1310003			Shutter Bracket Fitting Assembly
431B1310003			Shutter Bracket, Channel Assembly
431-1310004			Shutter Bracket
431B1310004			Channel, Shutter Locking

431-1310005			Shutter Fitting
431-1310006			Support Assembly
431-1310007			Support Details
431-1310008			Spring, Tension
431-1310009			Bushing
431B1310010			Drive Shaft
431B1310011			Connecting Link
431B1310012			Pin, Flat Head
431B1310013			Insulation Foil, Reservoir
431B1310014			Bracket, Shutter Locking
431-1310015			Upper Spring Pin
431-1310016			Screw, Stop
431B1310017			Actuator Shims
431-1310020			Tube Details
431-1310021			Bracket Details
431-1310022			Bracket Assembly
431B1310023		(CDI)	Assembly Procedure (Book Form)
431-1310024			Plug, Bellows Actuator
431-1310025			Clip, Actuator Tube
431B1310027			Eyebolt, Spring Adjustment
431B1310029			Shutter Assembly
431B1310030			Outer Shutter
431B1310031			Inner Shutter
431B1310032			Shutter Insulation
431B1310033			Dimpled Foil
431B1310034			Washers
431B1310035			Bolt, Plated
431B1310036			Bushings
431B1310037			Tee, Tubing

III. Shipping Cask

431B1110015		Shipping Cask Assembly
431B1110016		Graphite Details
431B1110017		Stand-off
431B1110018		Inner Shell
431B1110019		Outer Shell
431B1110020		Balsa Details
431B1110021		Pallet
431B1110022		Nameplates

IV. Field Test Kit

431B1700000	Sh 1	Field Test Kit Assembly
	Sh 2	Field Test Kit Assembly

V. DC-DC Converter

431A1120001	Casting
431A1120002	Housing
431A1120003	Converter Assembly
431A1120006	Printed Circuit Board
431A1120007	Insulators

VI. Shipping Container

PSK 326	Shipping Container for SNAP 11 Generator

VII. Module Test Fixtures

431-0210063	SNAP 11 Couple Assembly
431-0210064	SNAP 11 Test Module
431-0210065	Wiring Diagram
431-0210066	Test Fixture

VIII. Environmental Test Fixtures

88-3000501	Test Fixture for SNAP 11
88-3000502	Shock Adapter for SNAP 11

IX Purchased Parts

PN 7400001	Pressure Transducer
NPS 60420003	Bellows Actuator Assembly
NPS 60420004	Bellows Sealed Reservoir Assembly
NPS 81410002-005	Connector, Electrical
26 N2-1	Stud, Plain

APPENDIX D

LIST OF REPORTS AND MANUALS

I. Quarterly Reports

MND-P-2811-1	First Quarterly Progress Report	CDI
-2	Second Quarterly Progress Report	CDI
-3	Third Quarterly Progress Report	CDI
-4	Fourth Quarterly Progress Report	CDI
-5	Fifth Quarterly Progress Report	CDI
-6	Sixth Quarterly Progress Report	CDI
-7	Seventh Quarterly Progress Report	CDI
MND-2952-8	Eighth Quarterly Progress Report	CDI
-10	Ninth Quarterly Progress Report	CDI
-14	Tenth Quarterly Progress Report	CDI
-20	Eleventh Quarterly Progress Report	CDI
-26	Twelfth Quarterly Progress Report	CDI
-30	Thirteenth Quarterly Progress Report	CDI
-38	Fourteenth Quarterly Progress Report	CDI
-46	Fifteenth Quarterly Progress Report	CDI
-55	Sixteenth Quarterly Progress Report	CDI
-58	Seventeenth Quarterly Progress Report	CDI
-62	Eighteenth Quarterly Progress Report	CDI

II. Fueling and Safety Reports

MND-P-3103	Flight Model Impact Evaluation	CRD
MND-2952-32	Safety Analysis Hazards Report	CDI
-53	SNAP 11 Fueling Procedure	CDI
-54	SNAP 11 Fuel Block Assembly Design--Analysis Report	CDI

III. Operation Instruction Manuals

MND-2952-9	Operational Manual for SNAP 11 Project Surveyor	CDI
-35	Radioisotopic Power Supply Demonstration Test Plan & Operation Instruction Manual	CDI
-65	Operation Instructions Manual, SNAP 11 Q/N-3 Generator	CDI
-68	Operation Instructions Manual, SNAP 11 Q/N-4 Generator	CDI

IV. Reliability Reports

MND-2952-13	SNAP 11 Reliability Program Plan	--

BLANK